STRUCTURE AND BONDING 132

Series Editor D. M. P. Mingos
Volume Editor M. W. Hosseini

Molecular Networks

Springer

132
Structure and Bonding

Series Editor: D. M. P. Mingos

Structure and Bonding

Series Editor: D. M. P. Mingos

Recently Published and Forthcoming Volumes

Molecular Networks
Volume Editor: Hosseini, M. W.
Vol. 132, 2009

Molecular Thermodynamics of Complex Systems
Volume Editors: Lu, X., Hu, Y.
Vol. 131, 2009

Contemporary Metal Boron Chemistry I
Volume Editors: Marder, T. B., Lin, Z.
Vol. 130, 2008

Recognition of Anions
Volume Editor: Vilar, R.
Vol. 129, 2008

Liquid Crystalline Functional Assemblies and Their Supramolecular Structures
Volume Editor: Kato, T.
Vol. 128, 2008

Organometallic and Coordination Chemistry of the Actinides
Volume Editor: Albrecht-Schmitt, T. E.
Vol. 127, 2008

Halogen Bonding
Fundamentals and Applications
Volume Editors: Metrangolo, P., Resnati, G.
Vol. 126, 2008

High Energy Density Materials
Volume Editor: Klapötke, T. H.
Vol. 125, 2007

Ferro- and Antiferroelectricity
Volume Editors: Dalal, N. S., Bussmann-Holder, A.
Vol. 124, 2007

Photofunctional Transition Metal Complexes
Volume Editor: V. W. W. Yam
Vol. 123, 2007

Single-Molecule Magnets and Related Phenomena
Volume Editor: Winpenny, R.
Vol. 122, 2006

Non-Covalent Multi-Porphyrin Assemblies
Synthesis and Properties
Volume Editor: Alessio, E.
Vol. 121, 2006

Recent Developments in Mercury Science
Volume Editor: Atwood, David A.
Vol. 120, 2006

Layered Double Hydroxides
Volume Editors: Duan, X., Evans, D. G.
Vol. 119, 2005

Semiconductor Nanocrystals and Silicate Nanoparticles
Volume Editors: Peng, X., Mingos, D. M. P.
Vol. 118, 2005

Magnetic Functions Beyond the Spin-Hamiltonian
Volume Editor: Mingos, D. M. P.
Vol. 117, 2005

Intermolecular Forces and Clusters II
Volume Editor: Wales, D. J.
Vol. 116, 2005

Intermolecular Forces and Clusters I
Volume Editor: Wales, D. J.
Vol. 115, 2005

Molecular Networks

Volume Editor: Mir Wais Hosseini

With contributions by

D. Braga · S. Bureekaew · N.R. Champness · G. Férey
F. Grepioni · P. Hubberstey · J. Jia · S. Kitagawa
L. Maini · M. Polito · M. Schröder · S. Shimomura
M.D. Ward

Springer

Prof. Dr. Mir Wais Hosseini
Université de Strasbourg
Inst. Le Bel
Labo. de Tectonique Moléculaire
4 rue Blaise Pascal
67000 Strasbourg
France
hosseini@chimie.u-strasbg.fr

ISSN 0081-5993 e-ISSN 1616-8550
ISBN 978-3-642-01366-9 e-ISBN 978-3-642-01367-6
DOI 10.1007/978-3-642-01367-6
Springer Dordrecht Heidelberg London New York

Library of Congress Control Number: 2009926182

Cover design: KünkelLopka GmbH, Heidelberg, Germany

Printed on acid-free paper

Springer is part of Springer Science+Business Media (www.springer.com)

Structure and Bonding
Also Available Electronically

Structure and Bonding is included in Springer's eBook package *Chemistry and Materials Science.* If a library does not opt for the whole package the book series may be bought on a subscription basis. Also, all back volumes are available electronically.

For all customers who have a standing order to the print version of *Structure and Bonding*, we offer the electronic version via SpringerLink free of charge.

If you do not have access, you can still view the table of contents of each volume and the abstract of each article by going to the SpringerLink homepage, clicking on "Chemistry and Materials Science," under Subject Collection, then "Book Series," under Content Type and finally by selecting *Structure and Bonding.*

You will find information about the

– Editorial Board
– Aims and Scope
– Instructions for Authors
– Sample Contribution

at springer.com using the search function by typing in *Structure and Bonding*.

Color figures are published in full color in the electronic version on SpringerLink.

Aims and Scope

The series *Structure and Bonding* publishes critical reviews on topics of research concerned with chemical structure and bonding. The scope of the series spans the entire Periodic Table and addresses structure and bonding issues associated with all of the elements. It also focuses attention on new and developing areas of modern structural and theoretical chemistry such as nanostructures, molecular electronics, designed molecular solids, surfaces, metal clusters and supramolecular structures. Physical and spectroscopic techniques used to determine, examine and model structures fall within the purview of *Structure and Bonding* to the extent that the focus

is on the scientific results obtained and not on specialist information concerning the techniques themselves. Issues associated with the development of bonding models and generalizations that illuminate the reactivity pathways and rates of chemical processes are also relevant.

The individual volumes in the series are thematic. The goal of each volume is to give the reader, whether at a university or in industry, a comprehensive overview of an area where new insights are emerging that are of interest to a larger scientific audience. Thus each review within the volume critically surveys one aspect of that topic and places it within the context of the volume as a whole. The most significant developments of the last 5 to 10 years should be presented using selected examples to illustrate the principles discussed. A description of the physical basis of the experimental techniques that have been used to provide the primary data may also be appropriate, if it has not been covered in detail elsewhere. The coverage need not be exhaustive in data, but should rather be conceptual, concentrating on the new principles being developed that will allow the reader, who is not a specialist in the area covered, to understand the data presented. Discussion of possible future research directions in the area is welcomed.

Review articles for the individual volumes are invited by the volume editors.

In references *Structure and Bonding* is abbreviated *Struct Bond* and is cited as a journal.

Impact Factor in 2007: 4.041; Section “Chemistry, Inorganic & Nuclear”:
Rank 5 of 43; Section “Chemistry, Physical”: Rank 20 of 110

Preface

In the future, many modern materials will be increasingly based on the assembly of preformed molecular entities. Their structural characteristics and functional properties will be programmed at the molecular level and their formation as a completed entity will be achieved by self-assembly processes. This in essence is a bottom-up approach and its success will require a deep understanding not only of the chemistry of intermolecular interactions and associations but also of self-assembly processes in the condensed phase. Among various interesting innovations brought about by the development of supramolecular chemistry, supramolecular synthesis is a particularly powerful approach for the design and generation of molecular architectures displaying both structural and functional complexity. The combination of molecular synthesis (which allows chemists to design and prepare extremely sophisticated biotic and abiotic molecules through the interconnection of atoms or group of atoms by strong covalent bonds) and supramolecular synthesis (which orchestrates the association of molecules by recognition processes through the use of weak and reversible interactions) opens up endless structural and functional possibilities. Following the perceptive observation by Dunitz that "*A crystal is, in a sense, the supramolecule par excellence*", molecular crystals may be seen as infinite periodic architectures resulting from the interconnection of building blocks or tectons capable of self-assembling through specific recognising events. Thus, one may regard the formation of a molecular crystal as a subset of supramolecular synthesis based on the generation of crystalline materials with defined connectivity patterns between molecular components which makes up the solid material. The iterative recognition events responsible for the formation of crystalline architectures may be based on a variety of intermolecular interactions such as van der Waals' contacts, hydrogen- or coordination bonds and electrostatic interactions. These attractive forces may be employed separately or may be combined in a co-operative manner. This volume, by bringing together contributions by some of the most active and eminent researchers in this area, gives an updated overview of this important and emerging area of research.

Strasbourg, May 2009 *M. Wais Hosseini*

Contents

Struct Bond (2009) 132: 1–23
DOI:10.1007/430_2008_10

Published online: 25 February 2009

Charge-Assisted Hydrogen-Bonded Networks

Michael D. Ward

Abstract The importance of hydrogen bonds is widely recognized because of their role in defining the structure and properties of many compounds, including water, proteins, DNA, and polymers. Hydrogen bonding also has emerged as a critical tool in solid-state chemistry, in which the versatility of organic synthesis has been combined with the structure-directing properties of hydrogen-bond donor–acceptor pairs to steer molecular assembly into networks that reflect the symmetries of their molecular constituents. Although these efforts have been largely empirical, the dominance of hydrogen bonding among the multitude of intermolecular forces often leads to predictable control of crystal structure. Although charge-assisted hydrogen bonds (donors and acceptors with ionic character that reinforce the electrostatic character of the hydrogen bond) have been recognized for decades, their use in network design, particularly for "crystal engineering," has grown substantially in the past decade. The evidence suggests that charge-assisted hydrogen bonds introduce extraordinary robustness to molecular networks that reflects a combination of strong intermolecular forces and structural compliance, thus facilitating design of organic solid-state materials.

Keywords: Crystal engineering · Hydrogen bond · Molecular network

Contents

M. D. Ward (✉)
Molecular Design Institute, Department of Chemistry, New York University, 100 Washington St. East, New York, NY 10003, USA
e-mail: mdw3@nyu.edu

Abbreviations

GS	Guandinium sulfonate
CAHB	Charge-assisted hydrogen bond
EBA	2,2′-(1,2-Ethanediyl)pyrimidinium^{2+}] cation
PBA	2,2′-(1,4-Phenylene)pyrimidinium^{2+} dication

1 Introduction

The structure, organization, and properties of the living and nonliving world reflects a balance of the delicate forces (covalent, ionic, ion–dipole, dipole–dipole, van der Waals, hydrogen-bonding) that are well known to the scientific community. Although ubiquitous in animate and inanimate objects, hydrogen bonding is at once one of the best and poorly understood interactions. Its ability to direct structure is evident in biological macromolecules. The double helix structure of DNA is largely due to hydrogen bonding between the complementary base pairs, adenine (A) with thymine (T) and (G) with cytosine (C) in the Watson–Crick pairing scheme. Intramolecular N–H…O hydrogen bonds along a protein backbone can provoke secondary structure, generating an α-helix when the hydrogen-bonding groups are repeatedly located at i and $i+4$ positions, and a β-sheet when two strands of the protein associate through alternating residues. The function of DNA, its relative RNA, and proteins rely on finely tuned hydrogen bond forces in the midst of other competing interactions. Water – simple and yet complex – owes its peculiar properties to hydrogen bonding. Ice is unusual as it has a density lower than its liquid form, which can be attributed to the formation of a tetrahedral-like network, which in turn reflects the directional nature of hydrogen bonds and their unique structure-directing ability. This chapter focuses on the role of a particular kind of hydrogen bond, the charge-assisted hydrogen bond (CAHB), and its use in the design of molecular networks, which range from motifs in three-dimensional crystals to molecular monolayers.

2 The Dipolar Character of the Hydrogen Bond

The hydrogen bond has been studied exhaustively, and for no system more than water. An examination of the water molecule reveals the key attributes necessary for understanding the dipolar nature of the hydrogen bond and the role of ionic charge in CAHBs. Although many models have been invoked for water, one of the more commonly accepted ones is the ST2 model [1], in which each hydrogen atom is assumed to carry a $+0.24$e charge and each oxygen two -0.24e charges. The charges extend outward from the oxygen atom with tetrahedral symmetry, and the interaction between two water molecules is assumed to involve an isotropic Lennard-Jones

potential and sixteen Coulombic terms arising from the four point charges on the two molecules. The open tetrahedral-like ice network is a consequence of linear O…H…O hydrogen bonds that are situated along four vectors emanating from each oxygen atom. This was revealed by X-ray diffraction analysis of hexagonal ice performed separately by Dennison [2] and Bragg [3] in 1921. Liquid water, however, is estimated to have five nearest neighbors on average but an average of 3.5 hydrogen bonds per water molecule (instead of four in ice) [4] (Fig. 1).

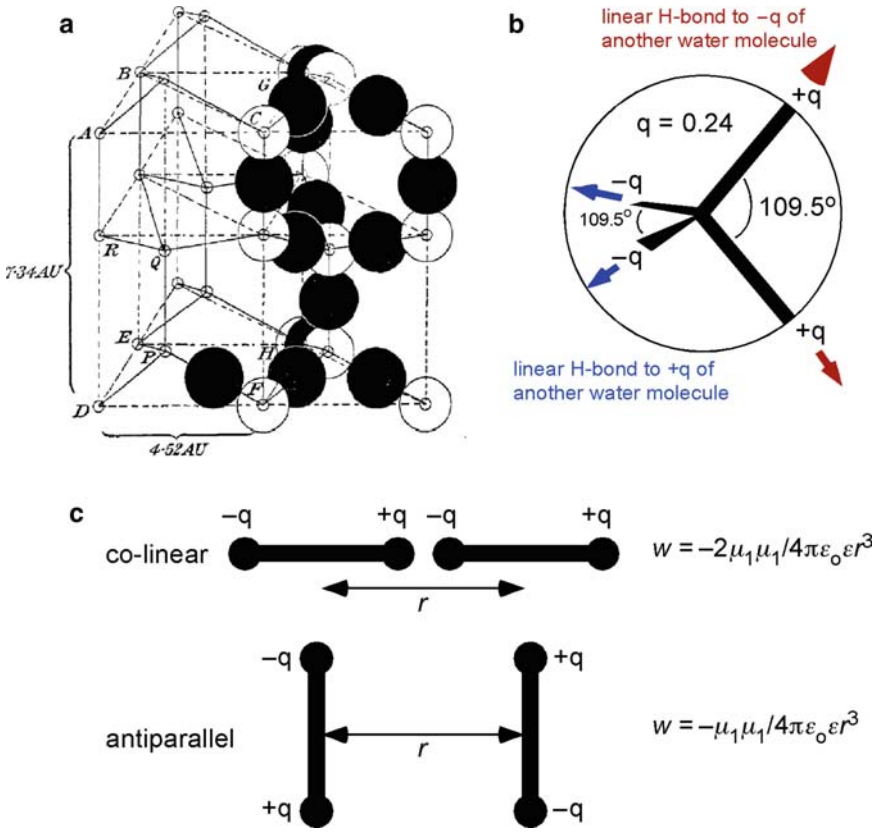

Fig. 1 **a** Hexagonal ice, a crystalline 3D open network in which each oxygen atom is associated with four neighboring oxygen atoms through four linear hydrogen bonds with local tetrahedral symmetry. *White spheres* are oxygen atoms, *black spheres* are hydrogen atoms (reproduced from [3]). **b**The "ST2" model for water, in which the electron lone pairs and hydrogen atoms are assigned partial charges of −0.24e and +0.24e, respectively. Energetically favorable colinear head-to-tail alignment of these dipoles with opposite dipoles on four neighboring water molecules, which are tantamount to hydrogen bonds, creates an infinite 3D network. **c** Schematic representation of collinear head-to-tail and antiparallel dipole–dipole interactions. The interaction energy of the colinear configuration is twice as favorable as the antiparallel configuration

The above description of the water molecule, as well as the structure of ice, suggests that hydrogen bonding is primarily electrostatic. Molecules regarded as having strong hydrogen bonds, such as ammonia (NH_3) and hydrogen fluoride (HF) tend to form order networks in the liquid state, even if only with short persistence lengths. These substances are often designated "associated liquids," and it has been suggested that hydrogen bonding in this state is cooperative, to the extent that hydrogen bonds between two molecules reinforce hydrogen bonds between other pairs in the network. The unique properties of these liquids stems from the unusually high dipole moments of the N–H and F–H bonds, which have bond moments of 1.31 D and 1.94 D, respectively. Therefore, these groups may be described better as strong dipoles with structures resembling N^-–H^+ and F^-–H^+. These dipoles supply a strong attractive force that can align dipoles on neighboring molecules, as expected from the interaction energy between two dipoles based on simple electrostatics for a dipole–dipole interaction. This interaction energy is greatest when both dipoles are colinear, as according to Eq. 1, where w is the interaction energy, μ_1 and μ_2 are the dipole moments of molecules 1 and 2, ε_0 and ε are permittivity terms, and r is the distance between the centroids of each dipole. This value is twice as large, for the same value of r, as for antiparallel two dipoles. Furthermore, the small size of the hydrogen atom, depleted of electron density so that it more resembles a proton, allows close approach of the N^-–H^+ and F^-–H^+ hydrogen-bond "donors" to electronegative "acceptor" sites on neighboring molecules. In fact, one of the criteria for a hydrogen bond is a distance between two electronegative atoms that is less than the sum of their van der Waals radii:

$$w = -2\mu_1\mu_2/4p\varepsilon_0\varepsilon r^3 \tag{1}$$

Collectively, these attributes reveal that (i) the hydrogen bond is primarily an electrostatic interaction that can be characterized as a very strong dipole–dipole interaction, (ii) the dipole–dipole interaction energy for the hydrogen bond can be greater that that calculated for the "textbook" point dipole because of the vanishingly small size of the hydrogen atom when it is depleted of electrons, and (iii) hydrogen bonds tend to be linear because the dipole–dipole interaction is maximized in this geometry. These attributes aptly describe charge-assisted hydrogen bonds (CAHBs) observed in networks in the crystalline solid state, and their description will comprise the major part of this chapter. CAHBs consist of a hydrogen bond acceptor and a hydrogen bond donor, *each carrying an ionic charge that further reinforces the electrostatic dipole–dipole character of the hydrogen bond*. Consequently, CAHBs tend to be among the strongest hydrogen bonds in the solid state. The strength of hydrogen bonds ranges from weak ($1\,kJ\,mol^{-1}$) to extremely strong ($>155\,kJ\,mol^{-1}$); most CAHBs can be expected to fall at least in the middle of this range. Gilli et al. classified CAHBs in crystals according to whether they were *negative charge assisted* (e.g., –O–H…O^-), *positive charge assisted* (e.g., = O…H^+…O =), or *resonance assisted* (where the two oxygens (or two nitrogens) are connected by a system of π-conjugated double bonds [5]. Taylor and Kennard found that N–H donors with formal positive charge tend to form shorter bonds than uncharged N–H groups, and

that the negatively charged carboxylate ion is a stronger acceptor than uncharged amides, ketones, and carboxyls [6]. This is illustrated by the so-called "Speakman salts," which contain strong hydrogen bonds between a carboxylic acid and a carboxylate ion [7]. Theoretical aspects associated with CAHBs, as well as with other types of hydrogen bonds, have been reviewed recently [8].

The peculiar properties of CAHBs make them especially promising with respect to directing molecular assembly and enabling the construction of networks in a rational manner aimed at the introduction of substituents for adjusting solid-state properties in a controllable manner. Notably, X-ray diffraction methods have been instrumental in the characterization of CAHBs, providing feedback into the further design of molecular networks. Because hydrogen atoms do not scatter X-rays strongly it is often difficult to determine their exact positions without resorting to neutron diffraction. This is particularly true for hydrogen bonds, where the electron density about the hydrogen atom is highly depleted. Consequently, hydrogen bonds and their directions are often located by identifying short distances between pairs of electronegative atoms, particularly if one of the atoms is known to carry a hydrogen atom and if there is clear evidence, usually geometric, for hydrogen bond formation [9]. Nonetheless, crystallographic methods are improving with respect to assigning the positions of hydrogen atoms.

3 Hydrogen Bonds and Network Design

Molecular crystals always can be described as consisting of some kind of network or a collection of networks, depending on how one wants to draw lines to connect points in some repeating fashion. Hydrogen bonds, however, are easily distinguished from less specific intermolecular interactions such as van der Waals and $\pi-\pi$ interactions. As such, the connectivity of a hydrogen-bonding network is usually straightforward. The term "network" has many definitions, chief among them:

1. A system of intersecting lines
2. Something resembling an openwork fabric or structure in form or concept
3. An openwork fabric or structure in which cords, threads, or wires cross at regular intervals
4. In information technology: a series of points or nodes interconnected by communication paths

Networks can interconnect with other networks and contain subnetworks. Each of these definitions suits hydrogen-bonded networks in crystalline solids. When two- or three-dimensional they can be represented as grids, they can be open or porous, they can cross at periodic intervals related to the translational symmetry of the crystal, and they can be constructed from molecules encoded with hydrogen bonds that effectively carry and communicate structural information to neighboring molecules, which results in the formation of a network. The term "semantophoretic," which means "carrying information," is often used to convey this concept in biological

macromolecules. A network also implies an infinite structure in one, two, or three dimensions, all of which are observed in molecular crystals. This chapter is limited to infinite networks, but the reader may want to explore the literature describing finite (a.k.a. discrete) molecular complexes assembled through charge-assisted hydrogen bonds.

The motivation behind the design and synthesis of molecular crystals is the promise of precise control of properties and function through manipulation of their molecular constituents, which can be readily prepared using conventional synthetic chemistry. The design and synthesis of crystalline organic materials often is thwarted, however, by the delicate and noncovalent nature of the intermolecular forces responsible for crystal packing, which is crucial to solid-state properties that rely on collective interactions. Sometimes the most innocent modification of a molecular constituent may produce an unanticipated solid-state structure. Furthermore, comprehensive crystal structure prediction of the lowest energy crystal forms through computational methods – complete with space group, lattice parameters, and atomic positions – remains elusive in general [10, 11], although it is advancing rapidly [12, 13]. These limitations have prompted the use of empirical strategies for crystal synthesis based on the use of generalized models of molecular packing modes surmised from selected sets of existing crystal structures. This approach, often referred to as crystal engineering, has enabled solid-state chemists to create well-defined lattice architectures with network topologies and lattice metrics prescribed by molecular building blocks adorned with multiple structure-directing functional groups arranged according to well-defined molecular symmetries. Although crystal engineering strategies usually do not result in precise control of atomic positions [14], often the control of network architecture coupled with systematic adjustment of lattice metrics is sufficient for the design of functional molecular materials. In this respect, hydrogen bonding, a long-standing favorite for crystal design [15, 16] has proven particularly useful.

One sensible tactic for regulating solid-state structure and properties involves the use of structurally robust one-dimensional (1D) and two-dimensional (2D) hydrogen-bonded networks. Persistent *n*-dimensional networks inherently simplify crystal synthesis by reducing the degree of freedom for crystal packing, effectively restricting crystal design to the remaining 3*n* dimensions. In order to manipulate solid-state properties these networks must be able to withstand modifications introduced by synthetic chemistry. These may involve swapping hydrogen-bonding components that preserve the generic features of the network or altering pendant substituents that do not participate directly in hydrogen bonding (Fig. 2). The robustness of CAHBs is proving very valuable in this regard.

It is quite natural to link robustness to bond strength, and strong hydrogen bonds have the potential to override the multitude of other intermolecular forces in the crystal lattice (e.g., van der Waals, dipole–dipole, multipolar) that otherwise can frustrate rational crystal design. On the other hand, modifications to the backbone of *n*-dimensional networks naturally will alter packing requirements, whether within the network or between pendant substituents, which could exert "strain" on the network. Consequently, networks may be more robust if they are somewhat

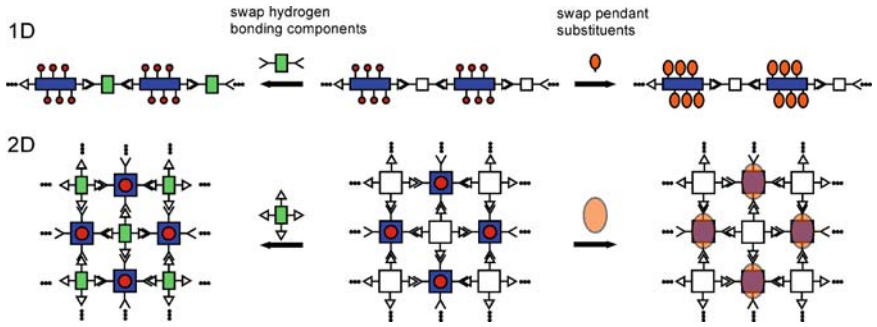

Fig. 2 Schematic representations of hypothetical binary 1D and 2D networks assembled through complementary hydrogen bonding. The networks can be modified by substituting one or both of the hydrogen bonding components or by exchanging pendant groups attached to the network. In the 2D case depicted here, the substituents projecting from the network surface can be altered (*red circles to orange ovals*)

compliant, that is, if they can deform, with minimal energetic penalty, to accommodate packing requirements while retaining their hydrogen-bonding connectivity and dimensionality. Borrowing from the parlance of materials science, such networks – strong yet pliable – could be regarded as "tough," a characteristic associated with the capacity of a material to undergo strain without fracture. In this respect, hydrogen bonds may prove ideal as they are intrinsically flexible. Although linear hydrogen bond geometries generally are preferred due to the dipole–dipole interactions described above, D–H…A bond angles range widely, implying shallow potential wells that are tantamount to compliant structures. Furthermore, some networks constructed from hydrogen bonds can deform readily while maintaining linearity of their hydrogen bonds, as described in Sect. 4.

4 Charge-Assisted Hydrogen Bonds in Molecular Crystals

During the past decade many compounds with rather sophisticated crystal architectures governed by CAHBs have been reported, some of which are depicted in Fig. 3. This chapter emphasizes networks that have been *assembled by design* using $(+)$N–H…O$(-)$ and $(+)$N–H…N$(-)$ hydrogen bonds, as these are quite common and probably the most robust of CAHBs. We note, however, that other types of CAHBs have been deployed for the design of molecular networks in the organic solid state, including $(+)$O–H…O$(-)$ and $(+)$C–H…O$(-)$. A particularly interesting example is the honeycomb host network formed by equal numbers of tartrate and tartaric acid, formed by loss of one proton for every two tartaric acid molecules (Fig. 4) [17]. These assemble into a honeycomb network through strong –C(O)O$^-$…H–O(O)C hydrogen bonds, identical to the aforementioned Speakman salts. This anionic framework can assemble around $Co(\eta^5-C_5H_5)_2^+$ cations, forming an inclusion complex with the cations stacked in the cylindrical pores of the honeycomb host framework.

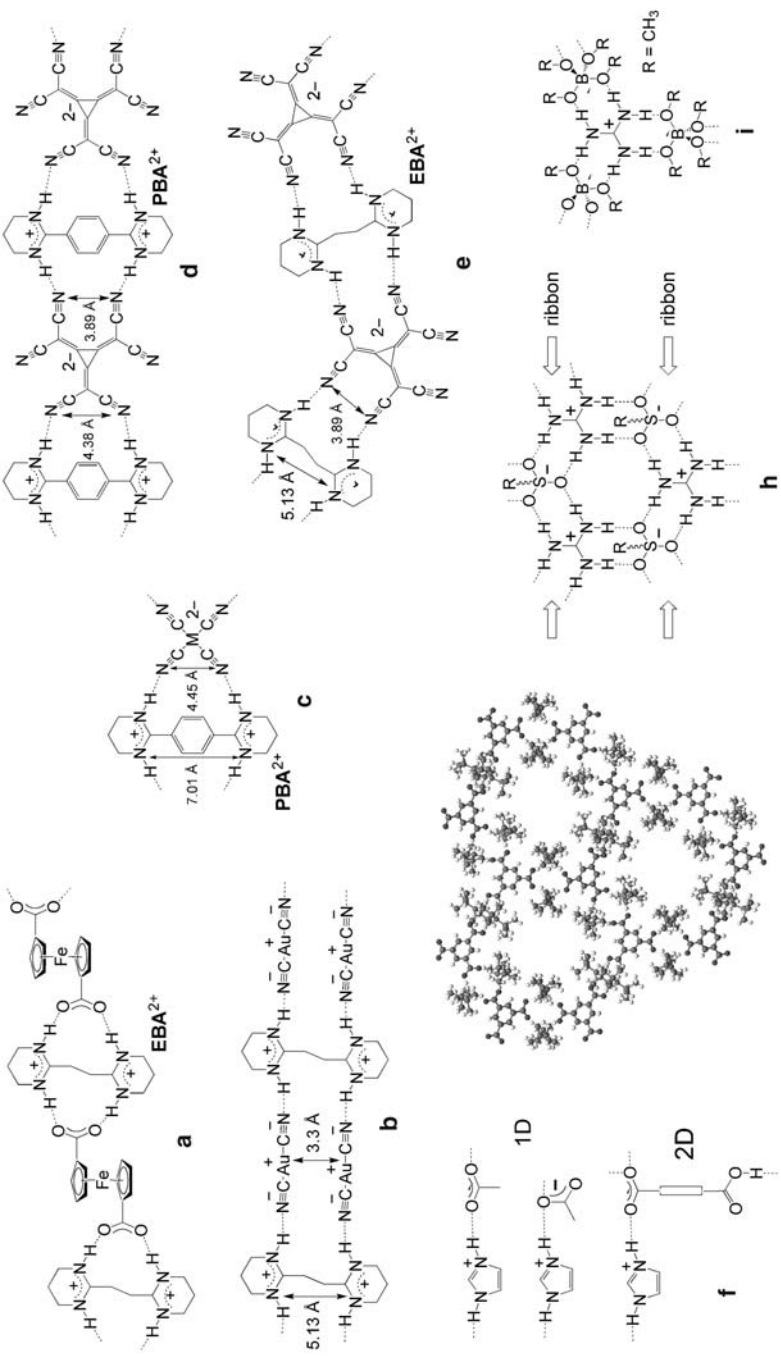

Fig. 3 Various charge-assisted hydrogen bonding motifs observed in molecular crystals

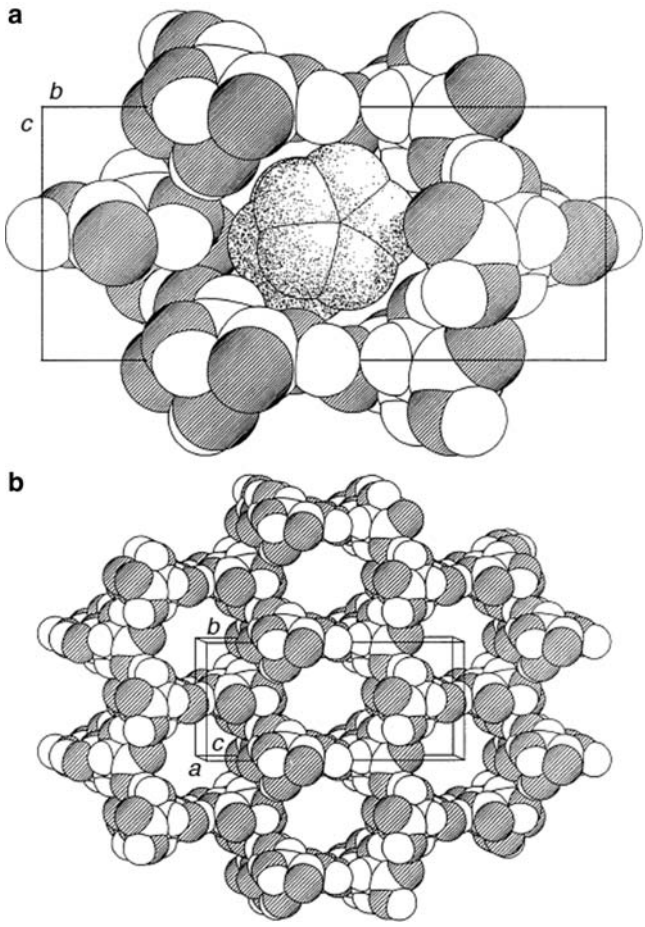

Fig. 4 **a** Space-filling representation of the tartaric acid template in crystalline $[Co(\eta^5\text{–}C_5H_5)_2]+$ $[(Hta)(H_2ta)]^-$. **b** Space-filling representation of the anionic honeycomb framework formed by the $[(Hta)(H_2ta)]_2$ units, the cobaltocenium cations stack inside the channels extending along the *a*-axis (reproduced with permission from [17])

The existence of charge-assisted $(+)$N–H$\ldots$O$(-)$ hydrogen bonds in crystalline phospholipids and amino acids (in zwitterionic form) has been recognized for decades. Therefore, these compounds are not described in detail here. We note, however, that the simplest amino acid, glycine, has three polymorphs [18–20], each differing with respect to the hydrogen-bonding networks responsible for molecular organization in the solid state. The interested reader is encouraged to examine the structures of these compounds, which are readily available in the literature as well as in the Cambridge Structural Database.

One of the more prolific series of CAHB building blocks is the family of bis(amidinium) dications (BA^{2+}), for which N–H substituents protrude from the flanks of an organic core to form hydrogen-bonded networks with a variety of

complementary anionic acceptors [21, 22]. For example, Figs. 3a and b illustrate 1D networks constructed with the [2,2′-(1,2-ethanediyl)pyrimidinium^{2+}] cation (EBA^{2+}) and the [1,1′-ferrocenedicarboxylate^{2-}] [23] and [dicyanoaurate^{-}]$_2$ anions [24], respectively (Fig. 5). The short Au…Au distance of 3.3 Å in Fig. 3b, enforced by the span of the N–H hydrogen-bond donors, produced strongly luminescent crystals. Expanding the separation between the Au centers to 4.2 Å by inserting the longer 2,2′-(1,4-phenylene)pyrimidinium^{2+} dication (PBA^{2+} in Fig. 3c) reduced the luminescence intensity, as anticipated. This elegant example demonstrates that the structure-directing character of CAHBs and well-defined molecular metrics can be combined to manipulate solid-state properties in a rational manner while retaining the overall architecture of the 1D network. Cyanometallate anions, specifically $Pt(CN)_4^{2-}$, also form 3D networks with bipyridinum dications, generating a $CdSO_4$-like lattice with channels [25].

The BA^{2+} dications form networks with various other polycyanometallates [26], as exemplified by Fig. 3c. This motif can be transposed to 1D networks with the doubly charged polycyanoanion $C_6(CN_6)^{2-}$ depicted in Fig. 3d, which contains geminal cyano groups that are isometric with the vicinal cyano ligands in the square-planar and octahedral polycyanometallates [27]. Metric control exerted by the dications is apparent here as well. The span of the N–H donors of PBA^{2+} is compatible with both the geminal and nongeminal pairs of cyano acceptors, resulting in the formation of linear chains held together by CAHBs (Fig. 5d). In contrast, the shorter span of the N–H donors in EBA^{2+} permits hydrogen bonding with only the nongeminal pairs of cyano acceptors, thus steering assembly into the zigzag 1D chains (Fig. 5e). These compounds exhibit different colors that were assignable to π-π charge-transfer interactions between the weak $C_6(CN)_6^{2-}$ electron donor and the weak PBA^{2+} electron acceptor in the solid state.

Charge-assisted (+)N–H…O(−) hydrogen bonds also promote the formation of 1D chains comprising imidazolium and arenecarboxylate ions (Fig. 3f). If dicarboxylic acids are used, the 1D chains can be stitched into 2D sheets by Speakman-type –COO^-…HOOC– hydrogen bonds [28]. The imidazolium–carboxylate hydrogen bond has also been used to construct a series of isostructural layered materials containing different transition metal ions [29].

Two-dimensional honeycomb networks assembled by (+)N–H…O(−) hydrogen bonds have been observed for the 1:3 complexes of the trimesate trianion and dicyclohexylammonium or di-*tert*-butylammonium ions, in which pairs of ammonium cations bridge carboxylate substituents on different trimesate ions (Fig. 3g) [30,31]. Notably, the 2D sheets pucker to different extents in these structures through deformations of the (+)N–H…O(−) hydrogen bonds, reflecting an intrinsic compliance that enables the network to accommodate differently sized alkyl groups and included solvent molecules while retaining the original hydrogen bond connectivity and the generic honeycomb architecture (Fig. 6).

The relationship of robust yet compliant networks based on CAHBs has been amply illustrated by the comprehensive series of lamellar inclusion compounds based on the guanidinium ion and numerous organomonosulfonates and disulfonates synthesized in our laboratory. The guanidinium ions (G) and the sulfonate

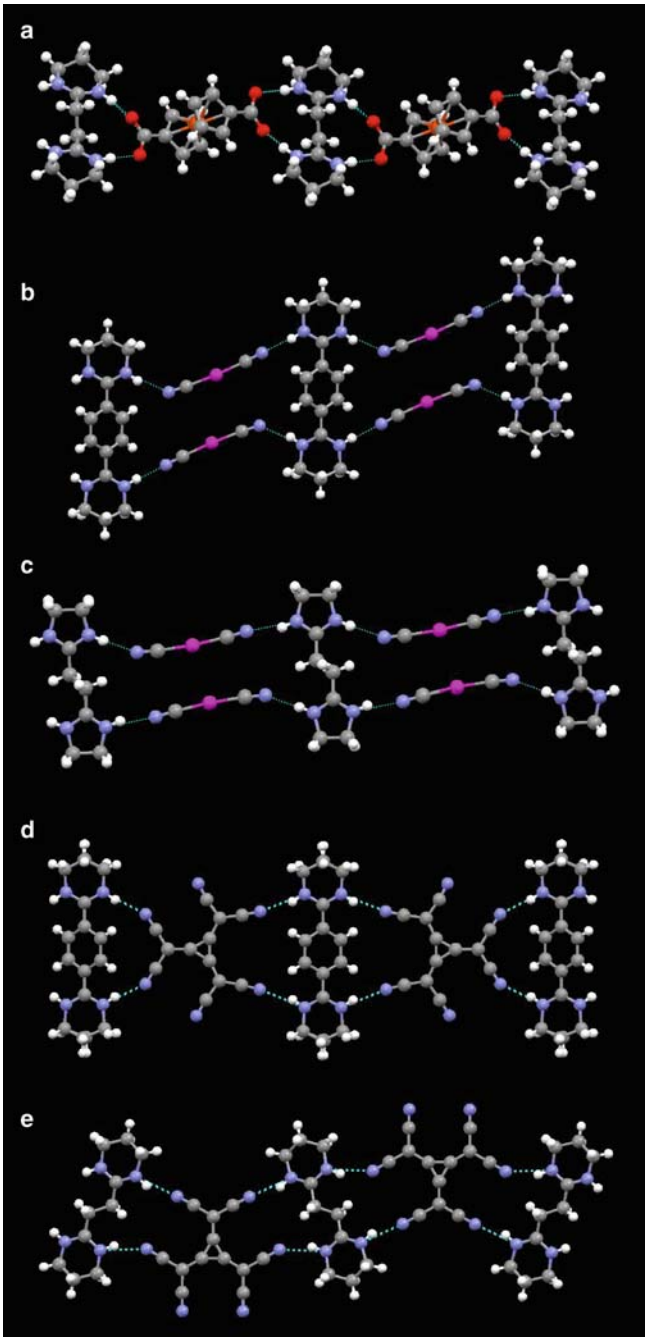

Fig. 5 Portions of the 1D networks in **a** $[EBA^{2+}][1,1'\text{-ferrocenedicarboxylate}^{2-}]$, **b** $[PBA^{2+}][Au(CN)^{2-}]$, **c** $[EBA^{2+}][Au(CN)^{2-}]$, **d** $[PBA^{2+}][C_6(CN_6)^{2-}]$, and **e** $[EBA^{2+}][C_6(CN_6)^{2-}]$. Only one polymorph of $[PBA^{2+}][C_6(CN_6)^{2-}]$ is depicted here

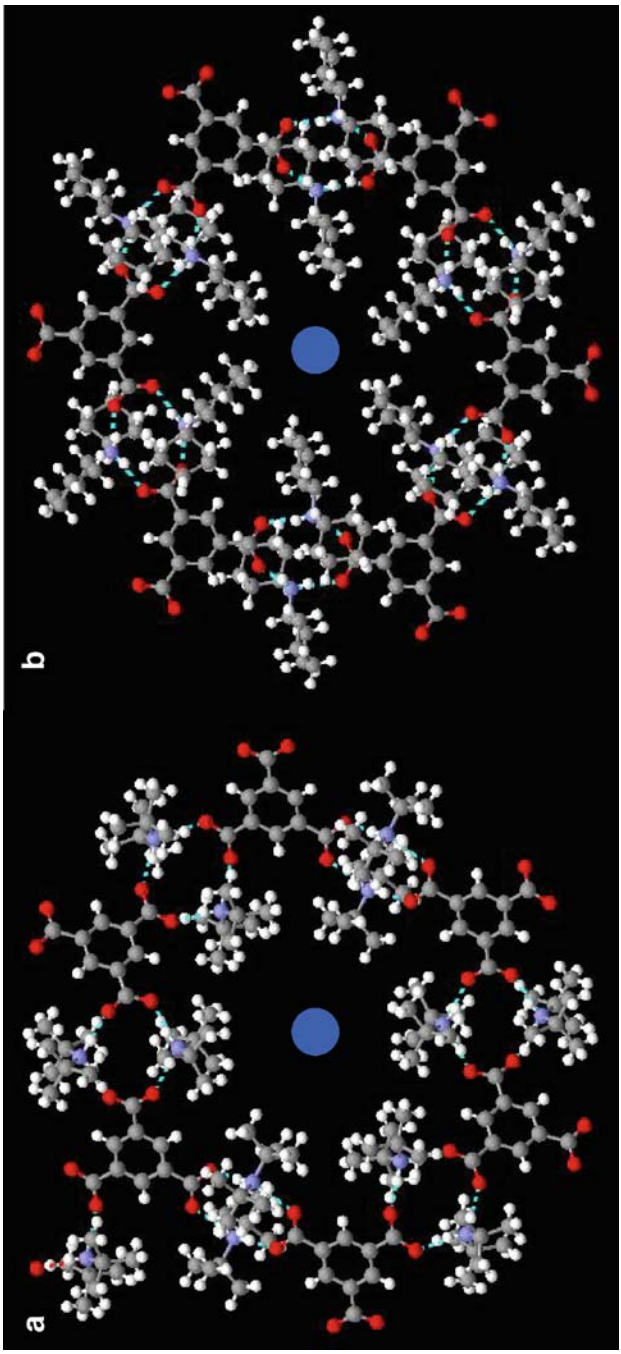

Fig. 6 Portions of the 2D hydrogen-bonded honeycomb networks in $[NH_2(But)]_3[TMA_3] \cdot Me_2CO$ and $[NH_2(c\text{-}C_6H_{11})^{2+}]_3[TMA_3] \cdot Me_2CO \cdot 0.5MeOH$ (*TMA* trimesic acid trianion)

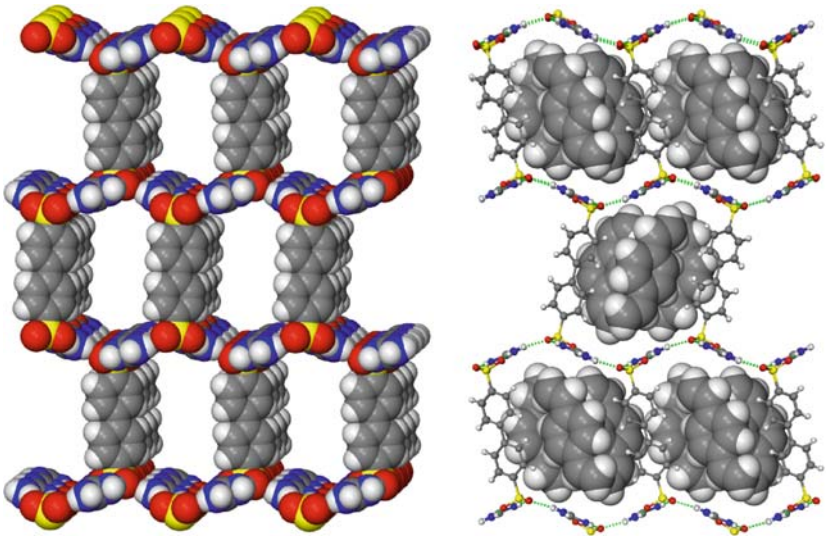

Fig. 7 *Left*: Space-filling model of the CAHB framework constructed from guanidinium cations and 4,4′-biphenyldisulfonate dianions. The GS sheet adopts a hexagonal motif like that depicted in Fig. 3h. *Right*: The same framework, rendered as ball-and-stick, with divinylbenzene guest molecules included, depicted as space-filling. The majority of the crystal volume (nearly 80%) is occupied by the guest molecules, which are present in a 3:1 divinylbenzene:biphenyldisulfonate ratio

group (S) form a quasihexagonal (6,3) 2D net in which each ion participates in six $(+)$N–H$\ldots$O$(-)$ hydrogen bonds (Fig. 3h) [32]. The organic substituents attached to the sulfonate moiety project from the sheet surface and serve as pillars that support inclusion cavities between the sheets (Fig. 7). The GS sheet is remarkably persistent, appearing in nearly one thousand different compounds, most of them inclusion compounds, derived from a broad range of organosulfonates [33–35]. Furthermore, these inclusion compounds exhibit an extraordinary diversity of architectures that differ with respect to the "up–down" pattern of the organic pillars on each sheet. These architectures are largely a response to the templating action of the guest, which governs the configuration of the pillars during assembly so that the cavities meet the requirements of the size and shape of the guest molecules. In this way, the GS network sets the stage for layered architectures, but the guest regulates the organization of the pillars that extend from the sheets. A particularly interesting guest-free compound, $[\text{guanidinium}]_2[\text{Fe}(\eta^5\text{-}C_5H_4SO_3)_2]$, exhibits a bilayer structure with ferrocene units between the sheets [36]. Powder compacts of this compound were electrochemically active (Fig. 8).

Although a large part of the tenacity of the GS sheet undoubtedly can be attributed to its large number of CAHBs, the network also derives its robustness from accordion-like puckering about the hydrogen bonds that fuse the edges of immutable 1D ribbons. This well-behaved deformation permits the lattice to shrink or expand perpendicular to the ribbons so that the organic constituents can achieve dense packing without disruption of the hydrogen-bond connectivity (the puckering angles range from 180°, which corresponds to a flat sheet, to a highly puckered

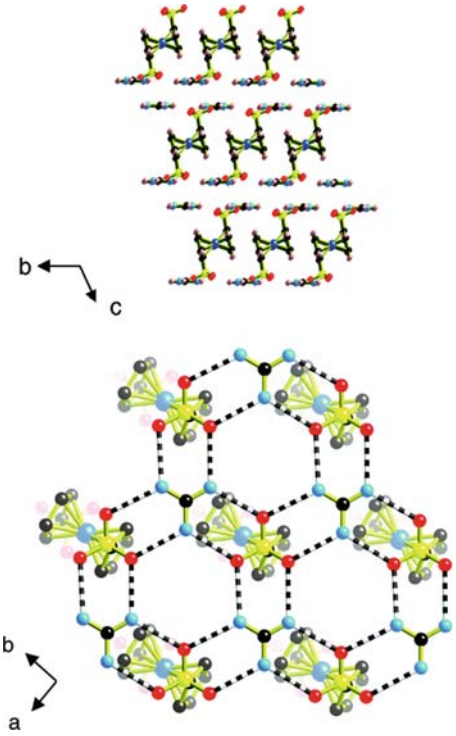

Fig. 8 *Top*: 2D network structure of [guanidinium]$_2$[Fe(η^5–$C_5H_4SO_3)_2$] (pillared discrete bilayer) as viewed along the *a*-axis. *Bottom*: Quasi-hexagonal (6,3) net formed by guanidinium and ferrocenedisulfonate ions as viewed along the *c*-axis (reproduced with permission from [36])

70°). The puckering occurs with retention of the linearity of the hydrogen bonds, implying a shallow potential well and a negligible energetic penalty associated with this deformation. This combines synergistically with the exceptional strength of the (+)N–H…O(−) hydrogen bonds, bestowing structural toughness to the GS sheet. Consequently, lattice metrics in the third dimension and the inclusion cavity size and character can be adjusted systematically and reliably by choice of the organosulfonate with retention of lamellar architecture [37]. When combined with the ability to achieve different architectures by adopting various "up–down" pillar configurations, these host frameworks are extraordinarily resilient.

The persistence and elastic nature of the GS sheet is also apparent for many combinations of organo*mono*sulfonates and guest molecules (Fig. 9). The diversity of architectures rivals that of the guanidinium organodisulfonates, producing analogs of the "simple brick," "double brick," and "zigzag brick" frameworks observed in the disulfonates. Furthermore, certain combinations of organo*mono*sulfonates and guest molecules produce "tubular inclusion compounds" in which the GS sheet curls into a cylinder. These cylinders pack on a hexagonal lattice through weak van der Waals forces between the organic groups projecting from the outer surface of the cylinders, crystallizing in either trigonal $P\bar{3}$ or hexagonal $P6_3/m$ space group

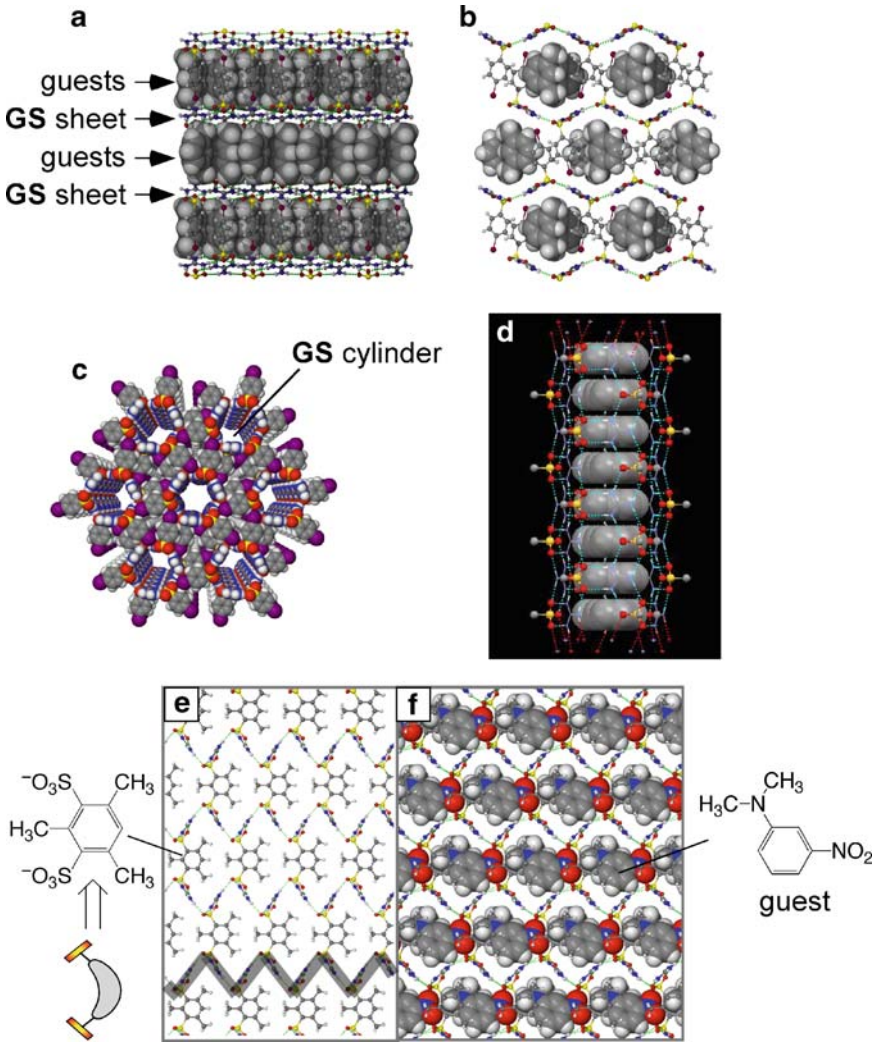

Fig. 9 **a**, **b** Lamellar inclusion compound [guanidinium][4-bromobenzenesulfonate)·(toluene) as viewed parallel and transverse to the major ribbons, respectively. The host framework is rendered as wire-frame and the included guests as space-filled. The puckering of the compliant GS sheet (Fig. 3h) is evident in **b**. **c** Hexagonal packing observed for the tubular inclusion compound [guanidinium][4-bromobenzenesulfonate)·2/3(*o*–xylene). The supramolecular connectivity of the GS sheet is identical in both the lamellar and cylindrical architectures. **d** View perpendicular to the cylinder axis of the tubular inclusion compound, illustrating the GS sheet wrapping around guests stacked in the cylinder. **e**, **f** Banana-shaped organodisulfonates force the GS sheet to pucker like an accordion while promoting formation of polar host frameworks, which have channels that can be occupied by guest molecules to produce materials with second harmonic generation activity

symmetry [38]. Notably, high space group symmetries are rare for molecular crystals (only 1.2 and 0.5% of molecular crystals crystallize in trigonal/hexagonal and cubic space groups, respectively). Interestingly, guanidinium–tetralkoxyborates (I) assemble via charge-assisted hydrogen bonds into the highly symmetric (10,3)-*a* net ($P\bar{4}3m$ space group). The topology of this network is a consequence of the 3-connecting symmetry of the G ion. The flexibility of the hydrogen bonds permits the network to conform to the highly restrictive symmetry requirements of the special positions in the cubic space group [39].

Such high symmetry structures suggest an interesting link to soft matter phases (surfactant assemblies and block copolymers), which form either lamellar, hexagonal, or cubic phases; the latter two requiring curvature of elastic interfaces between immiscible components. The purposeful design of molecular crystals with tough hydrogen-bonding networks capable of organizing into high symmetry structures through compliant hydrogen-bond networks could strengthen the link between molecular crystals and soft matter [40]. This connection was reinforced by the organization of more than 200 inclusion compounds, representing various combinations of guanidinium organomonosulfonates and guest molecules, on a "structural phase diagram" that was based on two simple molecular parameters – the host:guest volume ratio and the "ellipticity" (i.e., shape) of the guest (Fig. 10) [41].

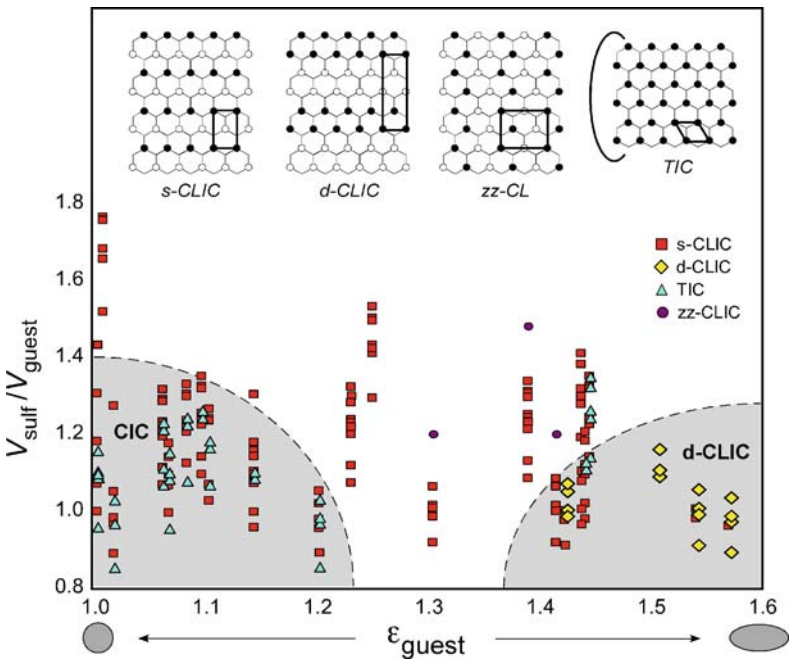

Fig. 10 Structural phase diagram for GMS inclusion compounds using V_{sulf}/V_{guest} and guest eccentricity (ε) as variables. This plot contains 206 data points representing unique host–guest combinations. Some of the data points are obscured by overlap. The diagrams at the *top* represent the "up–down" projections of organic residues from the sulfonate nodes on each GS sheet (the sheets stack by translational symmetry). *Open circles* correspond to a projection below the sheet and *filled circles* above

The diagram revealed that three of the four architectures – tubular (TIC), double continuously layered (d-CLIC), zigzag continuously layered zz-CLIC) – occupied well-defined sectors. The so-called simple continuously layered inclusion compound (s-CLIC) ranged across the entire phase diagram, consistent with its inherently high degree of framework flexibility. The ability to organize these architectures into specific sectors of a structural phase diagram resembles phase behavior for soft matter systems, which often adopt microstructures that can be organized on a phase diagram based on simple molecular parameters. It is important to note, however, that construction of this phase diagram is possible only because the GS sheet is so resilient and persistent, which enables the synthesis of a remarkably large number of inclusion compounds based a common supramolecular entity.

The peculiar compliance of the GS sheet also enables synthesis of polar host frameworks constructed from "banana-shaped" *meta*-arenedisulfonates, which enforce puckering of the GS sheets through geometric constraints (Fig. 9e,f). Inclusion of acentric guest molecules in these frameworks produced materials with second harmonic generation activity. The unique characteristics and structural consistency of the GS network enabled prediction of the space group symmetry and lattice metrics for these compounds using simple geometric principles [42], a rare occurrence for molecular crystals.

The robustness of CAHBs in guanidinium sulfonates was further demonstrated by its persistence in smectic liquid crystals prepared from a series of guanidinium alkylbenzenesulfonates and alkylbiphenyldisulfonates [43–45]. These smectic liquid-crystal phases, formed when their corresponding crystalline phases were heated, were observed when the number of carbons in the alkane chains was greater than seven. This chain length corresponded to single-crystal packing motifs that signaled the onset of a structure-directing role for alkane–alkane interactions. Furthermore, the viscosities of these smectic phases were exceptionally high due to the reinforcing nature of the CAHB network. The GS network was also found to persist in crystalline ternary inclusion monolayers, at the air–water interface, consisting of a 2D hydrogen-bonded host network of guanidinium ions and organosulfonate amphiphiles, with biphenylalkane guests [46]. Grazing incidence X-ray diffraction revealed that the inclusion monolayers were more crystalline than the corresponding guanidinium-free mixed monolayers.

Further proof of the robustness of CAHBs based on guanidinium and anionic acceptors can be gleaned from a variety of 2D hydrogen-bonded honeycomb grids bearing the same (6,3) network structure constructed with guanidinium cation and various anionic components, including the carbonate anion and stoichiometric mixtures of carbonate and boric acid (Fig. 11) [47, 48]. Because the carbonate carries a 2– charge, the 2D CAHB networks are anionic, carrying one excess charge per guanidinium–carbonate unit. This charge is balanced by tetraalkylammonium cations that occupied the region between the 2D networks, mimicking anionic clays intercalated with cations. In contrast, the sheet was nearly planar when oxalate was substituted with 1H-imidazole-4,5-dicarboxylate, producing $[(C_2H_5)_4N^+]\cdot[C(NH_2)_3^+]_7\cdot 3CO_3^{2-}\cdot[C_3N_2H_2(COO^-)_2]$. The guanidinium–carbonate (1:1) sheet in $4[(C_2H_5)_4N^+]\cdot 8[C(NH_2)_3^+]\cdot 3(CO_3)^{2-}\cdot 3(C_2O_4)^{2-}\cdot 2H_2O$

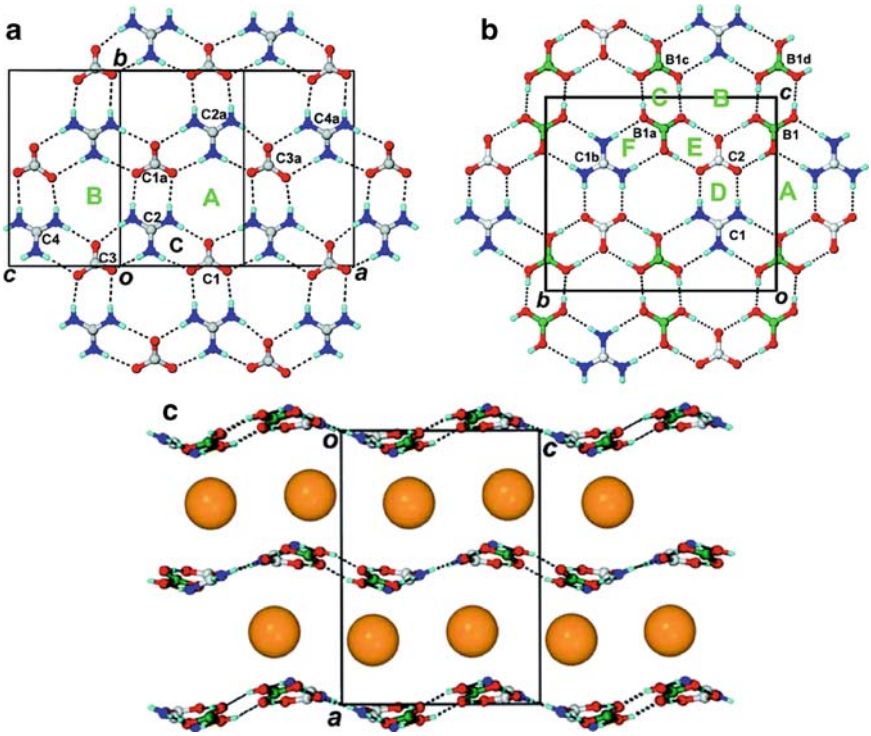

Fig. 11 **a** Quasi-hexagonal 1:1 guanidinium-carbonate (6,3) net in $[(C_2H_5)_4N^+] \cdot [C(NH_2)_3^+]_7 \cdot 3CO_3^{2-} \cdot [C_3N_2H_2(COO^-)_2]$. **b** The [1]2:1 guanidinium–boric acid–carbonate network in $[(n\text{-}C_3H_3)_3N^+] \cdot [C(NH_3)_3^+] \cdot CO_3^{2-} \cdot 2B(OH)_3$. **c** Molecular packing in $[(n\text{–}C_3H_3)_3N^+] \cdot [C(NH_3)_3^+] \cdot CO_3^{2-} \cdot 2B(OH)_3$ with charge-compensating nonpolar $(n-Pr)_4N^+$ cations between puckered layers, with guanidinium–boric acid–carbonate networks having a 1:2:1 composition (*yellow spheres*) (reproduced with permission from [49])

exhibited a corrugated, or wavy, texture also described as a "rosette layer." It adopted a nearly planar configuration using 1H-imidazole-4,5-dicarboxylate as an auxiliary template and spacer. Surprisingly, in the presence of boric acid an unusual three-component guanidinium–boric acid–carbonate (1:2:1) network was observed in $[(n\text{-}C_3H_3)_3N^+] \cdot [C(NH_3)_3^+] \cdot CO_3^{2-} \cdot 2B(OH)_3$. These rosette layers were also observed with constituents without C3 symmetry, albeit highly distorted. This also has been accomplished with 1,2-dithiosquarate and 1,1′-biphenyl-2,2′,6,6′-tetracarboxylate anions, even though these compounds do not have C3 symmetry.

Recent efforts have expanded cleverly on the GS networks, replacing the guanidinium ion with charged metal complexes with ligands that serve as hydrogen-bond donors with organosulfonates. For example, an unusual CAHB network was discovered in $[Co(NH_3)_6](\alpha,\alpha'\text{-}para\text{-xylenedisulfonate})_{1.5}(H_2O)$, based on a design principle by which the triangular faces of the $[Co(NH_3)_6]^{3+}$ octahedron, in a local C4 orientation, would be complementary to the triangular presentation of the sulfonate groups [49]. In the presence of aniline, however, the inclusion compound

$[Co(NH_3)_6](\alpha,\alpha'$-*para*-xylenedisulfonate$)_{1.5}$(aniline)$(H_2O)_3$ was formed (Fig. 12). Like behavior observed for guanidinium organodi- and organomonosulfonates [50–52], the second framework demonstrated selective inclusion; the desolvated framework selectively absorbed various amines (as guests) but not other substituted aromatics. This design strategy was also applied to the synthesis of $\{[Ni(tame)_2]_1(PES)2\}_\infty$ (tame = 1,1,1-tris(aminomethyl)ethane, PES = 2-phenylethynesulfonate) [53]. The single-crystal structure of this compound revealed the formation of quasihexagonal sheets assembled through CAHBs between $Ni(tame)_2^{2+}$ units and two sets of PES sulfonate groups and interaction in the third dimension through stacking of the PES aromatic rings (Fig. 13). A related compound prepared with a disulfonate pillar, $\{[Ni(tame)_2]_1(BSEB)_1\}_\infty$ (BSEB = 4,4′-bis(sulfoethynyl)biphenyl), formed a compound with a similar layered structure

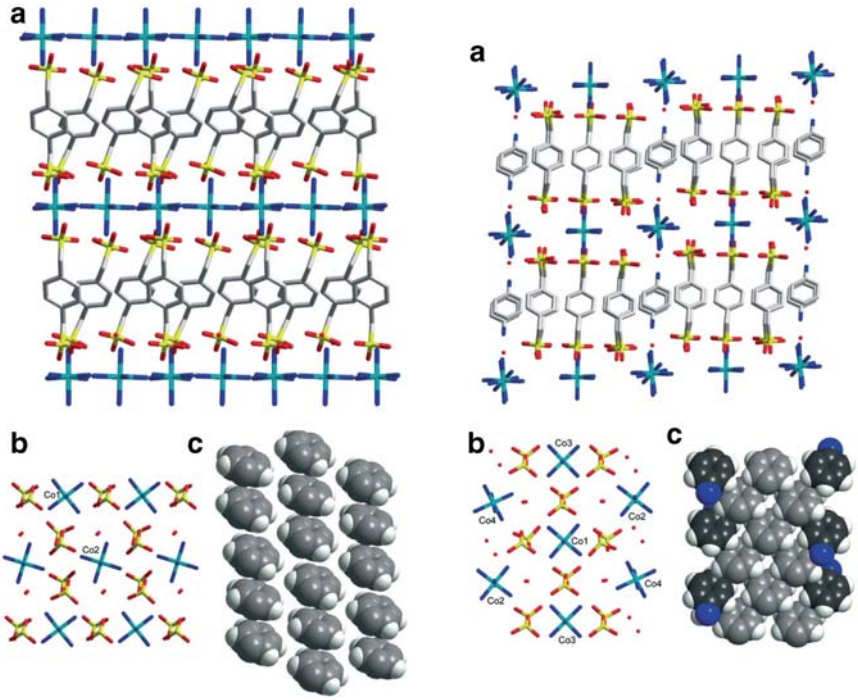

Fig. 12 *Left*: X-ray structure of the pillared, layered solid $[Co(NH_3)_6](\alpha,\alpha'$-*para*-xylenedisulfonate$)_{1.5}(H_2O)$. **a** View parallel to the layers. **b** View onto a single hydrogen-bonded layer with $Co(NH_3)_6$ centers aligned along their C4 axes. **c** Space-filling view showing the nondensely packed aryl rings of the disulfonate pillars in the interlayer. The *middle column* contains two repeating trimer "ABA" motifs. X-ray structure of compound $[Co(NH_3)_6](\alpha,\alpha'$-*para*-xylenedisulfonate$)_{1.5}$(aniline)$(H_2O)_3$. *Right*: **a** View parallel to the layers. The aniline guests appear above and below some Co centers and alternate in their orientation. *Red dots* are water molecules. **b** View onto a single hydrogen-bonded layer with $Co(NH_3)_6$ centers aligned along their C4 axes. Aniline molecules sit above the Co_2 and Co_4 centers. **c** Space-filling view of the interlayer showing the pillars packing with aniline guests (*darker grey*) (reproduced with permission from [49])

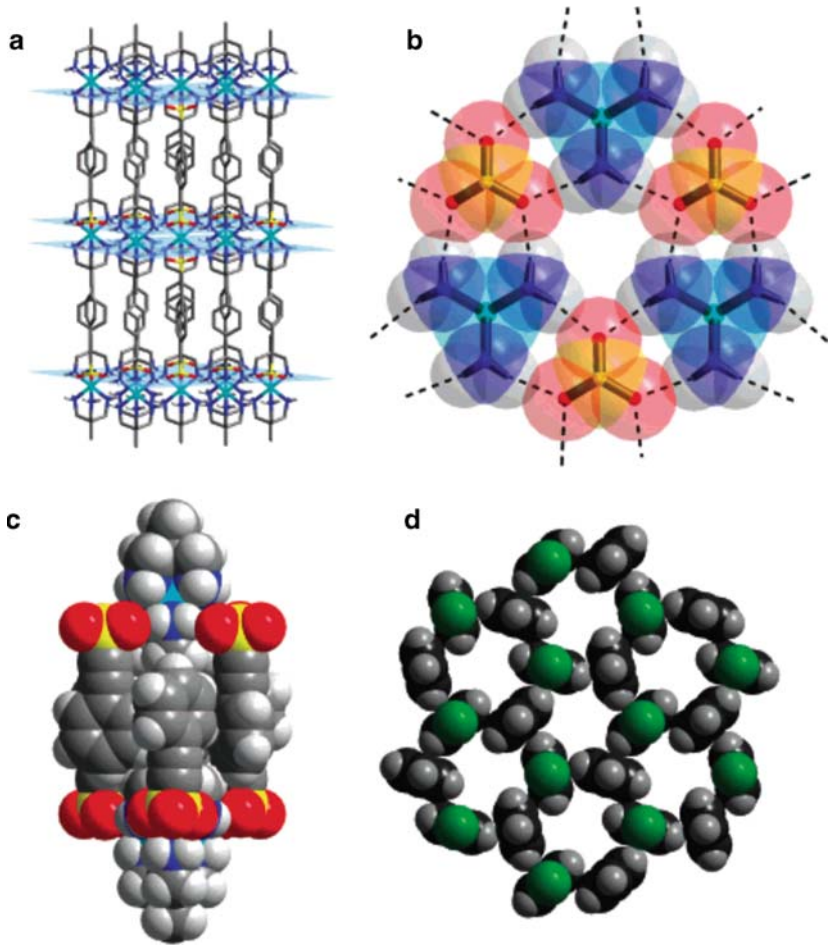

Fig. 13 Crystal structure of $[Ni(tame)_2]_1(PES)2\}_\infty$. **a** View of CAHB sheets (shown as *blue planes*) and the aromatic interlayer. **b** Overlaid space-filling diagram of the complementary hydrogen-bonds between $Ni(tame)_2^{2+}$ and PES SO_3 groups. **c** Space-filling view of $Ni(tame)_2^{2+}$ units and the interdigitation of PES ligands from adjacent sheets. **d** Aryl–aryl interactions in the interlayer with aromatic groups from the same sheets are marked in *green*. The voids are occupied, filled by the methyl groups of the tame ligands. For **a**–**c**: Ni *cyan*; N *blue*; C *gray*; H *white*; S *yellow*; O *red* (reproduced with permission from [53])

(deduced by PXRD only) that possessed permanent porosity, illustrating a rare occurrence of a permanently porous solid based on a hydrogen-bonded network (Fig. 13).

In a somewhat different adaption, CAHBs were used to assemble host frameworks based on the cationic metal complex $[Co(en)_2(ox)]^+$ and 2,6-naphthalenedisulfonate pillars (Fig. 14) [54]. These compounds exhibited the same kind of architectural isomerism that had been observed in the guanidinium

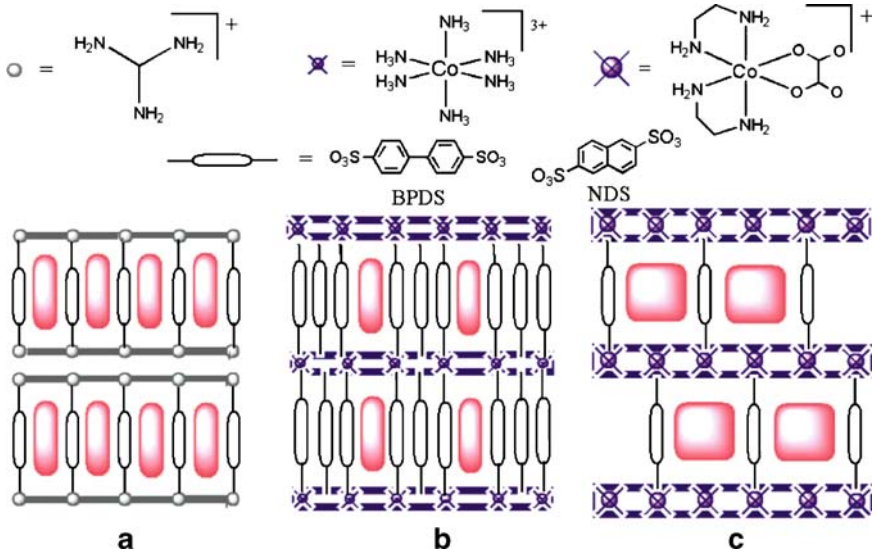

Fig. 14 **a** Typical guanidinium disulfonate bilayer structure with layers made of hydrogen-bonded guanidinium and sulfonate groups and pillars of the organic residue of the disulfonate. The ratio of the disulfonate to guanidinium is 0.5. **b** Proposed and later observed metal complex disulfonate structure with layers made of hydrogen-bonded $[Co(NH_3)_6]^{3+}$ and sulfonate groups. The ratio of disulfonate to metal complex is 1.5. **c** Proposed framework made of $[Co(en)_2(ox)]^+$ and disulfonate. The ratio of disulfonate to metal complex is 0.5 (reproduced with permission from [54])

organodisulfonates, wherein the orientations of the pillars on either side of a 2D hydrogen-bonded network adjust to meet the steric demands of included guest molecules. The structures of these compounds revealed that, compared with prior work [55, 56] with $[Co(NH_3)_6]^{3+}$, these compounds have larger interpillar galleries because of the lower charge of the $[Co(en)_2(ox)]^+$ complex (fewer disulfonates are required for charge compensation, thus the total volume occupied by the pillars is reduced). This clever twist nicely illustrates how simple molecular-level principles can be deployed to engineer solid-state structures if a robust supramolecular network, here realized through CAHBs, is used as a building block. Furthermore, the integration of metal complexes within the layers suggests a new pathway to functional materials, complementing approaches based on introducing function through guest molecules in the vacant galleries.

5 Summary

Collectively, these examples illustrate that CAHBs are effective for crystal design and molecular monolayers, often producing predictable crystal architectures while enabling manipulation of key structural features. The exceptional strength of

these hydrogen bonds and their natural flexibility can conspire to produce "tough" supramolecular networks that can withstand strains created by competing packing interactions in the crystal lattice. This combination of strength and softness may prove to be a potent strategy for the systematic engineering of molecular networks that determine solid-state structure in molecular crystals.

References

1. Stillinger FH, Rahman AJ (1974) Chem Phys 60:1545
2. Dennison DM (1921) Phys Rev 17:20
3. Bragg WH (1921) Proc Phys Soc Lond 34:98
4. Israelachvili J (1992) Intermolecular and surface forces, 2nd edn. Academic, London
5. Gilli P, Bertolasi V, Ferretti V, Gilli G (1993) J Am Chem Soc 116:909
6. Taylor R, Kennard O (1984) Acc Chem Res 17:320
7. Speakman JC (1972) Struct Bond 12:141
8. Grabowski SJ (2006) Annu Rep Prog Chem Sect C 102:131
9. Bernstein J, Etter MC, Leiserowitz L (1994) In: Burgi HB, Dunitz, JD (eds) Structure Correlation, vol 2, VCH, Weinheim, p 431
10. Dunitz JD (2003) Chem Commun, p 545
11. Dunitz JD, Gavezzotti A (2005) Angew Chem Int Ed 44:1766
12. Price SL (2004) Cryst Eng Commun 6:344
13. Price SL (2004) Adv Drug Deliv Rev 56:301
14. Moulton B, Zaworotko MJ (2001) Chem Rev 101:1629
15. Etter MC (1990) Acc Chem Res 23:120
16. Bernstein J, Etter MC, Leiserowitz L (1994) Struct Correl 2:431
17. Braga D, Angeloni A, Grepioni F, Tagliavini E (1997) Chem Commun, p 1447
18. Marsh RE (1958) Acta Cryst 11:654
19. Iitaka Y (1961) Acta Cryst 14:1
20. Iitaka Y (1960) Acta Cryst 13:35
21. Felix O, Hosseini MW, De Cian A, Fischer J (1998) New J Chem 12:1389
22. Ferlay S, Bulach V, Felix O, Hosseini MW Planeix JM, Kyritsakas N (2002) Cryst Eng Commun 4:447
23. Braga D, Maini L, Grepioni F, De Cian A, Felix O, Fischer J, Hosseini MW (2000) New J Chem 24:547
24. Paraschiv C, Ferlay S, Hosseini MW, Bulach V, Planeix JM (2004) Chem Commun, p 2270
25. Crawford PC, Gillon AL, Green J, Orpen AG, Podesta TJ, Pritchard SV (2004) Cryst Eng Commun 6:419
26. Ferlay S, Hosseini MW (2004) Chem Commun, p 788
27. Shacklady D, Lee SO, Ferlay S, Hosseini MW, Ward MD (2005) Cryst Growth Des 5:995
28. MacDonald JC, Dorrestein PC, Pilley MM (2001) Cryst Growth Des 1:29
29. MacDonald JC, Dorrestein PC, Pilley MM, Foote MM, Lundburg JL, Henning RW, Schultz AJ, Manson JL (2000) J Am Chem Soc 122:11692
30. Plaut DJ, Lund KM, Ward MD (2000) Chem Commun, p 769
31. Melendez RE, Sharma CVK, Zaworotko MJ, Bauer C, Rogers RD (1996) Angew Chem Int Ed Engl 35:2213
32. Russell VA, Etter MC, Ward MD (1994) J Am Chem Soc 116:1941
33. Russell VA, Evans C, Li W, Ward MD (1997) Science 276:575
34. Holman KT, Pivovar AM, Swift JA, Ward M D (2001) Acc Chem Res 34:107
35. Burke NJ, Burrows AD, Mahon MF, Teat SJ (2004) Cryst Eng Commun 6:429
36. Xie J, Ma, MT, Abrahams BF, Wedd, AG (2007) Inorg Chem 46:9027
37. Holman KT, Martin SM, Parker DP, Ward MD (2001) J Am Chem Soc 123:4421

38. Horner MJ, Holman KT, Ward, MD (2001) Angew Chem 40:4045
39. Abrahams BF, Haywood MG, Robson R (2005) J Am Chem Soc 127:816
40. Horner MA, Ward MD (2004) Crystal Eng Commun 6:401
41. Horner MJ, Holman KT, Ward MD (2007) J Am Chem Soc 129:14640
42. Holman KT, Pivovar AM, Ward MD (2001) Science 294:1907
43. Martin SM, Yonezawa Y, Horner MJ, Macosko CW, Ward MD (2004) Chem Mater 16:3045
44. Yonezawa Y, Martin SM, Macosko CW, Ward MD (2004) Macromolecules 7:6424
45. Mathevet F, Masson P, Nicoud JF, Skoulios A (2002) Chem Eur J 8:2248
46. Plaut DJ, Martin SM, Kjaer K, Weygand MJ, Lahav M, Leiserowitz L, Weissbuch I, Ward MD (2003) J Am Chem Soc 125:15922
47. Mak TCW, Xue F (2000) J Am Chem Soc 122:9860
48. Han J, Yau CW, Lam CK, Mak TCW (2008) J Am Chem Soc 130:10315
49. Dalrymple SA, Shimizu GKH (2006) Chem Commun, p 956
50. Pivovar AM, Holman KT, Ward MD (2001) Chem Mater 13:3018
51. Horner MJ, Grabowski S, Sandstrom K, Holman KT, Bader M, Kim WS, Ward MD (2004) Amer Crystall Assoc Trans 39:1
52. Kim J, Lee SO, Yi J, Kim WS, Ward MD (2008) Separ Purif Technol 62:519
53. Dalrymple SA, Shimizu GKH (2007) J Am Chem Soc 129:12114
54. Wang XY, Sevov SC (2008) Cryst Growth Design 8:1265
55. Wang XY, Justice R, Sevov SC (2007) Inorg Chem 46:4626
56. Wang XY, Sevov SC (2007) Chem Mater 19:4906

Struct Bond (2009) 132: 25–50
DOI:10.1007/430_2008_7

Published online: 25 February 2009

Crystal Polymorphism and Multiple Crystal Forms

Dario Braga, Fabrizia Grepioni, Lucia Maini, and Marco Polito

Abstract This chapter discusses the phenomenon of polymorphism in organic and organometallic compounds. Polymorphism is first introduced and then, to give the work some context, background information is given concerning properties and techniques for characterizing the solid phases. In particular, desolvation and interconverstion are examined, and the gas–solid reactions are presented as a successful route to obtaining new crystalline phases. Co-crystal definition is then described and the problem in distinguishing co-crystals and salts is evaluated.

Keywords: Co-crystal · Hydrogen bond · Organic salt · Polymorphism · Solid-gas reaction · Solid-state NMR · Solvate · X-ray diffraction

Contents

D. Braga (✉), F. Grepioni, L. Maini, M. Polito
Dipartimento di chimica G. Ciamician, Università degli Studi di Bologna, Via F. Selmi 2, 40126 Bologna, Italy
e-mail: dario.braga@unibo.it

1 Introduction

The isolation, identification and characterization of different crystal forms (polymorphs, solvates, salts and co-crystals) of the same molecule or of aggregates of the same molecule with other molecules represents one of the most active areas of modern solid state chemistry. The investigation of crystal forms impacts on fundamental science as well as on utilitarian objectives because different crystal forms may display a range of different physico-chemical properties, which may affect application and utilization of the solid materials.

Polymorphism [1] is one of the most fascinating phenomena of solid state chemistry and indeed is a "difficult" phenomenon, studied for many decades mainly, and separately, in the fields of organic and inorganic chemistry. In spite of the huge efforts of many researchers our knowledge of the phenomenon is still embryonic, and the relationship between growth of a crystalline phase and nucleation of the first crystallites is often mysterious. It is a fact that, despite the ambitions of the scientist, crystal construction is not yet strictly under human control. Many examples exist of *appearing* and *disappearing* polymorphs, some of which have had great practical consequences. The reader is addressed to the review by Dunitz and Bernstein for a number of intriguing examples [2].

2 Definition of Crystal Forms

Although the existence of three different crystal forms of calcium carbonate (calcite, vaterite and aragonite) was identified by Klaproth in 1788 [3], formal recognition of the phenomenon of *crystal polymorphism* is attributed to the work of Mitscherlich in 1823 [4]. In more general terms, the solid phase of a material, whether formed of organic molecules, inorganic ions or extended covalent networks, can exhibit different structures which, although possessing the same chemical composition, may manifest different properties. In addition to these polymorphic modifications the material may also lack long-range order and appear as an amorphous solid, which can be considered as another polymorph.

A number of authors have suggested that polymorphism is ubiquitous in crystal chemistry. McCrone stated long ago that: "…every compound has different polymorphic forms" and that, "…in general, the number of forms known for a given compound is proportional to the time and energy spent in research on that compound" [5]. In 1951 Findlay noted in his book that polymorphism: "…is now recognized as a very frequent occurrence indeed" [6]. Buerger and Bloom stated: "…polymorphism is an inherent property of the solid state and it fails to appear only under special conditions" [7]. Similarly, Sirota wrote in 1982: "Polymorphism is now believed to be characteristic of all substances, its actual non-occurrence arising from the fact that a polymorphic transition lies above the melting point of the substance or in the area of as yet unattainable values of external equilibrium factor or other conditions providing for the transition" [8].

In 1965 Kuhnert-Brandstätter investigated by hot stage microscopy three common classes of drug: 70% of barbiturates, 60% of sulphonamides and 23% of steroids exist in various polymorphic or solvate forms [9, 10].

A number of statistical estimates of the extent of polymorphism have also been carried out. A search of the Cambridge Structural Database on the keywords "polymorph", "form", "modification" and "phase" indicated that about 3.5% of the ~350,000 entries fall into this category. Approximately 25% of the entries are either solvates or hydrates. Other studies based on different selection criteria reveal a much larger occurrence [11–13]. For instance, Griesser and Burger have collected information on about 600 polymorphic forms and solvates (including hydrates) of pharmaceutical compounds that are solid at 25°C [14].

Even though crystal forms have been and are the subject of intense investigations, polymorphism as a *phenomenon* still represents a substantial scientific challenge. Indeed it is hard to predict whether a given molecule will crystallize in one or several crystal forms, whether it will form solvates with different stoichiometries or will ever be "happy" to link up with other molecules and form stable co-crystals. Such variability and unpredictability have been taken by some scientists as an intrinsic drawback of being able to construct desired crystal structures (and obtain relevant properties) from a purposeful choice of the molecular components, which is the paradigm of molecular crystal engineering [15–19].

In recent times the concept of crystal polymorphism has expanded beyond its original boundaries to encompass crystal forms of the same molecule with different molecular partners. These may be solvent molecules in solvates [20], or counterions if the molecule can be made non-neutral (by say proton or electron transfer [21]), or other molecules in co-crystals [22]. It is worth noting that the formation of solvate and hydrated forms is commonly observed during polymorph screening, therefore the use of the term "pseudopolymorphism" to describe solvate forms of a given molecular crystal ought to be discouraged, at least because solvates may, in turn, be polymorphic [23–25].

In this paper we shall discuss all four different types of crystal forms of the same molecule: polymorphs of the mere molecule, solvates and hydrates, molecular salts and co-crystals (when the same molecule can be co-crystallized with different co-crystal formers). All these crystal forms are summarized in Fig. 1.

3 Properties of Crystal Forms

From thermodynamic principles, under specified conditions only one polymorph is the stable form (except at a transition point) [26]. In practice, however, due to kinetic considerations, metastable forms can exist or coexist in the presence of more stable forms. The relative stability of the various crystal forms and the possibility of interconversion between crystal forms, between crystals with different degree of solvation, and between an amorphous phase and a crystalline phase can have very

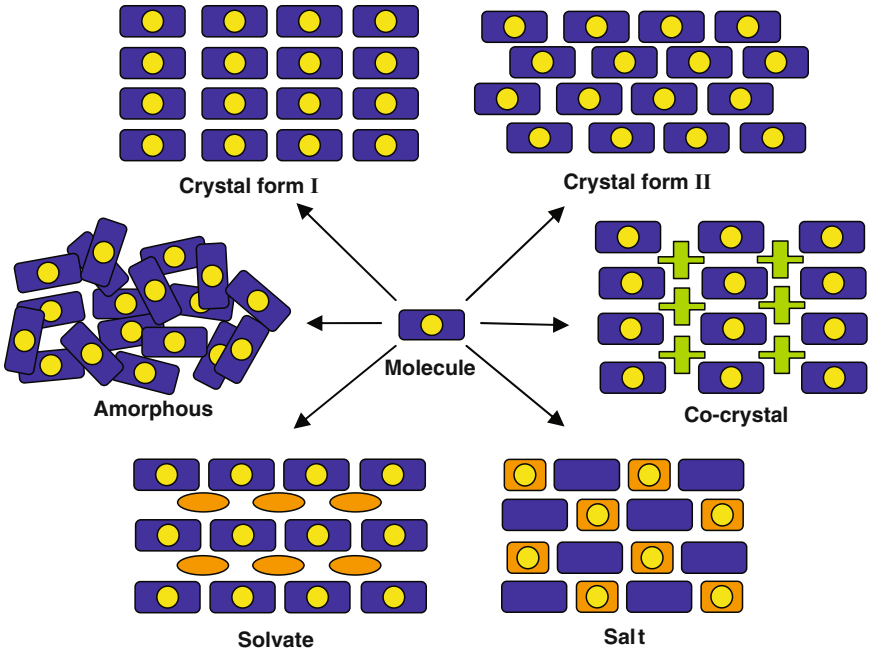

Fig. 1 Schematic representation of the structural relationship between "true" polymorphs, solvates, co-crystals, salts and the amorphous phase

serious consequences on the life and effectiveness of a polymorphic product and the persistence over time of the desired properties. The variety of phenomena related to polymorphism requires a thorough mapping of the "crystal space" of a substance that is ultimately intended for some specific applications (e.g. drugs, pigments, agrochemicals and food additives, explosives, etc.).

The industrial production and marketing lines need to know not only the exact nature of the material in the process, but also its stability with time, the variability of its chemical and physical properties as a function of the crystal form, etc. The search for and characterization of crystal forms is therefore a crucial step in the development of a new chemicals with relevant consequences on intellectual property issues [1, 27–29].

Different crystal forms are often recognized by differences in the colour and shape of crystals. A striking example of these two properties is provided by the differences in colour and form of the crystal forms of ROY (ROY = red, orange, yellow polymorphs of 5-methyl-2-[(2-nitrophenyl)amino]-3-thiophene carbonitrile) [30, 31]. Colour and shape are only some of the possible differences and Table 1 summarizes some major possible differences in chemical and physical properties between crystal forms and solvates of the same substance. In addition, one has to consider that new and different properties may derive from a change in the nature and chemical composition of the same molecule as a consequence of salt formation or co-crystallization. For each new crystal form obtained, a full characterization

PHYSICAL AND THERMODYNAMIC PROPERTIES	density and refractive index, thermal and electrical conductivity, hygroscopicity, melting points, free energy and chemical potential, heat capacity, vapor pressure, solubility, thermal stability
SPECTROSCOPIC PROPERTIES	electronic, vibrational and rotational properties, nuclear magnetic resonance spectral features
KINETIC PROPERTIES	rate of dissolution, kinetics of solid state reactions, stability
SURFACE PROPERTIES	surface free energy, crystal habit, surface area, particle size distribution
MECHANICAL PROPERTIES	hardness, compression, thermal expansion
CHEMICAL PROPERTIES	chemical and photochemical reactivity

Fig. 2 Examples of chemical and physical properties that can differ among crystal forms and solvates of the same substance

should be done since the new form can have different properties, such as higher solubility or higher melting point (Fig. 2).

4 Characterization of Multiple Crystal Forms

The exploration of the "crystal form space" of a substance is the search of polymorphs and solvates in order to identify the most stable form and the existence of unstable forms that interconvert (enantiotropism) or do not (monotropism) as a function of the temperature. This also applies to amorphous and solvate forms. The relationships between the various phases and commonly used industrial and research laboratory processes are schematically illustrated in Fig. 3.

It is worth stressing that polymorph assessment in industrial research and development as well as during processing is part of the system of quality control. Therefore it is necessary to make sure that the scale-up from laboratory preparation to industrial production does not introduce variations in crystal form. Polymorph assessment also guarantees that the product conforms to the guidelines of the appropriate regulatory agencies and does not infringe the intellectual property protection that may cover other crystal forms [32].

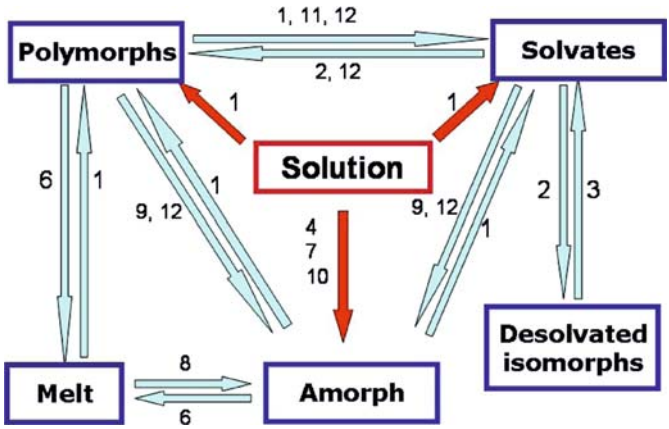

Fig. 3 Some general relationships between polymorphs, solvates and amorphous phases and the type of research laboratory or industrial or process for preparation and interconversion: *1* crystallization; *2* desolvation; *3* exposure to solvent/vapour uptake; *4* freeze drying; *5* heating; *6* melting; *7* precipitation; *8* quench cooling; *9* milling; *10* spray drying; *11* kneading; *12* wet granulation. Analogous relationships apply to polymorphic modifications of solvate forms. Note that the figure represents general trends rather than every possible transformation; the presence or absence of an arrow or number does not represent the exclusive existence or absence of a transformation

The screening of crystal forms is best achieved by the combined use of several solid-state techniques, such as hot stage microscopy, differential scanning calorimetry, thermogravimetric analysis and X-ray diffraction. Powerful complementary tools are also provided by solid-state spectroscopic techniques such as solid state nuclear magnetic resonance spectroscopy [33] and Raman spectroscopy [1]. Of great relevance is the possibility of determining the molecular and crystal structure of a crystal form by means of single crystal X-ray diffraction. This technique, although much more demanding than powder diffraction in terms of experiment duration and data processing, has the great advantage of providing detailed structural information on the molecular geometry. Furthermore, it affords insight into the factors controlling the packing of the molecules in the crystal and the nature and structural role of solvent molecules. Knowledge of the single-crystal structure allows a direct comparison between the X-ray powder diffraction pattern, calculated on the basis of the structure, with the one measured on the polycrystalline sample as it will be diffusely used in the following description of specific cases.

Importantly, the calculated diffraction pattern is not affected by the typical sources of errors of experimental powder diffraction (preferential orientation, mixtures, presence of amorphous phase) that often complicate or render uncertain the interpretation of measured powder diffractograms; hence the calculated powder pattern is often referred to as the "gold standard" pattern for a crystal form.

The search for various crystal forms requires that the behaviour of a solid phase is investigated as a function of the variables that can influence or determine the outcome of the crystallization process, e.g. temperature, choice of solvents,

crystallization conditions, rate of precipitation, interconversion between solid forms (from solvate to un-solvate and vice versa), pressure and mechanical treatment, absorption and release of vapour, etc. [24]. Techniques such as hot stage microscopy, DSC and micro-DSC can be used to obtain a semiempirical energy–temperature diagram [34, 35] that can be helpful in designing protocols for screening for crystal forms.

Another powerful tool for the investigation of the structural relationship between crystal forms is variable temperature X-ray diffraction that provides information on phase transitions and or on adsorption/desorption of solvent molecules (and chemical reactivity, of course, but this is of less concern in this context).

Beside the traditional thermal and solution methods for obtaining new crystal forms, many other methods are being used or developed in the quest for multiple crystal forms. Some of these methods are based on the knowledge of crystal structures in the literature [16], the application of crystal engineering principles (based on hydrogen-bonding patterns) to the preparation of new multicomponent solids [36,37], the induction of crystal forms by using polymeric substrates [38], the development of high-throughput crystallization technology [39], the utilization of solid–solid and solid–gas reactions [40], solvent-free synthesis [41,42], the desolvation of solvated crystals [43] and crystallization from a supercritical solvent [44,45]. These methods, combined with the development of new technology [39], the attempts to design and control crystal structure [46], combined with some spectacular encounters with new (and undesired) crystal forms [47] (see Sect. 5) and some high profile pharmaceutical patent litigations [1], have led to many new techniques for exploring the crystal form space of any particular substance.

5 Examples of Crystal Form Identification and Characterization

There is no protocol of polymorph screening that can guarantee the identification of *all* crystal forms of a given molecule. As pointed out in the previous section, the understanding of a system exhibiting multiple crystal forms is best achieved by studying the system with a wide variety of analytical tools. We have chosen to illustrate this aspect by means of two recent examples coming from our own work.

The first example is that of cinchomeronic acid, which has been known for almost a century [48]. The cinchomeronic acid 3,4-dicarboxypyridine is one of the six isomers of the acid pyridinedicarboxyl; all isomers are widely utilized in the construction of coordination networks [49–51]. The presence of two of cinchomeronic forms is reported in the PDF-2 [52], while the crystal structure has been determined only for one form [53]. We have investigated the structural relationship between these two crystal forms by a combined use of single-crystal X-ray diffraction, IR and Raman spectroscopy, and solid state NMR spectroscopy [54]. Form I crystallizes in an acentric orthorhombic group, while form II crystallizes in a centric monoclinic group (Fig. 4), due to a static disorder for the nitrogen position (Fig. 5). The zwitterionic nature of the acid in both forms has been confirmed by ^{1}H MAS,

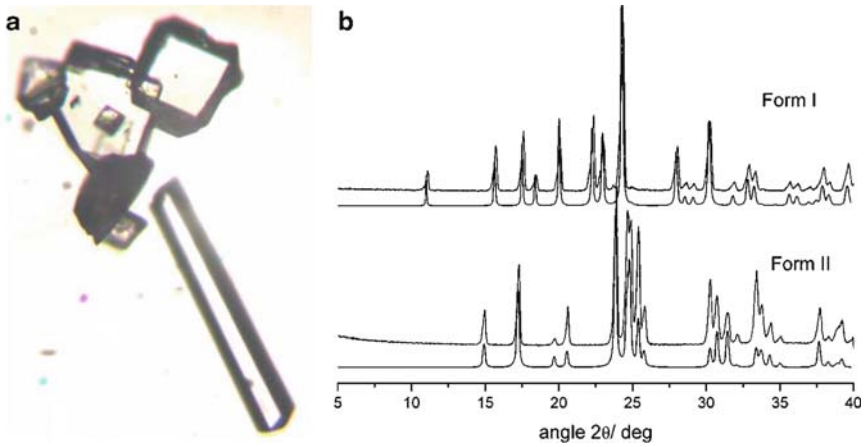

Fig. 4 Concomitant polymorphs obtained from an ethanol/water solution: *rods* form I, *blocks* form II **a** Comparsion between the experimental and calculated powder diffractograms of form I and form II **b**

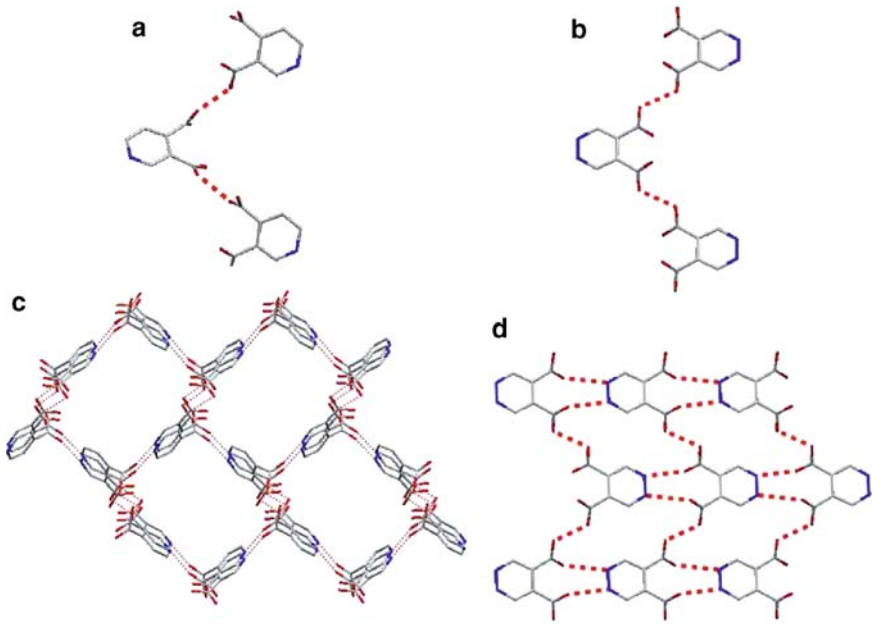

Fig. 5 Chains present in form I **a** and form II **b**; the adamantoid network formed by N–H + ···O− hydrogen bonds among the chains and the overall crystal structure formed by the three interpenetrating networks in form I **c**; interactions N–H + ···O− and C–H···O− among the chains and the 2D-network present in form II **d**

^{13}C CPMAS and ^{15}N CPMAS (Fig. 6). The single crystal structures give us a view of the hydrogen bonds formed by the molecule of cinchomeronic acid in the solid state; in both structures the molecules of cinchomeronic acid form infinite chains via

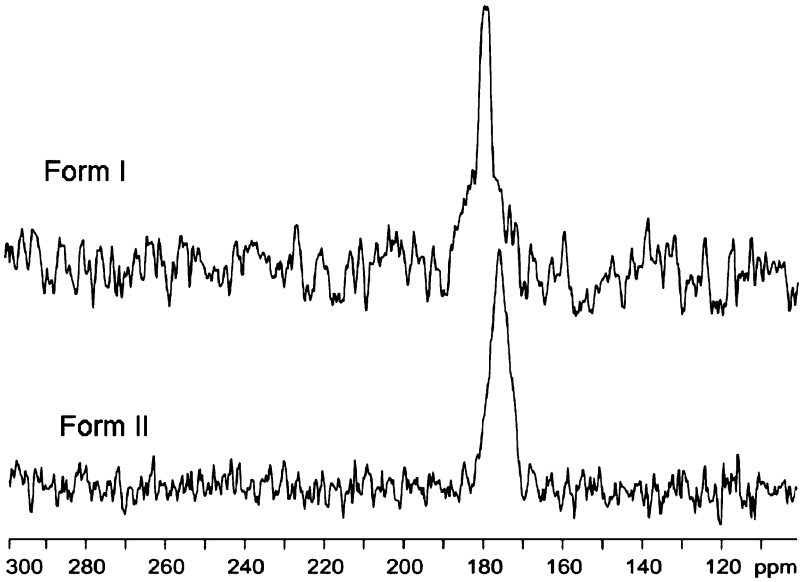

Fig. 6 ^{15}N CPMAS spectra of cinchomeronic acid: form I (*top*) and form II (*bottom*) recorded at 27.2 MHz with a spinning speed of 5 kHz which confirm the zwitterionic nature of cinchomeronic acid in both crystal phases

short O–H—O hydrogen bonds between the carboxylic and carboxylate groups (see Fig. 5). In form I the zwitterion chains are ordered and are connected via N–H—O interactions to form a threefold interpenetrating networks. In form II, on the other hand, the presence of static disorder leads to crystallographic equivalence between the –COO and –COOH groups (see Fig. 5) and the nitrogen atom is disordered over two positions, which leads to a longer and weaker N–H—O hydrogen bond consistent with the IR and Raman spectra. Both forms decompose before melting without any interconversion, which suggests the presence of a monotropic system, while the slurry experiment indicates that form I is the thermodynamically stable form. The crystal structure and spectroscopic analysis indicate that the difference in stability can be ascribed to the strength of the hydrogen bonding patterns established by the protonated N-atom and the carboxylic/carboxylate O-atoms. The possibility of optimizing the hydrogen bond interaction in form I, with respect to the somewhat *looser* interactions allowed by the packing in form II might be responsible for the stabilization of the crystal structure of form I.

Another example is provided by the two different crystal forms of the salt $[HN(CH_2CH_2)_3NH]$ $[OOC(CH_2)COOH]_2$ obtained depending on preparation technique (grinding or solution) and crystallization speed. Form I, containing mono-hydrogen malonate anions forming conventional intramolecular O–H$\cdots$O hydrogen bonds and inter-ionic N–H$\cdots$O hydrogen bonds, is obtained by solid-state co-grinding or by rapid crystallization, while form II, containing *both* intermolecular and intramolecular O–H$\cdots$O hydrogen bonds, is obtained by slow crystallization

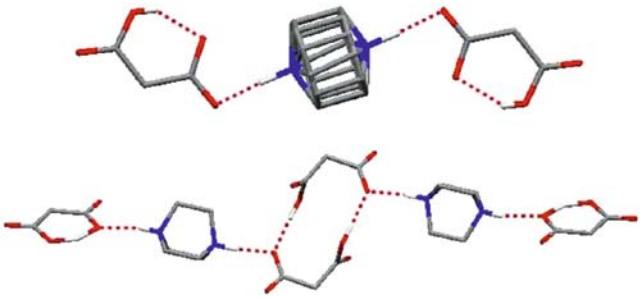

Fig. 7 Form I (*top*) and II (*bottom*) of $[HN(CH_2CH_2)_3NH][OOC(CH_2)COOH]_2$ and the hydrogen bonded anion · · · cation chains present in their crystals. Form I is obtained by solid-state co-grinding or by rapid crystallization, while form II is obtained by slow crystallization

(see Fig. 7). Form I and II do not interconvert, while form I undergoes an order–disorder phase transition on cooling. One can envisage the two crystalline forms as *hydrogen bond isomers* of the same *solid supermolecule* [55].

6 Examples of Solvate Crystal Forms and Interconversion

An intriguing case of interconversion between unsolvate and solvate crystals is observed when $[N(CH_2CH_2)_3N]$ is reacted with maleic acid [HOOC(HC=CH)COOH]. The initial product is the anhydrous salt $[HN(CH_2CH_2)_3N]$ [OOC(HC=CH)COOH], which contains chains of $^{(+)}N–H\cdots N^{(+)}$ bonded cations $[HN(CH_2CH_2)_3N]^+$ and "isolated" $[OOC(HC=CH)COOH]^-$ anions [56].

Upon exposure to humidity the anhydrous salt converts within few hours into the hydrated form $[HN(CH_2CH_2)_3N]$ $[OOC(HC=CH)COOH]\cdot 0.25H_2O$, which contains more conventional "charge-assisted" $^{(+)}N–H\cdots O^{(-)}$ hydrogen bonds between anion and cation (see Fig. 8). This latter form can also be obtained by co-grinding.

In a similar process, crystals of $[Ru(\eta^6–C_6H_6)_2][BF_4]_2$ have been crystallized from nitromethane as the solvate form $[Ru(\eta^6–C_6H_6)_2][BF_4]_2\cdot MeNO_2$. These solvate crystals, if exposed to air, rapidly convert to the unsolvate form $[Ru(\eta^6–C_6H_6)_2][BF_4]_2$. The nature of this latter compound was established from single crystals obtained from water in the presence of seeds of the powder material obtained from desolvated crystals $[Ru(\eta^6–C_6H_6)_2][BF_4]_2\cdot MeNO_2$ [57]. The opposite process, namely solvent uptake, can often be activated by mechanical treatment of unsolvate crystals. There are several reports that even gentle grinding of a powder product may lead to the formation of a hydrated product [58–60].

Another example is provided by the hydrated salt $[Co(\eta_5–C_5H_5)_2]^+[Fe(\eta_5–C_5H_4COOH)(\eta_5–C_5H_4COO)]^-\cdot H_2O$, which is obtained by simply grinding in air the crystalline powder of $[Co(\eta_5–C_5H_5)_2]^+[Fe(\eta_5–C_5H_4COOH)(\eta_5–C_5H_4COO)]^-$ that precipitates from THF or nitromethane on reacting $[Co(\eta_5–C_5H_5)_2]$ with $[Fe(\eta_5–C_5H_4COOH)_2]$ [61]. Once $[Co(\eta_5–C_5H_5)_2]^+[Fe$

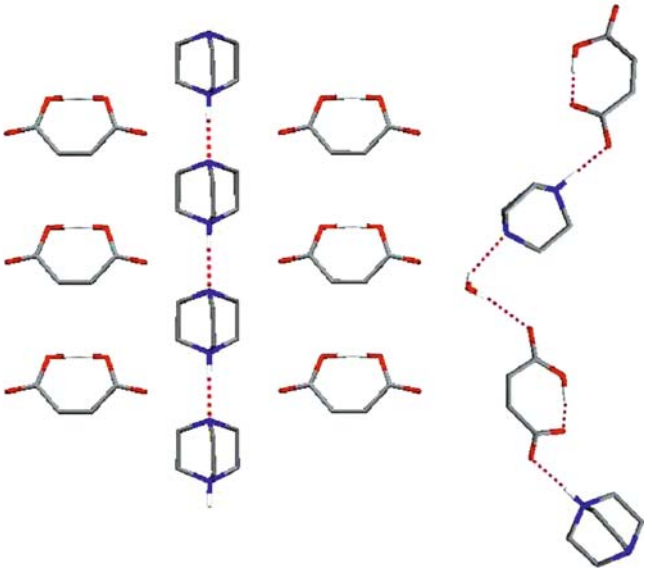

Fig. 8 Views of the packing and hydrogen bonding in the anhydrous salt $[HN(CH_2CH_2)_3N][OOC(HC{=}CH)COOH]$ (*left*) and of the hydrated salt $[HN(CH_2CH_2)_3N][OOC(HC{=}CH)COOH]H_2O_{0.25}$ (*right*)

$(\eta_5\text{–}C_5H_4COOH)(\eta_5\text{–}C_5H_4COO)]^- \cdot H_2O$ has been obtained by grinding, its single crystals can be grown from water or nitromethane, while crystals of the anhydrous form are no longer observed. However, on heating, the hydrated form loses water at 373 K and reverts to the starting material.

7 Solid–Gas Reactions: A Route to New Crystal Forms

Solid–gas reactions have been known for a long time and have recently attracted a renewed interest in the strive to find environmentally friendly processes. Since the reactant is a crystalline solid, the issue of whether different crystal forms would react in the same or a different way towards a gaseous reactant is of interest to the discussion. We have tackled this question by exploiting solid–gas reactions between crystal polymorphs of the same acidic substance and vapours of volatile bases, investigating in turn the inverse process, i.e. removal of the vapours from the crystal structures by thermal treatment.

The possibility of different chemical behaviour of polymorphic modifications has been explored before only in the case of indomethacine amorphous and crystal forms reacted with ammonia by Stowell, Griesser, Byrn et al. [62]. We have investigated two rather different systems, namely the polymorphic forms of barbituric acid [63] and of ferrocene dicarboxylic acids [64], which have been reacted with

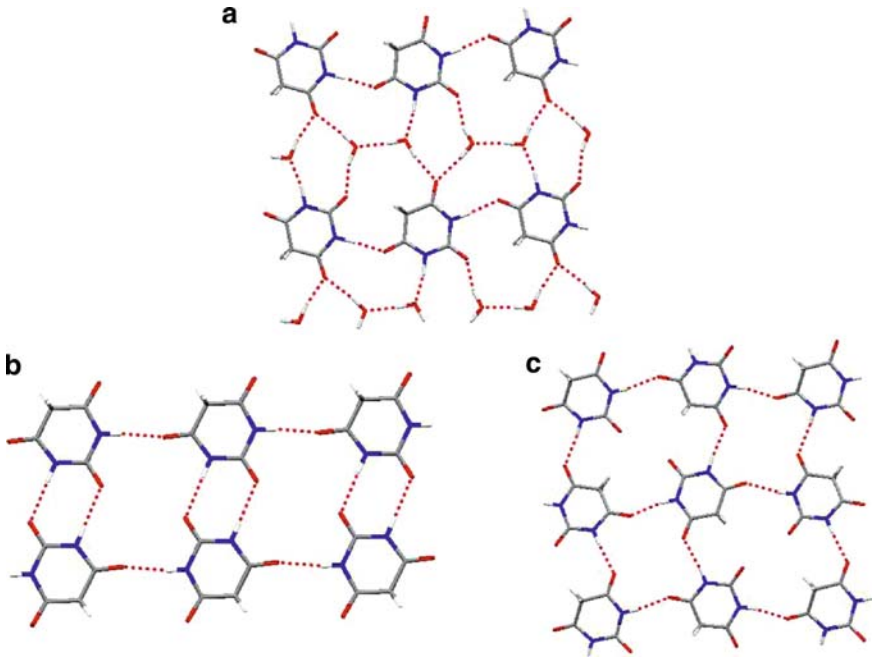

Fig. 9 Hydrogen bond networks present in the dihydrate form **a**, form I **b** and form II **c** of barbituric acid

volatile bases. Solid barbituric acid is known as two polymorphic forms (forms I and II) and as a dihydrate form for which single crystal data are available allowing computation of the theoretical powder diffractograms [65–68]. Views of the packings of the three forms are shown in Fig. 9. De-hydration of the dihydrate form has also been investigated, showing that it releases water to yield exclusively crystals of form II. We have been able to show that forms I, II and the dihydrate form of barbituric acid react with ammonia leading to the same crystalline ammonium barbiturate salt $NH_4(C_4H_3N_2O_3)$, while the gas–solid reactions of form II with methylamine and dimethylamine yield the corresponding crystalline salts $CH_3NH_3(C_4H_3N_2O_3)$ and $(CH_3)_2NH_2(C_4H_3N_2O_3)$, respectively. The processes are shown in Fig. 10.

Thermal desorption of the bases at ca. 200°C leads to formation of a new crystal form of barbituric acid, form III, as confirmed by H^1-NMR spectroscopy and by chemical behaviour. Unfortunately several attempts to crystallize compound III yielded only the formation of the dihydrate form (Fig. 11).

Similarly, the reactions between solid 1–3 dimethylbarbituric acid (dmb) with vapours of NH_3 and of the volatile amines $NH_2(CH_3)$, and $NH(CH_3)_2$ have been investigated [69]. The barbiturate salts $[NH_4]$dmb, $[NH_3(CH_3)]$dmb and $[NH_2(CH_3)_2]$dmb have been characterized by X-ray powder diffraction (XRPD), differential scanning calorimetry and thermogravimetric analysis. The solid–gas reactions were monitored by UV–Vis spectroscopy in the solid state. In the case of $[NH_2(CH_3)_2]$dmb, recrystallization from methanol yields the salt

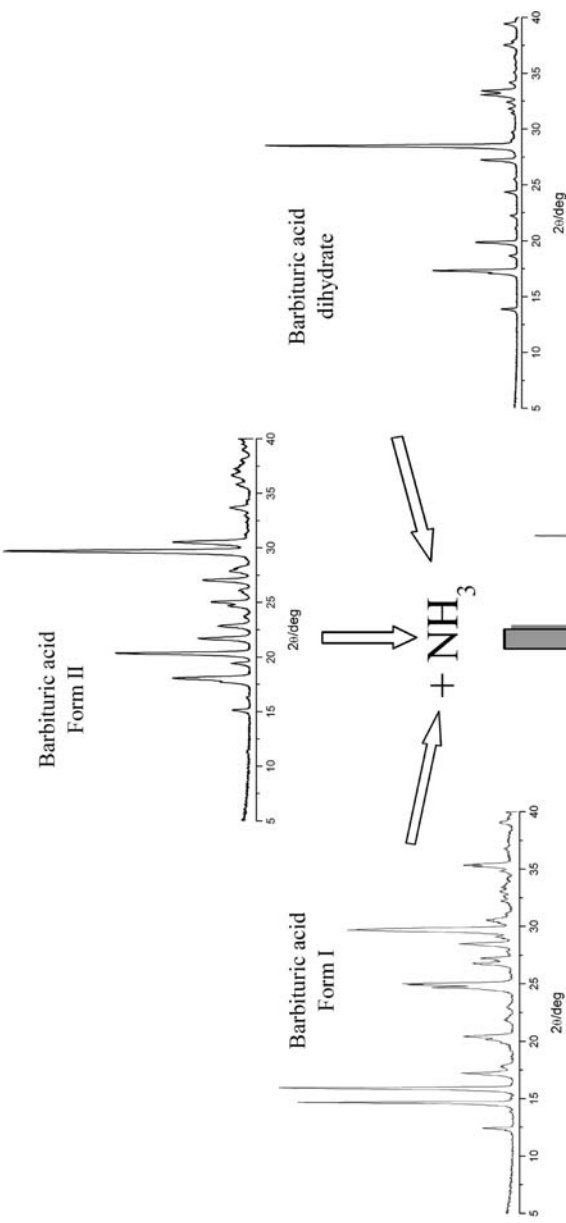

Fig. 10 Schematic representation of the XRPD patterns of the polymorphic forms of barbituric acid I and II and that of the dihydrate form. The interaction with NH_3 leads to the formation of the same product, $NH_4(C_4H_3N_2O_3)$

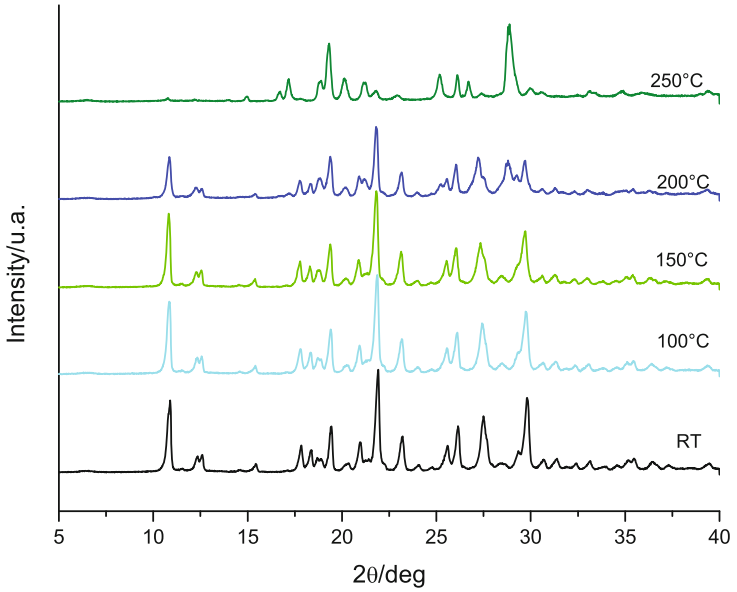

Fig. 11 XRPD recorded at different temperatures from room temperature to 250°C on crystalline $NH_4(C_4H_3N_2O_3)$ showing the presence of new reflections at 200°C

$[NH_2(CH_3)_2][DMB] \cdot 2[DMBA]$, while recrystallization of $[NH_3(CH_3)]$dmb yields both the dimerization product $[NH_3(CH_3)][(C_6O_3N_2H_6)_2–OH] \cdot 2H_2O$ and the hydurilate salt $[NH_3(CH_3)]_2[(C_6O_3N_2H_6)_2]$, i.e. the product $[NH_3(CH_3)]$dmb is only accessible via. the solid–gas reaction.

In an analogous study, crystalline form I (monoclinic) and form II (triclinic) of ferrocene dicarboxylic acid $[Fe(\eta^5–C_5H_4COOH)_2]$ have been reacted at room temperature with the gaseous bases NH_3, $NH_2(CH_3)$ and $NH(CH_3)_2$ [64]. The two crystal forms behave in exactly the same way in the solid–gas reaction generating the same products, identified as the anhydrous crystalline salts $[NH_4]_2[Fe(\eta^5–C_5H_4COO)_2]$, $[NH_3CH_3]_2[Fe(\eta^5–C_5H_4COO)_2]$, and $[NH_2(CH_3)_2]_2[Fe(\eta^5–C_5H_4COO)_2]$. Interestingly though, all these crystals revert via vapour release exclusively to the metastable crystalline form I, as shown in Fig. 12.

This is not surprising per se, because there is no reason why, if the reaction is quantitative, the crystalline salt product should “remember” which crystal form it comes from. It is instead of relevance that forms I and II of $[Fe(\eta^5–C_5H_4COOH)_2]$ are not known to interconvert via a solid–solid phase transition, hence they constitute a monotropic system. The ammonia absorption/release process, therefore, can be seen as a solid state way to convert the thermodynamically stable form II into the metastable form I. The process is schematically represented in Fig. 13.

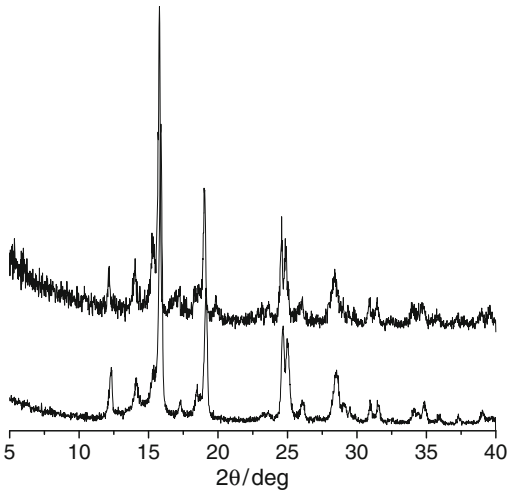

Fig. 12 Comparison between the experimental powder diffractograms of compound 1, obtained from the solid–gas reaction with ammonia of form I (*top*) and form II (*bottom*), respectively

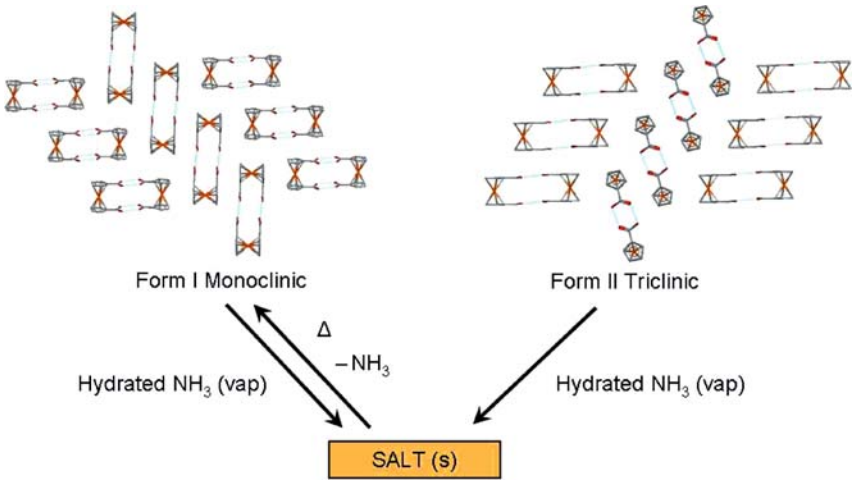

Fig. 13 Reaction of crystalline forms I and II with vapours of NH_3 yields the same salt, which upon heating and removal of NH_3 generates only the monoclinic form I

8 Co-Crystals and Salts, Co-Crystals or Salts?

In this last section we focus on co-crystals. Although co-crystals, i.e. multicomponent crystals containing chemically different molecular units in the asymmetric unit have long been known [70], they have recently become an important field of new discoveries and innovation under the strive to find new drugs and the potential of extension of IP protection on existing ones [71–73].

The definition of a co-crystal is still matter of debate [74, 75]. The definition initially put forward by Aakeroy focused on the aggregation state: "co-crystals are made from reactants that are solids at ambient conditions" [76] and has also been taken up by others [71, 77]. This definition, however, is not without ambiguity (see below). We prefer to take up Dunitz' more liberal view of co-crystals as "encompassing molecular compounds, molecular complexes, solvates, inclusion compounds, channel compounds, clathrates, and other types of multi-component crystals." This view has been echoed recently by Stahly [78] who wrote that: "co-crystals consist of two or more components that form a unique crystalline structure having unique properties." At the bottom line, these multicomponent systems ought to be looked at as crystals of supermolecules whereby the component units interacting via non-covalent interactions generate collective physico–chemical properties that are different from those of the homo-molecular crystals formed by the components.

One may wonder whether solvates would fall under the same broad definition. We would argue in favour, not only because solvent molecules themselves form their own crystalline materials at appropriate temperature (ice!) but also because, as we have argued above, solvate crystals do not necessarily come from solutions since vapour or any other volatile molecule can be taken up from the ambient atmosphere and become incorporated into the crystal. Since we are dealing with crystal forms, it is useful to also remind the reader that the term pseudopolymorphism is not appropriate to refer to solvate forms of a given molecular crystal [23, 79, 80] because solvate crystals can themselves be polymorphic!

In a recent paper, Bond listed a number of interesting controversial examples of co-crystals [81]. For example, dioxane, $C_4H_8O_2$, forms isostructural 1:1 two-component crystals with I_2, Br_2 or Cl_2, which at room temperature and 1 bar pressure are solid, liquid, and gas, respectively [82–84]. Clearly a distinction based on the aggregation state of one component has little significance.

The crystal structures of 13 co-crystals formed by *n*-alkylcarboxylic acids and pyrazine in 2:1 stoichiometry have been reported [85, 86]. The acids include formic acid, which is liquid at room temperature, up to the tridecandioic acid which is solid. Pyrazine is also a solid. Clearly, the early members of this series cannot be called solvates only because the co-former is liquid, while from decanoic to tridecandioic the acid/pyrazine systems are co-crystals. Another example is the two-component crystals formed by picric acid forms and benzene, naphthalene and anthracene (amongst others), which contain stacks of alternating molecular components that are clearly comparable in all three structures [87–89]. All of these crystals are stable at room temperature.

Not only it is difficult to distinguish between a co-crystal and a solvate (as a matter of fact all molecules are solid and form crystals at sufficiently low temperature) but it is also often difficult to distinguish between a crystal and a salt. As discussed above in the case of hydrogen-bonded systems between acids and bases the *transition* between a salt and a co-crystal may be a very semantic issue depending exclusively on the position of a proton along a N···O supramolecular link [90].

Proton transfer along a hydrogen bond poses an interesting question about polymorph definition. In fact, proton mobility along a hydrogen bond (say from

O–H···N to $^{(-)}$O···H–N$^{(+)}$) may not be associated with a phase transition, even though it implies the formal transformation of a molecular crystal into a molecular salt. This situation has been observed, for instance, for the proton migration along an O–H···O bond in a co-crystal of urea–phosphoric acid (1:1) as a function of temperature [91, 92].

Mootz and Wiechert have isolated two co-crystals of pyridine and formic acid: in the 1:1 co-crystal, proton transfer from formic acid to pyridine does not take place, while in the 1:4 co-crystal N–H$^{(+)}$···O interactions are present (see Fig. 14) [93]. Examples of this kind are rare, but serve to stress how the phenomenon of polymorphism can be, at times, full of ambiguity.

In order to tackle the problem of the co-crystal or salt nature of acid–base adducts we have used the same approach illustrated above in the case of the polymorphs of barbituric and cinchomeronic acid, namely a combined use of diffraction and spectroscopic methods in the investigations. We have shown that mechanical mixing of a di-nitrogen base [N(CH$_2$CH$_2$)$_3$N] (dabco) and of dicarboxylic acid HOOC(CH$_2$)$_n$COOH(n = 1–7) affords a series of hydrogen-bonded adducts of general formula [N(CH$_2$CH$_2$)$_3$N]–H–[OOC(CH$_2$)$_n$COOH](n = 1–7, that is to say **1C3**, **1C4**, **1C5, 1C6**, **1C7**, **1C8**, and **1C9**) (see Fig. 15) [21].

These compounds can be classified as co-crystals or salts depending on whether proton transfer from oxygen to nitrogen takes place or not along the O–H—N bonds [94]. In order to address this issue we have compared the results of an X-ray investigation carried out on single crystals grown from the solid-state products by seeding the corresponding methanol solutions with those obtained from the polycrystalline powder by solid-state ^{1}H and ^{15}N and ^{13}C spectroscopy.

For example, it has been possible to correlate the isotropic ^{1}H and ^{15}N chemical shift data with the N–O distances of the atoms involved in the hydrogen bond interaction in a series of solid adducts of formula [N(CH$_2$CH$_2$)$_3$N]–H–[OOC(CH$_2$)$_n$COOH](n = 1–7) (Fig. 16). The ^{1}H MAS and ^{15}N CPMAS NMR data are in agreement with the X-ray data and allow discrimination between the proton transfers for the **1C3** and **1C5** adducts and the strong N···H–O interactions

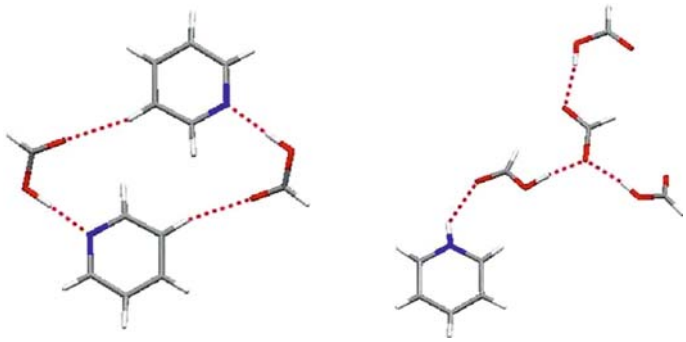

Fig. 14 The 1:1 co-crystal of pyridine and formic acid where the proton transfer does not occur (*left*) and the 1:4 co-crystal of pyridine and formic acid where the formate anion is present (*right*)

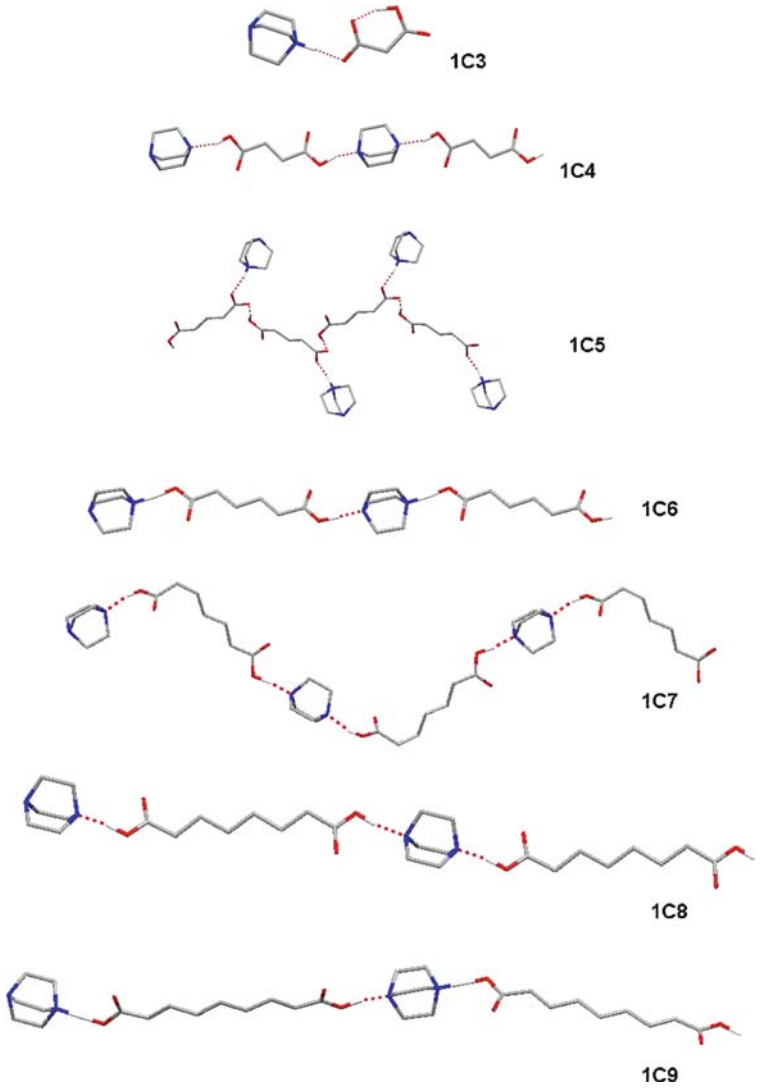

Fig. 15 Schematic representation of the packing motives in $[N(CH_2CH_2)_3N]$–H–$[OOC(CH_2)_n COOH]$($n = 1$–7, i.e. **1C3**, **1C4**, **1C5**, **1C6**, **1C7**, **1C8**, and **1C9**)

(without proton transfer) for the **1C4**, **1C7**, **1C8** and **1C9** co-crystals. **1C6** represents an intriguing case in which one of the nitrogen atoms of dabco is intermediate between the protonated and non-protonated forms. Density functional theory, applied to explore changes upon hydrogen bonding in the ^{1}H and ^{15}N shielding parameters, is in agreement with the experimental values found by solid-state NMR spectroscopy [95, 96].

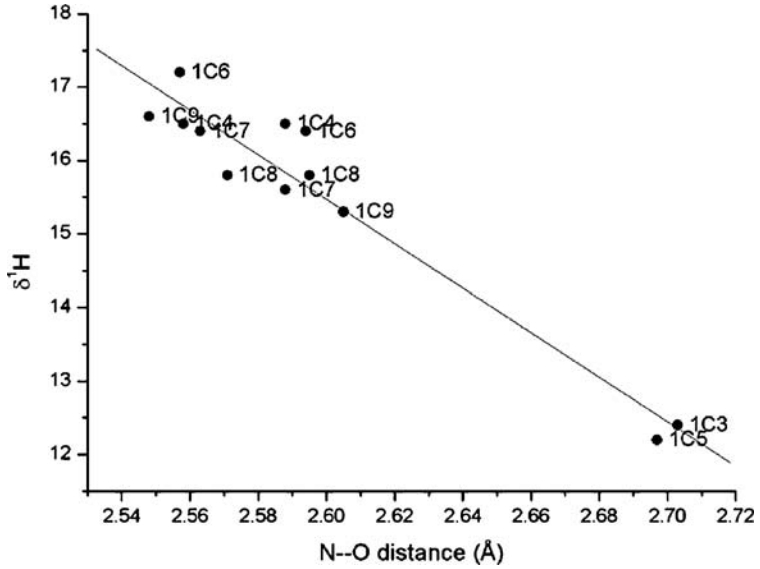

Fig. 16 Compact view of 1H chemical shifts as a function of N · · · O distance

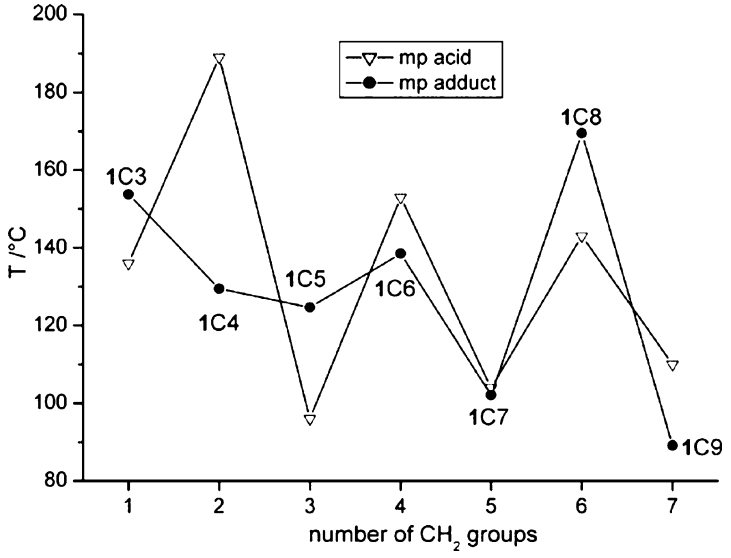

Fig. 17 Melting point alternation in neutral acids and in compounds **1C3–1C9**

Comparison of melting point data of the neutral organic acids and of the co-crystals and salts discussed herein yields another interesting observation. As shown in Fig. 17, the melting points of compounds **1C3–1C9** follow a trend very similar to that of the acids, i.e. they show an alternation of melting points as a function of the even–odd carbon chain length.

In summary, at room temperature malonic and glutaric adducts are salts; adipic is ambiguous; succinic, pimelic, suberic and azelaic adducts are co-crystals. Diffraction data and solid-state NMR data are in agreement except in the case of compound **1C6**, which shows proton motion on the NMR time scale. Salt or co-crystals – does it matter? The melting points of compounds **1C3–1C9** do not correlate with the salt-like or co-crystal nature of the adducts, but rather with the even–odd carbon chain length in spite of the substantial differences in supramolecular arrangements in the crystals of the adducts with respect to those of the parent diacids.

On closing this discussion on co-crystal systems, it is useful to cite few examples (selected from the many available in a rapidly expanding literature) of the importance of co-crystals in the pharmaceutical field. Piracetam, (2-oxo-1-pyrrolidinyl) acetamide), has been co-crystallized by Zaworotko et al. with gentisic acid and *p*-hydroxybenzoic acid (see Fig. 18) [22].

Co-crystals of 4-hydroxybenzoic acid (4HBA) and 2,3,5,6-tetramethylpyrazine (TMP) (2:1) have been reported as a case of supramolecular synthon polymorphism in a co-crystal (see Fig. 19); in fact the two forms exhibit different hydrogen bond interactions. The co-crystal form I does not follow the hierarchy of hydrogen bonding, and converts into the stable form II, which follows the hierarchy of hydrogen bonding [97].

In yet another example, a co-crystal of caffeine and adipic acid [98] has been isolated by a co-crystallization methods based on a suspension/slurry containing both components of the co-crystal system. This approach provides an optimal environment for the putative co-crystal formation because the activity values of both

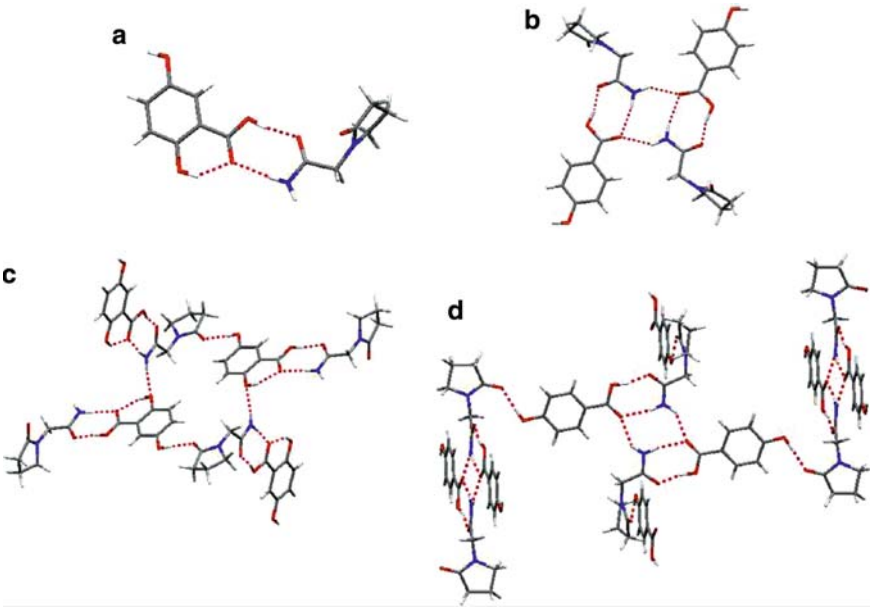

Fig. 18 Co-crystals of piracetam, (2-oxo-1-pyrrolidinyl) acetamide with gensitic **a** and **c**, and *p*-hydroxybenzoic acids **b** and **d**

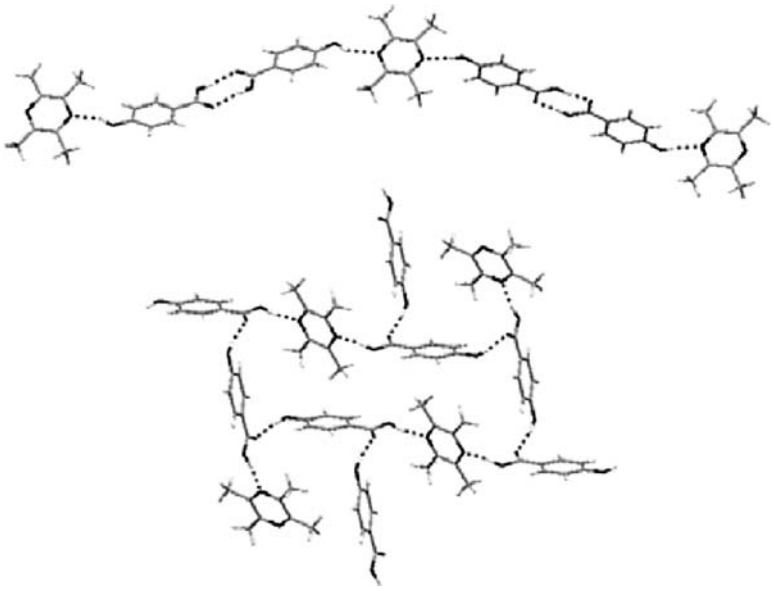

Fig. 19 Linear chain formed through carboxylic acid dimer and hydroxyl O–H···N hydrogen bonds in form I (*top*). Herringbone network in form II (*bottom*)

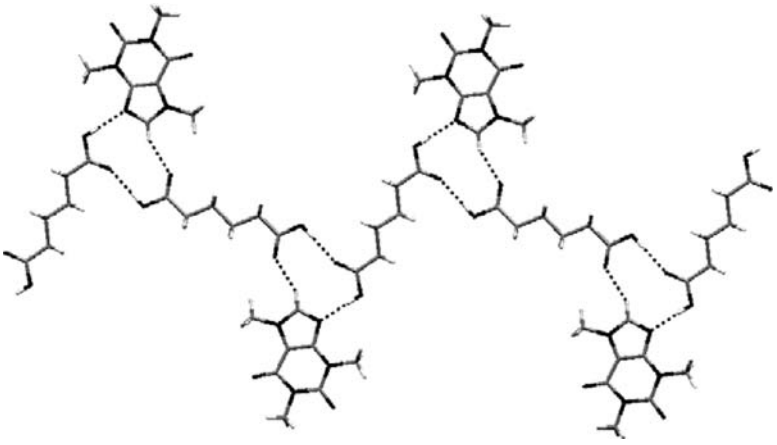

Fig. 20 View of caffeine–adipic acid trimers along the crystallographic plane (1 –2 0). The trimers are linked via hydrogen-bonded adipic acid molecules into molecular tapes

components are held at one. This method was applied to 16 pharmaceutically related co-crystal systems and was found to be 100% successful [99]. In the case of the co-crystal caffeine/adipic acid, a suspension of caffeine and adipic acid (1:1 molar ratio) in acetonitrile was prepared and equilibrated overnight at ambient temperature. The powder X-ray diffraction pattern of the solid after equilibration indicated formation of a new solid phase, which was then characterized as shown in Fig. 20.

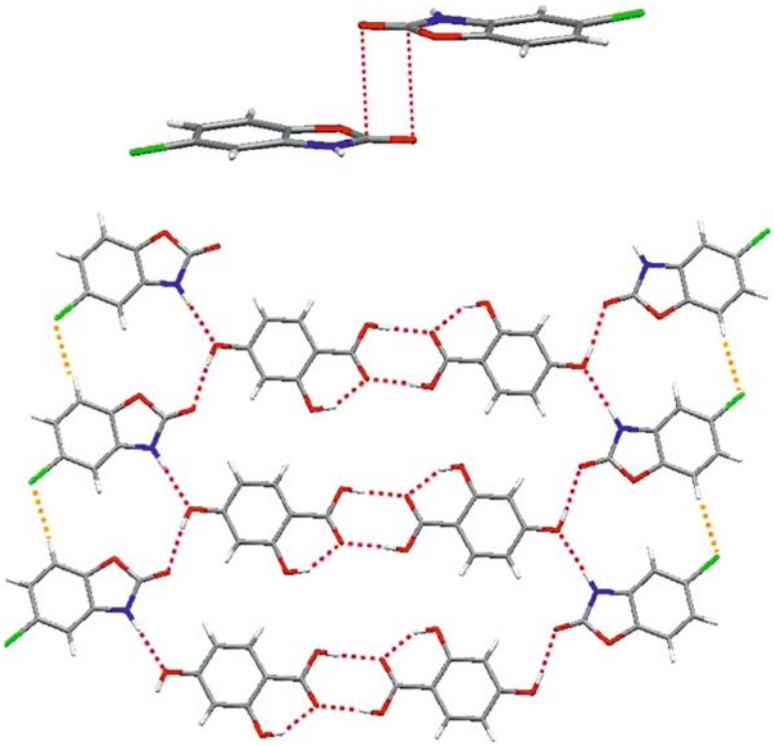

Fig. 21 Anti-parallel centrosymmetric carbonyl–carbonyl interaction between two molecules (*top*) and the packing motif (*bottom*) of chlorzoxazone in co-crystal form 1. Repulsive C–H · · · Cl–C interactions are in *light grey*

Evaporative crystallization experiments containing equimolar ratios of the API and guest has been instead used to obtain co-crystals of chlorzoxazone with carboxylic acids [100]. Two polymorphs of a chlorzoxazone:2,4-dihydroxybenzoic acid co-crystal and one form of a chlorzoxazone:4-hydroxybenzoic acid co-crystal have been characterized and the crystal structure of chlorzoxazone:2,4-dihydroxybenzoic acid (form 1) reported and analyzed, revealing an uncommon carbonyl–carbonyl interaction and a destabilizing C–H· · ·Cl–C interaction (see Fig. 21).

9 Conclusions

The scope of this review has not been that of providing the reader with a comprehensive coverage of the topic of crystal forms, rather we have aimed at an introductory view of the phenomena of multiple crystals forms in general, and polymorphism in particular. For reasons of space, many problems have not been addressed (e.g. theo-

retical methods to study polymorphism), in particular the computational exploration of the possible crystalline structures of a given molecule. The interested reader will find in the necessarily limited number of references a good starting point for further reading.

The question on whether a crystalline material contains only molecules A in different arrangements (e.g. polymorphs), or molecules A *and* molecules B, and whether this latter association ought to be considered a co-crystal or a solvate is somewhat semantic. It is unquestionable, however, that crystals of different composition not only have different crystal structures but also may possess different physical properties, such as solubility, thermal behaviour, resistance to mechanical stress, gas-absorption/release capacity, colour, melting point etc. These differences may be relevant, and carry economical and practical implications, when considering, for instance, the bio-availability of a drug or the thermal stability of a pigment.

Reproducibility and predictability are paradigms in the exact sciences. This is why, beside all the utilitarian reasons associated with the marketing of solid state materials, we would like to learn how to *make* polymorphs, or, which is the same, how to effectively *prevent* polymorph formation. If seeds of a polymorphic modification can be obtained from non-solution methods (i.e. mechanical, thermodynamical, perhaps solid state reactions) these can be used in the seeding process, which may allow growth of less kinetically favoured crystal forms. Seeding may be valuable not only to obtain the desired crystalline form, but also to prevent crystallization of undesired forms. One could argued that polymorphism, with its high degree of serendipity, could be the *nemesis* of crystal engineering because polymorphism is in logical contrast with a discipline that aims to control and reproduce univocally a given crystal structure. This is not true (rather the investigation of crystal forms) of the way a molecule recognizes another molecule, whether the same or a different one, and links to form stable or metastable supramolecular arrays, it is rather a way *to tune* synthetic and assembly strategies to obtain the desired crystal structure, which is the paradigm of crystal engineering.

References

1. Bernstein J (2002) Polymorphism in molecular crystals. Oxford University Press, Oxford, p 352
2. Dunitz JD, Bernstein J (1995) Acc Chem Res 28:193–200
3. Klaproth MH (1798) Bergmannische J I:294–299
4. Mitscherlich E (1823) Abhl Akad Berlin 43
5. McCrone WC (1965) In: Fox D, Labes MM, Weissemberg A (eds) Polymorphism in physics and chemistry of the organic solid state, vol 2. Interscience, New York, p 726
6. Findlay AF (1951) The phase rule and its applications, 9th edn. Dover, New York, pp 7–16
7. Buerger MJ, Bloom MC (1937) Z Kristallogr 96:182–200
8. Sirota NN (1982) Cryst Res Technol 17:661–691
9. Kuhnert-Brandstatter M (1965) Pure Appl Chem 10:133–144
10. Kuhnert-Brandstatter M (1971) Thermomicroscopy in the analysis of pharmaceuticals. International series of monographs in analytical chemistry, vol 45. Pergamon, Oxford

11. Sarma JARP, Desiraju GR (1999) In: Seddon KR, Zaworotko M (eds) Crystal engineering: the design and application of functional solids. Kluwer, Dorderecht, pp 325–356
12. Griesser UJ (2002) Acta Crystallogr A 58(suppl):c241
13. Gorbitz CH, Hersleth HP (2000) Acta Crystallogr B 56:526–534
14. Griesser UJ, Burger A (1999) Acta Crystallogr A 55(suppl):400
15. Desiraju GR (1989) Crystal engineering: the design of organic solids. Elsevier, Amsterdam
16. Braga D, Grepioni F, Orpen AG (eds) (1999) Crystal engineering: from molecules and crystals to materials. In: Proceedings of the NATO Advanced Study Institute. 12–23 May 1999, Erice, Italy, p 500
17. Braga D, Grepioni F, Desiraju GR (1998) Chem Rev 98:1375–1405
18. Blake AJ, Champness NR, Hubberstey P, Li W-S, Withersby MA, Schroder M (1999) Coord Chem Rev 183:117–138
19. Moulton B, Zaworotko MJ (2001) Chem Rev 101:1629–1658
20. Griesser UJ (2006) In: Hilfiker R (ed) The importance of solvates. Wiley, Weinheim, pp 211–233
21. Braga D, Maini L, de Sanctis G, Rubini K, Grepioni F, Chierotti MR, Gobetto R (2003) Chem Eur J 9:5538–5548
22. Vishweshwar P, McMahon JA, Peterson ML, Hickey MB, Shattock TR, Zaworotko MJ (2005) Chem Commun, pp 4601–4603
23. Seddon KR (2004) Cryst Growth Des 4:1087–1087
24. Bernstein J (2005) Chem Commun, pp 5007–5012
25. Nangia A (2006) Cryst Grow Des 6:2
26. Burger A (1983) Topics in pharmaceutical sciences. Elsevier, Amsterdam, p 347
27. Cabri W, Ghetti P, Pozzi G, Alpegiani M (2007) Org Process Res Dev 11:64–72
28. Lara-Ochoa F, Espinosa-Perez G (2007) Cryst Growth Des 7:1213–1215
29. Raw AS, Yu LX (2004) Adv Drug Delivery Rev 56:235–236
30. Yu L, Stephenson GA, Mitchell CA, Bunnell CA, Snorek SV, Bowyer JJ, Borchardt TB, Stowell JG, Byrn SR (2000) J Am Chem Soc 122:585
31. Chen S, Xi H, Yu L (2005) J Am Chem Soc 127:17439–17444
32. Braga D, Bernstein J (2007) In: Dario B, Grepioni F (eds) Crystal polymorphism: challenges at crossroads of science and technology. Wiley, Weinheim, pp 293–314
33. Gobetto R (2007) In: Braga D, Grepioni F (eds) Solid state NMR. Wiley, Weinheim, pp 266–292
34. Grunenberg A, Henck JO, Siesler HW (1996) Int J Pharm 129:147–158
35. Henck J-O, Kuhnert-Brandstatter M (1999) J Pharm Sci 88:103–108
36. Almarsson O, Zaworotko MJ (2004) Chem Commun, p 1889
37. Aakeröy CB, Beatty AM, Helfrich BA (2001) Angew Chem Int Ed 40:3240–3242
38. Price CP, Grzesiak AL, Matzger AJ (2005) J Am Chem Soc 127:5512–5517
39. Morissette SL, Almarsson O, Peterson ML, Remenar JF, Read MJ, Lemmo AV, Ellis S, Cima MJ, Gardner CR (2004) Adv Drug Delivery Rev 56:275–300
40. Braga D, Grepioni F (2005) Chem Commun, pp 3635–3645
41. Trask AV, Shan N, Motherwell WDS, Jones W, Feng S, Tan RBH, Carpenter KJ (2005) Chem Commun, pp 880–882
42. Braga D, Grepioni F (2004) Angew Chem Int Ed 43:4002–4011
43. Griesser UJ, Burger A (1991) Eur J Pharm Biopharm 37:118
44. York P (2005) Chem World 2:50
45. Shekunov YB, York P (2001) J Cryst Growth 211:122
46. Desiraju GR (2003) Crystal design: structure and function. Wiley, Chichester, p 420
47. Bauer J, Spanton S, Henry R, Quick J, Dziki W, Porter W, Morris J (2001) Pharm Res 18:859
48. Kirpal A (1907) Monatsh Chem 28:439–445
49. Tong ML, Wang J, Hu S (2005) J Solid State Chem 178:1518–1525
50. Tong ML, Wang J, Hu S, Batten SR (2005) Inorg Chem Commun 8:48–51
51. Senevirathna MKI, Pitigala P, Perera VPS, Tennakone K (2005) Langmuir 21:2997–3001
52. International Centre for Diffraction Data (2005) Powder diffraction file PDF-2. ICDD, Newton Square, PA

53. Takusagawa F, Hirotsu K, Shimada A (1973) Bull Chem Soc Jpn 46:2669–2675
54. Braga D, Maini L, Fagnano C, Taddei P, Chierotti MR, Gobetto R (2007) Chem Eur J 13:1222–1230
55. Braga D, Maini L (2004) Chem Commun, pp 976–977
56. Braga D, Rubini K, Maini L (2004) Cryst Eng Commun 6:236–238
57. Braga D, Cojazzi G, Abati A, Maini L, Polito M, Scaccianoce L, Grepioni F (2000) J Chem Soc Dalton Trans, pp 3969–3975
58. Caira MR (1998) Top Curr Chem 198:163–208
59. Caira MR, Nassimbeni LR, Timme M (1995) J Pharm Sci 84:884–888
60. De Villiers MM, Van der Watt JG, Lotter AP (1991) Drug Dev Ind Pharm 17:1295–1303
61. Braga D, Maini L, Grepioni F (1999) Chem Commun, pp 937–938
62. Chen X, Morris KR, Griesser UJ, Byrn SR, Stowell JG (2002) J Am Chem Soc 124:15012–15019
63. Braga D, Cadoni M, Grepioni F, Maini L, Rubini K (2006) Cryst Eng Commun 8:756–763
64. Braga D, Grepioni F, Polito M, Chierotti MR, Ellena S, Gobetto R (2006) Organometallics 25:4627–4633
65. Lewis TC, Tocher DA, Price SL (2004) Cryst Grow Des 4:979–987
66. Bolton W (1963) Acta Cryst 16:166–173
67. Jeffrey GA, Ghose S, Warwicker JO (1961) Acta Cryst 14:881–887
68. Al-Karaghouli AR, Abdul-Wahab B, Ajaj E, Al-Asaff S (1977) Acta Crystallogr Sect B Struct Sci B33:1655–1660
69. Braga D, Cadoni M, Grepioni F, Maini L, Streek JVD (2007) New J Chem 31:1935–1940 doi: 10.1039/b704772j
70. Etter MC, Reutzel SM, Choo CG (1993) J Am Chem Soc 115:4411–4412
71. Zaworotko MJ (2007) Cryst Grow Des 7:4–9
72. Hickey MB, Peterson ML, Scoppettuolo LA, Morrisette SL, Vetter A, Guzman H, Remenar JF, Zhang Z, Tawa MD, Haley S, Zaworotko MJ, Almarsson O (2007) Eur J Pharm Biopharm 67:112–119
73. Trask AV (2007) Mol Pharm 4:301–309
74. Desiraju GR (2003) Cryst Eng Commun 5:466–467
75. Dunitz JD (2003) Cryst Eng Commun 5:506
76. Aakeroy CB, Salmon DJ (2005) Cryst Eng Commun 7:439
77. Vishweshwar P, McMahon JA, Bis JA, Zaworotko MJ (2006) J Pharm Sci 95:499–516
78. Stahly GP (2007) Cryst Growth Des 7:1007–1026
79. Bernstein J (2005) Cryst Growth Des 5:1661–1662
80. Nangia A (2006) Cryst Growth Des 6:2–4
81. Bond AD (2007) Cryst Eng Commun 9:833–834
82. Bock H, Holl S (2001) Z Naturforsch B 56:111
83. Hassel OJH (1954) Acta Chem Scand 8:873
84. Hassel O, Stromme KO (1959) Acta Chem Scand 13:1775
85. Bond AD (2003) Chem Commun, pp 250–251
86. Bond AD (2006) Cryst Eng Commun 8:333–337
87. Takayanagi H, Toubai Y, Goto M, Yamaguchi S, Ogura H (1991) Chem Pharm Bull 39:2491
88. Banerjee A, Brown CJ (1985) Acta Crystallogr Sect C Cryst Struct Commun 41:82
89. Herbstein FH, Kaftory M (1976) Acta Crystallogr Sect B Struct Sci 32:387
90. Childs SL, Stahly GP, Park A (2007) Mol Pharm 4:323–338
91. Wilson CC (2001) Acta Crystallogr Sect B Struct Sci B57:435–439
92. Steiner T, Majerz I, Wilson CC (2001) Angew Chem Int Ed 40: 2651–2654
93. Wiechert D, Mootz D (1999) Angew Chem Int Ed 38:1974–1976
94. Braga D, Maini L, Polito M, Grepioni F (2004) Struct Bond 111:1–32
95. Gobetto R, Nervi C, Valfre E, Chierotti MR, Braga D, Maini L, Grepioni F, Harris RK, Ghi PY (2005) Chem Mater 17:1457–1466
96. Gobetto R, Nervi C, Chierotti MR, Braga D, Maini L, Grepioni F, Harris RK, Hodgkinson P (2005) Chem Eur J 11:7461–7471
97. Sreekanth BR, Vishweshwar P, Vyas K (2007) Chem Commun, pp 2375–2377

98. Bucar D-K, Henry RF, Lou X, Borchardt TB, Zhang GGZ (2007) Chem Commun, pp 525–527
99. Zhang GGZ, Henry RF, Borchardt TB, Lou X (2007) J Pharm Sci 96:990–995
100. Childs SL, Hardcastle KI (2007) Cryst Eng Commun 9:364–367

Struct Bond (2009) 132: 51–86
DOI:10.1007/430_2008_6

Published online: 25 February 2009

Porous Coordination Polymers Towards Gas Technology

Satoru Shimomura, Sareeya Bureekaew, and Susumu Kitagawa

Abstract Gas sorption is a key technology for solving the global issues of energy and the environment that beset the world. From the end of the twentieth century, porous coordination polymers have been synthesized and studied as candidates for advanced adsorbents with a wide variety of applications. The regular nanospace of porous coordination polymers shows unique gas molecule capture and creates a new chemistry in the field of porous materials. In this article, we focus on the gas sorption properties of porous coordination polymers. Their uniqueness is illustrated using current representative results and discussed together with perspectives on the gas technology.

Keywords: Gas sorption · Metal–organic framework · Microporous materials · Porous coordination polymer · Self-assembly

Contents

S. Shimomura, S. Bureekaew, and S. Kitagawa (✉)
Department of Synthetic Chemistry and Biological Chemistry, Kyoto University, Katsura, Nishikyo-ku, Kyoto 615-8510, Japan
e-mail: kitagawa@sbchem.kyoto-u.ac.jp

Abbreviations

adip	5,5′-(9,10-Anthracenediyl)di-isophthalate
azpy	4,4′-Azopyridine
1,4-bdc (bdc)	1,4-Benzenedicarboxylate
bdt	1,4-Benzeneditetrazol-5-yl
bipyen	*trans*-1,2-Bis(4-pyridyl)ethylene
BMIm	1-Butyl 3-methylimidazolium
bpdc	4,4′-Biphenyldicarboxylate
bptc	3,3′,5,5′-Biphenyltetracarboxylate
btapa	1,3,5-Benzenetricarboxylic acid tris[*N*-(4-pyridyl)amide]
1,3,5-btb (btb)	1,3,5-Benzenetribenzoate
1,3,5-btc (btc)	1,3,5-Benzenetricarboxylate
cbbdc	1,2-Dihydrocyclobutabenzene-3,6-dicarboxylate
dabco	1,4-Diazabicyclo[2.2.2]octane
DFT	Density functional theory
FCC	Fluidized catalytic cracking
eg	Ethylene glycol
GC	Gas chromatography
GCMC	Grand canonical Monte Carlo
MOF	Metal–organic framework
ndc	2,6-Naphthalenedicarboxylate
OMS	Open metal site
PCP	Porous coordination polymer
pd	Propanediol
pzdc	Pyrazine-2,3-dicarboxylate
pyz	Pyrazine
Pur	Purinate
QM	Quantum mechanics
qptc	Quaterphenyl-3,3‴,5,5‴-tetracarboxylate
tatb	4,4′,4″-*s*-Triazine-2,4,6-triyltribenzoate
TMA	Trimesic acid
tmbdc	Tetramethylterephthalate
tptc	Terphenyl-3,3″,5,5″-tetracarboxylate

ttdc	2,2′:5′,2″-Terthiophene-5,5″-dicarboxylate
Stdc	Styrene-2,5-dicarboxylate
STP	Standard temperature and pressure
UMS	Unsaturated metal center
XRPD	X-ray powder diffraction
ZIF	Zeolitic imidazolate framework

1 Introduction

Low molecular weight molecules such as O_2, N_2, CO_2, CH_4, and alkanes (C2–C3) are gases inevitably associated with human life and thus with global issues of energy and the environment. One of the important key technologies for these gases is "storage." Currently, there are three ways of storage: (i) as liquefied gas (LG) at low temperature, (ii) as compressed gas (CG) at high pressure, and (iii) as adsorption gas (AG) at ambient temperature and low pressure. Among these technologies, the AG method is highly preferable because it is safe, energy-efficient, and requires only light containers for transportation. Conventional materials (inorganic zeolites and activated carbons) are candidates for this purpose; however, they are still not at a practical stage for various reasons. At present, the invention of low pressure gas storage technology is urgent for vehicle fuel tanks and safe transportation of useful but dangerous gases. In addition, high efficiency separation technology, different from conventional distillation, is essential for low-energy separation of petroleum products, air, pollutant gases, and other industrial materials [1, 2].

In this context, porous materials could represent a breakthrough for future technologies in gas storage and separation. Control of pore size and shape is important for separation. For selectivity of the desired gas it is necessary to achieve a pore size in the region of less than 0.1 nm, associated with pore surface functionalization. For example, the kinetic dimensions of oxygen and nitrogen molecules are 0.346 and 0.364 nm, respectively. Therefore, to separate these gas molecules by molecular sieving, we must control pore size more acutely.

Creation of novel porous materials for these purposes is epoch-making in the field and represents a major breakthrough for the future technologies of environmentally, energetically, and biologically important gases such as H_2, CH_4, CO_2, NO etc.

2 Porous Materials

2.1 Conventional Materials

Porous materials have a long history and are always associated with the life of humankind. Activated carbons, which are the oldest and most famous porous materials, were used in a medical setting from as early as 1500 BC [3]. Industrial applications

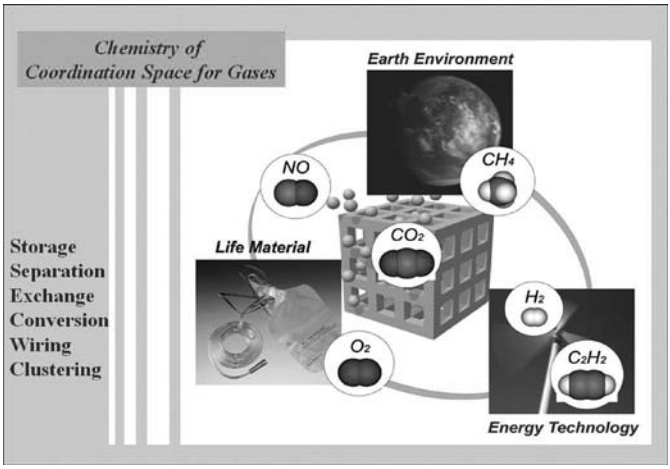

Fig. 1 Properties of porous coordination polymers with gas molecules

originated in the late eighteenth century, when it was discovered that activated carbons could adsorb gases and remove colored bodies from solution. The problems associated with activated carbons are the large distribution in physical and chemical properties, which make them difficult to use in exact studies and applications. These features come from the randomness of the amorphous structure, which has various pore sizes and pore shapes. However, activated carbons have been used extensively in manifold applications because of their inexpensive and convenient source and the simple synthetic method [3, 4]. Later, many kinds of porous materials, such as zeolites, were discovered and synthesized one after the other and used in various situations. Zeolites, which were found in the middle of the eighteenth century, are crystalline hydrated alkaline or alkaline-earth aluminosilicates containing pores and cavities [5]. Today, they are widely used in industrial applications due to their crystallographically defined pore structures and high thermal and chemical stabilities [6–8]. For example, the majority of the world's gasoline is produced by the fluidized catalytic cracking (FCC) of petroleum using zeolite catalysts [9]. On the other hand, there are some problems associated with them. It is difficult to control their exact structure and function, and we cannot design and modify the pore size, pore shape and surface condition with limited inorganic sources. Diversity of design remains as a big issue to be tackled, not only for zeolites but also for other porous materials (Fig. 1).

2.2 Porous Coordination Polymers

In the 1990s, the appearance of new porous compounds with an inorganic–organic hybrid framework made an impact on the field of porous materials and added a new

category to the conventional classification. Porous coordination polymers (PCPs), also known as metal–organic frameworks (MOFs), have completely regular micropores, resulting in a quite large pore surface area and in the highly designable framework, pore shape, pore size, and surface functionality [10–23]. Their structures are constructed with the organic ligands as linkers and the metal centers as connectors. PCPs have both the variety and functionality of the organic materials and the directivity and regularity of the inorganic materials. These components are connected by coordination bonds and other weak interactions or noncovalent bonds (H-bonds, π-electron stacking or van der Waals interactions) to form an infinite network. These interactions have a smaller binding energy than that of a covalent bond, which causes the structural flexibility and dynamics in the crystalline state. This heightens the singularity of PCPs in the field of porous materials [19, 24–26]. In addition, this infinite, absolutely regular structure is formed in a self-assembled system, without any difficulty or careful control. PCPs are adsorbing materials that meet scientific and industrial demands with these features. They have attracted the attention of chemists, physicists, and materials scientists because of interest in the creation of nanometer-sized spaces and the novel phenomena that occur in them. There is also commercial interest in their application in separation, storage, and heterogeneous catalysis.

2.3 Synthesis

The PCPs are generally synthesized in the liquid phase by using solvent as a media. There are four main synthetic methods for PCPs based on liquid phase reactions (saturation methods, diffusion methods, hydro(solvo)thermal methods, and microwave and ultrasonic methods) [20]. They have common procedures: All components (metal ions and organic ligands) are dissolved in the solvents. After that, they are mixed together, and then the solution matrix remains in equilibrium. This means that the final products depend on the synthetic method, even if same starting reactants are used. The products are often dictated by equilibrium solubility, product constant, and potential energy distribution on the synthetic conditions. In highly excited synthetic conditions (e.g., at high temperature) the product will be in the most thermodynamically stable state. Meanwhile, under mild reaction conditions, the product is often the kinetically stable state because of the absence of enough energy to cross an energy barrier. We can get a wide variety of structures by choosing the synthetic method and reaction conditions [27–32]. Recently, synthetic methods for PCPs based on solid phase reactions have started to garner attention.

In *mechanochemical* methods [33], all components are simply ground with no or tiny amounts of solvent media. Mechanochemical methods have the advantage of being able to use insoluble starting materials, which are not suitable for liquid phase reactions. However, the crystals produced from this method are microcrystals, which are too small for X-ray single crystal structural analysis. At this point, it is difficult

to analyze the exact structure of the microcrystals and these methods are used as a new synthetic approach for known materials.

In addition, a simple synthetic method has been studied to respond to the industrial requests for an *electrochemical* approach [34]. In this system, bulk metal plates are arranged as the anodes as well as the metal source in an electrochemical cell, with the organic ligands dissolved in solvent and a metal cathode. This method facilitates the quantity synthesis and the achievement of recyclability, but also remains to be exploited more efficiently and for the scope of the application to be widened.

To obtain fully-engineered PCPs with a desired structure, solvents and counterions should be involved as well as metal ions and organic ligands. They directly affect the equilibrium solubility product constants of all the potential products. In particular, they often play a crucial role in identifying the pore structure of PCPs. Generally, it is impossible to synthesize compounds containing vacant spaces, as nature abhors a vacuum [16]. Hence, the pores will always initially be filled with some sort of guest molecules such as solvent molecules, excess ligands, or counterions. After removal of guest molecules, the void space can be usable. The shape and size of the pores are determined by the included molecules, preventing the construction of dense structure. This means that different pore structures can be isolated with the same starting materials by employing appropriate guest molecules as a template.

Comparison of the following two compounds is a simple example of the template effect on PCPs synthesis. $\{[Co_3(ndc)_3(bipyen)_{1.5}] \cdot H_2O\}_n$ was synthesized by hydrothermal reactions of $Co(NO_3)_2 \cdot 6H_2O$, 2,6-naphthalenedicarboxylic acid (H_2ndc), and *trans*-1,2-bis(4-pyridyl)-ethylene (bipyen) in water (Fig. 2) [35]. The two-dimensional (2D) networks of interconnected $[Co_2(ndc)_{4/2}]$ paddle-wheels are bridged by the bipyen ligands to form threefold interpenetrated three-dimensional (3D) frameworks, which leaves 3D interconnected channels occupied by water molecules, with isolated pore cross-sections of $4.3 \times 4.3\,\text{Å}^2$. $\{[Co_2(ndc)_2(bipyen)] \cdot H_2O \cdot C_6H_6\}_n$ was synthesized under similar conditions except that benzene was added to the reaction mixture. This compound shows another threefold interpenetrated structure of similar primary framework as the former (Fig. 2). This compound has a distorted framework generating free space with two pore sizes that are occupied by lattice water and benzene molecules (6.6×6.2 Å for benzene and 4.4×3.5 Å for water). This result shows that the pore structure (size and shape) of PCPs can be easily designed by employing appropriate templates.

The chirality of the PCPs is also controllable by using the template effect. The three-connected helical (10,3)-a networks can be generated by using the achiral tridentate 1,3,5-benzenetricarboxylate (btc) ligand. The two kinds of related compounds are roughly isolated by selecting the solvent (template molecules) [36, 37]. The first compound $[Ni_3(btc)_2(py)_6(eg)_6] \cdot (eg)_x \cdot (H_2O)_y$ (x = 3, y = 4), in which the small solvent molecules bind in a unidentate fashion, contains fourfold interpenetrating (10,3)-a networks and has 28% accessible solvent volume. The alternative compound $[Ni_3(btc)_2(py)_6(1,2\text{-pd})_3] \cdot 11(1,2\text{-pd}) \cdot 8(H_2O)$, with relatively bulky diol solvent molecules acting as bidentate ligands, shows a greatly enhanced solvent accessible volume of 51%, because only two (distorted) (10,3)-a′ networks interpenetrate. In the latter case, the framework can be grown homochirally from

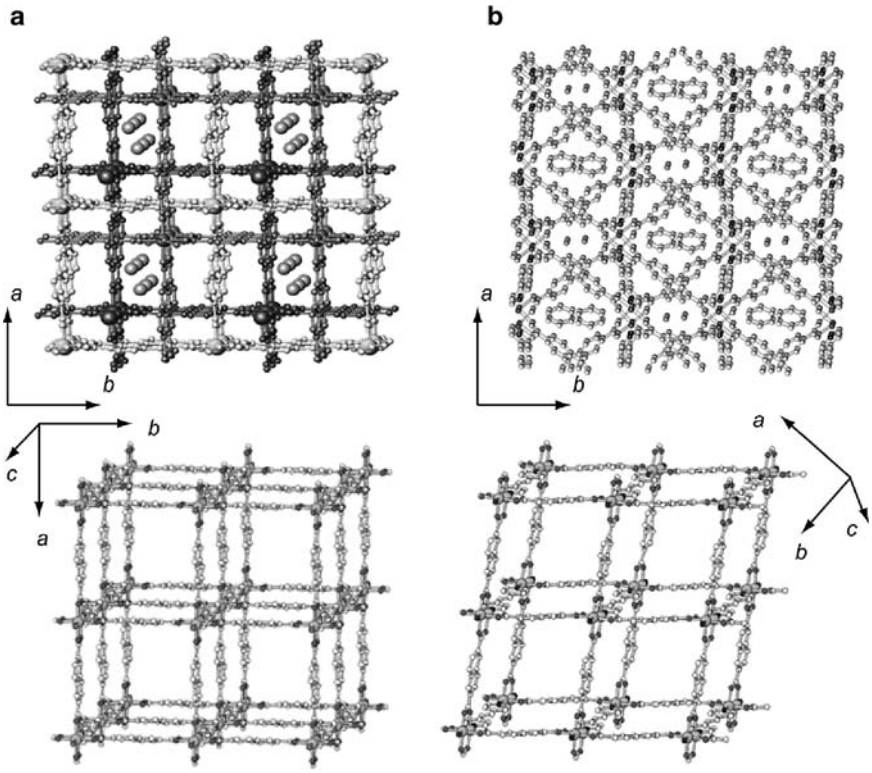

Fig. 2 **a** Structure of $\{[Co_3(ndc)(bipyen)_{1.5}]\cdot H_2O\}_n$ and **b** $\{[Co_3(ndc)(bipyen)_{1.5}]\cdot H_2O\cdot C_6H_6\}_n$. Single structures of **a** and **b** are shown by the *lower framework*. Copyright Wiley

enantiomerically pure diol template bound to the metal center. These structures $[Ni_3(btc)_2]$ represent a successful experience in controling the porosity and even the bulk chirality of PCPs with the template effect.

The use of chiral template that does not act as ligand appears to have considerable scope in the synthesis of chiral frameworks. This method allows the possibility of forming chiral solids from achiral building blocks, which would remove the need for a chiral center in the building units and so vastly increase the potential number of chiral solids. Recently, a chiral induction effect in the ionothermal synthesis was reported [38]. Use of the chiral ionic liquid 1-butyl 3-methylimidazolium (BMIm) L-aspartate produces a homochiral framework $[Ni(TMA-H)_2(H_2O)_2]\cdot(BMIm)_2$ (TMA = trimesicacid) from achiral building blocks that crystallizes in space group $P4_12_12$. In addition, replacing L-aspartate with D-aspartate in the ionic liquid induces a material that crystallizes with the opposite chirality. This result shows a new strategy for creating the homochiral open space with no chiral components. A chiral open framework is an important goal as there are many potential applications such as chiral separation and catalysis. Such an effect may open up new opportunities in the preparation of chiral materials and nanospace.

From this point of view, the key factors for achieving intentional PCPs are not only the selection and combination of metal joints and ligand linkers, but also the solvent or counterion used.

2.4 Relationship Between Porous Properties and Pore Structure

The adsorption of guest molecules onto the solid surface plays an essential role in determining the properties of porous compounds. This adsorption is governed not only by the interaction between guest molecules and the surfaces but also by the pore size and shape. Pores are classified according to their size, as shown in Table 1 [39]. There is no essential difference between adsorption by a macropore and adsorption onto a single surface, and both are explained well by the Brunauer–Emmett–Teller (BET) equation [40]. The adsorption by a mesopore is dominated by capillary condensation, which is responsible for a sharp adsorption rise around the mid relative-pressure region. This effect is not attributable to molecule–solid interactions but to a purely geometrical requirement, which is illustrated well by the Kelvin equation. The adsorption in the micropore should not be considered as that of molecules onto a solid surface but as the filling of molecules into a nanospace, where a deep potential field is generated by the overlapping of all the wall potentials. In this case, the adsorption isotherm shows a steep rise at very low relative pressure, and a plateau after saturation. This feature is effective for trapping gas molecules, which have only weak interactions at ambient condition. Microporosity and ultramicroporosity thus become more and more important in developing gas storage methods and technology.

There are six representative adsorption isotherms that reflect the relationship between porous structure and sorption type. This IUPAC classification of adsorption isotherms is shown in Fig. 3 [41]. These adsorption isotherms are characteristic of adsorbents that are microporous (type I), nonporous and macroporous (types II, III, and VI), and mesoporous (types IV and V). The differences between types II and III and between types IV and V arise from the relative strength of fluid–solid and fluid–fluid attractive interactions. When the fluid–solid attractive interaction is stronger than that of fluid–fluid, the adsorption isotherm will be of types II and IV, and the opposite situation leads to types III and V. The type VI isotherm represents adsorption on nonporous or macroporous solid surfaces where stepwise multiplayer adsorption occurs.

Table 1 Classification of pores

Pore type	Pore size [Å]
Ultramicropore	<5
Micropore	5–20
Mesopore	20–500
Macropore	>500

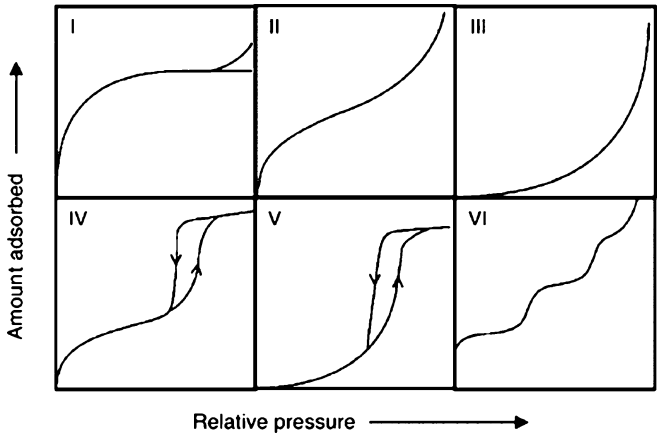

Fig. 3 IUPAC classification of adsorption isotherms. Copyright Wiley

2.5 Pore Structure and Classification of Porous Coordination Polymers

PCPs mainly have uniform micropore or ultramicropore structures. The pore shapes are crystallographically defined and not necessarily modeled by slit-like and cylindrical pores as in conventional porous materials such as activated carbons and inorganic zeolites. The uniform micropore or ultramicropore of PCPs whose sizes are close to the size of guest molecules show unprecedented adsorption properties. In addition, the definitive pore shape enables us to discuss and understand the details of the adsorption phenomena. For example, a square pore possesses four corner sites where a deeper attractive potential for guests is formed by the two pore walls than at the midpoint of the wall [42]. In this case, two-step adsorption is expected in the low relative-pressure region, corresponding to the presence of the two different sites. $[Cu(bpdc)(dabco)_{0.5}]_n$ (bpdc $= 4,4'$-biphenyldicarboxylate, dabco $= 1,4$-diazabicyclo[2.2.2]octane), with the B net of CaB_6, has a uniform square cross-sectional 1D channel with dimensions of $10.5 \times 10.5\,\text{Å}^2$ [43–45]. The Ar adsorption isotherm measured at 87.3 K shows two steps at relative pressure of around 10^{-2}, which correspond to pore sizes of about 9.5 and 12 Å, respectively [46].

Following a suggestion in 1998, PCPs were classified into three categories: first, second, and third generation (Fig. 4) [47]. The first generation compounds have microporous frameworks, which are sustained only with guest molecules and show irreversible framework collapse on removal of guest molecules. The second generation compounds have stable and robust porous frameworks, which show permanent porosity without any guest molecules in the pores. The third generation compounds have flexible and dynamic frameworks, which respond to external stimuli (such as light, electric field, and guest molecules) and change their channels or pores reversibly. Many inorganic porous materials constructed by covalent bonds

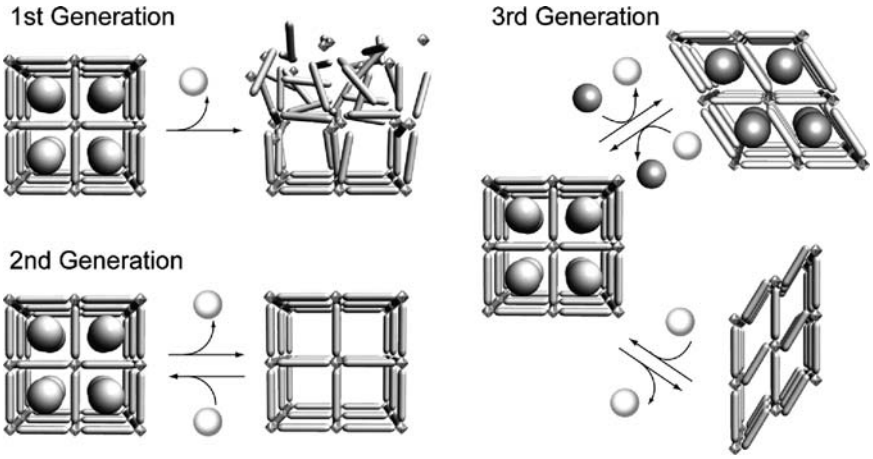

Fig. 4 Classification of porous compounds as first, second, and third generation

are classified as second generation compounds. On the other hand, PCPs could afford not only robust second generation compounds but also flexible and dynamic third generation ones.

The six types of adsorption isotherms assume that the porous host structures are not altered through the sorption process. If the porous hosts have a flexible and dynamic nature (e.g., when a structure transformation from nonporous to microporous occurs during the adsorption), the adsorption isotherm has a novel profile, dissimilar to the conventional type. This phenomenon is one of the advantages of third generation type PCPs with flexible and dynamic frameworks based on weak interactions, such as coordination bonds, hydrogen bonds, $\pi - \pi$ stacking interactions, and van der Waals forces. These dynamic uniform spaces in PCPs establish a platform of revolutionary host–guest chemistry with a transformation of the microscopic molecular motion to the macroscopic transition, which is precisely detected by crystallographic techniques [19,24–26]. They provide detailed information about sorption phenomena and show unconventional guest accommodations and unique porous applications.

3 Gas Sorption

PCPs have infinite networks with backbones constructed by metal ions as connectors and ligands as linkers, and form a family of "inorganic and organic hybrid polymers." The structural integrity of the building units, which can be maintained throughout the reactions, allows for their use as modules in the assembly of extended structures. Werner complexes, β-M(4-methylpyridyl)$_4$(NCS)$_2$ (M = Ni(II) or Co(II)) [48], Prussian blue compounds [49–51], and Hofmann clathrates and their

derivatives have frameworks that are built of CN-linkages between square-planar or tetrahedral tetracyanometallate(II) units and octahedral metal(II) units coordinated by complementary ligands [51], which are known to be materials that can reversibly absorb small molecules. An early report also exists regarding the use of the organic bridging ligand to form the PCP $[Cu(NO_3)(adiponitrile)_2]_n$ with a diamond net; however, the adsorption behavior was not reported [52].

Since the early 1990s, the amount of research on the structure of PCPs has increased greatly, and some examples with functional micropores have started to appear. The structural entity of a cavity could be related to a porous property. In 1990, Robson et al. reported the possibility of anion exchange by soaking a PCP crystal in anion-containing solvent [53]. Subsequently, a study on catalytic properties for 2D Cd(II)-4,4′-bpy (bpy = bipyridine) coordination polymer was done by Fujita et al. in 1994 [54]. In 1995, guest adsorption was studied in liquid/solid phases by the groups of Yaghi [55] and Moore [56]. However, with the use of organic molecules, the structural robustness after removal of guest molecules was hardly believed by researchers in inorganic materials because recrystallization is the preferable way for exchange/removal–inclusion of guest molecules or ions. Even though the experiments were carried out in liquid/solid phases, a gas/solid phase experiment had been expected to demonstrate that PCPs have porous structures without guests. Ultimately, the first gas adsorption at ambient temperature was carried out in 1997 by the authors' group [57], which showed that recrystallization is not the case for PCPs. Since the epoch-making work, the robustness of PCPs has been accepted and PCPs are recognized as porous compounds. In a surprisingly short period, their structural chemistry has attained a mature stage. A survey of the research works in recent years shows an extraordinary increase in the number of published articles. Now, PCPs are gaining an important position in porous materials and adding a new category to the conventional classification.

The adsorption enhancement occurs as a result of the multiple attractive interactions by confronting and neighboring pore walls; this is characteristic of the nanometer-sized space of a ultramicropore (pore size < 2 nm) [41]. This adsorption enhancement effect is useful not only for its application with gas storage materials and heterogeneous catalysts, but also for the unique properties of confined molecules that are different from those of the bulk fluid. Ultramicropore filling, also termed primary micropore filling [58], occurs at very low relative pressure (P/P_0); it is associated with enhanced adsorbent–adsorbate interaction and results in a significant distortion of the isotherm, as in the case of chemisorption. Generally, in chemisorption guest molecules are bound to specific adsorption sites via a chemical bond, whereas physisorption is nonspecific adsorption without any specific binding sites. This is because the dispersion force, which dominates physisorption, is not usually very sensitive to surface properties.

Small gas molecules under ambient condition have weak intermolecular interaction. To challenge the effective storage of these molecules at ambient temperature, PCPs possess many advantages compared to other porous compounds such as zeolites and activated carbons. Highly ordered and dense ultramicropores or micropores showing the strong adsorption enhancement effect as above can be easily

constructed by self-assembly synthetic schemes. The pores delimited by only one organic ligand achieve quite high porosity and effective storage in dilute conditions. The greatest superiority of PCPs is the designability of the framework and the pore surface, which provides a variety of surface properties based on organic ligands, affording unique functionalities on the channel surface. In the future this will provide a chemically interactive pore surface and make PCPs a groundbreaking adsorbent for the storage of small molecules, which are difficult to store by chemical binding and accommodation because of their weak intermolecular interactions.

The sorption of N_2 or Ar gas at low temperature is generally used for the evaluation of micropores [32, 45, 59–140]. N_2 and Ar are typical inert gases with no chemical interaction with the adsorbent. This nature is appropriate for application of α_s-analysis and the Dubinin–Radushkevich (DR) equation, which provides several micropore parameters such as micropore volume, surface area, and isosteric heat of adsorption.

The specific surface area is one of the most important factors for evaluating the pore capacity, and is associated with the number of guest molecules accommodated by direct contact. Recently, the specific surface areas attainable with coordination polymers have increased from $500\,m^2\,g^{-1}$, comparable to that of zeolites, to a very large value of $5000\,m^2\,g^{-1}$. This value is much higher than the ideal value of carbon materials, $2630\,m^2\,g^{-1}$, which is calculated as the sum of two surfaces of graphite planes. For instance, chromium compound $Cr_3OF(bdc)_3$ (bdc = 1,4-benzenedicarboxylate) (MIL-101) [87] and Zn(II) carboxylate cluster-based coordination polymer $Zn_4O(btb)_3$ (btb = 1,3,5-benzenetribenzoate) (MOF-177) [78] show exceptional N_2 sorption properties (MIL-101: type I, $1250\,cm^3\,(STP)\,g^{-1}$ at 78 K, 750 Torr; MOF-177: type I, $1030\,cm^3\,g^{-1}$, 78 K, 746 Torr) and have large surface areas (5900 and $4500\,m^2\,g^{-1}$, respectively) (STP = standard temperature and pressure). In practice, the thinner the walls of the pores, the higher the specific surface area. In the case of inorganic zeolites, the pore walls are constructed with a thickness of at least several Si, O, and Al atoms, whereas coordination polymers afford thin walls. For instance, when the wall is of 1,4-terephthalic acid it is only one carbon atom thick, which shows that almost all the atoms constructing porous frameworks can be used as a surface.

4 Gas Storage

4.1 Methane Storage

The ability to store a desired chemical substance is a typical property of porous materials. Methane (CH_4) is the main component of natural gas, which is an important candidate for clean transportation fuels. The storage of CH_4 by adsorbents has been pursued vigorously as an alternative to compressed gas storage at high pressure. However, the conventional adsorbents have afforded insufficient capacity

of CH_4 storage to meet the conditions required for commercial viability. Even in activated carbons with large specific surface area and micropores, a high percentage of the mesopores and macropores are not effective for CH_4 adsorption because the single surface cannot trap CH_4 molecules and therefore the large voids are useless. To achieve higher adsorption capacity, it is necessary to ensure that micropores with sizes well suited to methane molecules are densely and uniformly distributed in the solid. PCPs are therefore good candidates as adsorbents for CH_4 storage.

Measurement of CH_4 gas adsorption for PCPs was first carried out by using a coordination polymer, $\{[Co_2(4,4'\text{-bpy})_3(NO_3)_4]\cdot 4H_2O\}_n$, which adsorbs about $52\,cm^3\,(STP)\,g^{-1}$ of CH_4 at a temperature of 298 K and a pressure of 30 atm [57]. In 3D pillared-layer coordination polymers CPL-1, 2, and 6, approximately 18, 56, and $65\,cm^3\,(STP)\,g^{-1}$ of CH_4 are adsorbed at 298 K and 31 atm, respectively. The triply interpenetrated framework of $\{[Cd_2(NO_3)_4(azpy)_3]\cdot 2Me_2CO\}_n$, (azpy = 4,4′-azopyridine), which creates microporous channels despite the interpenetration, also adsorbs a certain amount of CH_4 ($40\,cm^3\,(STP)\,g^{-1}$ at 298 K and 36 atm) [141]. This is the first case to demonstrate gas adsorption for interpenetrated coordination polymers. Compounds $\{[Cu(AF_6)(4,4'\text{-bpy})_2]\cdot 8H_2O\}_n$ (A = Si and Ge) show a high CH_4 adsorption activity at room temperature and relatively low pressure (134 and $46\,cm^3\,(STP)\,g^{-1}$ for A = Si and Ge, respectively, at 298 K and 36 atm) [72, 142].

In this century, other types of complexes with high CH_4 capacity have been successively synthesized (Table 2) [26,43–45,57,60,70,72,74,77,88,106,108,110,115, 117,121,122,127,129,131,135,141–150]. IRMOF-6 affords a 3D cubic porous network and has high surface area of $2630\,m^2\,g^{-1}$, estimated by applying the Langmuir equation [70]. The CH_4 adsorption isotherm was found to have an uptake of $240\,cm^3$ (STP) g^{-1} ($156\,cm^3$ (STP) cm^{-3}) at 298 K and 36 atm. On the basis of volume (v/v), the amount of methane adsorbed by IRMOF-6 at 36 atm represents 70% of the amount stored in compressed methane cylinders in laboratories where much higher, unsafe levels of pressure (205 atm) are used. Other types of highly adsorbant PCPs are reported, in which 2D carboxylate-bridged polymers of $[Cu(OOC\text{-L-}COO)]_n$ (L = Ph, CH = CH, Ph–Ph, Ph–CH = CH), which have methane adsorption ability in

Table 2 CH_4 storage of porous coordination polymers

Compound	CH_4 uptake	Conditions		Apparent surface area	Pore diam.	Ref
		Temp.	Pressure			
	$[cm^3\ (STR)\ g^{-1}]$	[K]	[atm]	$[m^2g^{-1}]$	[Å]	
$[Co_2(4,4'\text{-bpy})_3(NO_3)_4]$	52	298	30	–	$3,3\times 6$	[57]
$[Cu(SiF_6)(4,4'\text{-bpy})_2]$	134	298	36	1337	8	[142]
$[Zn_4O(cbbdc)_3]$ (IRMOF-6)	240	298	36	2630	9.3	[70]
$[Cu_2(bpdc)_2(dabco)]$	212	298	35	3265	10.8	[43]
$[Cu_2(Stdc)_2(dabco)]$	213	298	35	3129	9.5	[43]
$[Cu_2(H_2O)_2(adip)]$	253	290	35	1753	9.23	[150]

themselves [144], are bridged by dabco to form more highly porous 3D networks of $[Cu(OOC\text{-}L\text{-}COO)(dabco)_{0.5}]_n$ with the topology of the net of B in CaB_6 [43–45]. In particular, the polymers with L=Ph–Ph and Ph–CH=CH adsorb 212 and 213 cm^3 (STP) g^{-1} (179 and 199 cm^3 (STP) cm^{-3}), respectively, at 298 K and 35 atm [43,45]. Analyses of high-resolution Ar adsorption isotherms at 87.3 K yield BET surface areas of 3265 and 3129 $m^2 g^{-1}$ for L=Ph–Ph and Ph–CH=CH, respectively. The adsorption amount of CH_4 molecules at around 35 atm appears to increase with the increase of cross-sectional channel size; however, this is not true. There could be an upper limit to the size of square pores of $(11–12) \times (11–12)$ $Å^2$, where a size suitable to fit CH_4 molecules and potential deep enough to store methane are realized.

4.2 Hydrogen Storage

Hydrogen (H_2) has attracted a great deal of attention as an energy source. Once it is generated, its use as a fuel creates neither air pollution nor greenhouse gas emissions. However, no practical H_2 storage and transportation have yet been developed. So, the development of H_2-fueled vehicles and portable electronics will require new materials that can store large amounts of H_2 at ambient temperature and relatively low pressures with small volume, low weight, and fast kinetics for recharging. In the field of PCPs, H_2 adsorption is the noticeable issue and, recently, has been carried out with various compounds [32,79,81,83,84,86,89,90,93, 97–107,109,110,115,117–122,126–130,132,134–137,140,149,151–174].

There are two different approaches for H_2 storage in solid-state porous materials. The first one is to achieve chemisorption, making a chemical bonding between H_2 molecules and solids, which allows a very high volumetric density at near ambient temperatures and pressures. The second one is to achieve physisorption of hydrogen on the surface of solids, whose binding energies are much lower than for chemisorption. This process has significant capacity but at a low temperature, typically that of liquid nitrogen.

Several PCPs showed the uptake of H_2 and there are new findings on improving the efficiency and uptake value (Table 3, 4). For example, MOF-5, a Zn(II) cluster–dicarboxylate coordination polymer with large cubic cavities, adsorbs up to 4.7 wt% under 60 bar at 77 K and 1.0 wt% under 20 atm at room temperature [151]. MOF-505, with $Cu_2(CO_2)_4$ paddle-wheel units, shows good H_2 adsorption properties, adsorbing an exceptional 2.47 wt% at 1 atm and 77 K [83]. MIL-101b, with trimeric chromium(III) octahedral clusters and abnormally large cavities, exhibits H_2 uptake at ambient temperatures (0.43 wt% under 8 MPa) and at 77 K (6.1 wt% at 8 MPa), but saturation is almost reached above 4 MPa [164]. These compounds contain open metal sites (OMSs) or unsaturated metal centers (UMCs) functionalizing the pore surface to interact with H_2 molecules (Fig. 5).

Several neutron diffraction studies revealed that OMSs act as the binding sites for H_2 molecules in PCPs [99, 166]. This result provides the possibility for strong

Table 3 H_2 storage of porous coordination polymers at low temperature

Compound	H_2 uptake	Conditions		Apparent surface area	Pore diam.	Ref
		Temp.	Pressure			
	[wt%]	[K]		$[m^2g^{-1}]$	[Å]	
$Zn_3(bdt)_3$	1.46	77	880 Torr	640[a]	19.6	[100]
$Cu_3[Co(CN)_6]_2$	1.8	77	890 Torr	730[a]	–	[156]
$Co_3(bpdc)_3(4,4'\text{-bpy})$	1.98	77	1 atm	922[a]	8	[158]
$Cu_3(TMA)_2$ (HKUST-1)	2.27	77	1 bar	1154[a]	3.5/9	[168, 174]
$Mo_3(TMA)_2$	1.75	77	1 atm	1280[a]	–	[103]
$Zn_2(bdc)_2(dabco)$	2.0	78	1 atm	1450[a]	7.5	[79]
Zn_2(bdc)(tmbdc)(dabco)	2.0	78	1 atm	1100[a]	3.5/8	[84]
Cu_2(bptc) (MOF-505)	2.59	77	1 bar	1670[a]	6.7/8.3/ 10.1	[84, 105]
Cu_2(tptc)	2.52	77	1 bar	2247[a]	7.3	[105]
Cu_2(qptc)	2.24	77	1 bar	2932[a]	8.3	[105]
$Cu_3(tatb)_2$	1.9	77	760 Torr	3800[b]	5/9.2	[113]

[a]BET surface area
[b]Calculated from N_2 adsorption datacollected at 77 K using the Langmuir model, except where indicated

Table 4 H_2 storage of porous coordination polymers at high pressure condition

Compound	H_2 uptake	Conditions		Apparent surface area	Pore diam.	Ref
		Temp.	Pressure			
	[wt%]	[K]	[bar]	$[m^2g^{-1}]$	[Å]	
[Al(OH)(bdc)] (MIL-53(Al))	3.8	77	1.6 MPa	1100[b]	8.4	[152]
CrOF$(btc)_2$ (MIL-100(Cr))	3.3	77	25	2700[b]	25/29	[164]
$Cr_3OF(bdc)_3$ (MIL-101(Cr))	6.1	77	60	5500[b]	8.6/29/34	[164]
Cu2(bptc)	4.02	77	20	1670[a]	6.5	[105]
Cu2(tptc)	6.06	77	20	2247[a]	7.3	[105]
Cu2(qptc)	6.07	77	20	2932[a]	8.3	[105]
$Cu_3(btc)_2$ (HKUST-1)	3.6	77	50	1958[b]	3.5/9	[165, 167]
$Zn_4O(bdc)_3$ (MOF-5)	4.7	77	50	2296[a]	11.2	[165, 167]
$Zn_4O(cbbdc)_3$ (IRMOF-6)	4.8	77	50	3300[b]	9.3	[168]
$Zn_4O(ttdc)_3$ (IRMOF-20)	6.7	77	70	4590[b]	14	[168]
$Zn_4O(btb)_3$ (MOF-177)	7.5	77	70	5640[b]	11/17	[168]

[a]BET surface area
[b]Calculated from N_2 adsorption data collected at 77 K using the Langmuir model, except where indicated

accommodation, which may explain the present hydrogen-storage properties observed at ambient temperature. However, although these compounds have large pores, high porosity, and highly interactive sites, the H_2 sorption properties are not enough for practical use. An interesting study on the effect of pore size of PCPs on adsorption reveals that H_2 sorption is pore-size dependent [105]. The three Cu complexes with biphenyl, terphenyl, and quaterphenyl tetracarboxylic ligands forming

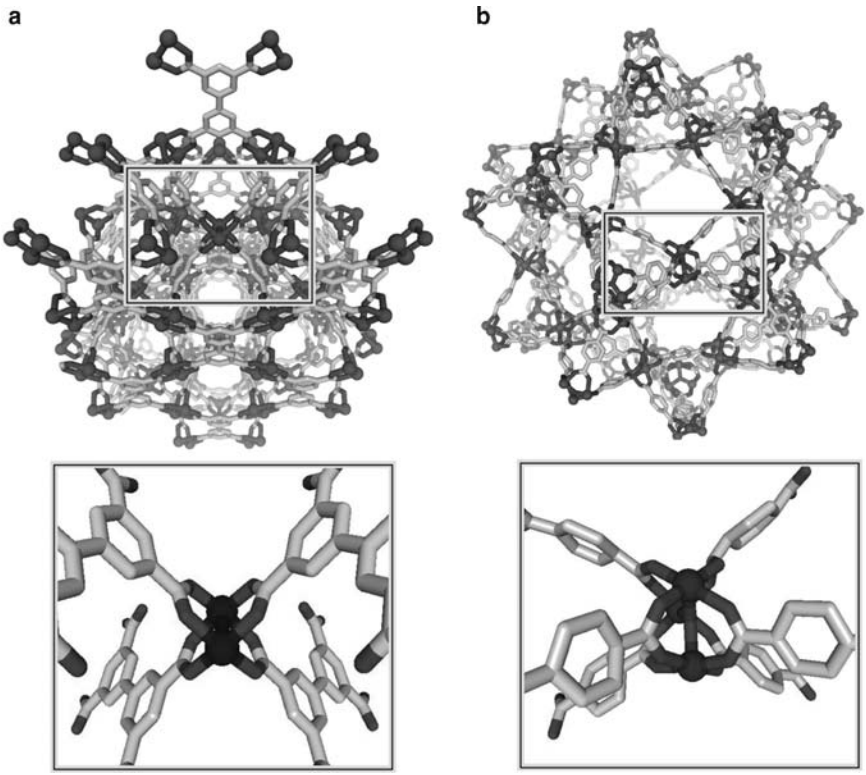

Fig. 5 Structure and coordination geometry around OMS of **a** MOF-505 and **b** MIL-101b

$Cu_2(CO_2)_4$ paddle-wheel units show good H_2 sorption capacities of 2.59, 2.52, and 2.24 wt% at 78 K (1 bar). Interestingly, the quaterphenyl compound has the lowest H_2 adsorption despite having the largest pore size and pore surface area. The saturated H_2 sorption of this compound at 20 bar is almost same as the H_2 sorption of terphenyl compound with smaller pore volume and pore surface (terphenyl compound: 6.06%; quaterphenyl compound: 6.07%). When we aim to achieve H_2 sorption at ambient conditions, a key factor is an affinity for H_2 molecules, but not big pores nor high porosity.

4.3 Carbon Dioxide Capture

Global warming is a serious environmental issue. The technology for selective capture and immobilization of carbon dioxide (CO_2), which is the main greenhouse gas, is required today. Adsorption-based processes can help to develop this. Some studies have raised the possibility of zeolites and activated carbons as candidates for adsorbent materials to achieve the separation and storage of CO_2, but they are not

adequate in terms of efficiency and cost. There is a demand for an effective strategy and an improvement in providing CO_2 sorption technology within an environmentally friendly and low-cost system.

In the field of PCPs, CO_2 sorption is also one of the important targets [26, 59, 62–64, 68, 73, 77, 88, 92, 97, 106, 107, 115, 117, 121, 122, 127, 129, 135, 137, 145, 148, 149, 153, 175–187]. MOF-177 shows high CO_2 adsorption capacity at ambient temperature (33.5 mmol g^{-1}, 35 bar), which is far greater than that of the other porous materials reported [180]. Compared with zeolite 13X (7.4 mmol g^{-1}, 32 bar) and MAXSORB (25 mmol g^{-1}, 35 bar), PCPs have the possibility to be materials with remarkable CO_2 capture capability, which is based on the high microporosity and completely regular pore structure.

The interactive pore surface of MIL-53(Cr) with bridged hydroxyl groups can trap CO_2 molecules and enhance the CO_2 adsorption capacity [188]. In MIL-53, the unique vibration modes of CO_2, which are not observed in the gas phase, can be observed. In addition, adsorption of increasing amounts of CO_2 leads to the appearance of two new bands, which are assigned to the perturbations of both $\nu(\mathrm{OH})$ and $\delta(\mathrm{OH})$ bands (Fig. 6). These phenomena show the existence of CO_2 interacted

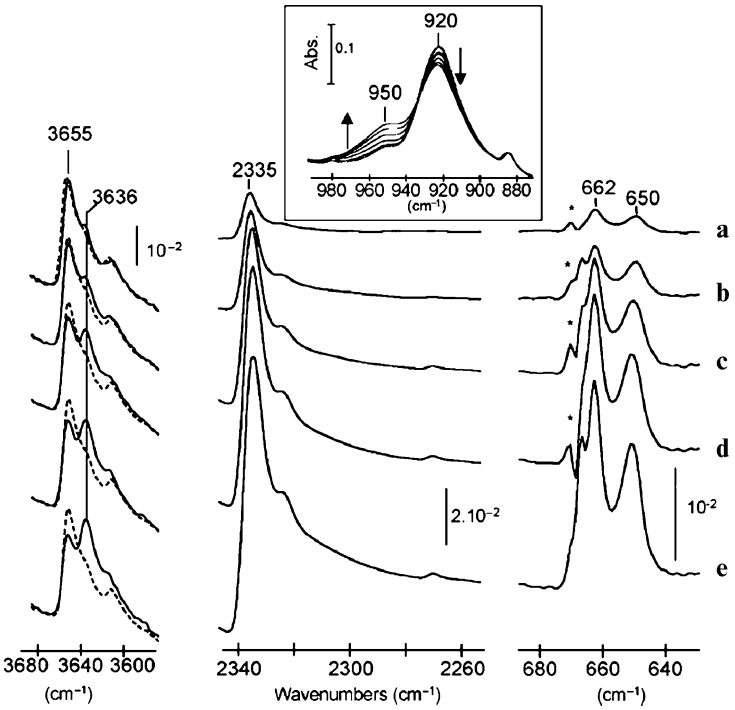

Fig. 6 CO_2 introduction on MIL-53(Cr) activated at 473 K. Spectra of activated MIL-53(Cr) deposited on silicon wafer (*dotted lines*) and then after introduction of increasing CO2 equilibrium pressures into the cell (*solid lines*): **a** 1066 Pa, **b** 2400 Pa, **c** 3850 Pa, **d** 5000 Pa, **e** 5850 Pa. *Inset*: perturbation of the $\delta(\mathrm{OH})$ mode upon CO_2 adsorption. * indicates a residual contribution of the $\nu 2$ band of CO_2 gas in the spectra. Copyright RCS

with the oxygen atom of μ_2-OH groups. Design of such interaction between gas molecules and framework is one of the most important factors in achieving high adsorption properties.

4.4 Gas Molecule Array

The properties of small molecules in ordered, solid form are particularly interesting. In the case of oxygen (O_2), it exhibits a form of magnetism known as antiferromagnetism (in which the spins of neighboring electrons align pointing in opposite directions) and displays metallic conductivity and superconductivity [189]. In addition, the lower-dimensionally confined forms of gas molecules are expected to provide novel magnetic and optical properties [190]. However, it is difficult to achieve these molecular in confined forms with existing methods without extremely high pressures and/or cryogenic conditions.

PCPs are one of the most plausible candidates for the formation of specific molecular arrays under mild conditions because of their highly designable nature and pore homogeneity [18, 70, 84, 91, 142, 143]. Sometimes, 1D arrays of solvent molecules result from the crystallization process [191–194]. O_2 and NO are among the smallest stable paramagnetic molecules under ambient conditions and have the potential to form new molecular-based magnetic and/or dielectric materials. However, there have not been many successful attempts to form 1D arrays of these paramagnetic gas molecules through confinement of the molecules in PCPs [195] or microporous carbon materials [58, 196]. Therefore, to form a regular assembly of simple molecules in nanochannels, an important key idea is that we use not only the strong confinement effect of nanospace but also the commensurability between the host structure and the guest molecule.

As mentioned above, the amount of gas adsorbed in each unit pore of $[Cu_2(pzdc)_2(pyz)]$ (pzdc = pyrazine-2,3-dicarboxylate, pyz = pyrazine) (CPL-1) shows precisely integral values [88, 197]. This commensurate adsorption clearly indicates the formation of molecular arrays in the 1D channel of CPL-1. Therefore, to elucidate the structure of the adsorbed molecules, we first performed in-situ X-ray powder diffraction (XRPD) measurements for CPL-1 accommodating O_2 molecules, and succeeded in determining a 1D ladder structure of the O_2 molecular array. Direct observation of guest molecules accommodated in porous materials by X-ray and neutron structural analysis is very useful for studying guest adsorption phenomena [79, 88, 138, 147, 159, 160, 177, 179, 198–212]. The overall crystal structure and geometry of O_2 molecules are represented in Fig. 6. Two O_2 molecules are aligned parallel to each other along the *a*-axis with an inclination of 11.8° and an intermolecular distance of 3.28(4) Å. This intermolecular distance is close to the nearest distance in solid α–O_2 phase, whose close-packed structure appears below 24 K. This result indicates that O_2 molecules adsorbed in nanochannels form van der Waals dimers, $(O_2)_2$. Each dimer aligns along the axis to form a 1D ladder-like structure.

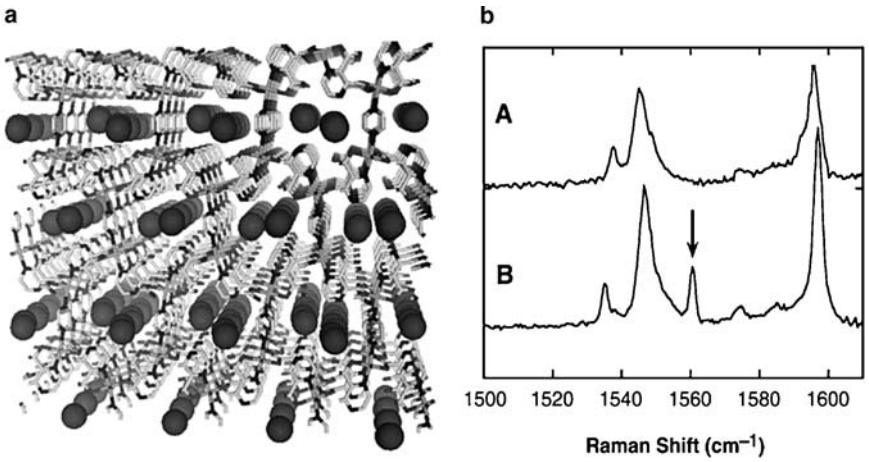

Fig. 7 **a** Overall crystal structure of O_2-accommodated CPL-1. The framework and O_2 molecules are represented by stick and van der Waals surface models, respectively. **b** Raman spectra of **A** CPL-1 and **B** CPL-1 with O_2 molecules. A peak due to the stretching of O_2 molecules (marked by an *arrow*) is shown in **B**. The abscissas were calibrated using the standard lines from a neon lamp, and the resolution of the data is $0.6\,cm^{-1}$. Copyright Elsevier

The X-ray structure analysis reveals that O_2 molecules are in the solid state rather than the liquid state, even at 130 K under 80 kPa, which is much higher than the boiling point of bulk O_2 under atmospheric pressure (54.4 K). This result is ascribed to the strong confinement effect of CPL-1. The magnetic susceptibility for adsorbed O_2 molecules approaches zero with decreasing temperature, which indicates a nonmagnetic ground state of the antiferromagnetic dimer $(O_2)_2$. The Raman spectrum of the O_2 stretching-vibration mode appears as a sharp peak at a higher energy than that of solid α–O_2 under atmospheric pressure and comparable to that of α–O_2 under 2 GPa (Fig. 7) [213].

Interestingly, even under the pressure lower than the saturated vapor pressure, the densities of the adsorbed phases of O_2 were much greater than those of the corresponding bulk liquid phases. This indicates that the adsorbed molecules are significantly different from the bulk state and, therefore, are considered to be a new state characteristic of molecules confined in the ultramicropore of CPL-1. These phenomena have been observed in the linear chain of a coordination polymer; O_2 molecules are trapped and form the structure in the space between the 1D coordination polymers [147, 212, 214].

CPL-1 can show a high adsorption capability for specific molecules as a result of the designed channel surface. As-synthesized complex CPL-$1 \cdot 2H_2O$ shows an interesting aspect of the pore. The water molecules, acting as guest molecules, are connected to the oxygen atoms of the carboxylate groups on the pore surface in a one-to-one fashion, indicating that the oxygen atoms act as basic adsorption sites for guest molecules (Fig. 8). Accordingly, it is expected that CPL-1 would exert an effective sorption ability on small molecules having acidic parts by a deep van

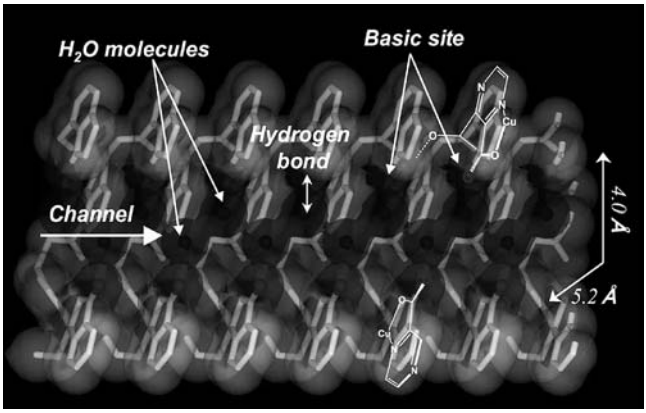

Fig. 8 Channel structure of as-synthesized CPL-1. 1D array of water molecules supported by oxygen atoms on the pore surface in CPL-1, displayed by stick and van der Waals surface models. Copyright Elsevier

der Waals-type potential energy well [215] and additional hydrogen-bonding interaction. The C_2H_2 molecule has a linear form with acidic hydrogen atoms at both ends ($pK_a = 25$). On the other hand, the CO_2 molecule has a rod-shaped form with the dimension of 3×5 Å, similar to that of C_2H_2. However, it has no acidic protons, therefore, we call attention to CPL-1 as a feasible adsorbate for the C_2H_2 molecule.

A marked difference in the C_2H_2 and CO_2 adsorption isotherms was observed. The adsorption isotherms of C_2H_2 show a steep rise at the very low-pressure region and reach saturation, whereas those of CO_2 show a gradual adsorption (Fig. 9). The saturated amount of C_2H_2 corresponds to just one molecule per unit pore. The maximum ratio of the adsorbed amount of C_2H_2 relative to that of CO_2 is 26.0 (at 1.1 kPa) at 270 K, indicating that CPL-1 accommodates C_2H_2 more preferentially than CO_2. The isosteric heat (q_{st}) at the fractional filling ratio of 0.2 of C_2H_2 is 42.5 kJ mol^{-1}, higher than that of CO_2, 31.9 kJ mol^{-1}. These results indicate a higher enhancement in the interaction of C_2H_2 with CPL-1 than that of CO_2.

In the acetylene-accommodated structure, only one C_2H_2 molecule locates in the middle of the channels, whose stoichiometry is in good agreement with that of the adsorption measurement. In the channel, the C_2H_2 molecules align along the axis with an inclination of 78.1° and an intermolecular distance of 4.8 Å. This indicates that they are densely packed with a short intermolecular distance, while avoiding the close contact that induces an explosion. Each end of the C_2H_2 molecule is oriented to the two noncoordinated oxygen atoms on the pore wall. The distance between one hydrogen atom of C_2H_2 and the oxygen atom was found to be 2.2 Å, which is smaller than the sum of the van der Waals radius of hydrogen and oxygen atoms (2.6 Å) indicative of the typical O–HC hydrogen bond. These interactions strongly fix the C_2H_2 molecule in every periodic unit pore and isolate the C_2H_2 in

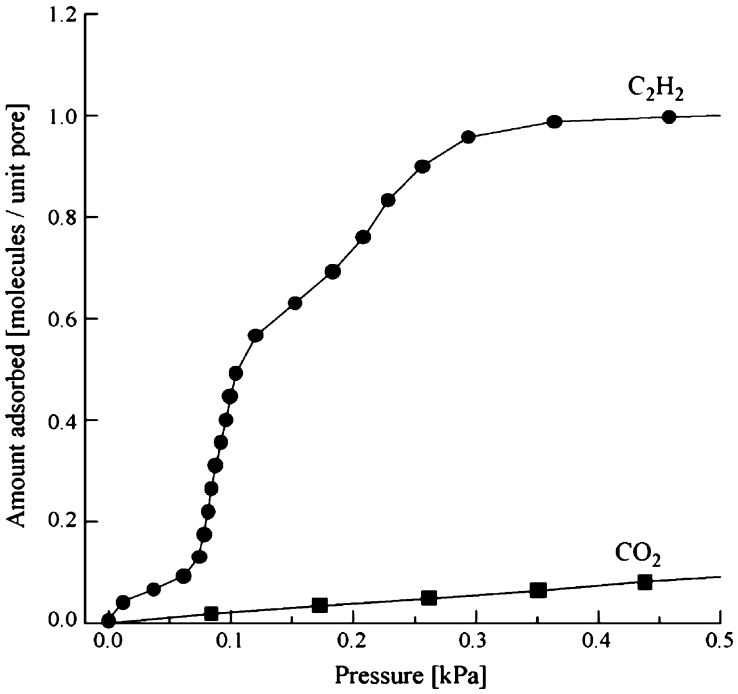

Fig. 9 Adsorption isotherms of C_2H_2 and CO_2 on CPL-1. Copyright Elsevier

the 1D channel, which gives rise to the enhancement of the "confinement effect" and enables the stable accommodation.

It is worth noting that the density of adsorbed C_2H_2 is estimated to be $0.434\,g\,cm^{-3}$; the density is equivalent to that of an extrapolated state of acetylene at 41 MPa at room temperature, and is 200 times larger than the value of the compression limit for the safe use of C_2H_2 at room temperature (0.20 MPa, $0.0021\,g\,cm^{-3}$) [216].

The specific sorption ability of CPL-1 for C_2H_2 is ascribed to the proper and regular arrangement of the two basic oxygen atom sites for an acetylene molecule. Usually, small molecules are adsorbed in a micropore, where van der Waals-type potential operates efficiently. When functional sites are added to the pore, the enhancement of the confinement effect is evidently observed. Furthermore, the stoichiometric guest incarceration is obtained with a commensurate structure of guest array with respect to that of host. According to the results, when the multiple specific interaction sites are located at suitable positions on the regular micropore, the specific adsorption system to the target molecule can be realized.

4.5 Computational Study

Recently, some computational studies on the sorption properties of PCPs have been performed [124, 217–227]. They not only provide a rationale for the sorption phenomena but also are able to predict the potential sorption capacity.

The host–guest interactions between CPL-1 and C_2H_2 are elucidated by binding energy estimations of various configuration of C_2H_2 in the pore [199]. As the molecule does not collide during the rotation, one rotation axis was defined as the axis existing in a plane perpendicular to the *b*-axis, among axes perpendicular to the acetylene molecule. The effective hydrogen bond would be cleaved immediately as the rotational angle increases; the relative energy increases by up to $45\,\mathrm{kJ\,mol^{-1}}$ as the rotational angle increases from 0° to 80° and, similarly, it increases as the rotational angle decreases from 0° to −90°. This results shows that the acetylene molecule is highly stabilized by two hydrogen bonding supports (Fig. 10)

Based on the accumulated crystallographic and adsorption data of PCPs, Monte Carlo (MC) simulations of small-molecule adsorption have been performed, which is an approach that is common in carbon and inorganic materials chemistry [58, 228, 229]. For the simulation, the PCPs have an advantage in that their well-characterized regular structure precludes the need to make assumptions about the host structures. The MC simulations were carried out using formal HF-based and B3LYP-based charge densities for the frameworks $[Zn(1,4\text{-bdc})]_n$ and $[Cu_3(1,3,5\text{-btc})_2]_n$ [230]. The isosteric heats of adsorption for N_2, Ar, and H_2, are small and lie in the range of values for physisorption ($<10\,\mathrm{kcal\,mol^{-1}}$). In the case of the $[Cu_3(1,3,5\text{-btc})_2]_n$ framework, the adsorbed Ar tends to distribute in a four-leaf-clover-like shape. The effect of axially coordinated water molecules influences the adsorption; the amount of adsorbed Ar at low pressure in the presence of coordinated water is higher than that of water-free $[Cu_3(1,3,5\text{-btc})_2]_n$, while the value for water coordinated $[Cu_3(1,3,5\text{-btc})_2]_n$ is smaller than that for water-free $[Cu_3(1,3,5\text{-btc})_2]_n$

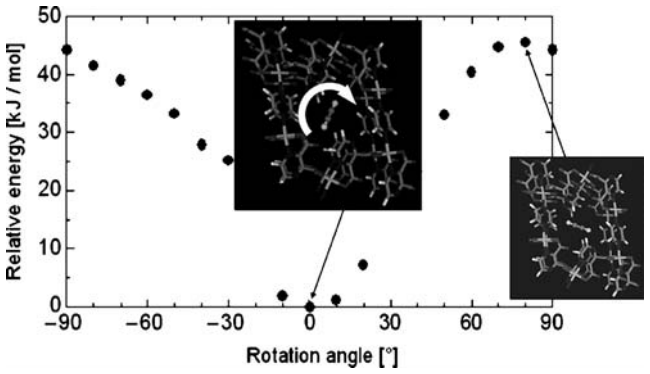

Fig. 10 Relative energy diagrams accompanying the rotation of the acetylene molecule, estimated by the first-principles calculations. Copyright Nature Publishing Group

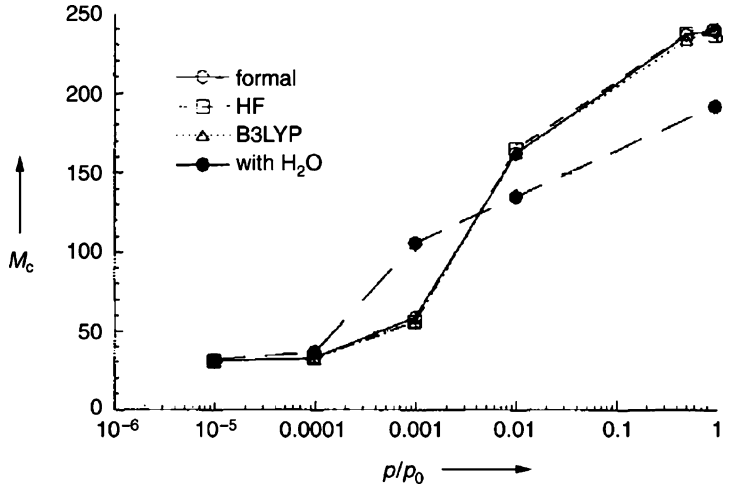

Fig. 11 Calculated isotherms of adsorbed Ar in [Cu3(1,3,5-btc)$_2$]. Three models for the charge densities on each atom of the framework are used: formal charge, HF/4–31G, and B3LYP4–31G (M_c = molecules per cell). Copyright Wiley

(Fig. 11). The coordinating water enhances adsorption but also narrows the cavity available for Ar.

IRMOF materials have been examined for high CH_4 adsorption capacity by using grand canonical MC (GCMC) simulations [217]. The experimental adsorption isotherms of IRMOF-1 and IRMOF-6 have been quantitatively predicted and the simulation suggested that the CH_4 uptake observed experimentally in IRMOF-6 (155 cm^3 (STP) cm^{-3} at 35 bar) is due to physical adsorption. In addition, the simulation for new, not yet synthesized isostructural materials of IRMOF using 1,4-tetrabromobenzenedicarboxylate and 9,10-anthracenedicarboxylate as linker molecules showed substantially higher uptake of CH_4 than IRMOF-6 (by 23 and 36%, respectively); however, those pore surface areas are smaller than for IRMOF-6. These results indicated that the key to high CH_4 adsorption is not pore surface area but strong energetic interaction between the framework and the methane molecules, and indicates the benefit of GCMC simulations as a screening tool for identifying new candidates for methane storage and other adsorption applications and to guide the design of new materials.

There is a suggestive report providing a strategy for achieving practical hydrogen storage [220]. The effects of doping of MOF materials with electropositive metals for hydrogen uptake have been calculated by quantum mechanics (QM) calculations (X3LYP flavor of DFT) and GCMC. For the pure MOF materials, the H_2 molecule binds weakly with both the metal oxide clusters and the aromatic linkers with binding energies of 1.5 and 0.9 kcal mol^{-1}, respectively. However, Li doped into MOF materials promotes charge separation and acts as an acidic site providing strong stabilization of H_2 molecules with effective binding energies of 4.0 kcal mol^{-1}, enhancing ambient temperature H_2 uptake.

5 Other Properties

5.1 Separation

Unlike those of conventional porous zeolites, the surfaces and voids of PCP are typically composed of aromatic rings and other organic moieties, and thus their pore structures are often quite complex and different from those of oxide-based porous materials. High framework stability of PCPs is important for many practical applications, therefore the quest for metal–organic materials with robust frameworks has been the subject of intense research. Moreover, these PCPs possess flexible and dynamic frameworks. Some flexible PCPs show unusual sorption properties in response to specific external stimuli that are not observed in other conventional porous solids. According to this feature, PCPs are offered as an alternative to prepare high capacity and selectivity sorption, mainly determined by size-exclusive effects in which smaller molecules can go through the microporous channels while larger substrates are blocked [35, 77, 117, 140, 148, 153, 176, 199, 231–234]. Furthermore, recent research demonstrates the selective separation properties of PCPs from miscible systems [55, 97, 121, 194, 235–237].

Compound $[Zn(Pur)_2]_n$, ZIF-20 (Pur = purinate), a zeolitic imidazolate framework (ZIF) with zeolite A (LTA) topology, has two types of separate cages (α and β) (Fig. 12) [121]. There are two types of α-cages whose pore diameters are 14.5 and 15.4 Å, with a pore aperture of 2.8 Å in diameter. The β-cage has smaller cavity (5.3 Å) and smaller pore aperture (2.0 Å). Thus, the α-cage can be accessed by some small molecules through the pore window. The adsorption of CO_2 and CH_4 gas by ZIF-20 were also examined at 273 K. The CO_2 uptake at 760 Torr is five times higher than that of CH_4, suggesting a stronger interaction between the framework and the CO_2 molecules. A gas separation property of ZIF-20 using CO_2/CH_4 (about 50:50 v/v) gas mixture was examined. Indeed, the breakthrough curves clearly show that ZIF-20 can separate CO_2 from CH_4.

In the petroleum industry, the separation of alkane isomers is a very important process, and some narrow-pore zeolites have been used to sieve linear from branched alkanes, to boost octane ratings in gasoline. A doubly interpenetration microporous compound, $[Zn_2(1,4\text{-bdc})_2(4,4'\text{-bpy})]_n$ (MOF-508) shows highly selective separation of alkanes in gas chromatography (GC) based on their different van der Waals interactions arising from subtle size- and shape-selective matching [97]. This compound has 1D channels of approximately 4.0×4.0 Å in cross section and these channels can selectively accommodate linear alkanes and discriminate branched alkanes. This framework exhibits a reversible open–dense transformation, which is attributed to the rigid and flexible nature of the $4,4'$-bpy linkers and the variable distortion of the paddle-wheel clusters. The GC separation was examined for linear and branched isomers of pentane and hexane, because of their availability and industrial relevance in petroleum refining. The MOF-508 column can clearly separate *n*-pentane from *n*-hexane (Fig. 13). Branched 2-methylbutane can be separated from its linear isomer *n*-pentane with different retention times.

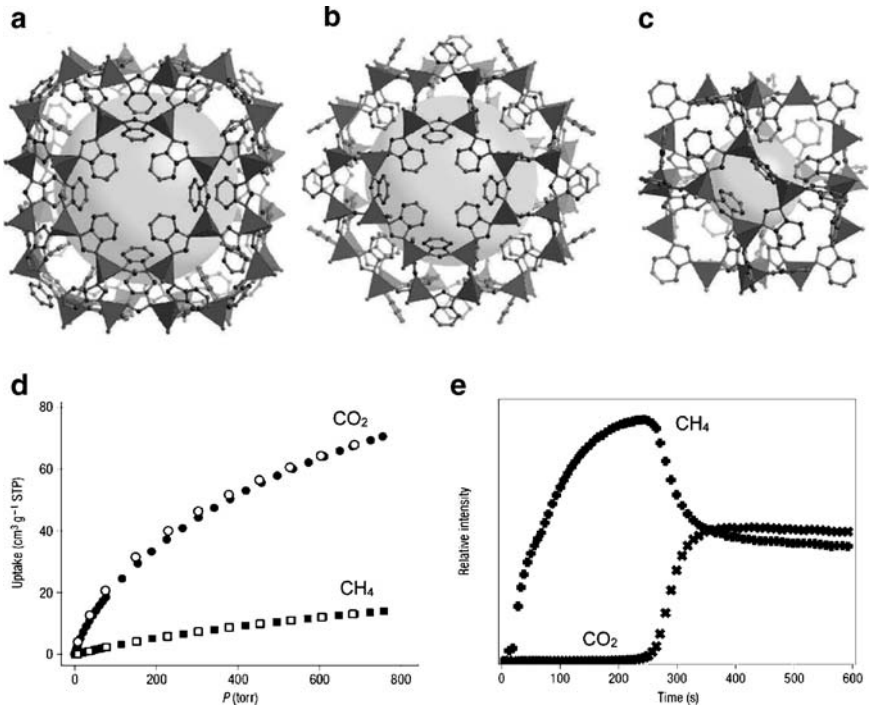

Fig. 12 The structure of ZIF-20. **a**,**b** Two expanded α-cages, and **c** β-cage. **d** Gas adsorption isotherms of ZIF-20 for CO_2 and CH_4 at 273 K. **e** Breakthrough curves of CO_2 and CH_4 for ZIF-20 using a CO_2/CH_4 gas mixture. The relative intensities of each gas passing through the ZIF-20-packed column were obtained using a mass spectrometer to detect ion peaks at $m/z = 44$ (CO_2) and 16 (CH_4). Copyright Nature Publishing Group

Similarly, 2-methylpentane runs through the column faster than its linear isomer *n*-hexane, while 2,2-dimethylbutane, the isomer of hexane with the shortest linear chain, elutes even faster. Thus, mixtures of 2-methylbutane, *n*-pentane, 2,2-dimethylbutane, 2-methylpentane, and *n*-hexane can be easily separated with this new type of microporous MOF column. The potential applications of this microporous MOF column in the efficient GC separation of natural gas and alkane mixtures are remarkable and foreseeable. The column could be used to identify the impurities in natural gas, and to monitor the amounts of mono- and multibranched alkanes formed in cracking reactions.

Moreover, this porous compound is also applicable for efficient separation of mixed gases, CO_2/N_2 and CO_2/CH_4, which are useful in air purification and methane transportation systems [235]. Kinetic diameters of CO_2, N_2, and CH_4 are 3.30, 3.64, and 3.80 Å, respectively. The small pores of $4.0 \times 4.0\,\text{Å}^2$ within this compound has limited the packing of these three gas molecules within the micropores to a single-layer packing that simplifies the complicated adsorption phenomena and process. The adsorption isotherms for each component at different temperatures

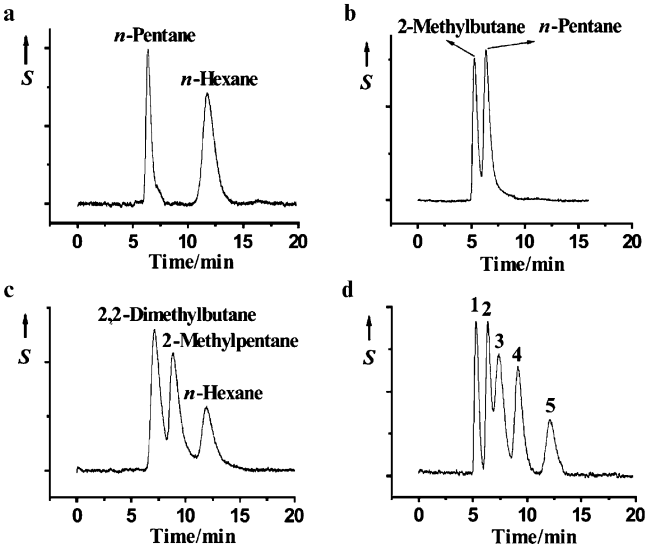

Fig. 13 Chromatograms of alkane mixtures separated on a MOF-508 column: **a** separation of *n*-pentane and *n*-hexane; **b** separation of 2-methylbutane and *n*-pentane; **c** separation of 2,2-dimethylbutane, 2-methylpentane, and *n*-hexane; and **d** separation of an alkane mixture containing 2-methylbutane (**1**), *n*-pentane (**2**), 2,2-dimethylbutane (**3**), 2-methylpentane (**4**), and *n*-hexane (**5**). S = thermal conductivity detector response. Copyright Wiley

have been investigated. The adsorption capacity for CO_2 is significantly dependent on the temperature, but for CH_4 and N_2 it is almost independent of the temperature. The adsorbed amount of CO_2 decreases as the temperature increases. These significantly different temperature-dependent adsorption behaviors might be specifically useful for optimizing the temperature for the binary and ternary separation of CO_2/N_2 and CO_2/CH_4.

5.2 Catalytic Properties

One potential application for PCPs is catalytic reaction because of their functional cavity surface, high regioselectivity, stereoselectivity, and shape or size selectivity. The activation of small gas molecules is a quite big challenge and an important target in the field of PCPs. However, there are few reports about this area and the topic is currently being explored [238,239]. Today, most PCPs with catalytic properties have been used only for organic reactions [54, 93, 96, 134, 192, 240–260].

Compared with conventional zeolite, whose catalytic function depends on Bronsted or Lewis acidic sites that are intimately associated with the Al^{3+} substitutional defects in the tetrahedral zeolite framework, PCPs would be inferior for applications in catalysis because of their relative instability, their lack of strong acidity,

and their relatively costly synthesis. However, organic and inorganic hybrids offer certain advantages:

1. The relative ease with which they can be functionalized, postsynthesis
2. The range of substrates that can be handled by zeolites is limited by the maximum window size
3. The simplicity with which the pore size can be tuned over a wide range of sizes in PCPs
4. The manner in which enatiomerically-pure chiral frameworks can be created

The examples shown below will illustrate that many of these advantages are now beginning to be realized; further details are given in a recent review of the area.

The early study of catalysis by PCPs used a simple lamellar coordination polymer $[Cd(4,4'\text{-bpy})_2](NO_3)_2$, whose inner cavities are surrounded by $4,4'$-bpy units [54]. Several aldehydes were tested for cyanosilation with cyanotrimethylsilane. Although smaller substrates, α- and β-naphthaldehyde are good substrates to give the adducts in 62 and 84% yields, respectively, the more sterically demanding 9-anthraldehyde hardly reacted. These shape specificities may be ascribed to the cavity size of the network material. A control experiment using $Cd(NO_3)_2$ and $4,4'$-bpy as catalysts resulted in no reaction, confirming the role of the coordination polymer's porosity in catalyzing the reaction. Even though there are a few reports on liquid-phase catalytic reactions, catalysis of gas-phase reactions by PCPs is rare. Compound $\{[Na_{20}(Ni_8L3_{12})(H_2O)_{28}](H_2O)_{13}(CH_3OH)_2\}_n$ is constructed from cubic building blocks $[Ni_8L3_{12}](H_3L3 = 4,5\text{-imidazoledicarboxylic acid})$ with bridging by Na^I [243]. It exhibits not only significant gas-adsorption properties but also stable catalytic activity for the oxidation of CO to CO_2. This complex is the first example of a porous MOF catalyst for the oxidation of CO, and the stable catalytic activity makes an intriguing forerunner for other new environmentally relevant materials. A PCP with amide groups $\{[Cd(btapa)_2(NO_3)_2]\cdot 6H_2O{\cdot}2DMF\}_n$ (btapa = 1,3,5-benzene tricarboxylic acid tris[*N*-(4-pyridyl)amide]), a new base-type catalytic pore framework, has channels with dimensions of $4.7 \times 7.3\,\text{Å}^2$ [244]. These amide groups on the surfaces of channels act as guest interaction sites for selective sorption and/or catalysis inside the channel because they possess two types of hydrogen bonding sites: the –NH moiety acts as an electron acceptor and the –C=O group acts as an electron donor (Fig. 14). To confirm base catalytic properties, Knoevenagel condensation reactions of benzaldehyde with each of the active methylene compounds (malononitrile, ethyl cyanoacetate, and cyano-acetic acid *tert*-butyl ester) catalyzed by this framework were performed. The malononitrile was a good substrate, producing 98% conversion of the adduct, whereas the other substrates reacted negligibly. This guest-selective reaction suggests that the reaction occurs in the channels and not on the surface of framework.

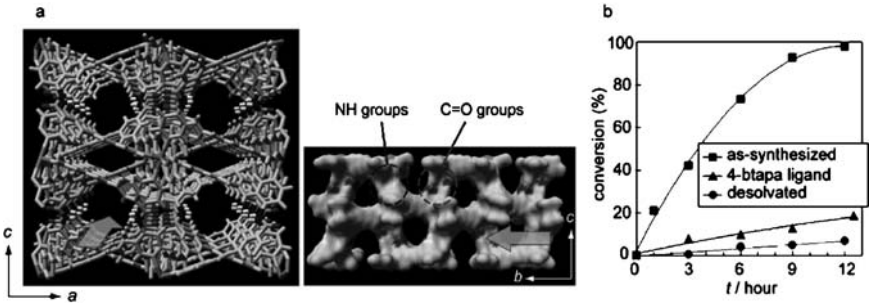

Fig. 14 **a** Crystal structure of $\{[Cd(4\text{-btapa})_2(NO_3)_2] \cdot 6H_2O \cdot 2DMF\}_n$. The amide groups are regularly embedded on the pore surface. **b** Conversion (%) vs. time (h) for Knoevenagel condensation reaction of benzaldehyde with malnonitrile in benzene-catalyzed as-synthesized (*square*), desolvated (*circle*), and 4-btapa ligand (*triangle*)

6 Perspectives

Gas molecules are associated with important issues of global environment, energy, and life. In addition to the well-traveled lands, there is the vast unexplored land regarding cooperative performances by gas and porous materials: gas molecule-inspired materials or porous material-inspired gas assemblies. This could be an important target for the next generation of porous materials.

In this context, understanding and control of gas molecules confined in nanoscale space would lead to interesting properties that are not observed in the corresponding bulk state and provide significant development in the field of chemistry and physics.

In the nanospace of PCPs, small molecules are strictly confined because a well-suited framework traps and makes ordered arrangement of molecules in a channel. In addition, the flexibility of the framework, which is categorized as a third generation compound, and the designability of the pore shape and its environment will create unprecedented phenomena and applications. Some potential applications of future PCPs are outlined below.

6.1 Energy Storage and Conversion

Porous compounds are sometimes called energy storage materials as the adsorbents of gaseous fuels. However, PCPs possess the potential to be energy storage materials in the real sense of the term. When gas molecules are adsorbed into the porous compound, they generated heat by the adsorption enthalpy alone. This energy has been only emitted into the atmosphere in the case of conventional materials and leads to a critical decrease in adsorption efficiency. In case of PCPs, a part of this energy can be absorbed as energy of structural transformation, such as distortion

of coordination geometry, a rotational rearrangement of the organic part. Furthermore, it will be possible to convert this thermal energy into an optical, electric, or anisotropic kinetic energy by incorporating adequate organic and inorganic components into the framework. [261]

6.2 Responsive Properties

The dynamic nanospace of PCPs still has many potential properties. Introduction of the flexible part makes frameworks responsive to the external stimuli; for instance, switching of adsorption and desorption by light or electric field with no change of temperature and pressure. The presence of controllable multiple states is quite important for practical use. It is also possible to control the affinity for guest molecules with structural transformation induced by an external stimulus. An interesting idea is that guest molecules and porous function (such as storage, separation, and catalysis) are intimately correlated. This is a new field, called "nanospace manipulation," which should provide new host–guest chemistry to porous materials.

6.3 Reaction Field

The controllable nanospace of PCPs is a competent candidate for the accurately controlled reaction field. In these micropores, guest molecules are strictly arranged and oriented uniformly, and gas molecules are no exception. Guest molecules and reactants approach each other spatially and react regioselectively through excitation by the external stimuli. After the reaction, the products are released outside of the pores because the pores are not suitable for the size and shape of the products and have no affinity for them. The products of this ideal reaction cycle rely heavily on the shape and size of the nanospace. By choosing the pore structure, different products can be obtained from the same reactants. Moreover, this spatial reaction control may produce unparalleled reaction paths and products that cannot be realized in homogeneous systems.

References

1. Abraham S, Evans DL, Marburger JH (2003) Strategic plan for the climate change science program, final report, July 2003. US Climate Change Science Program, Washington, DC
2. Gutierrez CM, Bodman SW, Marburger JH, Eule SD (2006) US climate change technology program strategic plan, September 2006. US Climate Change Technology Program, Washington, DC
3. Matisova E, Skrabakova S (1995) J Chromatogr A 707:145
4. Wigmans T (1989) Carbon 27:13
5. Davis ME, Lobo RF (1992) Chem Mater 4:756

6. Ozin GA, Kuperman A, Stein A (1989) Angew Chem Int Ed Engl 28:359
7. Cheetham AK, Ferey G, Loiseau T (1999) Angew Chem Int Ed 38:3268
8. Tao YS, Kanoh H, Abrams L, Kaneko K (2006) Chem Rev 106:896
9. Cundy CS, Cox PA (2003) Chem Rev 103:663
10. Batten SR, Robson R (1998) Angew Chem Int Ed 37:1460
11. Moulton B, Zaworotko MJ (2001) Chem Rev 101:1629
12. Eddaoudi M, Moler DB, Li HL, Chen BL, Reineke TM, O'Keeffe M, Yaghi OM (2001) Acc Chem Res 34:319
13. James SL (2003) Chem Soc Rev 32:276
14. Yaghi OM, O'Keeffe M, Ockwig NW, Chae HK, Eddaoudi M, Kim J (2003) Nature 423:705
15. Kesanli B, Lin WB (2003) Coord Chem Rev 246:305
16. Kitagawa S, Kitaura R, Noro S (2004) Angew Chem Int Ed 43:2334
17. Rowsell JLC, Yaghi OM (2005) Angew Chem Int Ed 44:4670
18. Ferey G, Mellot-Draznieks C, Serre C, Millange F (2005) Acc Chem Res 38:217
19. Bradshaw D, Claridge JB, Cussen EJ, Prior TJ, Rosseinsky MJ (2005) Acc Chem Res 38:273
20. Robin AY, Fromm KM (2006) Coord Chem Rev 250:2127
21. Kitagawa S, Matsuda R (2007) Coord Chem Rev 251:2490
22. Maspoch D, Ruiz-Molina D, Veciana J (2007) Chem Soc Rev 36:770
23. Kawano M, Fujita M (2007) Coord Chem Rev 251:2592
24. Kitagawa S, Uemura K (2005) Chem Soc Rev 34:109
25. Fletcher AJ, Thomas KM, Rosseinsky MJ (2005) J Solid State Chem 178:2491
26. Ferey G (2008) Chem Soc Rev 37:191
27. Cheetham AK, Rao CNR, Feller RK (2006) Chem Commun, p 4780
28. Forster PM, Burbank AR, Livage C, Ferey G, Cheetham AK (2004) Chem Commun, p 368
29. Borkowski LA, Cahill CL (2004) Inorg Chem Commun 7:725
30. Yucesan G, Golub V, O'Connor CJ, Zubieta J (2005) Solid State Sci 7:133
31. Dan M, Rao CNR (2006) Angew Chem Int Ed 45:281
32. Chen JX, Ohba M, Zhao DY, Kaneko W, Kitagawa S (2006) Cryst Growth Des 6:664
33. Garay AL, Pichon A, James SL (2007) Chem Soc Rev 36:846
34. Mueller U, Schubert M, Teich F, Puetter H, Schierle-Arndt K, Pastre J (2006) J Mater Chem 16:626
35. Choi EY, Park K, Yang CM, Kim H, Son JH, Lee SW, Lee YH, Min D, Kwon YU (2004) Chem Eur J 10:5535
36. Kepert CJ, Prior TJ, Rosseinsky MJ (2000) J Am Chem Soc 122:5158
37. Bradshaw D, Prior TJ, Cussen EJ, Claridge JB, Rosseinsky MJ (2004) J Am Chem Soc 126:6106
38. Lin ZJ, Slawin AMZ, Morris RE (2007) J Am Chem Soc 129:4880
39. Rouquerol J, Avnir D, Fairbridge CW, Everett DH, Haynes JH, Pernicone N, Ramsay JDF, Sing KSW, Unger KK (1994) Pure Appl Chem 66:1739
40. Brunauer S, Emmett PH, Teller E (1938) J Am Chem Soc 60:309
41. Sing KSW, Everett DH, Haul RAW, Moscou L, Pierotti RA, Rouquerol J, Siemieniewska T (1985) Pure Appl Chem 57:603
42. Bojan MJ, Steele WA (1998) Carbon 36:1417
43. Seki K (2001) Chem Commun, p 1496
44. Seki K, Takamizawa S, Mori W (2001) Chem Lett, p 332
45. Seki K, Mori W (2002) J Phys Chem B 106:1380
46. Horvath G, Kawazoe K (1983) J Chem Eng Jpn 16:470
47. Kitagawa S, Kondo M (1998) Bull Chem Soc Jpn 71:1739
48. Barrer RM (1974) Molecular sieves. American Chemical Society, Washington
49. Wilde RE, Ghosh SN, Marshall BJ (1970) Inorg Chem 9:2512
50. Buser HJ, Schwarzenbach D, Petter W, Ludi A (1977) Inorg Chem 16:2704
51. Dunbar KR, Heintz RA (1997) Prog Inorg Chem 45:283
52. Kinoshita Y, Matsubara I, Higuchi T, Saito Y (1959) Bull Chem Soc Jpn 32:1221
53. Hoskins BF, Robson R (1990) J Am Chem Soc 112:1546
54. Fujita M, Kwon YJ, Washizu S, Ogura K (1994) J Am Chem Soc 116:1151

55. Yaghi OM, Li GM, Li HL (1995) Nature 378:703
56. Venkataraman D, Gardner GB, Lee S, Moore JS (1995) J Am Chem Soc 117:11600
57. Kondo M, Yoshitomi T, Seki K, Matsuzaka H, Kitagawa S (1997) Angew Chem Int Ed Engl 36:1725
58. Kaneko K, Cracknell RF, Nicholson D (1994) Langmuir 10:4606
59. Li H, Eddaoudi M, Groy TL, Yaghi OM (1998) J Am Chem Soc 120:8571
60. Takamizawa S, Mori W, Furihata M, Takeda S, Yamaguchi K (1998) Inorg Chim Acta 283:268
61. Chui SSY, Lo SMF, Charmant JPH, Orpen AG, Williams ID (1999) Science 283:1148
62. Eddaoudi M, Li HL, Yaghi OM (2000) J Am Chem Soc 122:1391
63. Li D, Kaneko K (2000) J Phys Chem B 104:8940
64. Reineke TM, Eddaoudi M, Moler D, O'Keeffe M, Yaghi OM (2000) J Am Chem Soc 122:4843
65. Chae HK, Eddaoudi M, Kim J, Hauck SI, Hartwig JF, O'Keeffe M, Yaghi OM (2001) J Am Chem Soc 123:11482
66. Chen BL, Eddaoudi M, Hyde ST, O'Keeffe M, Yaghi OM (2001) Science 291:1021
67. Fletcher AJ, Cussen EJ, Prior TJ, Rosseinsky MJ, Kepert CJ, Thomas KM (2001) J Am Chem Soc 123:10001
68. Li D, Kaneko K (2001) Chem Phys Lett 335:50
69. Barthelet K, Marrot J, Riou D, Ferey G (2002) Angew Chem Int Ed 41:281
70. Eddaoudi M, Kim J, Rosi N, Vodak D, Wachter J, O'Keeffe M, Yaghi OM (2002) Science 295:469
71. Millange F, Serre C, Ferey G (2002) Chem Commun, p 822
72. Noro S, Kitaura R, Kondo M, Kitagawa S, Ishii T, Matsuzaka H, Yamashita M (2002) J Am Chem Soc 124:2568
73. Onishi S, Ohmori T, Ohkubo T, Noguchi H, Di L, Hanzawa Y, Kanoh H, Kaneko K (2002) Appl Surf Sci 196:81
74. Seki K (2002) Phys Chem Chem Phys 4:1968
75. Sun JY, Weng LH, Zhou YM, Chen JX, Chen ZX, Liu ZC, Zhao DY (2002) Angew Chem Int Ed 41:4471
76. Guillou N, Livage C, van Beek W, Nogues M, Ferey G (2003) Angew Chem Int Ed 42:644
77. Kitaura R, Seki K, Akiyama G, Kitagawa S (2003) Angew Chem Int Ed 42:428
78. Chae HK, Siberio-Perez DY, Kim J, Go Y, Eddaoudi M, Matzger AJ, O'Keeffe M, Yaghi OM (2004) Nature 427:523
79. Dybtsev DN, Chun H, Kim K (2004) Angew Chem Int Ed 43:5033
80. Ferey G, Serre C, Mellot-Draznieks C, Millange F, Surble S, Dutour J, Margiolaki I (2004) Angew Chem Int Ed 43:6296
81. Lee EY, Suh MP (2004) Angew Chem Int Ed 43:2798
82. Xu HT, Liang JH, Zhuang J, Kou HZ, Wang RJ, Li YD (2004) J Mol Struct 689:177
83. Chen BL, Ockwig NW, Millward AR, Contreras DS, Yaghi OM (2005) Angew Chem Int Ed 44:4745
84. Chun H, Dybtsev DN, Kim H, Kim K (2005) Chem Eur J 11:3521
85. Devic T, Serre C, Audebrand N, Marrot J, Ferey G (2005) J Am Chem Soc 127:12788
86. Dinca M, Long JR (2005) J Am Chem Soc 127:9376
87. Ferey G, Mellot-Draznieks C, Serre C, Millange F, Dutour J, Surble S, Margiolaki I (2005) Science 309:2040
88. Kitaura R, Matsuda R, Kubota Y, Kitagawa S, Takata M, Kobayashi TC, Suzuki M (2005) J Phys Chem B 109:23378
89. Lee EY, Jang SY, Suh MP (2005) J Am Chem Soc 127:6374
90. Lee J, Li J, Jagiello J (2005) J Solid State Chem 178:2527
91. Ma BQ, Mulfort KL, Hupp JT (2005) Inorg Chem 44:4912
92. Maji TK, Ohba M, Kitagawa S (2005) Inorg Chem 44:9225
93. Perles J, Iglesias M, Martin-Luengo MA, Monge MA, Ruiz-Valero C, Snejko N (2005) Chem Mater 17:5837

94. Rosi NL, Kim J, Eddaoudi M, Chen BL, O'Keeffe M, Yaghi OM (2005) J Am Chem Soc 127:1504
95. Wang ZM, Zhang B, Kurmoo M, Green MA, Fujiwara H, Otsuka T, Kobayashi H (2005) Inorg Chem 44:1230
96. Alaerts L, Seguin E, Poelman H, Thibault-Starzyk F, Jacobs PA, De Vos DE (2006) Chem Eur J 12:7353
97. Chen BL, Liang CD, Yang J, Contreras DS, Clancy YL, Lobkovsky EB, Yaghi OM, Dai S (2006) Angew Chem Int Ed 45:1390
98. Dietzel PDC, Panella B, Hirscher M, Blom R, Fjellvag H (2006) Chem Commun, p 959
99. Dinca M, Dailly A, Liu Y, Brown CM, Neumann DA, Long JR (2006) J Am Chem Soc 128:16876
100. Dinca M, Yu AF, Long JR (2006) J Am Chem Soc 128:8904
101. Jia JH, Lin X, Blake AJ, Champness NR, Hubberstey P, Shao LM, Walker G, Wilson C, Schroder M (2006) Inorg Chem 45:8838
102. Kongshaug KO, Fjellvag H (2006) Inorg Chem 45:2424
103. Kramer M, Ulrich SB, Kaskel S (2006) J Mater Chem 16:2245
104. Lin X, Blake AJ, Wilson C, Sun XZ, Champness NR, George MW, Hubberstey P, Mokaya R, Schroder M (2006) J Am Chem Soc 128:10745
105. Lin X, Jia JH, Zhao XB, Thomas KM, Blake AJ, Walker GS, Champness NR, Hubberstey P, Schroder M (2006) Angew Chem Int Ed 45:7358
106. Moon HR, Kobayashi N, Suh MP (2006) Inorg Chem 45:8672
107. Navarro JAR, Barea E, Salas JM, Masciocchi N, Galli S, Sironi A, Ania CO, Parra JB (2006) Inorg Chem 45:2397
108. Noro SI, Kitaura R, Kitagawa S, Akutagawa T, Nakamura T (2006) Inorg Chem 45:8990
109. Rood JA, Noll BC, Henderson KW (2006) Inorg Chem 45:5521
110. Senkovska I, Kaskel S (2006) Eur J Inorg Chem 4564
111. Sudik AC, Cote AP, Wong-Foy AG, O'Keeffe M, Yaghi OM (2006) Angew Chem Int Ed 45:2528
112. Sun DF, Ke YX, Mattox TM, Parkin S, Zhou HC (2006) Inorg Chem 45:7566
113. Sun DF, Ma SQ, Ke YX, Collins DJ, Zhou HC (2006) J Am Chem Soc 128:3896
114. Sun JY, Zhou YM, Fang QR, Chen ZX, Weng LH, Zhu GS, Qiu SL, Zhao DY (2006) Inorg Chem 45:8677
115. Surble S, Millange F, Serre C, Duren T, Latroche M, Bourrelly S, Llewellyn PL, Ferey G (2006) J Am Chem Soc 128:14889
116. Wang XS, Ma SQ, Sun DF, Parkin S, Zhou HC (2006) J Am Chem Soc 128:16474
117. Chen BL, Ma SQ, Zapata F, Fronczek FR, Lobkovsky EB, Zhou HC (2007) Inorg Chem 46:1233
118. Chun H, Moon J (2007) Inorg Chem 46:4371
119. Furukawa H, Miller MA, Yaghi OM (2007) J Mater Chem 17:3197
120. Goto M, Furukawa M, Miyamoto J, Kanoh H, Kaneko K (2007) Langmuir 23:5264
121. Hayashi H, Cote AP, Furukawa H, O'Keeffe M, Yaghi OM (2007) Nat Mater 6:501
122. Humphrey SM, Chang JS, Jhung SH, Yoon JW, Wood PT (2007) Angew Chem Int Ed 46:272
123. Kondo A, Noguchi H, Carlucci L, Proserpio DM, Ciani G, Kajiro H, Ohba T, Kanoh H, Kaneko K (2007) J Am Chem Soc 129:12362
124. Krungleviciute V, Lask K, Heroux L, Migone AD, Lee JY, Li J, Skoulidas A (2007) Langmuir 23:3106
125. Liang J, Shimizu GKH (2007) Inorg Chem 46:10449
126. Liu YL, Eubank JF, Cairns AJ, Eckert J, Kravtsov VC, Luebke R, Eddaoudi M (2007) Angew Chem Int Ed 46:3278
127. Ma S, Sun D, Wang XS, Zhou HC (2007) Angew Chem Int Ed 46:2458
128. Ma SQ, Sun DF, Ambrogio M, Fillinger JA, Parkin S, Zhou HC (2007) J Am Chem Soc 129:1858
129. Ma SQ, Wang XS, Manis ES, Collier CD, Zhou HC (2007) Inorg Chem 46:3432
130. Mulfort KL, Hupp JT (2007) J Am Chem Soc 129:9604

131. Noguchi H, Kondo A, Hattori Y, Kajiro H, Kanoh H, Kaneko K (2007) J Phys Chem C 111:248
132. Park H, Britten JF, Mueller U, Lee J, Li J, Parise JB (2007) Chem Mater 19:1302
133. Park YK, Choi SB, Kim H, Kim K, Won BH, Choi K, Choi JS, Ahn WS, Won N, Kim S, Jung DH, Choi SH, Kim GH, Cha SS, Jhon YH, Yang JK, Kim J (2007) Angew Chem Int Ed 46:8230
134. Sabo M, Henschel A, Froede H, Klemm E, Kaskel S (2007) J Mater Chem 17:3827
135. Suh MP, Cheon YE, Lee EY (2007) Chem Eur J 13:4208
136. Yoon JH, Choi SB, Oh YJ, Seo MJ, Jhon YH, Lee TB, Kim D, Choi SH, Kim J (2007) Catal Today 120:324
137. Zou Y, Hong S, Park M, Chun H, Lah MS (2007) Chem Commun, p 5182
138. Kachi-Terajima C, Akatsuka T, Kohbara M, Takamizawa S (2007) Chem Asian J 2:40
139. Chun H (2008) J Am Chem Soc 130:800
140. Pan L, Parker B, Huang XY, Olson DH, Lee J, Li J (2006) J Am Chem Soc 128:4180
141. Kondo M, Shimamura M, Noro S, Minakoshi S, Asami A, Seki K, Kitagawa S (2000) Chem Mater 12:1288
142. Noro S, Kitagawa S, Kondo M, Seki K (2000) Angew Chem Int Ed 39:2082
143. Kondo M, Okubo T, Asami A, Noro S, Yoshitomi T, Kitagawa S, Ishii T, Matsuzaka H, Seki K (1999) Angew Chem Int Ed 38:140
144. Seki K, Takamizawa S, Mori W (2001) Chem Lett, p 122
145. Bourrelly S, Llewellyn PL, Serre C, Millange F, Loiseau T, Ferey G (2005) J Am Chem Soc 127:13519
146. Noguchi H, Kondoh A, Hattori Y, Kanoh H, Kajiro H, Kaneko K (2005) J Phys Chem B 109:13851
147. Takamizawa S, Nakata E, Saito T, Akatsuka T (2005) Inorg Chem 44:1362
148. Llewellyn PL, Bourrelly S, Serre C, Filinchuk Y, Ferey G (2006) Angew Chem Int Ed 45:7751
149. Loiseau T, Lecroq L, Volkringer C, Marrot J, Ferey G, Haouas M, Taulelle F, Bourrelly S, Llewellyn PL, Latroche M (2006) J Am Chem Soc 128:10223
150. Ma S, Sun D, Simmons JM, Collier CD, Yuan D, Zhou HC (2008) J Am Chem Soc 130:1012
151. Rosi NL, Eckert J, Eddaoudi M, Vodak DT, Kim J, O'Keeffe M, Yaghi OM (2003) Science 300:1127
152. Ferey G, Latroche M, Serre C, Millange F, Loiseau T, Percheron-Guegan A (2003) Chem Commun, p 2976
153. Dybtsev DN, Chun H, Yoon SH, Kim D, Kim K (2004) J Am Chem Soc 126:32
154. Rowsell JLC, Millward AR, Park KS, Yaghi OM (2004) J Am Chem Soc 126:5666
155. Zhao XB, Xiao B, Fletcher AJ, Thomas KM, Bradshaw D, Rosseinsky MJ (2004) Science 306:1012
156. Kaye SS, Long JR (2005) J Am Chem Soc 127:6506
157. Kesanli B, Cui Y, Smith MR, Bittner EW, Bockrath BC, Lin WB (2005) Angew Chem Int Ed 44:72
158. Lee JY, Pan L, Kelly SR, Jagiello J, Emge TJ, Li J (2005) Adv Mater 17:2703
159. Rowsell JLC, Eckert J, Yaghi OM (2005) J Am Chem Soc 127:14904
160. Takamizawa S, Nakata E (2005) Cryst Eng Commun 7:476
161. Dailly A, Vajo JJ, Ahn CC (2006) J Phys Chem B 110:1099
162. Fang QR, Zhu GS, Xue M, Zhang QL, Sun JY, Guo XD, Qiu SL, Xu ST, Wang P, Wang DJ, Wei Y (2006) Chem Eur J 12:3754
163. Forster PM, Eckert J, Heiken BD, Parise JB, Yoon JW, Jhung SH, Chang JS, Cheetham AK (2006) J Am Chem Soc 128:16846
164. Latroche M, Surble S, Serre C, Mellot-Draznieks C, Llewellyn PL, Lee JH, Chang JS, Jhung SH, Ferey G (2006) Angew Chem Int Ed 45:8227
165. Panella B, Hirscher M, Putter H, Muller U (2006) Adv Funct Mater 16:520
166. Peterson VK, Liu Y, Brown CM, Kepert CJ (2006) J Am Chem Soc 128:15578
167. Rowsell JLC, Yaghi OM (2006) J Am Chem Soc 128:1304

168. Wong-Foy AG, Matzger AJ, Yaghi OM (2006) J Am Chem Soc 128:3494
169. Dinca M, Long JR (2007) J Am Chem Soc 129:11172
170. Fang QR, Zhu GS, Jin Z, Ji YY, Ye JW, Xue M, Yang H, Wang Y, Qiu SL (2007) Angew Chem Int Ed 46:6638
171. Farha OK, Spokoyny AM, Mulfort KL, Hawthorne MF, Mirkin CA, Hupp JT (2007) J Am Chem Soc 129:12680
172. Jia JH, Lin X, Wilson C, Blake AJ, Champness NR, Hubberstey P, Walker G, Cussen EJ, Schroder M (2007) Chem Commun, p 840
173. Lee JY, Olson DH, Pan L, Emge TJ, Li J (2007) Adv Funct Mater 17:1255
174. Xiao B, Wheatley PS, Zhao XB, Fletcher AJ, Fox S, Rossi AG, Megson IL, Bordiga S, Regli L, Thomas KM, Morris RE (2007) J Am Chem Soc 129:1203
175. Reineke TM, Eddaoudi M, O'Keeffe M, Yaghi OM (1999) Angew Chem Int Ed 38:2590
176. Pan L, Adams KM, Hernandez HE, Wang XT, Zheng C, Hattori Y, Kaneko K (2003) J Am Chem Soc 125:3062
177. Takamizawa S, Nakata E, Yokoyama H, Mochizuki K, Mori W (2003) Angew Chem Int Ed 42:4331
178. Fletcher AJ, Cussen EJ, Bradshaw D, Rosseinsky MJ, Thomas KM (2004) J Am Chem Soc 126:9750
179. Maji TK, Mostafa G, Matsuda R, Kitagawa S (2005) J Am Chem Soc 127:17152
180. Millward AR, Yaghi OM (2005) J Am Chem Soc 127:17998
181. Chandler BD, Cramb DT, Shimizu GKH (2006) J Am Chem Soc 128:10403
182. Kondo A, Noguchi H, Ohnishi S, Kajiro H, Tohdoh A, Hattori Y, Xu WC, Tanaka H, Kanoh H, Kaneko K (2006) Nano Lett 6:2581
183. Takamizawa S, Kojima K, Akatsuka T (2006) Inorg Chem 45:4580
184. Wu CD, Lin WB (2006) Dalton Trans, p 4563
185. Hawxwell SM, Espallargas GM, Bradshaw D, Rosseinsky MJ, Prior TJ, Florence AJ, van de Streek J, Brammer L (2007) Chem Commun, p 1532
186. Maji TK, Matsuda R, Kitagawa S (2007) Nat Mater 6:142
187. Taylor JM, Mahmoudkhani AH, Shimizu GKH (2007) Angew Chem Int Ed 46:795
188. Vimont A, Travert A, Bazin P, Lavalley JC, Daturi M, Serre C, Ferey G, Bourrelly S, Llewellyn PL (2007) Chem Commun, p 3291
189. Shimizu K, Suhara K, Ikumo M, Eremets MI, Amaya K (1998) Nature 393:767
190. Ritter SK (2004) Chem Eng News 82:29
191. Biradha K, Hongo Y, Fujita M (2000) Angew Chem Int Ed 39:3843
192. Pan L, Liu HM, Lei XG, Huang XY, Olson DH, Turro NJ, Li J (2003) Angew Chem Int Ed 42:542
193. Soldatov DV, Ripmeester JA, Shergina SI, Sokolov IE, Zanina AS, Gromilov SA, Dyadin YA (1999) J Am Chem Soc 121:4179
194. Lu JY, Babb AM (2002) Chem Commun, p 1340
195. Mori W, Kobayashi TC, Kurobe J, Kumada T, Amaya K, Narumi Y, Kindo K, Katori HA, Goto T, Miura N, Takamizawa S, Nakayama H, Yamaguchi K (1997) Mol Cryst Liq Cryst Sci Technol Sect A 306:1
196. Kanoh H, Kaneko K (1996) J Phys Chem 100:755
197. Matsuda R, Kitaura R, Kitagawa S, Kubota Y, Kobayashi TC, Horike S, Takata M (2004) J Am Chem Soc 126:14063
198. Kitaura R, Kitagawa S, Kubota Y, Kobayashi TC, Kindo K, Mita Y, Matsuo A, Kobayashi M, Chang HC, Ozawa TC, Suzuki M, Sakata M, Takata M (2002) Science 298:2358
199. Matsuda R, Kitaura R, Kitagawa S, Kubota Y, Belosludov RV, Kobayashi TC, Sakamoto H, Chiba T, Takata M, Kawazoe Y, Mita Y (2005) Nature 436:238
200. Kubota Y, Takata M, Matsuda R, Kitaura R, Kitagawa S, Kato K, Sakata M, Kobayashi TC (2005) Angew Chem Int Ed 44:920
201. Kubota Y, Takata M, Matsuda R, Kitaura R, Kitagawa S, Kobayashi TC (2006) Angew Chem Int Ed 45:4932
202. Shimomura S, Matsuda R, Tsujino T, Kawamura T, Kitagawa S (2006) J Am Chem Soc 128:16416

203. Kachi-Terajima C, Akatsuka T, Kohbara MA, Takamizawa S (2007) Polyhedron 26:1876
204. Tanaka D, Masaoka S, Horike S, Furukawa S, Mizuno M, Endo K, Kitagawa S (2006) Angew Chem Int Ed 45:4628
205. Ohmori O, Kawano M, Fujita M (2005) Angew Chem Int Ed 44:1962
206. Choi HJ, Suh MP (2004) J Am Chem Soc 126:15844
207. Rowsell JLC, Spencer EC, Eckert J, Howard JAK, Yaghi OM (2005) Science 309:1350
208. Kubota Y, Takata M, Kobayashi TC, Kitagawa S (2007) Coord Chem Rev 251:2510
209. Halder GJ, Kepert CJ (2005) J Am Chem Soc 127:7891
210. Hartman MR, Peterson VK, Liu Y, Kaye SS, Long JR (2006) Chem Mater 18:3221
211. Takamizawa S, Saito T, Akatsuka T, Nakata E (2005) Inorg Chem 44:1421
212. Takamizawa S, Nakata E, Saito T (2004) Angew Chem Int Ed 43:1368
213. Jodl HJ, Bolduan F, Hochheimer HD (1985) Phys Rev B 31:7376
214. Takamizawa S, Nakata E, Akatsuka T (2006) Angew Chem Int Ed 45:2216
215. Radhakrishnan R, Gubbins KE, Sliwinska-Bartkowiak M (2000) J Chem Phys 112:11048
216. Budavari S (1996) The Merck index, 12th edn. Merck Research Laboratories, New Jersey
217. Duren T, Sarkisov L, Yaghi OM, Snurr RQ (2004) Langmuir 20:2683
218. Frost H, Duren T, Snurr RQ (2006) J Phys Chem B 110:9565
219. Han SS, Deng WQ, Goddard WA (2007) Angew Chem Int Ed 46:6289
220. Han SS, Goddard WA (2007) J Am Chem Soc 129:8422
221. Jiang JW, Sandler SI (2006) Langmuir 22:5702
222. Keskin S, Sholl DS (2007) J Phys Chem C 111:14055
223. Kim D, Kim J, Jung DH, Lee TB, Choi SB, Yoon JH, Kim J, Choi K, Choi SH (2007) Catal Today 120:317
224. Walton KS, Millward AR, Dubbeldam D, Frost H, Low JJ, Yaghi OM, Snurr RQ (2008) J Am Chem Soc 130:406
225. Walton KS, Snurr RQ (2007) J Am Chem Soc 129:8552
226. Yang QY, Zhong CL (2006) J Phys Chem B 110:17776
227. Yang QY, Zhong CL (2006) J Phys Chem B 110:655
228. Ohkubo T, Miyawaki J, Kaneko K, Ryoo R, Seaton NA (2002) J Phys Chem B 106:6523
229. Setoyama N, Suzuki T, Kaneko K (1998) Carbon 36:1459
230. Nakamura A, Ueyama N, Yamaguchi K (2002) Organometallic conjugation: Structures, reactions and functions of d-d and d-π conjugated systems. Kodansha-Springer, Tokyo
231. Maji TK, Uemura K, Chang H-C, Matsuda R, Kitagawa S (2004) Angew Chem Int Ed 43:3269
232. Chen BL, Ma SQ, Hurtado EJ, Lobkovsky EB, Zhou HC (2007) Inorg Chem 46:8490
233. Chen BL, Ma SQ, Hurtado EJ, Lobkovsky EB, Liang CD, Zhu HG, Dai S (2007) Inorg Chem 46:8705
234. Pan L, Olson DH, Ciemnolonski LR, Heddy R, Li J (2006) Angew Chem Int Ed 45:616
235. Bastin L, Barcia PS, Hurtado EJ, Silva JAC, Rodrigues AE, Chen B (2008) J Phys Chem C 112:1575
236. Makinen SK, Melcer NJ, Parvez M, Shimizu GKH (2001) Chem Eur J 7:5176
237. Shimomura S, Horike S, Matsuda R, Kitagawa S (2007) J Am Chem Soc 129:10990
238. Han JW, Hill CL (2007) J Am Chem Soc 129:15094
239. Zou RQ, Sakurai H, Han S, Zhong RQ, Xu Q (2007) J Am Chem Soc 129:8402
240. Seo JS, Whang D, Lee H, Jun SI, Oh J, Jeon YJ, Kim K (2000) Nature 404:982
241. Evans OR, Ngo HL, Lin WB (2001) J Am Chem Soc 123:10395
242. Gomez-Lor B, Gutierrez-Puebla E, Iglesias M, Monge MA, Ruiz-Valero C, Snejko N (2005) Chem Mater 17:2568
243. Zou RQ, Sakurai H, Xu Q (2006) Angew Chem Int Ed 45:2542
244. Hasegawa S, Horike S, Matsuda R, Furukawa S, Mochizuki K, Kinoshita Y, Kitagawa S (2007) J Am Chem Soc 129:2607
245. Ohmori O, Fujita M (2004) Chem Commun, p 1586
246. Cho SH, Ma BQ, Nguyen ST, Hupp JT, Albrecht-Schmitt TE (2006) Chem Commun, p 2563
247. Dybtsev DN, Nuzhdin AL, Chun H, Bryliakov KP, Talsi EP, Fedin VP, Kim K (2006) Angew Chem Int Ed 45:916

248. Wu CD, Lin WB (2007) Angew Chem Int Ed 46:1075
249. Wu CD, Hu A, Zhang L, Lin WB (2005) J Am Chem Soc 127:8940
250. Xamena FXLI, Abad A, Corma A, Garcia H (2007) J Catal 250:294
251. Sato T, Mori W, Kato CN, Yanaoka E, Kuribayashi T, Ohtera R, Shiraishi Y (2005) J Catal 232:186
252. Tanski JM, Wolczanski PT (2001) Inorg Chem 40:2026
253. Gomez-Lor B, Gutierrez-Puebla E, Iglesias M, Monge MA, Ruiz-Valero C, Snejko N (2002) Inorg Chem 41:2429
254. Tannenbaum R (1994) Chem Mater 6:550
255. Tannenbaum R (1996) J Mol Catal A Chem 107:207
256. Feinsteinjaffe I, Efraty A (1987) J Mol Catal 40:1
257. Naito S, Tanibe T, Saito E, Miyao T, Mori W (2001) Chem Lett 1178
258. Nuzhdin AL, Dybtsev DN, Bryliakov KP, Talsi EP, Fedin VP (2007) J Am Chem Soc 129:12958
259. Schlichte K, Kratzke T, Kaskel S (2004) Microporous Mesoporous Mater 73:81
260. Alvaro M, Carbonell E, Ferrer B, Xamena FXLI, Garcia H (2007) Chem Eur J 13:5106
261. Uemura K, Kitagawa S, Fukui K, Saito K (2004) J Am Chem Soc 126:3817

Struct Bond (2009) 132: 87–134
DOI:10.1007/430_2008_8

Published online: 25 February 2009

The Long Story and the Brilliant Future of Crystallized Porous Solids

Gérard Férey

Abstract This article presents the state of the art in the topical domain of crystallized inorganic or hybrid porous solids and describes their comparison and the strategic approaches currently being developed for understanding their formation, for discovering new multifunctional materials and for improved applications. From recent outstanding results in various fields, this paper suggests some new trends for using rational and predictive chemistry to bring chemical solutions to current societal problems like energy, sustainable development and health.

Keywords: CO_2 sequestration · Drug delivery · Hydrogen storage · Luminescence · Multifunctional materials · Porous materials · Structural prediction

Contents

G. Férey (✉)
Institut universitaire de France and Institut Lavoisier, University of Versailles (UMR CNRS 8180), 78035, Versailles, France
e-mail: gferey@wanadoo.fr

1 Introduction

In materials science, the search for new porous solids, either with an inorganic or hybrid organic–inorganic framework, is very topical [1,2], fuelled by the strong incentives related for instance to their use in catalysis, gas separation [3] or strategic gas storage [4–7]. Their unique structural particularities and the numerous applications they find in all the fields concerning current societal problems (energy, sustainable development, health etc.) render them strategic materials.

Indeed, when compared to other materials, porous solids are unique (Fig. 1). They alone exhibit *at the same time* (i) a framework, purely inorganic or hybrid,

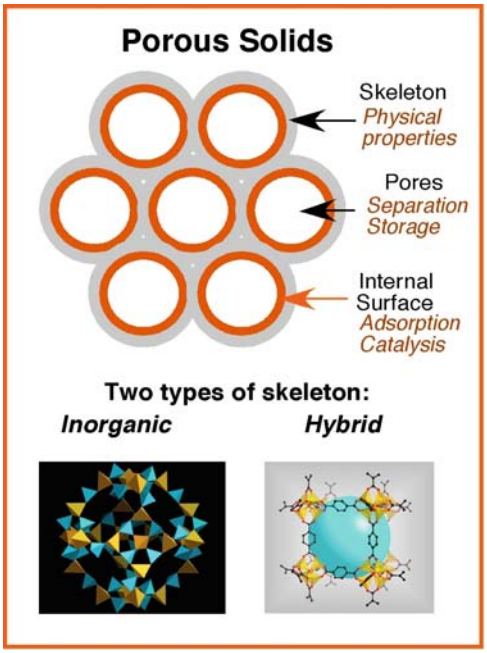

Fig. 1 Representation of the two types of porous solids in terms of skeleton, pores and internal surfaces with, for each, the type of dedicated properties

responsible, as in dense solids, for physical properties like magnetism, conductivity and optical features; (ii) pores that can store species; and (iii) an internal surface, which is at the origin of the catalytic and separation properties of these materials.

The concept of porous solids arose in 1756 with Crönstedt [8]. This Swedish mineralogist, studying the thermal behaviour of the mineral stilbite (a hydrated calcium and sodium aluminosilicate), observed that bubbles appeared on the surface of the solid when heated. He named such compounds zeolites (from the Greek words $\zeta\varepsilon\iota\nu$ (zein) meaning to boil and $\lambda\iota\upsilon o\varsigma$ (lithos) meaning stone). The phenomenon was structurally explained in 1930 with the first crystal structures of zeolites [9, 10]. Water molecules, located with sodium and calcium atoms within the tunnels of stilbite, evaporate through heating and leave empty spaces in the tunnels, creating the porosity.

Many natural zeolites were discovered later, and began to find applications as early as 1850 with the discovery of their ion-exchange properties [11] applied to water softeners. Further, Friedel showed that the pores created by dehydratation could be filled by gases like NH_3, CO_2, H_2S, ethanol etc., opening the field of separation and gas storage [12]. However, the strategic importance of this family really appeared when chemists were able to synthesize them. Sainte Claire Deville opened the way in 1862 [13] with the synthesis of levynite. Even now, the tremendous research in the chemistry and structure of new systems provides new porous solids.

With time, different types of porous solids were discovered, whose properties depended on the size of the pores, the nature of the elements of the skeleton, the coordination of the cations and the dimensionality of the inorganic subnetwork (Table 1). Whatever the characteristics of the skeleton, the size of the pores ($\varnothing$) is the first criterion and offers the first classification:

- *Microporous solids* ($\varnothing < 2$ nm): they correspond to inorganic or hybrid frameworks and are all crystallized
- *Mesoporous solids* ($50 > \varnothing > 2$ nm): the inorganic members (discovered in 1992) have all-amorphous frameworks in contrast to hybrid ones (discovered in 2004), which are crystallized
- *Macroporous compounds* ($\varnothing > 50$ nm): they are amorphous and their representatives are opals

Most of the porous solids described up to now have a purely inorganic skeleton. It was only at the end of the 1980s [14] that a new class of materials emerged at the crossroads of inorganic materials science and coordination chemistry [1, 15–23]: hybrid porous solids or metal–organic frameworks (MOFs), in which the framework is ensured by the linkage of inorganic moieties (mono- or oligomeric) with functionalized organic molecules through only strong covalent or ionocovalent bonds. Now, porous solids are considered to be strategic materials both in academic research and in industry, owing to their numerous applications (Table 2) in finding solutions to current societal problems like energy, environment and health. According to some sources [24], this family of solids, directly or indirectly, represents ca. 20% of the gross domestic product of the industrial countries. Table 2 presents the main types of applications, according to the nature of the porous solids.

Table 1 Different classes of porous solids with their criteria of classification

Dimensions of the pores	Denomination of the solid	Nature of the skeletons	Nature of the template	Coordination of the cation	Dimensionality of the inorganic subnetwork	Family
$\varnothing \leq 20$ Å	Nanoporous	Inorganic (crystallized)	Organic amines, complexes	4	3D	Zeolites, aluminosilicates (phosphates)
				≥ 4	3D	Germanates, metalophosphates, arsenates
		Hybrid (crystallized)	Solvant	≥ 4	0–3D	Coordination polymers, MOFs – MILs
$20 \leq \varnothing \leq 500$ Å	Mesoporous	Inorganic, (amorphous)	Micelles, polymers	≥ 4	3D	MCM and related solids
500 Å $\leq \varnothing$	Macroporous	Inorganic (amorphous)	Micelles, polymers	≥ 4	3D	Opals

Table 2 Some applications of the most important of porous solids. For more information see [3]

Related to	Properties used	In	Some examples
The surface (catalysis)	Acido-basic	Acid catalysis	Activation of alkanes and alcenes Breaking of C–C bonds in aliphatics Formation of C–C bonds in aliphatics Rearrangements of C–C bonds Reactions of isomerisation Reactions of nucleophilic substitution and addition Cyclization reactions Reactions of electrophilic substitution on aromatic rings
		Basic catalysis	Dehydrogenation of alcohols Isomerization of the double bonds of olefins
	Oxydo-reduction	–	Hydroxylation of aromatics (Ti) Oxydation of heavy hydrocarbons (Fe) Oxidizing dehydrogenation of propane and methanol
	Electrostatic	Adsorption	Greenhouse gases, H_2
The pores	Geometry of windows	Selectivity	Selectivity of reactants Selectivity of products Selectivity of isomers
		Molecular sieves	Separation
	Geometry of cages	Gas storage	H_2, CO_2, CH_4, NO_x, SO_x, C_2H_2 etc.
		Adsorption and drug delivery	–
		Nanosciences	Monodisperse nanoparticles
The skeleton	Physical	Magnetism	Ferromagnetic transition metal phosphates
		Conductivity	Mixed valence transition metal hybrids
		Luminescence	Rare-earth-based hybrids

2 What is a Good Porous Solid?

The ideal porous solid must present a maximum of properties, in particular:

- Good thermal stability (1000°C)
- Pores easily generated and easily accessible, with sizes tuneable by chemical substitutions
- A specific surface area as large as possible in order to favour a maximum of interactions between the adsorbed species and the wall for use in catalysis, separation and storage

Beyond these classical properties, a good porous solid must also have a skeleton that can accept a maximum of chemical substitutions on the sites occupied by the cations and the anions of the structure. This allows modulation of the size of the pores, but mainly allows introduction of physical properties (magnetism, conductivity,

optical properties) usually encountered in dense solids and the transformation of these solids into efficient multifunctional materials with sometimes unexpected applications. These ideal specifications have not yet been fulfilled, but the progress realized during the last 20 years make this aim reachable. The number of materials approaching this goal has increased drastically in the last 5 years.

3 Common Points in the Family

Whatever the subclass of solids, they share methods of synthesis and also a common description of structures. Indeed, almost of all these solids are prepared using solvothermal synthesis under autogeneous pressure at temperatures of 100–250°C. The solvents, including water, are either pure or mixed. The yields are very often high but pure phases sometimes require very strict chemical conditions. One can note several recent advances in the methods of synthesis. The first [25], uses a mixture of non-miscible solvents for the hydrothermal synthesis (heavy alcohols and water, for instance). The solid is formed at the interface of the biphasic mixture and, most of the time, provides single crystals of the desired phase. The second method is represented by the first trial for synthesizing MOFs using an electrochemical route [26]. The third method involves microwave synthesis, a method already applied to dense solids and inorganic porous compounds [27–34] and seems very promising for MOFs. The microwave method has already attracted growing attention for the synthesis of nanoporous inorganic materials, which normally require several days for their hydrothermal crystallization. It provides an efficient way to synthesize them with short crystallization times, narrow particle size distributions, facile morphology control, and efficient evaluation of process parameters, etc. However, the microwave method has rarely been applied to the synthesis of porous hybrid materials to date [35]. Chang and coworkers [36, 37] have recently shown that the microwave synthesis of the latter offers several advantages such as fast crystallization and phase selective synthesis.

Hybrid solids with giant pores, chromium trimesate and terephtalate (MIL-100 and MIL-101), have been formed under microwave irradiation after less than 1 h at 220°C instead of 96 h using the conventional route. Moreover, at very short synthesis times (1 min), MIL-101 is obtained as quasi-monodisperse nanoparticles, a feature that could very quickly afford applications in nanosciences. In addition, while the formation of the cubic nickel glutarate (MIL-77), previously synthesized by conventional heating in several hours or days depending on synthesis temperature, was greatly accelerated by microwave irradiation, the more stable tetragonal nickel glutarate appeared within only a few minutes. The cubic phase was preferentially formed at low pH, low temperature and predominantly with conventional electrical heating. In contrast, the tetragonal phase was favourably obtained at high pH, high temperature and especially with microwave irradiation. These selective results suggest the efficiency of the microwave technique in the synthesis of MOFs. The exceptionally rapid crystallization of nickel glutarates was attributed to

different formation pathways compared to those for conventional zeolites. While the formation of aluminosilicate zeolites appeared to involve complex crystallization pathways via hydrolysis, hydrophobic hydration, gelation, nucleation, and crystal growth [38], the porous nickel glutarates apparently grow directly from the reactants once the solution is raised to the appropriate reaction temperature. Consequently, the long induction periods required for zeolite formation are not necessary in the synthesis of nickel glutarates. Morris and coworkers recently reported the synthesis of porous solids using ionic liquids, which can act both as solvent and template [39]. Using both classical and microwave conditions, they conclude that the MOFs prepared under microwave conditions are purer and have higher crystallinity.

Finally, some authors recently developed a dedicated application of high throughput (HT) synthesis to MOFs systems [40–44]. This method has already been employed for zeolites, inorganic frameworks and polymers for applications in catalysis and phosphors [45]. High-throughput methods imply four major steps: design of experiment, synthesis, characterization and data evaluation. Each step has to be integrated in a workflow in order to reach a maximum of productivity and innovation. While HT methods can produce a tremendous amount of data in a very short time, their success depends on the proper application. Thus, the experimental design is a step of paramount importance. Statistical methods in combination with data evaluation programs, genetic algorithms and neural networks have been shown to be powerful tools. The number of reactions must also be minimized by including chemical data and chemical knowledge into the synthesis set-up. In addition, investigations are most often limited to certain parameters, mainly composition, but can also process parameters such as temperature, time and pressure. In a typical experiment, 48 miniautoclaves are filled by various compositions within the same system.

In both subclasses (inorganic or hybrid skeletons), a tremendous variety of systems were chemically and structurally tested. However, it rapidly became necessary to introduce rational approaches besides these "trial and error" experiments, with the aim of reaching tailor-made structures for specific applications. For templated inorganic frameworks like silicates, metal phosphates, metal halides or chalcogenides, mainly obtained under hydrothermal conditions (200°C, 10–30 bar), an approach to their mechanisms of formation was needed in order to play further on conditions of synthesis for obtaining the desired product. For hybrid frameworks, which combine an inorganic part (single polyhedra, clusters or chains) and an organic moiety, the directivity of the covalent bonds introduces more initial geometric information as soon as the inorganic brick is known and stable. Moreover, whatever the subclass, another challenge [46–48] was to increase the size of the pores, limited 15 years ago to ca. 10 Å in diameter. Indeed, larger pores imply enhanced specific surfaces, an important parameter for catalytic properties, and more possibilities for the storage of species. This last point becomes more and more crucial in the twenty-first century where problems of energy and sustainable development will increase dramatically. The challenge of large pores is relevant to *molecular gigantism* [46,49–51], and this review will be concerned exclusively with crystallized porous solids. Mesoporous

solids, despite their larger pore diameters, will not be considered. Their amorphous skeletons rule out their characterization at the atomic scale. Information about them can be found in [3].

The second point that inorganic and hybrid solids have in common is their structural *description*. On a primary basis, their skeletons are based on the connection of polyhedral entities (considered primary building units), which can be described either in a ball-and-stick representation (often used by molecular chemists) or in terms of polyhedra (preferred by solid state scientists). The increasing complexity of the inorganic frameworks has incited researchers to simplify their representation, first in terms of connected polyhedra instead of linked atoms (Fig. 2), but even with that a further simplification was needed. The centres of the polyhedra were therefore assimilated to nodes. Their linkage defined clear figures of nets, which characterized the connectivity of the solid. This approach, initiated by Wells [52], was applied to zeolites by Smith [53] and now the structures of the latter are described using this way [54].

Another way of description of the structures [55] uses, instead of single polyhedra, assemblies of polyhedra (Fig. 2c) that, by translation/rotation in the three directions of space, regenerate the whole framework. These are called secondary building units (SBU) and the concept has been very useful for defining the large pore strategy.

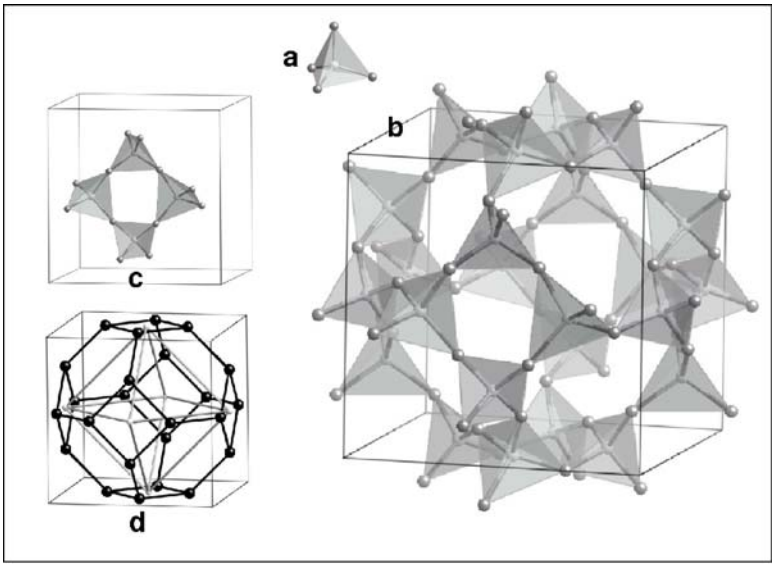

Fig. 2 **a** SiO_4 tetrahedra used for **b** the description of the sodalite structure; **c** the tetrameric SBU able to regenerate its structure; **d** the latter in terms of nets. The linked *black spheres*, which correspond to the centres of tetrahedra, form a truncated octahedron whereas the *grey spheres*, which relate to the centres of the SBU, determine an octahedron

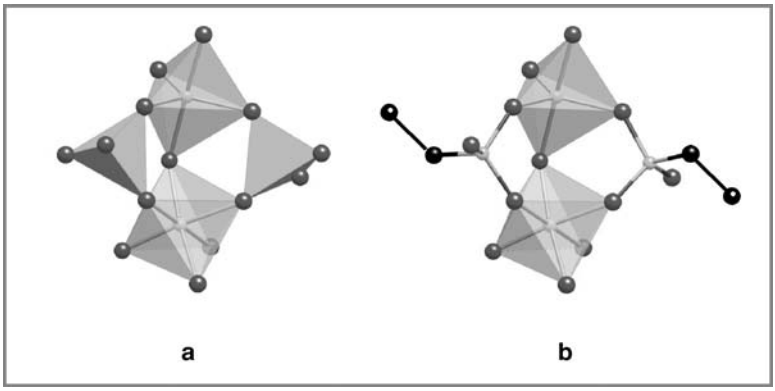

Fig. 3 Relation between the SBUs in inorganic (*right*) and hybrid (*left*) solids

The same concept of SBU applies when hybrid solids are concerned (Fig. 3). Indeed, the three-dimensional skeleton can be described for both of them by the association of SBU. However, whereas the inorganic SBU contain only inorganic parts (tetrahedral species like SiO_4, PO_4, AsO_4, SO_4, associated with metallic cations in four-, five- or six-coordination), in the hybrid SBU, the anionic species are replaced by organic linkers. This creates a contrast between the bonds within the framework: mainly covalent for the organic parts and ionocovalent for the inorganic. Moreover, as far as the porous character is concerned, organic ligands with multiple bonds must be preferred in order to ensure rigid topologies as for inorganic solids with an open framework.

In view of the tremendous number of inorganic–inorganic and inorganic–organic combinations, basic principles are needed for a classification of porous structures. Curiously, in 2000, in the same issue of the same journal, O'Keeffe [56] and Férey [49] paved the way for the development of the topological rules governing the structures of porous solids. Their starting point was the same. They both observed that some structures of MOFs corresponded to extended versions of simple structures (diamond, sodalites etc.). Even if their approaches were slightly different (nets for O'Keeffe, SBUs for Férey), both concepts were concerned by the topology of structures and their invariance whatever the chemical associations. They also aimed at finding porous solids with larger and larger pores [46] for the specific applications that are allowed with mesoporous solids and not with micropores.

O'Keeffe defined the geometrical design principles for frameworks of extended solids [56] based on the concept of *augmented* nets. Every solid can indeed be described by the geometric figure (net) obtained by the connection of the entities of the structure. The idea of these connecting nets is underlined by the old concept of coordination. For instance, in an [N, M] connected net, some vertices are connected to N neighbours and some to M ones. With the idea of creating low density structures, and formalizing a previous idea of Hansen [57], O'Keeffe defined the concept of *decoration* [58] to describe the process of replacing a vertex by a group of vertices. *Augmentation* [56] corresponds to the case where each vertex of a N-connected net

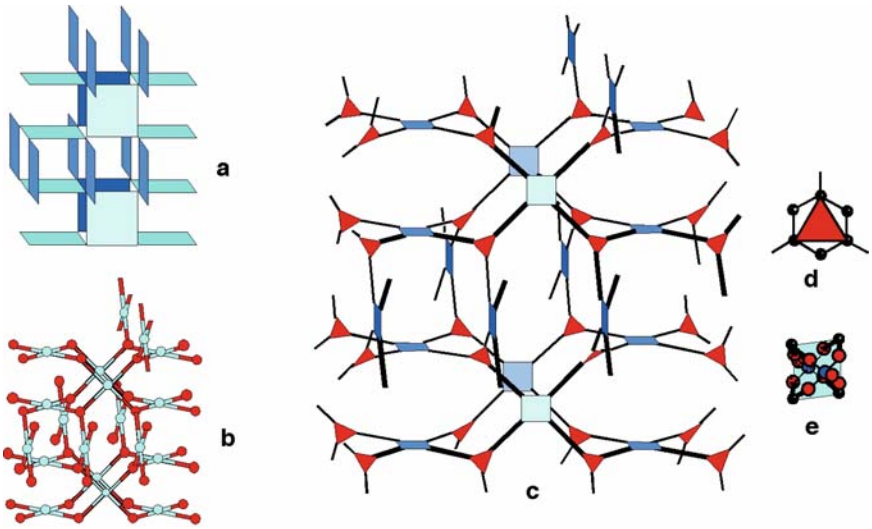

Fig. 4 Principle of augmented nets. **a** Description of Pt_3O_4 in terms of connection of squares. **b** Ball-and-stick representation of Pt_3O_4 (Pt *blue*, O *red*) showing the fourfold coordination of Pt and the threefold coordination of O. **c** Augmented version of Pt_3O_4; O is replaced by a *triangle* and Pt by a *square*. Both polygons are related by linkers; keeping the same topology in copper(II) 4,4′,4″-benzene-1,3,5-triyl-tribenzoic carboxylate, the *triangles* correspond to the connecting points of the central phenyl ring of benzene-1,3,5-triyl-tribenzoic carboxylate **d** and the square by the Cu dimer linked to four carbons of the carboxylate functions **e**

is replaced by a group of N-vertices. In other words, this replacement does not affect the connectivity of the parent net.

The example of platinum oxide Pt_3O_4 taken as a parent structure (Fig. 4) illustrates this concept. In this solid, platinum ions are in square-planar coordination by oxygen atoms, and the latter are connected to three Pt atoms (Fig. 4a), thus creating a [3,4] net and a structure based on the three-dimensional assembly of square planes (Fig. 4b). The augmented net will replace the Pt atom by a square (which provides the same connectivity as Pt) and the oxygen atom by a triangle (which provides the same connectivity as O). Once related by a line, the vertices of these two polygons create the augmented net (Fig. 4c). The squares and the triangles may be referred to as the topological SBU; that is, they represent species whose connectivity is four for the squares and three for the triangles, whatever their chemical nature. Moreover, the line joining the polygons can be a bond, but also a sequence of bonds, the latter case being called *expansion* by O'Keeffe [56]. With this approach, a copper(II) 4,4′, 4″-benzene-1,3,5-triyl-tribenzoic carboxylate corresponds to an augmented Pt_3O_4 net [59]. In this solid, the squares are taken up by a binuclear Cu carboxylate moiety (Fig. 4d) and the triangles correspond to the three corners of the benzene ring acting as the vertices of the inner triangle, the linkers being phenyl groups (Fig. 4e).

The O'Keeffe principle of *augmented nets* was not only a tool for describing complex structures in a simple manner, but was also very inspiring for the synthe-

sis of new MOFs with large pores showing very simple basic topologies dictated by the shape and connectivity of the building units. O'Keeffe anticipated that a few simple high symmetry topologies would be of paramount importance in the future for such a purpose. In a further work based on this principle, his group detailed the rules for reticular synthesis [60] (defined by the authors as "the process of assembling judiciously designed rigid molecular building blocks into predetermined ordered structures which are held together by strong bonding") and the design of new materials. They also proposed a classification of the known structure types of MOFs [61], labelled, as for inorganic porous solids [54], by three small letters with oblique characters, often referring to an abbreviation of the formula of the parent structure.

The tool of description of Férey, known as the *scale chemistry* concept [49], started from his analysis of solids in terms of secondary building units (SBUs). Instead of describing structures by the connection of single polyhedra, he showed that it was possible to analyse them using larger units (SBUs or "bricks") which, by translation and/or rotation and further sharing of vertices, built up the final solid. Playing on the size of the SBU, he illustrated his concept by numerous examples, for instance the following (Fig. 5): If the brick is an atom, for example metallic, the topology of the resulting solid is generally face-centred cubic (fcc); if the brick is a cube of atoms, the resulting structure is the fluorite type, always fcc; if the brick is a C60, the fullerene structure is obtained, which also exhibits a fcc arrangement. This means that, whatever the size of the SBU, the topology of the resulting structure remains invariant and, in terms of porosity, *the larger the brick, the larger the pores*. This defined one of his strategies for a possible access to giant pores and to new applications related to their large sizes.

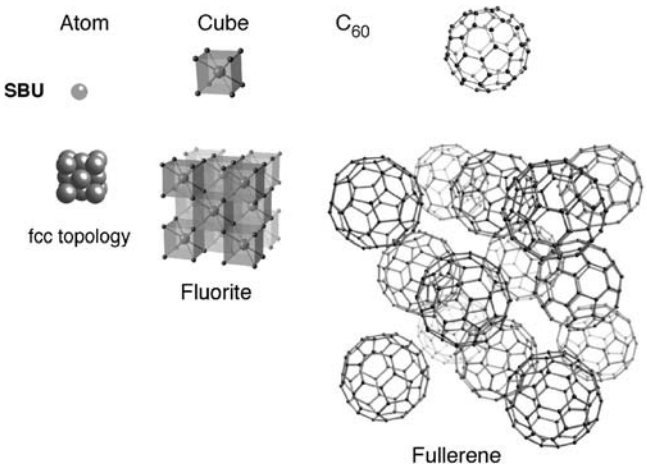

Fig. 5 Principle of scale chemistry: whatever the size of the brick, the three-dimensional arrangement keeps the same topology (here fcc)

As seen in Sect. 4, Férey's in situ studies on the mechanisms of formation of inorganic porous solids [62–67] proved the existence within the solution of SBUs identical to those that existed in the final solid. These SBUs, initially a tool of description, became a reality and then could act as "bricks" for the construction of the solid. Moreover, he proved that the increase of the size of the inorganic moiety (and therefore the extent of oligomeric condensation of inorganic species in the solution) is strongly dependent on the weakening of the charge density of the template. This allowed the rational synthesis of MIL-74 [68] an aluminophosphate using TREN as a template. MIL-74 has a supersodalite structure (Fig. 6). The square brick of four tetrahedra existing in the pure sodalite is replaced by a square of nine tetrahedra, which create a cage eight times larger than that of the sodalite.

Both concepts are complementary for the creation of new topologies. They have in common the key notion of connectivity (number of atoms shared with other SBUs and their spatial geometry) of the SBUs (Fig. 7).

Both concepts are simple, inspiring for the search of solids with dedicated applications. Even if they do not pretend to exhaustivity, they provide elements of thought that stimulate the imagination of researchers without neglecting the unexpected results of serendipity, which will refine the concepts. Indeed, both principles have limitations. In the case of MOFs (but not in the case of inorganic porous solids), the O'Keeffe principle seems to be restricted, at least for most of the cases, to the creation of coordination polymers in which the inorganic part is a cluster because the augmentation of the primitive net always respects the alternation of the cation and the anion of the original simple structure and therefore the alternation of organic and inorganic moieties. In terms of predictability, the principle does not consider the variability of the inorganic SBU with the chemical conditions. It is applicable for

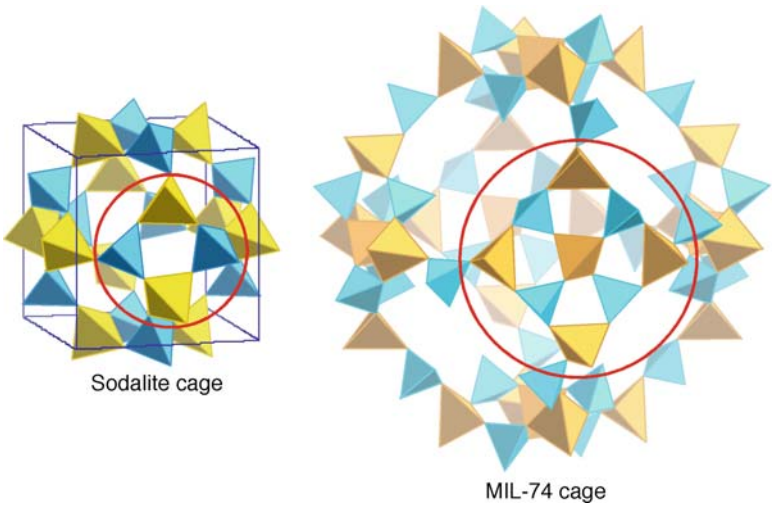

Fig. 6 Comparison of the sodalite and MIL-74 cages with the same topology. The latter is eight times larger than the former

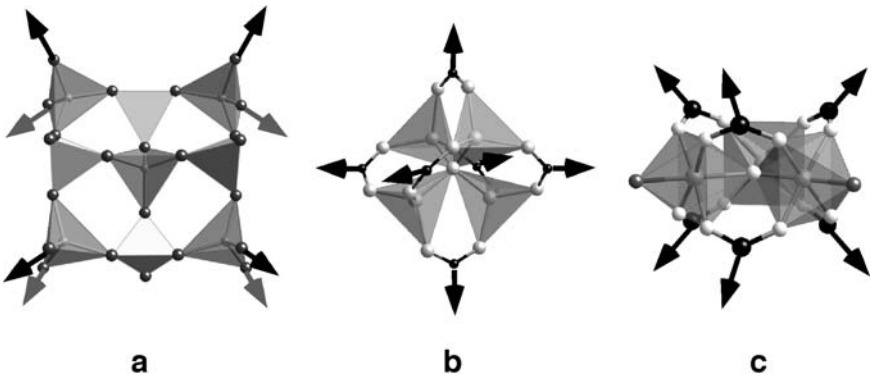

Fig. 7 Some examples of connectivities (Cnc) of the SBU, either inorganic (**a** MIL-74: Cnc 8 cubic) or hybrid (**b** MOF-5: Cnc 6 (octahedral) and **c** MIL-101 Cnc 6 (prismatic))

already known bricks with a variation on the organic linker. In contrast, the Férey principle takes into account this variability of the bricks, but considers the same linkage in a whole series. At least at the beginning, the extension concerned only the inorganic brick, the connection being invariant, but recent examples [69–71] have proved that scale chemistry can also apply to the shared vertices. Moreover, it is not restricted to organic–inorganic connections, but also accepts inorganic–inorganic ones for explaining, for instance, the existence of MOFs with 1D or 2D inorganic subnetworks. However, it must be kept in mind that these two principles correspond to geometrical rules. One must never forget that the structures of porous solids are governed by thermodynamics and not by geometry. At variance to the opinion of some authors, the above rules can only *suggest* some possibilities of arrangements of the SBU. They cannot *predict* them. This point will be discussed further in this paper.

4 Templated Porous Inorganic Solids

Templated porous inorganic solids are obtained by precipitation in hydrothermal conditions from an aqueous solution that contains, beside the inorganic species, organic moieties like amines or ammonium ions acting as templates during the precipitation. Zeolites [3] are the most known of this category. Their framework, based on corner-sharing of SiO_4 and AlO_4 tetrahedra, delimits cages and/or tunnels, which represent the pores of the structures. Later, other porous solids [2] (metal phosphates and arsenates, halides and chalcogenides) involving not only tetrahedral but also pentahedral and octahedral coordinations for the metals were discovered.

4.1 SBUs: Mechanisms of Formation and Simulation of Structures

When the concept of SBU as a useful tool for the *description* and classification of the porous structures was proposed, there was no experimental proof of their real existence in solution. The dogma was the invariance of these SBU during the precipitation process. This hypothesis had to be validated. Our group looked at this on porous alumino- and gallophosphates [63] and titanophosphates [72] using in- and ex-situ NMR experiments under the conditions of hydrothermal synthesis after a careful analysis of the pertinent chemical parameters governing these systems (pH, temperature, nature of the amine template, concentrations etc.) [73]. The existence of SBUs in the solution was confirmed for these systems and it was proved that the driving force of the synthesis was the charge density of the template, which (i) governs the extent of the oligomeric condensation that gives rise to the SBU in the solution, (ii) is responsible for the creation of neutral ion pairs leading to precipitation and (iii) determines, by its size and plasticity, the structural organization.

Once the existence of the bricks was established, and therefore the chemical conditions of their stability, it became possible to create new materials based on a given brick by playing on the nature of the amine template. It was an approach to tailor-made solids that had some successes [74, 75]. As it is impossible for chemists to explore the whole space of phases in a system, we introduced an original computer simulation method based on Monte Carlo simulated annealing for generating candidate crystal structures (automated assembly of secondary building units or the AASBU method), based on the concept of SBUs and their linkage in 3D space [76]. For a given brick, the AASBU method produces virtual libraries of energetically viable inorganic structures based on pre-defined SBU. These bricks are implemented according to the following criteria:

1. One constraint on the nature or size of the SBUs involved: $M/P = 1$ for AlPOs and GaPOs
2. No explicit constraints on cell dimensions, but optionally on space group symmetry
3. An ability to accommodate one or more types of SBU
4. Accommodation of differing modes of inter-SBU connection, allowing, for example, corner-, edge- and face-sharing modes
5. A broad flexibility in the definition of the linkage points

The wide applicability of the method in inorganic chemistry was demonstrated by finding the known families of inorganic structures using simple SBUs. It also provided numerous hypothetical frameworks, using several types of SBUs [77, 78], which were classified as not-yet discovered or virtual [78, 79] according to their relative energy compared to that of dense phases. Chemical studies are currently in progress to discover some of them. Note that a similar approach [80] was used by Foster et al. for zeolites. It now provides a virtual library of several millions of possible structures for zeolites.

4.2 SBUs and "Scale Chemistry": a Route Towards Large Pores

This concept, based on the invariance of the topology whatever the size of the SBU, has a direct consequence for the search of large pores. Indeed, if it is possible to create large SBUs instead of the small ones discovered up to now, larger SBUs would create larger pores, and therefore solve the problem. Owing to the special role played by the charge density of the amine on the size of the SBU (the lower the charge density, the larger the SBU) [73], the search for large pores requires the use of large, multifunctional amines with weak deprotonation for providing a low charge density and initiating large SBUs. The supersodalite MIL-74 (see Fig. 6) came from this strategy, using TREN as templating agent. The usual tetrameric squares of tetrahedra are replaced by enneamers. The hexagonal windows of the sodalite structure become dodecagonal and create a large cage ($\varnothing = 10\,\text{Å}$), eight times that of the sodalite.

Scale chemistry also applies to a fascinating new family of templated porous indium-metal chalcogenides coming from two American groups [81]. The structures are all based on T_p supertetrahedra, which are formed by the corner sharing of single InX_4 tetrahedra, p (currently ≤ 5) corresponding to the number of single tetrahedra along one edge of the supertetrahedron. The latter share vertices. The cages are occupied by the templates. Moreover, these supertetrahedra can assemble into hypertetrahedra labelled $T_{p,q}$ for the description of a T_q hypertetrahedra composed of T_p supertetrahedra. If the templates could leave the cages without collapse of the framework, this would provide a free volume of more than $1800\,\text{Å}^3$! These phases represent the upper homologues of dense structures like diamond, sodalite, cristoballite and CrB_4 types.

4.3 First Limits

The above examples show some limits in the evolution toward large cavities in porous inorganic solids. Chemically, in some systems, the reactivity of the components decreases with the complexity of the SBU and, even if some topologies can be predicted, their experimental discovery becomes sometimes doubtful. Moreover, the increase in cell volume decreases the facility to obtain single crystals, as already true for protein crystallography. Despite the tremendous progresses in ab initio structural determination from powder diffraction data, a crystal is necessary for structures with cells larger than ca. $300{,}000\,\text{Å}^3$ [82]. For good data collection, the threshold in crystal size was recently lowered to $1\,\mu^3$ [83]. Correlatively with the cell expansion, the thermal stability also decreases when the template is extracted. Whereas in zeolites and most aluminophosphates, the evacuation of the template maintains the integrity of the skeleton, a collapse of the structure is more and more frequent when the pores become larger. Some of these limits, which restrict the field of new porous inorganic compounds, do not exist for hybrid solids, as will be shown in Sect. 5.

5 Porous Metal–Organic Frameworks (MOFs)

5.1 State of the Art

The substitution of inorganic tetrahedra by organic molecules dramatically increases the number of possibilities, owing to the infinite variety of functionalized organic molecules that can be used (N donors, polycarboxylates, polyphosphonates and polysulfonates with either aliphatic or rigid carbon skeletons, fixed by ionocovalent bonds to the metallic centres). One can play on the length of the carbon chain, on the connectivity and the chirality of the ligand, on the nature and the oxidation state of the metal [1], leading to a quasi-infinite number of possible compounds.

Within the hybrid 3D network, if this inorganic part is zero-dimensional (single polyhedra or clusters), one speaks about porous coordination polymers. They represent the major part of the discovered solids, up to now. More rarely, however, the dimensionality of the inorganic subnetwork can also be 1D [84, 85], 2D [86, 87] and even 3D [88–90] (Fig. 8).

It was recently shown [91] that within a given system the reaction temperature plays a major role in the degree of condensation of the inorganic subnetwork, which can range from 0D to 3D in a few tenths of a degree. If one adds that the reaction of the organic ligands is effective with almost all the metallic elements including transition metals and rare earths, the result has been the discovery of hundreds of new compounds over the past 10 years. Compared to the solids with a pure inorganic skeleton, which require extraction of the template to become porous, MOFs have the great advantage of giving directly accessible porosity, modulated by the size of the ligand, after extracting the solvent molecules. They have, however, in most cases, a lower thermal stability than inorganic frameworks.

Once the richness of the field was discovered, it was necessary to rationalize the synthesis of MOFs to provide tailor-made architectures. At the beginning, the *reticular chemistry* of the augmented net concept of O'Keeffe et al. [56] was nicely applied for defining the chemical and topological rules governing this possible design. The derived structures of MOF-5 [4] provide the most famous example of this approach.

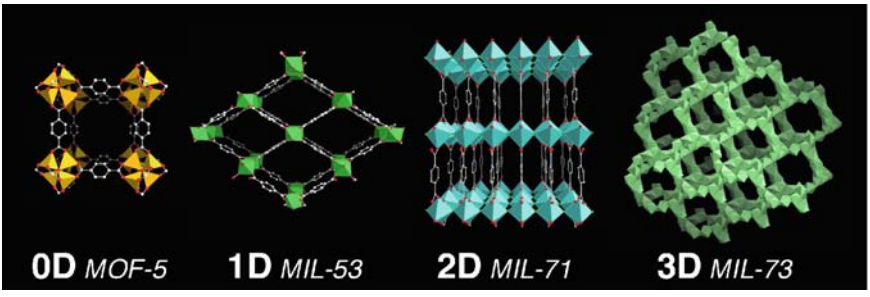

Fig. 8 Examples of MOFs with various dimensionalities of the inorganic subnetwork: MOF-5 [4], MIL-53 [100], MIL-71 [87], MIL-73 [90]

However, the concept is confronted by chemical reality, and two steps limit this strategy: (i) as far as the search for giant pores is concerned, the first difficulty comes from the tendency of the framework to be interpenetrated or interwoven [17], which decreases the porosity of the solid and must be avoided wherever possible; and (ii) the difficult chemical control of the existence, size and connectivity of the inorganic SBU, mainly in solvothermal conditions. In MOFs, knowledge of the inorganic SBU for mastering the structure is a key point, since the organic part is structurally inert and just plays the role of linker. The currently used SBUs are well known by inorganic chemists for their room or moderate temperatures of reaction and the rare inorganic bricks evidenced up to now are stable; they exist in a large range of temperature and have been known for a long time with their associated chemical conditions of existence. In contrast, nothing is established as soon as hydrothermal conditions are applied because the properties of the solvent change drastically and, correlatively, so does the nature of the species in the solution. A systematic study of the conditions of the existence of each SBU is therefore needed for a better mastery of the "design" of MOFs. Our group currently performs in situ studies for finding new inorganic SBU able to increase the number of possibilities and of new connectivities to enrich once more the possibilities of obtaining tailor-made solids. The two first examples are the discovery of the hexameric cluster of corner-shared octahedra [92] and the invariance of the trimeric cluster of three octahedra during the reaction with carboxylic acids [93]. The mastery of the latter was at the origin of the discovery of the two first mesoporous crystallized MOFs, as explained in detail below.

Moreover, it is worth noting that reticular chemistry, despite its richness, needs a parent structure and concerns only the realization of a reasonable expectation (based on intuition), assuming that thermodynamic conditions are fulfilled, for obtaining an augmented architecture. Even under these conditions, it does not explore *all the possibilities* of connection of the appropriate inorganic and organic building blocks. In particular, it does not predict polymorphs, which exist for instance with vanadium(III) terephtalates MIL-47 [94] and MIL-68 [95]. Only original global structural simulations, like those we performed on inorganic skeletons (see above), are appropriate to an exploration of the whole space of configurations.

5.2 SBUs and Prediction of Possible MOF Structures

With these ideas, our group has developed a new method [96]. It combines the determination of the chemical conditions of existence and integrity of the inorganic SBU in solvothermal medium [97] with a computer simulation approach, derived from our initial AASBU method [76], for the prediction of hybrid structures [98]. The latter also uses a simulated annealing Monte Carlo procedure and generates the whole set of possible connections between organic and inorganic SBUs. If there is a reaction between the organic and inorganic counterparts, the resulting product must adopt one of the virtual structures obtained from the simulations. Moreover,

just the comparison between the experimental and the calculated powder diffraction patterns provides the structural solution.

Our first chemical approach aimed at originality and concerned the search for the conditions of stability of a trimeric inorganic unit (a scarce SBU, previously reported only with divalent cations), but with trivalent ions, for which no example exists up to now in the domain of MOFs. Our strategy was to start from soluble precursors that already contained these trimers and to establish the conditions for its chemical integrity during the reaction. Already confirmed by an in-situ EXAFs study [93], these conditions, primitively determined for Fe^{3+} [97], have been extended recently to Cr^{3+} and V^{3+} and lead to new MOFs containing the desired SBU.

Our simulation method takes advantage of the SBU concept, already used in our previous AASBU method [76], through the assembly of predefined organic and inorganic SBUs. It is performed in 3D space with minimal input, aiming at computationally exploring the possibilities of connection. The inorganic and organic counterparts may be treated independently, i.e. as two different building units (the "mixture" method in [98]) or encapsulated in a single hybrid building block. Both approaches were explored. The simulations provide a list of hybrid candidates, with their space group, cell parameters and atomic positions. Our aim was not only to simulate existing structures, but more importantly to predict not-yet-synthesized structures, aiding the often difficult task of crystal structure determination, rationalizing different but related structure types, while tackling the issue of polymorphism by limiting the domain of structures that are possible for a given metal–organic ligand pair.

The preliminary step consists in elaborating a suitable library of SBUs, directly extracted from known MOFs. The inorganic unit is modelled by a rigid body, and the organic unit as a flexible body. The computational assembly is further controlled through the use of pre-defined "sticky-atoms", all ligand atoms on both units being defined as equally possible linkage points. The rules that control the possible assembly of the two SBUs during the subsequent simulation steps are defined in a force-field that includes sticky-atom *pairs*, parameterized on an atom–atom basis by a simple Lennard-Jones expression for the "energy" of interaction. A repulsive potential between organic pairs avoids their overlapping. For a run, the amount of input data is minimal: the number of organic and inorganic units per asymmetric unit and, optionally, the space group.

The validity of the method was proved by finding the existing and well-characterized MOFs based on mono-, di- and tetrameric inorganic SBUs and organic ligands like benzene 1,4 dicarboxylate (BDC) or benzene 1,3,5 tricarboxylate (BTC) with a very good accuracy. However, the most attractive feature of the simulations remains the generation of new topologies.

The application of the method to trimeric units with the same ligands as above (BDC and BTC) in a 1:1 ratio for BDC and 2:3 for BTC leads to a whole series of plausible and very open MOFs with hitherto unknown topologies for most of them. Among all the discovered topologies, only three present reasonable lattice energies, but only one fits with the experimental data of powder diffraction. This topology is of particular interest for the unprecedented giant cubic cells they provide (380,000 $Å^3$ for BTC and 706,000 for BDC), far beyond all the known ones.

Last but not least, the Bragg peaks of their calculated diffraction pattern exactly fit with those of solids (MIL-100 for BTC and MIL-101 for BDC) obtained in a powdered form in the systems Cr(III)-BDC and Cr(III)-BTC for a 1:1 Cr/BxC ratio (x = D or T). The only difference concerns the discrepancy between calculated and experimental intensities; the first corresponding only to the skeleton, whereas the experimental takes also into account the contribution of the occluded species. Astonishingly, despite the large number of parameters (> 200 for BTC), the Rietveld refinements of powder data, obtained using synchrotron radiation, converge toward good *R* values and improve the prediction by the location of the inserted species, i.e. free water molecules in these cases.

The resulting cubic structures of MIL-100 [96] and MIL-100 [99] (S.G. Fd–3m) are based on trimers (Fig. 9a). They have in common the occurrence of supertetrahedra (ST) as building blocks (Fig. 9b), formed in such a way that the four vertices of the ST are occupied by the trimers. For MIL-101, the position of the organic linker corresponds to the edges of the ST. Within it, the microporous cage corresponds to a free internal diameter of 8.7 Å. More interestingly, the corner-sharing of the ST (Fig. 9c) delimits a framework (Fig. 9d) with two types of cages (Fig. 9e–f), whose dimensions are now typically in the range of *mesopores*. With BDC, the smallest one, limited by 20 ST, has only pentagonal windows (free openings $\sim 12.5 \times 12.5$ Å) and an internal *free* diameter of ≈ 29 Å. The connection of the pentagonododecahedral cages creates larger cavities, limited this time by 28 ST, with 12 pentagonal and four hexagonal windows (free aperture $\sim 16.3 \times 16.3$ Å).

The internal *free* diameter becomes close to 34 Å. This is another breakthrough of our method. Indeed, in inorganic chemistry, such dimensions were only reached with mesoporous solids with amorphous walls. Thus, MIL-100 and MIL-101 provide the first example of mesoporous solids with crystallized walls, with a unique hierarchical system of three types of cages of different dimensions ranging from nano- to mesoporosity. This leads to pore volumes near $1.96\,cm^3\,g^{-1}$ and an apparent Langmuir surface area of $5900(100)\,m^2\,g^{-1}$ for MIL-101, which constitutes a new record compared to [101]. Interestingly, the arrangement of the ST in MIL-100 and MIL-101 present (Fig. 9d) the same topology as a well-known zeolite (MTN-type) [54], the ST replacing the single tetrahedra in the latter. It therefore illustrates once more the "scale chemistry" concept.

Computer simulations found two polymorphs of this new structure type, with the same relative energy cost. One is cubic (Pm–3n) (volume 64,500 $Å^3$) and is the upper analogue of another zeolite: MEP. The other is hexagonal ($P6_3/mmc$), (volume 23,600 $Å^3$) and has no known equivalent in denser structures. They are all built from the same ST. In all of them, the pentagonododecahedra are present. Only their connection in 3D space is different and leads to large cages with 26 vertices instead of 28 in the cubic polymorph, while the hexagonal one exhibits the same large cages as MIL-100 and MIL-101. So, to reply to the provocative sentence of John Maddox:"One of the continuous scandals in the physical sciences is that it remains in general impossible to predict the structure of even the simplest crystalline solids from the knowledge of their chemical composition", we can now say: "It is done for MOFs, Mr Maddox! And, as a bonus, we give you the polymorphs!"

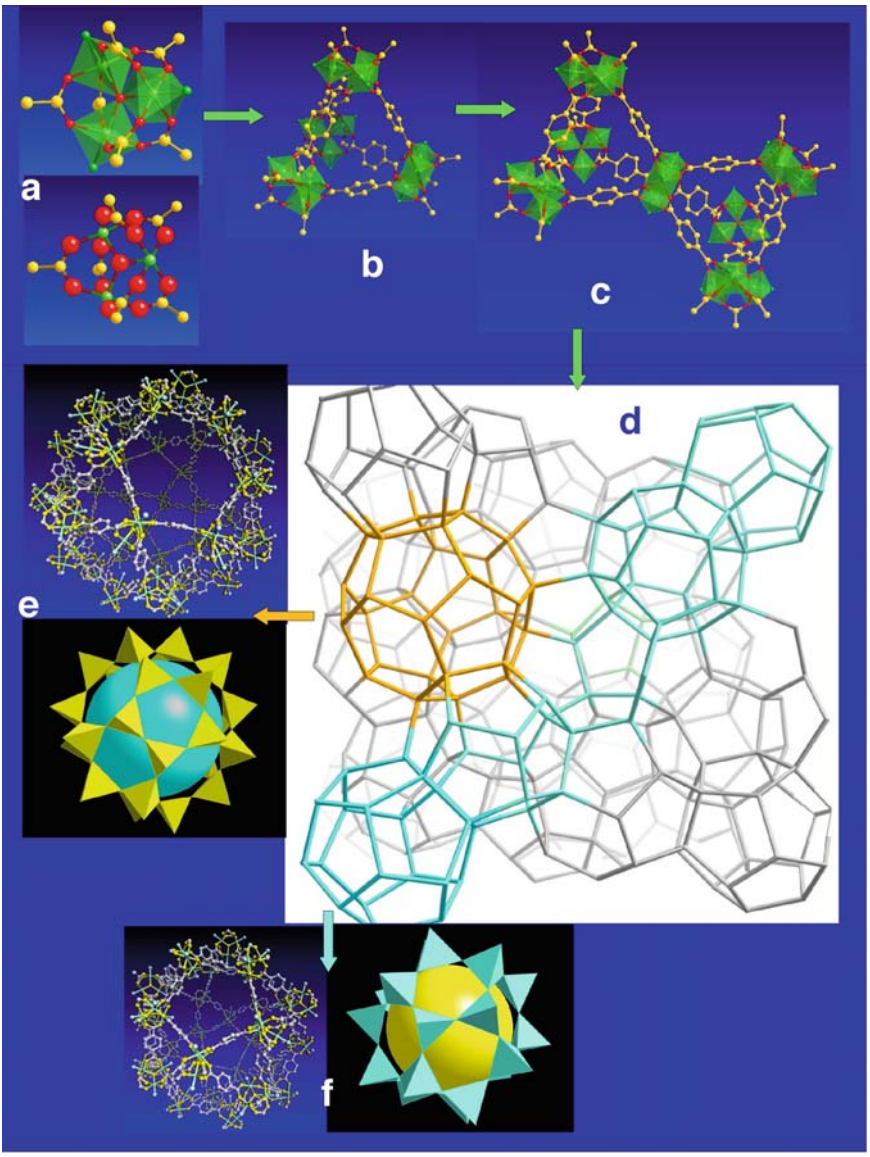

Fig. 9 Structure and building of MIL-101. **a** Trimeric inorganic cluster, **b** supertetrahedral SBU, **c** their connection, **d** framework of MIL-101. The *lines join* the centres of the supertetrahedra and show two types of cages (*yellow* and *blue*). **e** Ball-and-stick and polyhedral representations of the large cage; **f** ball-and-stick and polyhedral representations of the small cage

Despite their large volumes, these solids are thermally stable up to 350°C and can support the effect of electronic beams without damage [102]. In general, MOFs are resistant to heat. Their stability can even reach 500°C. The tremendous research

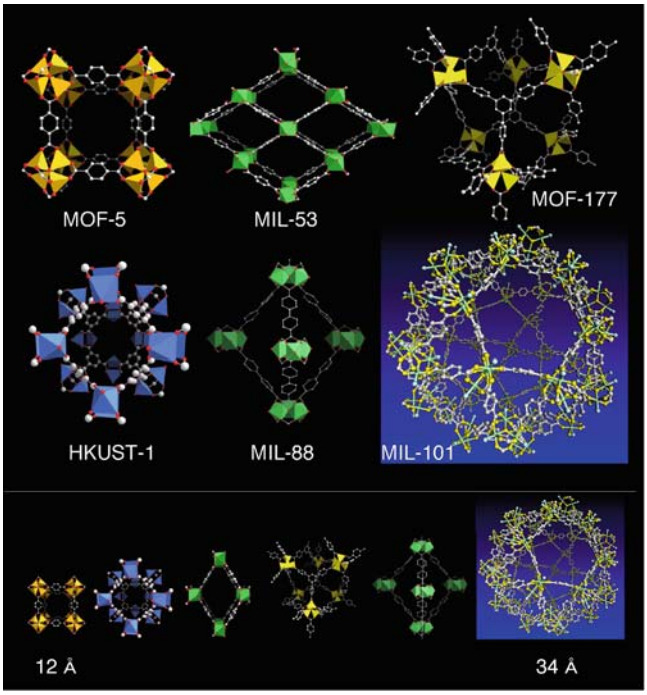

Fig. 10 The currently most cited MOFs (*upper part*). In the lower part, their cages are represented at the same scale

on new MOFs is always increasing and every month, new solids are discovered. However, within the huge family discovered up to now, only a few are studied due to their outstanding characteristics, the first being the existence of large pores that induce both academic and industrial interest. Figure 10 presents their structural characteristics.

5.3 Structural Originality of MOFs; Dynamic Frameworks and Breathing

Beside all these topologies, a strange feature arises with some MOFs, which relates to their flexibility. It is a general problem that concerns not only 0D coordination polymers, but all the dimensionalities of the inorganic subnetwork. As early as 1997, Kitagawa [103] suggested classifying the hybrid porous frameworks into three categories, which he called "generations". The first concerns frameworks that are sustained only with guest molecules and collapse on removal of the guest, most of the time irreversibly. The second generation corresponds to stable and robust porous frameworks that exhibit permanent porosity without any guest in the pores. The last

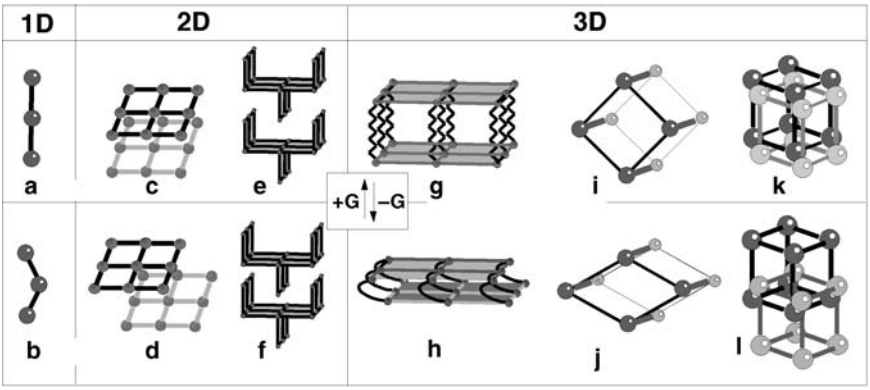

Fig. 11 The six classes of Kitagawa (**a–l**)

category refers to flexible frameworks that change, most of the time reversibly, their structure to respond to external stimuli. The stimulus can be temperature, pressure, light, electric or magnetic field, guests etc. Depending on the structure itself, the input is associated with either an expansion or a contraction of the cell volume and can generate induced movements larger than 10 Å during the transformation.

Such a phenomenon, illustrated by several examples, has lead Kitagawa [104] to distinguish six classes of dynamic frameworks (Fig. 11) in relation to the dimensionality of the inorganic subnetwork. In the 1D class (Fig. 11a, b), the voids between the chains are occupied by small molecules and can exhibit ion exchange [104]. In the first case of the 2D class (Fig. 11c, d), the manner of stacking of the layers (superimposed or shifted) is strongly dependent on the nature of the guest and the weak interactions the guests have with the layers. In the second case (Fig. 11e, f), the interdigitated layers are superimposed and form 1D channels [105–107]. Closed without guests, they open with some of them, resulting in an elongation of the stacking parameter.

In the 3D cases, three situations occur. When pillared layers are involved (Fig. 11g, h), the reversible phenomenon of interlayer elongation and shortening is realized by non-rigid pillars [108]. The expanding and shrinking frameworks (Fig. 11i, j) act as sponges. Keeping the same topology, the drastic volume change is induced by strong host–guest interactions. Depending on the structure, the volume increase is associated with either the evacuation [94] or the inclusion of the guests [109–113]. Finally, in the case of interpenetrated grids, they are densely packed in the absence of guests and the introduction of molecules generates a sliding of one network (Fig. 11k, l) [114, 115]. Most of the cases imply significant atomic movements during the transition, typically in the range 2–4 Å. However, these displacements can reach values in the range 5–10 Å whereas the topology of the framework is maintained. This is observed in class 5 (expanded and shrunken grids) and concern two structure types (MIL-53 and MIL-88) isolated in our laboratory.

The MIL-53 type [94, 100] [(M^{III}(OH)L, guest) with M = Al, V, Cr, Fe; L = terephtalate, naphtalene dicarboxylate] is built up from chains of octahedra sharing

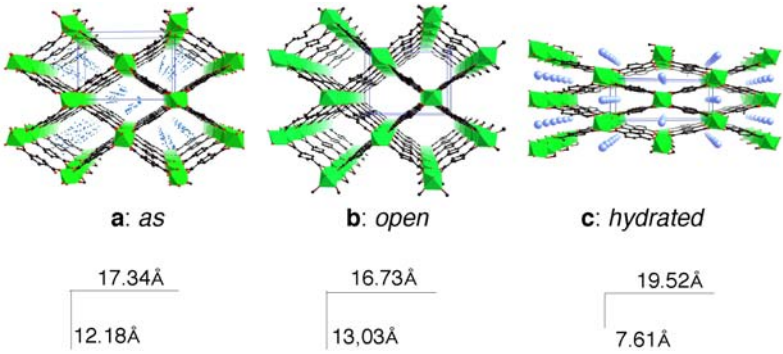

Fig. 12 Different forms of MIL-53: **a** as synthesized (*as*), disordered terephtalic acid molecules lie within the tunnels; **b** high temperature (*open*); **c** room temperature hydrated form (*hydrated*). Note the changes in the cell parameters during the thermal treatments

OH vertices, which are linked in the two other directions by linkers (Fig. 12) in order to create 1D lozenge-shaped tunnels.

The expanded empty form occurs at high temperature. By cooling, a water molecule is trapped in the tunnels and induces a drastic shrinkage of the framework with a decrease of the cell volume of ca. 40% associated with atomic displacements of -5.2 Å in one direction and of $+3$ Å in the other one. The transition is fully reversible. It is worth noting that, in the case of MIL-53, the input (water) provokes a contraction of the framework. An in-situ solid state NMR study proved [85] that two types of strong hydrogen bonds between water and the skeleton were responsible for the shrinkage. This very large breathing induces some selectivity during the exchange of water by other solvents. Acetone and ethanol are not exchangeable, whereas DMF is, owing to the sufficiently strong hydrogen bonds they form with the skeleton. This large breathing effect induces new applications, described in the last section.

The MIL-88 type, (MIL-88A for muconate, B for terephtalate, C and D for naphtalene and biphenyl dicarboxylates, respectively) with an hexagonal symmetry [93, 97, 116, 117] corresponds to a coordination polymer based on trimeric units with three octahedra sharing a μ_3-oxygen (Fig. 13). Within the 3D structure, the carboxylates linking the trimers create both tunnels and triangular bipyramidal cages in such a way that, in the latter, there is no connection between the trimers in the equatorial plane of the bipyramid.

This peculiarity induces unprecedented very large breathing effects, but in contrast to MIL-53, the input (solvent) is associated with an expansion of the framework (Fig. 14). The extent of these swellings (most of the time reversible) strongly depends on the nature of the dicarboxylate linking the trimers in the solids.

The as-synthesized solids always contain a few solvent molecules and drastically increase their volume by solvent exchange while keeping the same topology. The evacuation of the solvent molecules by heating provides the dry forms, with the same symmetry, but with a strong decrease in the cell volume. For example,

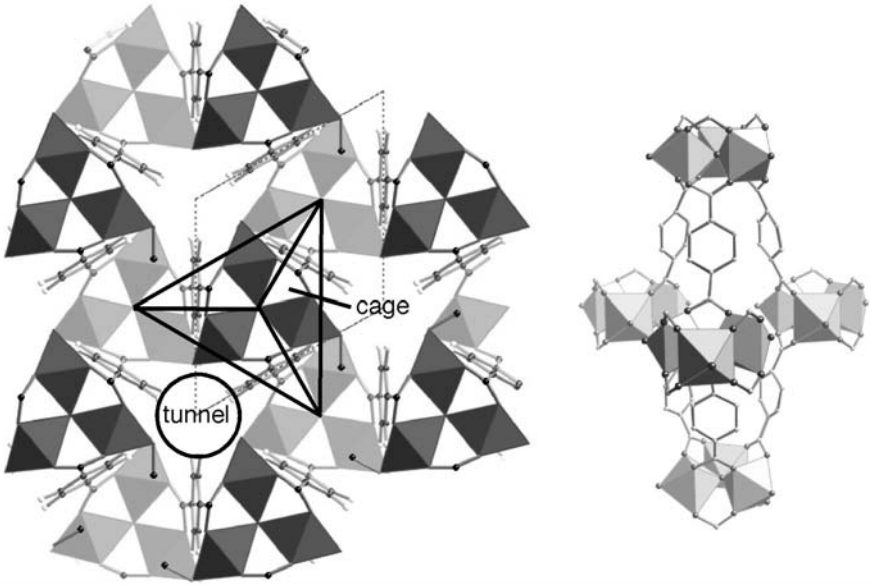

Fig. 13 (001) projection (*left*) of MIL-88B and perspective view of its cage (*right*)

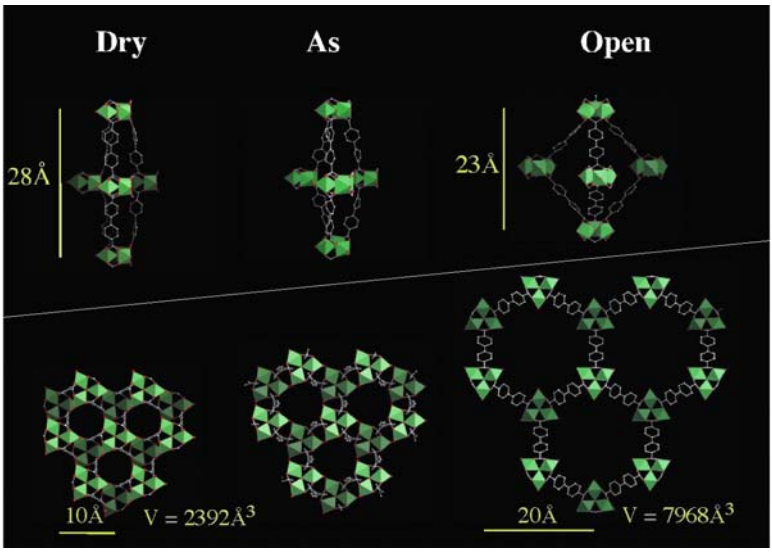

Fig. 14 Evolution of the breathing of MIL-88D. The (001) projection and the view of the cages are represented: *from left to right*, the dry closed form, the as synthesized structure (*as*) and the open extended one (*open*)

in MIL-88D (chromium(III) biphenyl dicarboxylate), the ratio V_{open}/V_{dry} is larger than three, which means a difference of more than 300% between the two states [118]. Correlatively, this expansion/shrinkage implies very large reversible atomic displacements in the structures (> 10 Å for MIL-88D), the topology remaining invariant with apparently no bond breaking.

Structural reasons must exist for explaining such a behaviour. They concern two types of situations: (i) the intrinsic flexibility of the framework itself, induced by the existence of "weak points" within the skeleton, which allow the deformation of the network under the action of the stimulus (this was explained for MIL-88 and MIL-53 [118]) and (ii) the host–guest interactions (hydrogen bonds, VDW forces, $\pi - \pi$ interactions)

On the last point, the interactions created by the guest must be sufficiently energetic to induce the structural changes described by Kitagawa and, once this condition is fulfilled, the extent of breathing will depend on the strength of the host–guest interactions. For instance, with MIL-88C, and as far as hydrogen bonds are concerned, the volume expansion when the dry form is put in contact with a solvent is ten times more important for DMF than for H_2O [118]. This could find application in separations.

There is finally a topological restriction for breathing. As exemplified by MIL-68 [95], a structure cannot breathe if odd cycles exist in the structure. Indeed, MIL-68 is a polymorph of MIL-53. Despite the same formula and the same inorganic chain, the structures are different. Instead of lozenge-shaped tunnels in MIL-53, MIL-68 exhibits large hexagonal and small triangular tunnels. The latter confers a strong rigidity to the structure, which was verified as a function of temperature, excluding any breathing. The same rule applies for MOF-5.

6 Advantages and Disadvantages of Hybrids for Inorganic Frameworks

In contrast to zeolite-related inorganic solids, which require the use of inorganic or organic templates (amines, quaternary ammoniums etc.) in addition to the components of the skeleton and the solvent, the situation is much simpler for MOFs: *the solvent itself acts as the main template*. Such a feature presents a great advantage, *the skeleton of most MOFs is therefore neutral*. Indeed, many structures of zeolitic inorganic solids with a cationic skeleton often collapse during the extraction of the template owing to the strong electrostatic host–guest interactions, which energetically represent an important contribution to the lattice energy. In MOFs, the solvents have weaker interactions with the framework and therefore easily evolve the structure at low temperature, often keeping the framework intact and providing very quickly an important and *readily accessible porosity*. Moreover, the existence of inorganic and organic moieties in the structure allows hydrophilic and hydrophobic parts to coexist within the pores and may have some influence on the adsorption properties.

Another interesting feature of MOFs concerns the number of cations that can participate in the framework. Indeed, compared to inorganic ones [3], which are more based on a few cations (Si and Al for zeolites, eventually doped with some transition metals, with the exception of titanosilicates [119]; Zr, Al, Ga, In phosphates and arsenates, sometimes fully substituted by transition metals Ti [72], V [120], Fe [121, 122], Co [123, 124], Ni [125], Zn [126, 127]), MOFs can accept almost all the cations of the classification, at least those which are di-, tri- (including rare earth) or tetravalent. Keeping in mind the tremendous number of species previously isolated in coordination chemistry, this provides a huge number of possibilities for creating new MOFs.

This number is drastically increased considering the large choice of functionalized organic linkers that can be associated with the inorganic parts. The functions borne by the linker contain O or N donors. When O is concerned, they are mainly mono- or polycarboxylates, mono- or polyphosphonates, but rarely sulfonates. All of them, even combined, can provide different possibilities of linkage with the inorganic cations (chelating, single bond, etc.). The nitrogen derivatives (cyanides, pyridine, imidazoles, etc.) are fixed directly to the cation. Moreover, the carbon subnetwork (rigid or not) of the linker can itself be functionalized, depending on the expected application (halogeno-, amino groups, etc.). This means that, potentially, the possibilities of combination within this new family of hybrids tend towards infinity. It is both the richness and the weakness of this family. The richness is clear, but the weakness comes from the quasi-infinite number of potential products. Among them, which are potentially interesting for applications? One cannot imagine testing all these products for eventual applications, and the recourse to a predictive approach for this family, initiated in our group (see above), will be more and more useful in the future for converging more easily towards potentially interesting compounds.

While inorganic zeolitic solids, within a given topology, accept only a few substitutions of the groups ($PO_4 \Rightarrow AsO_4$ etc.) and of metals, MOFs have the immense advantage of being extremely tuneable in terms of size and shape of the pores, for instance by playing on the length, the curvature and the functionalization of the ligands, without affecting the crystallinity of the resulting compounds. This explains the discovery of the first crystallized mesoporous MOFs [96, 99], which opened a new window for potential applications. This tunability also concerns the inorganic parts because the temperature of reaction modifies the coordination of the metallic species, the nuclearity and/or the dimensionality of the inorganic subnetwork. Within the same system, the other synthesis parameters being fixed, the increase of temperature favours first an enhanced condensation of supplementary metallic polyhedra on the starting cluster (increased nuclearity and modified connectivity). Then, the increase of inorganic dimensionality (from 0D to 3D) creates the onset of long-range interactions (for instance, magnetic) and, therefore, the appearance of physical properties usually encountered in dense solids. This induces new potential applications beside the usual properties of porous solids (separation and storage, catalysis etc.).

Have MOFs disadvantages? For the moment, only one is apparent: their weaker thermal stability (limited to 350–400°C, rarely more than 500°C) [85], which rules out any application at high temperatures.

7 Porous Solids are Multifunctional Materials

Inorganic porous solids, and the first rank of zeolites, have for a long time been strategic materials [3]. Their applications are primarily concerned with petrochemistry, catalysis molecular sieves and selective separation using both their porous character, their high thermal stability and their interesting surface areas. Their principal limitation was the relatively small size of the pores in the crystallized solids, until the discovery of inorganic mesoporous compounds, which were further shown to be rather disappointing regarding applications.

MOFs provided a breakthrough. They indeed combine all the desired possibilities of the classical porous solids, with potentially unlimited pore size and surface area, with the physical properties of dense solids that were quasi-inexistent for zeolites and related compounds. This means that, most of the time, whatever their nature, the applications of porous solids (both real and potential) will concern the same domains (catalysis, separation and storage of energetic and greenhouse fluids, drug delivery, etc.) related to the current societal problems of energy, sustainable development and health. However, depending on the nature of the porous solids, the intensity of dedicated research varies within a given type of application, according to the novelty of the compounds. As the field of application of inorganic micro- and mesoporous solids is well documented, this review will mainly focus on the potential applications of MOFs. In general, and even if some of them are unprecedented, the concerned domains are the same. In general, the performances of MOFs are better than those of inorganic solids, in relation to the high tunability of the former.

7.1 Catalysis

Although catalysis is potentially one of the most important applications of metal–organic porous materials, as was the case for microporous zeolites and mesoporous materials, only a handful of examples have been so far reported for MOFs [128–131]. For catalytic applications using metal–organic open-framework materials, apparently five types of catalyst systems or active sites have been utilized:

1. Homochiral metal–organic frameworks
2. Metal ions or ligands in the metal–organic frameworks
3. Coordinatively unsaturated metal (CUM) centres in metal–organic porous materials

4. Metal complexes in supramolecular porous frameworks
5. Highly dispersed metal or metal oxide nanoparticles loaded onto porous MOF host lattices

Homochiral, porous MOFs that look like heterogeneous enzymatic catalysts are particularly attractive as heterogeneous asymmetric catalysts for the production of optically active organic compounds due to the lack of chiral, inorganic zeolites. However, despite considerable efforts, attempts to synthesize homochiral metal–organic porous materials capable of enantioselective catalysis have met with only limited success. Only a few groups have recently provided preliminary evidence for the potential utility of homochiral porous MOFs in enantioselective separation and catalysis [132–135]. Recently, Dybtsev et al. [135] have isolated a Zn-based MOF with bdc and lactate ligands, intrinsically homochiral, with size- and enantioselective guest sorption properties and a remarkable catalytic activity with size- and chemoselectivity, and high conversion in the oxidation of thioethers to sulfoxides.

Most popular examples for catalytic applications belong to framework catalysis by metal ions in the MOFs even though the metal ion and the ligand are usually selected as the building blocks rather than as catalysts. After the pioneer works of Clearfield on phosphonates [136–138], framework catalysis by MOFs now includes cyanosilylation, the Diels–Alder reaction, hydrogenation, esterification, CO etc. [139–143].

The introduction of CUM centres into porous MOFs can offer a promising tool in catalysis because a regular arrangement of metal centres in the pore channels induces regioselectivity or shape- or size-selectivity towards guest molecules or reaction intermediates. For example, Kitagawa and coworkers [144, 145] have shown that pore surface engineering using a metaloligand as a building unit could provide the introduction of CUM centres. Some of examples in framework catalysis may have been achieved by CUM centres in MOFs although it was not clearly mentioned.

Given that inorganic porous materials that contain metal complexes encapsulated in their porous cavities take advantages of heterogeneous catalysts, it might be a good approach to encapsulate metal complexes into MOFs through supramolecular self-assembly. A few authors recently illustrated this strategy [146, 147]. The resulting supramolecular frameworks show size- and shape-selective catalytic activity in the oxidation of phenols with H_2O_2 to form dihydroxybenzenes.

The use of highly dispersed metal or metal oxide nanoparticles inside porous MOF host lattices is very rare. Pd and Pt phosphonates are active catalysts for the photochemical production of H_2 [148] and the production of hydrogen peroxide from streams of H_2 and O_2 [149, 150]. Recently, Fischer and coworkers have shown that metal–organic chemical vapour deposition gave inorganic nanoparticles (Cu and Pd) in MOF-5 to be moderately active for methanol synthesis (Cu@MOF-5) and hydrogenation of cyclooctene (Pd@MOF-5), respectively [147]. However, the surface functionalization of pores for catalytic applications remains still unexplored in porous MOFs in spite of it being a promising research area, previously exemplified in mesoporous materials.

Whereas catalytic applications concern the surface of the pores, many others use either the pores and their possibility of being filled by inserted species, or the skeleton, as soon as properties close to those of dense solids (magnetism, conductivity, optical properties) are required.

7.2 Insertion of Species and Their Applications

Solvents are easily evacuated from the pores of MOFs. The tunability of pore size renders MOFs particularly attractive for insertion of species, including gases, liquids, molecules, inorganic nanoparticles and metals. On the point of tunability, a false debate is emerging: which are better: large pores or small pores? Such a question is not reasonable. The choice will only depend on the required application and on the size of the species to be inserted. It is clear that if a selectivity between small species is looked for, there is no need for large pores. In contrast, if the aim is to insert drugs into the pores, the larger the cage, the better the storage. In other words, instead of seeing the two ways as opposite, it is better to use all the possibilities of dimensions described in the literature to fit a given application and to optimize it. This does not prevent the search for larger and larger pores. Apart from the idea of a world record (but every record is to be beaten), it is more important to enlarge the possibilities of insertion for dedicated applications.

7.3 Gas Adsorption/Separation/Storage and Energy

This domain is increasingly important. The decrease in fossil energies urgently needs solutions of substitution, and MOFs might represent one of them for their capacity to adsorb large amounts of strategic gases like H_2, CO_2, CH_4, CO, O_2, NO_x, C_2H_2 etc. within the cages. The American Department of Energy recently fixed the lower limits of adsorption (6.5 wt% for hydrogen) needed for realistic energy applications in this domain [151, 152].

The first success, due to Kitagawa in 1997 [103], was the introduction of large amounts of methane in a coordination polymer. This opened the way for a tremendous search for materials able to store these gases, due both to their high specific surface areas (SSA) and large pore sizes. For the moment, the main efforts concentrate on H_2, CH_4 and CO_2 with, however, a striking difference between the first and the others. Indeed, MOFs adsorb large amounts of hydrogen only at 77 K; at room temperature, adsorption is negligible, in contrast to CH_4 and CO_2, which exhibit interesting performances at 300 K and above. This low temperature adsorption of H_2 prevented, for a long time, applications for its use in cars. Recent technical solutions are in progress (Eberle, private communication).

At this point, two general remarks must be made. The first concerns the performances of MOFs and their reproducibility. Indeed, the performance of a MOF is

strongly dependent on the way of synthesis, on the scale of production (laboratory or large-scale preparations) and on the efficiency of activation of the MOF. It is currently difficult to compare the real performances because the data (for instance wt%) refer to a given P/P_0 ratio (often at 1 bar) whereas the true capacity must be measured at high pressure (60–70 bar). For the future, there is an urgent need for normalization, with a complete set data including isotherms of adsorption (classical) and desorption (currently rare), gas capacity at high pressure (wt%; $cm^3\,g^{-1}$; $cm^3\,cm^{-3}$) as well as surface areas (BET, Langmuir). At the laboratory scale, the performances of only three MOFs have been currently validated: MOF-5 [153], MIL-53 [154] and HKUST-1 [155]. The second remark concerns an emerging trend. The improvement of the performances in gas adsorption will allow a better understanding of the mechanisms and thermodynamics of adsorption, and of a better structural knowledge of the adsorption sites. This has been done for zeolites. Measurements of heats of adsorption are currently very scarce [156, 157], as well as the localization of adsorbed molecules, experimentally (using X-ray and neutron diffraction) [158–160] or theoretically using computer simulations [161–169]. This shall be a major requirement for the future. The identification of the active sites, either on the inorganic or organic moieties, will be very important for elaborating new syntheses.

7.4 Hydrogen Adsorption and Storage

This is currently one of the major challenges for energy purposes and for fuel cell-driven cars [169–174]. Hydrides seemed attractive for such a purpose, but both their high density (which leads to low weight-based storage) and the obligation to heat them for delivering hydrogen were drastic limitations for their industrial use, even if alanates [175, 176] represent a significant progress. MOFs do not have these limitations since their density is very low ($< 1\,g\,cm^{-3}$) and their hydrogen storage is governed by physisorption and not redox reactions.

Up to now, the best-verified MOFs for hydrogen storage at 77 K are MOF-177 (7.5 wt% at 70 bar) [177], MOF-5 (5.1 wt% at saturation), MIL-53(Al) (4.5 wt% at saturation) and HKUST-1 (3.6 wt% at saturation). The heats of adsorption were calculated to be -3.8 and $-4.5\,kJ\,mol^{-1}$ for MOF-5 and HKUST-1, respectively. The adsorption–desorption curve of MIL-53 presents an hysteresis, which is due to the breathing effect in this solid. Some 90% of its total capacity is reached in less than 1 min; 2.2 wt% of hydrogen is recovered at 0.1 bar. All these MOFs show H_2 capacities much larger than those reported for zeolites A, X, Y and RHO (1.8 wt%) [178] and compare favourably to high-grade activated carbon [179, 180].

These high capacities make MOFs very efficient for industrial applications. As shown by Müller et al. [26], comparing the pressurization of an empty container with hydrogen, the above MOFs increasingly take up higher amounts of hydrogen, exceeding the standard pressure–volume–temperature (PVT) uptake curve of the empty container. At 40 bar, the PVT relation of hydrogen in an empty canister is registered as $12.8\,g\,H_2\,L^{-1}$ [179, 180], whereas Cu-BTC-MOF filled into containers

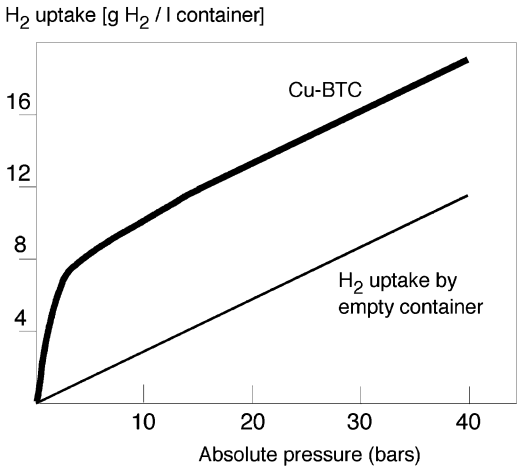

Fig. 15 Effect of MOF introduction in a container for hydrogen storage

reaches a plus 44% capacity of up to $18.5\,g\,H_2\,L^{-1}$. For comparison, the volume-specific density of liquid hydrogen at its boiling point (20 K) is $70\,g\,H_2$. On a per weight calculation, the saturation of MOFs with hydrogen is already achieved at pressures of less than 15 bar (Fig. 15). Some dedicated reviews appeared on the subject in 2005 [170–172].

For a few experimental determinations of the localization of H_2 molecules in MOFs [158–160], several computer simulations have been performed, which either anticipated experience or agreed with it [161–169]. Whatever the case, experience and simulation show that it is molecular dihydrogen that is adsorbed, and that the metal–oxygen clusters are the preferential adsorption sites for H_2 in MOFs; the effect of the organic linkers becomes evident only at high pressure.

The H_2 storage capacity of MOFs is definitively larger than that of carbon nanotubes, which is much higher than that of zeolites. Furthermore, diffusion of H_2 in MOFs is an activated process, similar to diffusion in zeolites. This domain is currently a great challenge, combining targeted storage capacities, thermodynamics and kinetics of exchange. It will become more and more interdisciplinary, using chemistry, physics and engineering science.

7.5 CO_2 *and* CH_4 *Adsorption and Storage*

These two gases are also strategic for pollution and energy problems. In particular, the current elimination of CO_2 uses chilling, pressure, contact with amine solutions [181], chemisorption on oxide surfaces or adsorption within zeolites, carbons, or membranes [182], but MOFs present a valuable alternative for this removal.

In contrast to hydrogen, CO_2 and CH_4 are both adsorbed at room temperature. However, studies on their adsorption are by far less numerous than for hydrogen [157, 183–190], even if it is with CH_4 that the story of gas adsorption began for MOFs [103]. In a general way, methane is less adsorbed than CO_2. Even if it is not yet clearly understood, it seems that the difference in adsorption is due to the existence of a large quadrupolar moment for CO_2 (-1.4×10^{-35} C – m) [157], which does not exist with CH_4. This moment induces specific interactions with adsorbents (molecular orientation, hydrogen bonding etc.) which, depending on the host structure, will give different behaviours for the adsorption isotherms.

Currently, the best adsorbers are MOF-177 [189] (Langmuir surface area (LSA) 4500 $m^2 g^{-1}$, 11 × 17 Å pores) and MIL-101 [191] (LSA 5900 $m^2 g^{-1}$, 29 and 34 Å diameters), which correspond to the solids having the largest pores ever evidenced (Fig. 16). They adsorb more than 30 mmol g^{-1} (33.5 at 40 bar for MOF-177 and 40

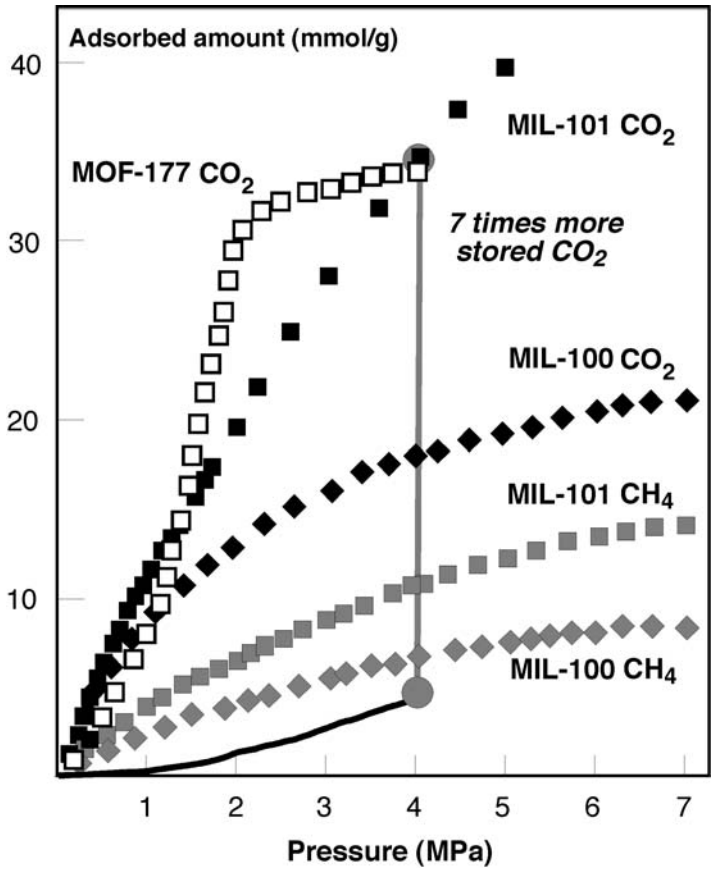

Fig. 16 CO_2 and CH_4 adsorption isotherms of MIL-101 and MOF-177 at 300 K. Comparison with pure CO_2

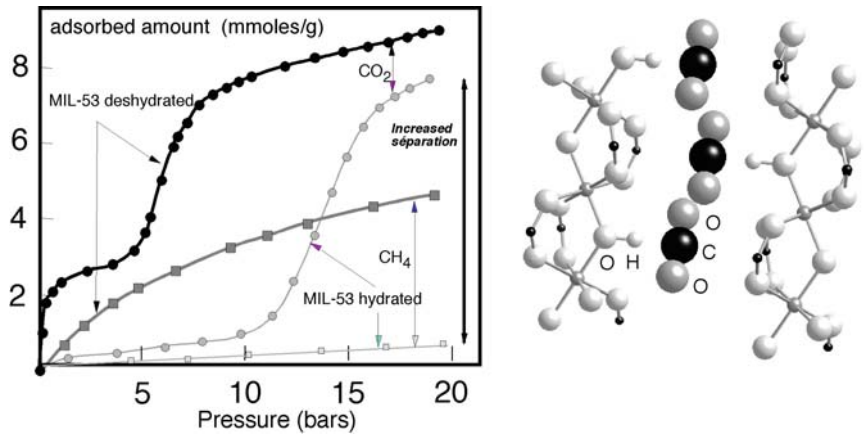

Fig. 17 CO_2 and CH_4 adsorption isotherms of anhydrous and hydrated MIL-53 and location of CO_2 molecules within the tunnels

at 50 bar for MIL-101), which means about seven times the amount of pure CO_2 in a container pressurized at the same pressure.

Only two structural studies on CO_2 adsorption exist [158, 192]. Both show that flexibility might have an influence. In both cases, the enthalpy of adsorption is close to $35\,kJ\,mol^{-1}$. Anhydrous MIL-53 presents the most pronounced behaviour, related to its already mentioned large breathing effect (ca. 40%). Whereas the isotherm is classical with CH_4, the CO_2 isotherm presents a two-step behaviour (Fig. 17). After a first increase of CO_2 uptake, it marks a clear plateau at $3\,mmol\,g^{-1}$ up to 5 bar before a second increase up to $9\,mmol\,g^{-1}$ at 20 bar. In situ diffraction studies [192] provide the explanation. When dehydrated under vacuum before CO_2 adsorption, MIL-53 adopts its expanded structure, but at low pressures of CO_2 its structure readopts the shrunken form up to 5–6 bar. At higher pressure, the structure reopens to give the expanded form.

A complete structural study at 1 bar shows that the CO_2 molecules lie at the centre of the tunnels, as water molecules did, but the interactions are different, even if the OH groups shared between the octahedra of the skeleton are concerned in both cases. Whereas with H_2O, the interactions occurred between the OH groups and the oxygens of the water molecules of the tunnels, with CO_2 it is the carbon and not the oxygen of CO_2 that interacts with OH. This induces a strong but continuous modification of the IR spectrum, followed by in situ measurements [193], and correlatively, a clear bending of the CO_2 molecule by 6°.

This tends to demonstrate an influence of the polar character of the adsorbed molecules on the host–guest interactions and on the shape of the isotherms. This could have applications in selective adsorption of polar molecules. It is the reason why our group recently studied the adsorption of CO_2 and CH_4 by the hydrated form of MIL-53 [190] in order to see the behaviour of a non-polar and polar probes in the presence of a second polar molecule (here water). The isotherms are drastically

changed (Fig. 17). Whereas CH_4 is almost not adsorbed up to 20 bar ($0.2\,\mathrm{mmol\,g^{-1}}$), there is a very little uptake of CO_2 up to 10 bar and a sudden increase ($8\,\mathrm{mmolg^{-1}}$) after. XRPD patterns show that, up to 10 bar, the shrunken form of MIL-53 prevails, and in situ IR spectroscopy indicates a progressive displacement of the water. This could find applications in the recovery of CO_2 in mixed gas streams, particularly natural gas.

7.6 Adsorption and Storage of Other Gases and Liquids

In these cases, most papers just mention the corresponding amount vs. P/P_0 curves and element databases, but do not go further. This a cruel deficiency in knowledge because progress in understanding adsorption requires, as already noted, structural information on the host–guest interactions. Two outstanding exceptions exist, coming from the Kitagawa group [108, 109, 194–201] and Howard et al. [160]. The first systematically performed in situ synchrotron radiation studies on the adsorption of many gases by some of their solids and determined the adsorption sites. In particular, they proved that for C_2H_2 adsorption results in an unprecedented acidobasic reaction between the oxygens of the framework and the hydrogens of C_2H_2, with the formation of a weak O–H bond during the phase transitions [200, 201] that occur during adsorption. This provides one more example that adsorption is favoured by flexibility of the framework (breathing, gate effects), a behaviour that was nicely reviewed by Rosseinsky [202–204]. The second exception concerns the location of argon and dinitrogen in MOF-5. The first adsorption sites are also close to the inorganic cluster.

The tunability of the pore size in MOFs is also a big advantage for the separation of alcanes. This application, well known for zeolites, is just emerging for MOFs. A recent structural paper by Li et al. [205] proves that the pore size of one of their coordination polymers is sufficiently large for trapping methane, ethane and propane, while butane is not inserted. Moreover, in the petroleum industry, the separation of alkane isomers is a very important process. Narrow pore zeolites can sieve linear from branched alkanes to boost octane ratings in gasoline. Recently, a solid described simultaneously by different groups [206–208] exhibits a similar behaviour and is used for gas-chromatographic separation of linear and branched alkanes [208]. Whereas the first example described real trapping of small alkanes, the second, owing to the small dimensions of the cage (4×4 Å), concerns only the window's accessibility to the pores. They can accommodate only the linear part of the branched isomer, and the retention of alkanes on the column mainly depends on the length of the linear part of the alkane and its van der Waals interactions with the microporous MOF walls.

The immense possibilities of adsorption of MOFs also apply liquids. Recently, Jacobson et al. [209] introduced aniline, thiophene and acetone in crystals of MIL-47 (V^{4+}) by impregnation and localized the species within the tunnels. The intercalated aniline molecules show substantial ring–ring $\pi-\pi$ interactions between them

and with the BDC ligand over short distances. The $\pi-\pi$ interactions are complemented by weak C–H$\cdots\pi$ and N–H$\cdots\pi$ interactions between the aniline molecules and the BDC ligands. The packing of thiophene molecules is similar to that of aniline. A clear C–H$\cdots\pi$ interaction between the thiophene molecules and the framework BDC seems to play a major role in determining the thiophene orientation.

Breathing occurs during insertion and induces non-centrosymmetry. This was confirmed by second harmonic generation (SHG) measurements. The SHG efficiency of intercalated solids is comparable to that of quartz. This shows the importance of non-covalent orientated weak interactions in the packing of organic molecules within nanopores of MOFs. As mentioned by Jacobson, such interactions, although relatively weak, may readily cause remarkable deformation and symmetry change of the framework, which point to effective ways of manipulating known materials or designing new materials with targeted properties through intercalation chemistry. As recently shown by De Vos et al. [210], the same solid MIL-47 also exhibits remarkable properties of separation between the different isomers of xylene. These features open new opportunities of application for MOFs.

7.7 Adsorption/Storage of Molecular Species, Catalysis and Drug Delivery

These molecular species can be either organic or inorganic. The variety of inserted moieties is strongly dependent on the size of the pores. This justifies the current search for very large pores limited by crystalline walls. Compared to inorganic porous solids with their pores limited to 24-membered rings, MOFs indeed represent a gap in this domain. With larger pores, the trapping of larger molecules or polyions becomes possible. For instance, by impregnation, crystals of MOF-177 [211] incorporate in their cages (accessible diameter 11 Å) several aromatics, C_{60} and dyes.

A decisive gap has been reached with the discovery of the mesoporous MOFs MIL-100 and MIL-101. Their augmented MTN zeolite topology exhibits two types of cages with 20 and 28 vertices, the first with exclusively pentagonal windows and the other with pentagonal and hexagonal windows with large apertures (up to 16 Å). These windows allow the introduction of large molecular species, particularly drugs. The analgesic Iboprofen was used as a probe for validation [212].

MIL-100 and MIL-101 show remarkable Ibuprofen uptake (0.35 and 1.4 g per gram of dehydrated MILs, respectively) (Fig. 18). The difference is the result of their different pore sizes (25 and 29 Å for MIL-100; 25 and 29 Å for MIL-101). This is very important as only very small amounts of material are required for the administration of high dosages. The free apertures of the windows of the cages compared to those of Ibuprofen (6×10.3 Å) [4.8 Å (MIL-100) and 12 Å (MIL-101) for the pentagonal; 8.6 Å (MIL-100) and 16 Å (MIL-101) for the hexagonal] explain this discrepancy. Therefore, Ibuprofen fills only the large cages in MIL-100, and all of them in MIL-101. Each small and large cage of MIL-101 hosts approximately 56 and 92

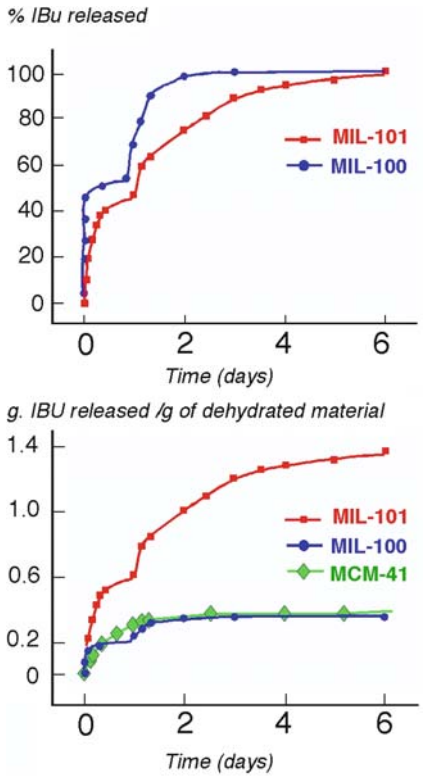

Fig. 18 Compared adsorptions of ibuprofen by MCM-41, MIL-100 and MIL-101

Ibuprofen molecules, which represents four times the capacity of MCM-41 toward Ibuprofen [213]. Moreover, the release of the drug at physiological pH occurs in 3 days with MIL-100 and 6 days with MIL-101, in two steps. The faster release concerns the molecules that fill the cages, whereas the slower release relates to the molecules in noticeable interaction with the framework.

This unprecedented behaviour illustrates three facts:

1. The ever-growing need for very large pores
2. When tuneable, the hierarchy of mesopores can act as an internal molecular sieve for a given guest of important dimensions with a selective occupation of the cages; the empty cages remain able to host a different species
3. Such matrices may provide tools for the study of nanoassemblies of organic compounds and help the development of nanoorganic chemistry

Moreover, this behaviour adds a new route for drug storage and release. Two routes have been previously set up: the "organic route", which uses either biocompatible dendritic macromolecules or polymers [214, 215], and the "inorganic route", in which the hosts are inorganic porous solids, such as zeolites [216, 217]

or mesoporous silicate materials [218]. In the first case, a wide range of drugs can be encapsulated but a controlled release is difficult to achieve in the absence of a well-defined porosity [214, 215]. In the second case, this release is performed by grafting organic molecules onto the pore walls, but implies a decrease in the drug-loading capacity [219]. Crystallized mesoporous MIL-100 and MIL-101 introduce a third way, the "hybrid" route. Indeed, the combination of a high and regular porosity with the presence of organic groups within the framework may accumulate the advantages to achieve both a high drug loading and a controlled release.

These mesopores also allow the introduction of large molecular inorganic species within the cages. For instance, MIL-101 incorporates [99] the Keggin polyanion $PW_{11}O_{40}^{7-}$. Owing to the large dimension of this anion (ca. 13 Å), only the large cages can host it. From XRPD, TGA, specific surfaces and solid state NMR measurements, it was proven that each cage can accept five Keggin ions, representing 50% of the volume of the cage. This successful incorporation of large amounts of Keggin anions strongly suggests that MIL-101 is an ideal candidate for the introduction of other nanoobjects with chemical, physical, biological or medicinal properties.

In a general way, a fit must exist between the size of the guest and the dimensions of the windows. A recent example [147] illustrates this point. Fischer looked at the absorption of volatile or very soluble metal organic CVD precursors $[(\eta^5-C_5H_5)Pd(\eta^3C_3H_5)$, $(\eta^5-C_5H_5)Cu(PMe_3)$, $(CH_3)Au(PMe_3)$ and $Cu(OR)_2$ where $R = CH(CH_3)CH_2NMe_2]$. Only the latter does not incorporate the structure because its dimensions exceed those of the pore window of MOF-5 (8 Å). Reduction of the intercalated compounds by H_2 leads to the formation of metallic nanoparticles. In the case of Pd, the framework of MOF-5 is strongly affected by the treatment whereas, with Cu and Au, it remains intact. However, the range of observed particle sizes (13–15 Å for Pd, 30–40 Å for Cu, 50–200 Å for Au) is far above the dimensions of the cage, indicating a biphasic metal–MOF mixture instead of incorporation at the nanometric scale, which is at variance to that observed with MCM [220]. However, the corresponding solids exhibit some catalytic properties.

Inclusion of metallic nanoparticles in MOFs remains a challenge. Suh et al. [221] recently tried to generate in situ nanoparticles of Ag and Au within a flexible two-dimensional MOF $[Ni^{II}(cyclam)_2][BPTC]$ through the reduction of noble metals by the Ni^{2+} of the cyclam complex. Reduction effectively occurs but a thorough study, including many types of characterization, proved that the MOF network remained intact and that the nanoparticles (40 Å for Ag, 20 Å for Au) are not incorporated between the layers but form a metal–MOF composite. The authors suggest that Ag(I) metal ions are introduced between the host layers and react with the Ni(II) species incorporated in the host to form Ag(0) atoms, which diffuse to the surface of the solid to grow into nanoparticles. Since the Ag nanoparticles grow on the surface of the solid, the host structure can be maintained even after the nanoparticles of ca. 4 nm are formed. Such an explanation also seems valid for the above metalocenes.

7.8 MOFs as Nanoreactors and Nanomoulds for Nanosciences and Applied Physics

Despite being unsuccessful, the work of Suh was an elegant trial for using MOFs as reactors within which nanospecies could be synthesized in situ and confined in the pores. The high reactivity and diffusion of metallic aggregates was probably responsible for the failure. However, as soon as such a strategy becomes applicable, a myriad of new possibilities will arise in relation to the physical properties usually encountered in dense solids (magnetism, conductivity, optical properties etc.), but this time at the nanoscale. The specific advantage of MOFs is to provide large, tuneable and well-defined crystallized pores. Besides their now-classical role of storage and sieving, they can act as *nanoreactors* and allow chemical reactions and the formation of known (or unknown) products within the cages, with the possibility of seeing the *effect of confinement* on the structure of the included species. Once this nanoreactor role is realized, the cages will act as *nanomoulds* for the synthesized species because the size of the latter is fixed by the dimensions of the cage, therefore leading to calibrated monodisperse nanoparticles, a feature that is scarcely reached by the usual ways of obtaining nanoobjects. This opens the way to a new step in the knowledge of nanophysics with the study of *strictly* monodisperse assemblies, their size being tuneable as a function of the size of the cage.

The first example of such a strategy is provided by MIL-101 [99]. Once desolvated and impregnated in a Zn^{2+} solution, it provides nanoparticles of the semiconductor ZnS when the carefully washed Zn-impregnated solid is treated by an H_2S stream at 300 K. High resolution electron microscopy with associated chemical nanoanalysis on small crystals unambiguously proves that the semiconductor particles reside only within the pores and not on the surface. Both types of cages are partially occupied with four ZnS/trimers, which means 80 and 40 ZnS assemblies within each type of cage, corresponding to a 50% occupancy of the volume of the pores. From preliminary studies, it seems that the sphalerite form of ZnS is privileged in the aggregates, whereas for 60 ZnS, computer simulation of the nucleation and growth of ZnS nanoparticles predicted the existence of bubbles close to a sodalite arrangement [222]. Evolution of the semiconducting properties is currently in progress. Such a result opens larger perspectives for nanoscience: it becomes possible to imagine the introduction of known dense materials in mesoporous MOFs, such as semiconductors (or a mixture of them), photocatalysts (TiO_2), oxide conductors (YBaCuO), ferro- and ferrimagnets (CrO_2, spinels, etc.) as soon as the dedicated chemistry is developed for such a purpose. For that, the accumulated knowledge on the preparation of these nanophases, but in a non-confined form, will be useful.

Conductivity of porous MOFS seemed impossible until recently. Conductivity implies either mobility of species (ionic conductivity) or delocalization (electronic conductivity, isotropic or anisotropic). For MOFs, if ionic conduction is theoretically possible when dedicated inserted species are chosen, electronic conduction seems to be almost inaccessible for at least two reasons: (i) there is no clear mention

of MOFs containing mixed-valence species, a necessary condition for eventual electronic delocalization, and (ii) most of the MOFs are coordination polymers (0D for the inorganic framework), whereas, except in a few cases, at least a 1D inorganic subnetwork is required.

A recent breakthrough circumvents these limitations in terms of mixed-valence and at least of ionic conductivity [223]. The progressive electrochemical insertion of lithium in the breathing MIL-53(Fe^{3+}) with one dimensional Fe(III) chains induces the onset of Fe^{2+} within the chains, proved by a Mössbauer study. Used as an electrode in a Li-half cell, this material shows a reversible redox process around 3.0 V vs. Li^{+}/Li° exchanging 0.6 Li per formula unit with excellent capacity retention and rate capability, even if the induced electronic conductivity is rather low. Moreover, the magnetic properties change from antiferromagnetic for MIL-53(Fe^{3+}) to ferrimagnetic for Li-MIL-53(Fe^{3+}). It finally reveals an interesting property of MOFs with large galleries, related to the breathing effect: the uptake of electrolyte molecules within their channels facilitating ionic transport in MOFs. Mixed valence in MOFs opens a wealth of opportunities for the elaboration of materials with tuneable properties for various applications.

Magnetic properties of MOFs are an emerging field, recently reviewed by Veciana et al. [224]. As for inorganic porous solids [122], the results are rather scarce. Due to the very low magnetic ordering temperatures, this field is currently restricted to academic interest. However, magnetic MOFs present interesting features, some of them being specific to the hybrid nature of the related structures. An example is the use of ligands with phenyl rings which, through their delocalized π electrons, can transmit the magnetic information between several inorganic moieties and create long-range interactions even for 0D coordination polymers.

Transition metal-containing MOFs (*d* and *f*) with various dimensionalities of the inorganic subnetwork satisfy the rules of molecular magnetism and of the Kanamori–Goodenough laws [225–227]. The sign and the strength of the magnetic superexchange interactions depend on both the nature of the magnetic carriers, which can give either isotropic (Mn^{2+}, Fe^{3+}) or anisotropic (Co^{2+}) couplings, and on geometrical criteria concerning the M–X–M superexchange angles. Depending on these angles, the coupling can change from antiferromagnetic to ferromagnetic, and the strength from strong (when the M–X–M angle is close to 180°) to weak (when the M–X–M angle is close to 90°). For 2D solids, dipolar magnetic interactions must also be taken into account for the long-range interactions. This means that all the magnetic behaviours encountered in dense solids are also encountered in MOFs, including frustrating problems when odd cycles of cations in antiferromagnetic interactions are involved in the structure [228, 229].

Veciana et al. [230–233] recently introduced a new strategy for enhancing the magnetic properties of MOFs. They used the purely organic radical (polychlorinated triphenylmethyl tricarboxylate or PTMTC) as "spacer" paramagnetic ligands, which interact magnetically with the transition metal. The so-called MOROFs series exhibit interesting properties. The layered Cu-MOROF-1 is a ferrimagnet below 2 K and exhibits a spectacular reversible breathing behaviour upon solvent uptake

and release with a change of 30% of the volume, the desolvated phase exhibiting turbostratic disorder. In the 3D Co-MOROF-3, ferro- and antiferromagnetic interactions coexist.

The guest dependence on the magnetic properties is nicely illustrated by the porous manganese(II) formate [234] $[Mn_3(HCOO)_6]MeOH.H_2O$ with a diamond-type framework built up from $MnMn_4$ supertetrahedra. This exhibits a guest-modulated ferrimagnetic behaviour, owing to the steric effects of the guest which induce subtle changes in the framework. The Curie temperature, originally measured as 8 K, can vary from 5 to 10 K according to the nature of the guests reinserted in the porous framework. Such effects could also explain the complex $4f-3d$ interactions in the trimetallic Cu–Gd–Fe coordination polymer [235].

Finally, one could expect an increase of the critical magnetic temperatures for higher dimensionalities. They currently do not exceed 100 K, even if a remnant magnetization has been mentioned at room temperature for $Cu_2(py)_2(BDC)_2$ [236]. Until now, only Ni^{2+} carboxylates exhibit 3D inorganic subnetworks. Higher T_c values could therefore be expected but, despite interesting ferri- and ferromagnetic properties, they occur only at $T < 10$K [237–239] because the polyhedra in these structures only share edges and faces, a characteristic that is not favourable for high critical temperatures.

The optical properties of MOFs mainly concern luminescence. Here also, the possibility for MOFs to accept many metals, including rare-earths, and the tunability of the chromophores as ligands offer great opportunities for new phosphors and probes. Numerous lanthanide carboxylates have been isolated [240–265] but only some of them were submitted to spectroscopic investigations, often restricted to the presentation of the emission spectra. The small interest is due to the fact that, in Ln-MOFs, the rare-earth polyhedra have water ligands, which are well known to quench fluorescence due to the loss of excited-state energy to vibrational energy of an OH oscillator in close proximity, even though it was shown that the evolution of Eu^{3+} lifetimes can serve as an indicator of the degree of hydration of some Ln-glutarates [266].

However, a characteristic of lanthanide fluorescence is their low absorbance coefficients, and a coordinated ligand with a π delocalized system can stimulate energy transfer to the metal centre via an intramolecular pathway. This effect, named the *antenna effect* [267, 268] can realize efficient UV light conversion devices. This goal has incited research in many fields and new concepts have emerged [269, 270]. MOFs could be good candidates for such a purpose but serious and quantitative studies are currently extremely rare [265, 271]. For example, the rare earth trimesate $Ln[(C_6H_3)(COO)_3]$ [271] has demonstrated such an antenna effect. The ligand triplet state is located $200\,cm^{-1}$ higher than the $^5D_0$ (Eu^{3+}) emitting level, and the migration of the excitation occurs along the chains of rare-earth polyhedra with an activation energy quite similar to the energy separation between the triplet state and the $^5D_0$ (Eu^{3+}) level.

8 Conclusion

Only a few topics have known such a tremendous development in 15 years. Besides the current explosion of new products and the increase in understanding of their formation, the current trends over the last 3 years offer a myriad of potential applications. The only limit is the imagination of researchers. Within a few years, hybrid solids have passed from curiosities to strategic materials. Not only do they amplify most of the performances of the usual porous solids (sieving, adsorption, storage, etc.) but they reach domains usually reserved for other disciplines: solid state chemistry and physics with the introduction of physical properties usually devoted to dense phases; life sciences with their ability to store and deliver drugs; the emerging nanosciences with the possibility of providing monodisperse nanoparticles of many kinds of solids. Even polymer science is now concerned [272] with the polymerization of monomers and their dependence on the confinement effects provided by the restricted space of the pores. These solids represent a new world. We just discover it.

8.1 Biographical Sketch

Gérard Férey was born in Bréhal, France (1941). After education in Caen, he became Professor at Le Mans University(1981) and moved to Versailles in 1996 to create the Institut Lavoisier. Currently interested in the field of porous solids, he is now Professor at the Institut universitaire de France and member of the French Academy of Sciences.

References

1. Férey G (2008) Chem Soc Rev 37:191
2. Cheetham AK, Férey G, Loiseau T (1999) Angew Chem Int Ed 38:3268
3. Schüth F, Sing KSW, Weitkamp J (eds) (2002) Handbook of porous solids. Wiley, Weinheim
4. Eddaoudi M, Kim J, Rosi, N, Vodak D, Wachter J, O'Keeffe M, Yaghi OM (2002) Science 295:469
5. Forster PM, Eckert J, Chang JS, Park SE, Férey G, Cheetham AK (2003) J Am Chem Soc 125:1309
6. Rosi N, Eckert J, Eddaoudi M, Vodak D, Kim J, O'Keeffe M, Yaghi OM (2003) Science 300:1127
7. Férey G, Latroche M, Serre C, Millange F, Percheron-Guégan A (2003) Chem Commun, p 2355
8. Cronstedt AF (1756) Kongl Wetenskaps Akad Handl Stockh 17:120
9. Taylor NA (1930) Z Kristallogr 74:1
10. Pauling L (1930) Proc Natl Acad Sci 16:453
11. Thompson HS (1850) J R Agric Soc Engl 11:68
12. Friedel G (1896) Bull Soc Fr Mineralog 19:94
13. Sainte C, Deville H (1862) C R Acad Sci 54:524

14. Hoskins BF, Robson R (1989) J Am Chem Soc 111:5962
15. Eckert H, Ward M (2001) Organic-inorganic nanocomposite materials. Chem Mater (special issue) 13:3061
16. Kitagawa S, Kitaura R, Noro S (2004) Angew Chem Int Ed 43:2334
17. Batten SR, Robson R (1998) Angew Chem Int Ed 37:1460
18. Hargman PL, Hargman D, Zubieta J (1999) Angew Chem Int Ed 38:2638
19. Moulton B, Zaworotko M (2001) Chem Rev 101:1629
20. Eddaoudi M, Moler DB, Li H, Chen B, Reineke TM, O'Keeffe M, Yaghi OM (2001) Acc Chem Res 34:319
21. Yaghi OM, O'Keeffe M, Ockwig NW, Chae HK, Eddaoudi M, Kim J (2003) Nature 423:705
22. Yaghi OM, O'Keeffe M, Kanatzidis M (2000) J Solid State Chem (special issue) 152:1
23. Rao CNR, Natarajan S, Vaidhyanathan R (2004) Angew Chem Int Ed 43:1466
24. Davies ME, Maxwell IE (1996) Curr Opin Solid State Mater 1:35
25. Forster PM, Thomas PM, Cheetham AK (2002) Chem Mater 14:17
26. Mueller U, Schubert M, Teich F, Puetter H, Schierle-Arndt K, Pastré J (2006) J Mater Chem 16:626
27. Mingos DMP, Baghurst DR (1991) Chem Soc Rev 20:14
28. Tompsett GG, Conner WC, Yngvesson KS (2006) Chem Phys Chem 7:296
29. Park SE, Chang JS, Hwang YK, Kim DS, Jhung SH, Hwang JS (2004) Catal Surv Asia 8:91
30. Hwang YK, Lee UH, Chang JS, Kwang YU, Park SE (2005) Chem Lett, 34:1596
31. Jhung SH, Yoon JW, Hwang JS, Cheetham AK, Chang JS (2005) Chem Mater 17:4455
32. Jhung JS, Lee JH, Yoon JW, Hwang JS, Park SE, Chang JS (2005) Mic Mes Mater 80:147
33. Hwang YK, Chang JS, Park SE, Kim DS, Kwon YU, Jhung SH, Hwang JS, Park MS (2005) Angew Chem Int Ed 44:557
34. Jhung SH, Chang JS, Kim DS, Park SE (2004) Mic Mes Mater 71:135
35. Kitagawa S, Okubo, Kawata TS, Kondo M, Katada M, Kobayashi H (1995) Inorg Chem 34:4790
36. Jhung SH, Lee JH, Chang JS (2005) Bull Kor Chem Soc 26:880
37. Jhung SH, Lee JH, Forster PM, Férey G, Cheetham AK, Chang J-S (2006) Chem Eur J 12:7899
38. Mintova S, Olson NH, Senker J, Bein T (2002) Angew Chem Int Ed 41:2558
39. Lin Z, Wragg DS, Morris RE (2006) Chem Commun, p 2021
40. Stock N, Bein T (2003) Solid State Sci 5:1207
41. Stock N, Bein T (2004) Angew Chem Int Ed 43:749
42. Bauer S, Bein T, Stock N (2005) Inorg Chem 44:5882
43. Serre C, Groves JA, Lightfoot P, Slawin AMZ, Wright PA, Stock N, Bein T, Haouas M, Taulelle F, Férey G (2006) Chem Mater 18:1451
44. Forster PM, Burbank AR, O'Sullivan MC, Guillou N, Livage C, Férey G, Stock N, Cheetham AK (2005) Solid State Sci 7:1549
45. Akporyaye D, Dahl IM, Karlsson A, Plassen M, Wendelbo R, Bem DS, Broach RWLewis GJ, Miller M, Moscoso J (2001) Mic Mes Mater 48:367
46. Férey G, Cheetham AK (1999) Science 283:1125
47. Li H, Laine A, O'Keeffe M, Yaghi OM (1999) Science 283:1145
48. Férey G (2001) Science 289:994
49. Férey G (2000) J Solid State Chem 152:37
50. Müller A, Krickemeyer E, Bögge H, Schmidtmann M, Roy S, Berkle A (2002) Angew Chem Int Ed 41:3604
51. Müller A, Das SK, Talismanov S, Roy S, Beckmann E, Bögge H, Schmidtmann M, Merca A, Berkle A, Allouche L, Zhou Y, Zhang L (2003) Angew Chem Int Ed 42:5039
52. Wells AF (1979) Further studies of three-dimensional nets. ACA monograph 8. American Crystallographic Association, San Diego
53. Han S, Smith JV (1999), Acta Crystallogr A 55:332
54. Baerlocher C, McCusker LB, Olson DH (2007) Atlas of zeolite framework types, 6th edn. International Zeolite Association. http://www.iza-structure.org/databases/. Last accessed 26 Sept 2008

55. Meier WM, Olson DH (1970) Adv Chem Ser 101:155
56. O'Keeffe M, Eddaouadi M, Li H, Reineke T, Yaghi OM (2000) J Solid State Chem 152:1
57. Hansen S (1990) Nature 346:799
58. O'Keeffe M (1991) Z Kristallogr 196:21
59. Chen B, Eddaouadi M, Li H, Hyde ST, O'Keeffe M, Yaghi OM (2001) Science 291:1021
60. Yaghi OM, O'Keeffe M, Ockwig NW, Chae HK, Eddaouadi (2003) Nature 423:705
61. Ockwig NW, Delgado-Friedrichs, O'Keeffe M, O, Yaghi OM (2005) Acc Chem Res 38:176
62. Haouas M, Gérardin C, Taulelle F, Estournes C, Loiseau T, Férey G (1998) J Chim Phys 95:302
63. Taulelle F, Haouas M, Gérardin C, Estournes C, Loiseau T, Férey G (1999) Colloids Surf 158:299
64. Taulelle F, Pruski M, Amoureux JP, Lang D, Bailly A, Huguenard C, Haouas M, Loiseau T, Férey G (1999) J Am Chem Soc 121:12148
65. Francis RJ, O'Brien S, Fogg AM, Halasyamani PS, O'Hare D, Loiseau T, Férey G (1999) J Am Chem Soc 121:1002
66. Walton RI, Loiseau T, O'Hare D, Férey G (1999) Chem Mater 11:3201
67. Loiseau T, Beitone L, Millange F, Taulelle F, O'Hare D, Férey G (2004) J Phys Chem B 108:20020
68. Beitone L, Huguenard C, Gansmuller A, Henry M, Taulelle F, Loiseau T, Férey G (2003) J Am Chem Soc 125:9102
69. Huang XC, Lin YY, Zhang JP, Chen XM (2006) Angew Chem Int Ed 45:1557
70. Zhang JP, Chen XM (2006) Chem Commun, p 1689
71. Liu Y, Kravtsov VC, Laren R, Eddaoudi M (2006) Chem Commun, p 1488
72. Serre C, Taulelle F, Férey G (2003) Chem Commun, p 2755
73. Férey G (1998) C R Acad Sci 1:1
74. Sassoye C, Loiseau T, Taulelle F, Férey G (2000) Chem Commun, p 943
75. Sassoye C, Marrot J, Loiseau T, Férey G (2002) Chem Mater 14:1340
76. Mellot-Draznieks C, Newsam JM, Gorman AM, Freeman CM, Férey G (2000) Angew Chem Int Ed 39:2270
77. Mellot-Draznieks C, Girard S, Férey G (2002) J Am Chem Soc 124:15326
78. Mellot-Draznieks C, Girard S, Férey G, Schön C, Cancarevic Z, Jansen M (2002) Chem Eur J 8:4103
79. Férey G, Mellot-Draznieks C, Loiseau T (2003) Solid State Sci 5:79
80. Foster MD, Treacy MMJ (2004) Atlas of prospective zeolite frameworks. http://www. hypothetical zeolites.net/. Last accessed 26 Sept 2008
81. Férey G (2003) Angew Chem Int Ed 42:2576
82. Le Bail A (1997) ACA'97 conference on new developments in microstructure analysis via rietveld refinement, 19–25 July 1997, Saint Louis, Missouri
83. Volkringer C, Popov D, Loiseau T, Guillou N, Férey G, Haouas M, Taulelle, Mellot-Draznieks C, Burghammer, Riekel C (2007) Nature Mater 6:760
84. Serre C, Millange F, Thouvenot C, Nogues M, Marsolier G, Louër, D, Férey G (2002) J Am Chem Soc 124:13519
85. Loiseau T, Serre C, Huguenard C, Fink G, Taulelle F, Henry M, Bataille T, Férey G (2004) Chem Eur J 10:1373
86. Serpaggi F, Férey G (2003) J Mol Struct 656:201
87. Barthelet K, Adil K, Millange F, Serre C, Riou D, Férey G (2003) J Mater Chem 13:2208
88. Forster PM, Cheetham AK (2002) Angew Chem Int Ed 41:457
89. Prior TJ, Rosseinsky MJ (2003) Inorg Chem 42:1564
90. Guillou N, Livage C, Drillon M, Férey G (2003) Angew Chem Int Ed 42:5314
91. Forster PM, Burbank AR, Livage C, Férey G, Cheetham AK (2004) Chem Commun, p 368
92. Guillou N, Livage C, Férey G (2005) Angew Chem Int Ed 44:6488
93. Surblé S, Millange F, Serre C, Férey G, Walton RI (2006) Chem Commun, p 1518
94. Barthelet K, Marrot J, Riou D, Férey G (2002) Angew Chem Int Ed 41:281
95. Barthelet K, Marrot J, Riou D, Férey G (2004) Chem Commun, p 520

96. Férey G, Serre C, Mellot-Draznieks C, Millange F, Dutour J, Surblé S, Margiolaki I (2004) Angew Chem Int Ed 43:6296
97. Serre C, Millange F, Surblé S, Férey G (2004) Angew Chem Int Ed 43:6285
98. Mellot-Draznieks C, Dutour J, Férey G (2004) Angew Chem Int Ed 43:6290
99. Férey G, Mellot-Draznieks C, Serre C, Millange F, Dutour J, Surblé S, Margiolaki I (2005) Science 309:2040
100. Serre C, Millange F, Thouvenot C, Nogues M, Marsolier G, Louer D, Férey G (2002) J Am Chem Soc 124:13519
101. Chae HK, Siberio-Perez DY, Kim, J, Go YB, Eddaoudi M, Matzger AJ, O'Keeffe M, Yaghi OM (2004) Nature 427:523
102. Lebedev OI, C, Millange F, Serre C, Van Tendeloo G, Férey G (2005) Chem Mater 17:6525
103. Kitagawa S, Kondo M (1997), Angew Chem Int Ed 36:1725
104. Kitagawa S, Uemura K (2006) Chem Soc Rev 34:109
105. Uemura K, Kitagawa S, Kondo M, Fukui K, Kitaura R, Chang HC, Mizutani T (2002) Chem Eur J 8:3586
106. Uemura K, Kitagawa S, Fukui K, Saito K (2004) J Am Chem Soc 126:3817
107. Birhada K, Hongo Y, Fujita M (2002) Angew Chem Int Ed 41:3395
108. Kitaura R, Seki K, Akiyama G, Kitagawa S (2003) Angew Chem Int Ed 42:428
109. Kitaura R, Fujimoto K, Noro SI, Kondo M, Kitagawa S (2002) Angew Chem Int Ed 41:133
110. Alberti G, Murcia-Mascaros S, Vivani R (1998) J Am Chem Soc 120:9291
111. Tabares LC, Navarro JAR, Salas JM (2001) J Am Chem Soc 123:383
112. Makinen SK, Melcer J, Parvez M, Shimizu GKH (2001) Chem Eur J 7:5176
113. Lu JY, Babb AM (2002) Chem Commun, p 1340
114. Carlucci L, Ciani G, More Mt, Proserpio DM, Rizzato S (2000) Angew Chem Int Ed 39:1506
115. Kepert CJ, Prior TJ, Rosseinsky MJ (2000) J Am Chem Soc 122:5158
116. Mellot-Draznieks C, Serre C, Surblé S, Férey G (2005) J Am Chem Soc 127:16273
117. Surblé S, Serre C, Mellot-Draznieks C, Millange F, Férey G (2006) Chem Soc 284
118. Serre C, Mellot-Draznieks C, Surblé S, Audebrand N, Filinchuk Y, Férey G (2007) Science 315:1828
119. Rocha J, Anderson MW (2000), Eur J Inorg Chem, p 801
120. Khan MI, Meyer LM, Haushalter RC, Schweitzer AL, Zubieta J, Dye JL (1996) Chem Mater 8:43
121. Cavellec M, Riou D, Férey G (1994) J Solid State Chem 112:441
122. Cavellec M, Riou D, Férey G (1999) Inorg Chem Acta 291:317
123. Chen J, Jones RH, Natarajan S, Hursthouse MB, Thomas JM (1994) Angew Chem Int Ed 33:639
124. Natarajan S, Neeraj S, Choudhury A, Rao CNR (2000) Inorg Chem 39:1426
125. Guillou N, Gao Q, Nogues M, Morris RE, Hervieu M, Férey G, Cheetham AK (1999) C R Acad Sci 2:387
126. Feng P, Bu X, Stucky G (1997) Nature 388:735
127. Feng P, Bu X, Stucky G (1997) Science 278:2080
128. Fujita M, Kwon YJ, Washizu S, Ogura K (1994) J Am Chem Soc 116:1151
129. Forster PM, Cheetham AK (2003) Top Catal 24:79
130. Mori W, Takamizawa S, Kato CN, Ohmura T, Sato T (2004) Mic Mes Mater 73:31
131. Lin W (2005) J Solid State Chem 178:2486
132. Seo JS, Whang D, Lee H, Jun SI, Oh J, Jeon YJ, Kim K (2000) Nature 404:982
133. Kesanli B, Lin W (2003) Coord Chem Rev 246:305
134. Wu DD, Hu A, Zhang L, Lin W (2005) J Am Chem Soc 127:8940
135. Dybtsev DN, Nuzhdin AL, Chun H, Bryliakov KP, Talsi EP, Fedin VP, Kim K (2006) Angew Chem Int Ed 45:916
136. Yang CY, Clearfield A (1987) React Polym 5:13
137. Clearfield A, Wang ZK (2002) Dalton Trans, p 2937
138. Clearfield A, Wang ZK, Bellinghausen P (2002) J Solid State Chem 167:376
139. Evans OR, Ngo HL, Lin W (2001) J Am Chem Soc 123:10395
140. Sawaki T, Aoyama Y (1999) J Am Chem Soc 121:4793

141. Gomez-Lor B, Gutierrez-Puebla E, Iglesias M, Monge MA, Ruiz-Valero C, Snejko N (2002) Inorg Chem 41:2429
142. Forster PM, Stock N, Cheetham AK (2005) Angew Chem Int Ed 44:7608
143. Zou Q, Sakurai H, Xu Q (2006) Angew Chem Int Ed 45:2542
144. Kitagawa S, Noro SI, Nakamura T (2006) Chem Commun, p 701
145. Kitaura R, Onoyama G, Sakamoto H, Matsuda R, Noro SI, Kitagawa S (2004) Angew Chem Int Ed 43:2684
146. Qiu LG, Xie AJ, Zhang LD (2004) Angew Chem Int Ed 43:2680
147. Hermes S, Schröter MK, Schmid R, Jhodeir L, Muhler M, Tissler A, Fischer RW, Fischer RA (2005) Angew Chem Int Ed 44:6237
148. Byrd H, Clearfield A, Poojary D, Reis KP, Thompson ME (1996) Chem Mater 8:2239
149. Dokoutchaev A, Krishnan VV, Thompson ME (1998) J Mol Struct 470:191
150. Reis KP, Joshi VK, Thompson ME (1996) J Catal 161:62
151. US Department of Energy (2005) Hydrogen, fuel cells & infrastructure technologies program: multi-year research, development and demonstration plan. US Department of Energy, Washington DC, Chap 3. http://www1.eere.energy.gov/hydrogenandfuelcell/mypp/. Last accessed 26 Sept 2008
152. US Department of Energy (2004) Basic research needs for the hydrogen economy: report of the BES workshop on hydrogen production, storage and use. US Department of Energy Office of Basic Energy Sciences, Washington DC. http://www.science.doe.gov/production/bes/hydrogen.pdf. Last accessed 26 Sept 2008
153. Panella B, Hirscher M, Pütter H, Müller U (2006) Adv Funct Mater 16:520
154. Férey G, Latroche M, Serre C, Millange F, Loiseau T, Percheron-Guégan A (2003) Chem Commun, p 2976
155. Krawiec P, Kramer M, Sabo M, Lunschke R, Fröde H, Kaskel S (2006) Adv Eng Mater 8:293
156. Mueller U, Schubert M, Teich F, Puetter H, Schierle-Arndt K, Pastré J (2006) J Mater Chem 16:626
157. Bourrelly S, LLewellyn P, Serre C, Loiseau T, Millange F, Férey G (2005) J Am Chem Soc 126:13519
158. Takamizawa S, Nakata EI (2005) Cryst Eng Commun 7:476
159. Yildirim T, Hartman MR (2005) Phys Rev Lett 95:215504
160. Spencer EC, Howard JAK, McIntyre GJ, Rowsell JLC, Yaghi OM (2006) Chem Commun, p 278
161. Yang Q, Zhong C (2005) J Phys Chem B 109:11862
162. Yang Q, Zhong C (2005) J Phys Chem B 110:655
163. Düren T, Sarkizov L, Yaghi OM, Snurr RQ (2004) Langmuir 20:2683
164. Mueller T, Ceder G (2005) J Phys Chem B 109:17974
165. Sagara T, Klassen J, Ganz E (2004) J Chem Phys 121:12543
166. Sagara T, Klassen J, Ortony J,Ganz E (2005) J Chem Phys 123:14701
167. Garberoglio G, Skoulidas AI, Johnson JK (2005) J Phys Chem B 109:13094
168. Skoulidas AI, Sholl DS (2005) J Phys Chem B 109:15760
169. Kaye S, Long JR (2005) J Am Chem Soc 126:13519
170. Fichtner M (2006) Adv Eng Mater 7:443
171. Rowsell JLC, Yaghi OM (2004) Mic Mes Mater 73:3
172. Rowsell JLC, Yaghi OM (2005) Angew Chem Int Ed 44:6670
173. Zhou L ((2005) Renew Sust Eng Rev 9:395
174. Barrett S (2005) Fuel Cells Bull, p 12
175. Bogdanovitch B, Felderhoff M, Kaskel S, Pommerin A, Schlichte K, Schüth F (2003) Adv Mater 15:1012
176. Schüth F, Bogdanovitch B, Felderhoff M (2004) Chem Commun, p 2249
177. Wong-Foy AG, Matzger AJ, Yaghi OM (2006) J Am Chem Soc 128:3494
178. Langmi HW, Walton A, Al-Mamouri MM, Johnson SR, Book D, Speight JD, Edwards PP, Gameson I, Anderson PA, Harris IR (2003) J Alloys Compd 356–357:710
179. Panella B, Hirscher M, Roth S (2005) Carbon 109:13094
180. Benard P, Chahine R (2001) Langmuir17:1950

181. Miller C, Rudolf P, Teles HJ (2004) WO 2004/009523, BASF
182. Johnson J (2004) Chem Eng News 82:36
183. Mori W, Yoshida F, Nakayama H, Takamizaka S, Kishita M (1997) Chem Lett 1219
184. Yong Z, Mata V, Rodrigues AE (2002) Sep Purif Technol 26:195
185. Takamizaka S, Nakata EI, Yokoyama H, Mochizuki K, Mori W (2003) Angew Chem Int Ed 42:4331
186. Takamizaka S, Nakata EI, Akatsuka T (2006) Angew Chem Int Ed 45:2216
187. Takamizaka S, Saito T, Akatsuka T, Nakata EI (2005) Inorg Chem 44:1421
188. Li H, Eddaoudi M, Groy TL, Yaghi OM (1998) J Am Chem Soc 120:8571
189. Millward AR, Yaghi OM (1998) J Am Chem Soc 127:17998
190. Llewellyn P, Bourrelly S, Serre C, Filinchuk Y, Férey G (2006) Angew Chem Int Ed 45:7751
191. Llewellyn P, Bourrelly S, Serre C, Vimont A, Daturi M, Hamon L, De Weireld G, Chang JS, Hong DY, Hwang YK, Férey G (2008) Langmuir 24:7245
192. Serre C, LLewellyn P, Bourrelly S, Maurin G, Filinchuk Y, Vimont A, Daturi M, Leynaud O, Barnes P, Férey G (2007) Adv Mater 19:2246
193. Vimont A, Leclerc H, Maugé F, Daturi M, Lavalley JC, Surblé S, Serre, Férey G (2007) J Phys Chem C 111:383
194. Noro S, Kitagawa S, Kondo M, Seki T (2000) Angew Chem Int Ed 39:2082
195. Kitaura R, Kitagawa S, Kubota Y, Kobayachi TC, Kindo K, Mita Y, Matsuo A, Kobayachi A, Chang MC, Ozawa TC, Suzuki M, Sakata, Takata MM (2002) Science 298:2358
196. Uemura T, Kitagawa S (2003) J Am Chem Soc 125:7814
197. Horike S, Matsuda R, Kitaura R, Kitagawa S, Ijima T, Endo K, Kubota Y, Takata MM (2002) Chem Commun, p 2152
198. Kubota Y, Takata MM, Matsuda R, Kitaura R, Kitagawa S (2005) Angew Chem Int Ed 44:920
199. Matsuda R, Kitaura R, Kitagawa S, Kubota Y, Belovsludov RV, Kobayachi TC, Sakamoto H, Chiba T, Takata MM, Kawazoe Y, Mita Y (2005) Nature 436:238
200. Kitaura R, Matsuda R, Kubota Y, Kitagawa S, Takata M, Kobayachi TC, Suzuki M (2005) J Phys Chem B 109:23278
201. Matsuda R, Kitaura R, Kitagawa S, Kubota Y, Belovsludov RV, Kobayachi TC, SakamotoH, Chiba T, Takata MM, Kawazoe Y, Mita Y (2006) Nature 441:584
202. Fletcher AJ, Thomas KM, Rosseinsky MJ (2005) J Solid State Chem 178:2491
203. Bradshaw D, Claridge JB, Cusen EJ, Prior TJ, Rosseinsky MJ (2005) Acc Chem Res 38:273
204. Zhao X, Xiao B, Fletcher AJ, Thomas KM, Rosseinsky MJ (2004) Science 306:1012
205. Pan L, Olson LR, Ciemnolonski, Heddy R, Li J (2006) Angew Chem Int Ed 45:616
206. Chun H, Dybtsev DN, Kim H, Kim K (2005) Chem Eur J 11:3521
207. Ma B, Mulfort KL, Hupp JT (2005) Inorg Chem 44:4912
208. Chen B, Liang C, Contreras DS, Clancy YL, Lobkovsky EB, Yaghi OM, Dai S (2006) Angew Chem Int Ed 45:1390
209. Wang XQ, Liu LM, Jacobson AJ (2006) Angew Chem Int Ed 45:6499
210. Alaerts L, Kirschhok CEA, Maes M, van der Veen MA, Finzy V, Depla A, Martens JA, Baron GV, Jacobs PA, Denayer JFM, De Vos DE (2006) Angew Chem Int Ed 46:4293
211. Chae HK, Siberio-Pérez DY, Kim J, Go Y, Eddaoudi M, Matzger AJ, O'Keeffe M, Yaghi OM (2004) Nature 427:523
212. Horcajada P, Serre C, Vallet-Regi M, Sebban M, Taulelle F, Férey G (2006) Angew Chem Int Ed 45:5974
213. Horcajada P, Ramila A, Férey G, Vallet-Regi M (2006) (2006) Solid State Sci 8:1243
214. Freiberg S, Zhu XX (2004) Int J Pharm 282:1
215. Soppimath KS, Aminabhavi TM, Kulkarni AR, Rudzinski WE (2001) J Control Release 70:1
216. Dhivanand P, Sprockel OL (1998) Int J Pharm 167
217. Rivera A, Farias T (2005) Mic Mes Mater 80:337
218. Vallet-Regi M, Ramila A, del Real RP, Perez-Pariente J (2001) Chem Mater 13:308
219. Munoz B, Ramila A, Perez-Pariente J, Vallet-Regi M (2003) Chem Mater 15:500

220. Becker R, Parala H, Hipler F, Birkner A, Wöll C, Hinrichsen O, Tkachenko OP, Klementiev KV, Grünert W, Schäfer S, Wilmer H, Muhler M, Fischer RA (2004) Angew Chem Int Ed 43:2839
221. Suh MP, Moon HR, Lee EY, Jang SY (2006) J Am Chem Soc 128:4710
222. Spano E, Hamad S, Catlow CRA (2004) Chem Commun, p 864
223. Férey G, Millange F, Morcrette O, Grenèche JM, Doublet ML, Tarascon JM (2007) Angew Chem Int Ed 46:3259
224. Maspoch D, Ruiz-Molina D, Veciana J (2004) J Mater Chem 14:2713
225. Drillon M, Miller JS (2001–2005) Magnetism: molecules to materials, vols I–V. Wiley, Weinheim
226. Kahn O (1993) Molecular magnetism. Wiley, New-York
227. Goodenough JB (1963) Magnetism and the chemical bond. Wiley, New York
228. Shrikanth H, Hajndl R, Moulton B, Zaworotko M (2003) J Appl Phys 93:7089
229. Barthelet K, Riou R, Férey, G (2002) Chem Commun, p 1492
230. Maspoch D, Ruiz-Molina D, Wurtz K, Domingo N, Cavallini M, Biscarini F, Tejada J, Rovira C, Veciana J (2003) Nat Mater 2:190
231. Maspoch D, Domingo N, Ruiz-Molina D, Wurtz K, Vaughan G, Tejada J, Rovira C,Veciana J (2004) Angew Chem Int Ed 43:1828
232. Maspoch D, Ruiz-Molina D, Wurtz K, Rovira C,Veciana J (2004) Dalton Trans 43:1073
233. Maspoch D, Domingo N, Ruiz-Molina D, Wurtz K, Hernandez JM, Vaughan G, Rovira C, Lloret FTejada J, Veciana J (2005) Chem Commun, p 5035
234. Wang Z, Zhang B, Fujiwara H, Kobayashi H, Kurmoo M (2004) Chem Commun, p 416
235. Kou HZ, Zhou BC, Wang RJ (2003) Inorg Chem 42:7658
236. Bourne SA, Lu J, Mondal A, Moulton B, Zaworotko MJ (2001) Angew Chem Int Ed 40:2111
237. Guillou N, Pastre S, LIvage C, Férey G (2002) Chem Commun, p 2358
238. Guillou N, LIvage C, Van Beck M, Nogues M,Férey G (2003) Angew Chem Int Ed 42:644
239. Guillou N, LIvage C, Rabu P, Drillon M, Férey G (2003) Angew Chem Int Ed 42:5314
240. Serpaggi F, Férey G (1998) J Mater Chem 8:2737
241. Serpaggi F, Férey G (1998) J Mater Chem 8:2749
242. Serpaggi F, Férey G (1999) Inorg Chem 38:4741
243. Serpaggi F, Férey G (1999) Mic Mes Mater 32:311
244. Serre C, Millange F, Marrot J, Férey G (2002) Chem Mater 14:2409
245. Serre C, Férey G (2002) J Mater Chem 12:3053
246. Millange F, Serre C, Marrot J, Gardant N, Pelé F, Férey G (2004) Chem Mater 16:1177
247. Millange F, Serre C, Marrot J, Gardant N, Pelé F, Férey G (2004) J Mater Chem 14:642
248. Surblé S (2006) Ph.D. Thesis Versailles (France)
249. Serre C, Marrot J, Férey G (2002) Inorg Chem 44:654
250. Devic T, Serre C, Audebrand N, Marrot J, Férey G (2005) J Am Chem Soc 127:12788
251. Reineke TM, Eddaoudi M, Fehr M, Kelley D, Yaghi OM (1999) J Am Chem Soc 121:1651
252. Reineke TM, Eddaoudi M, O'Keeffe M, Kelley D, Yaghi OM (1999) Angew Chem Int Ed 38:2590
253. Rosi NL, Kim J, Eddaoudi M, Chen BL, O'Keeffe M, Yaghi OM (2005) J Am Chem Soc 127:1504
254. Alleyne BD, Williams AR, Hall LA (2001) Inorg Chem 40:1045
255. Chui SSY, Siu A, Feng X, Zhang ZY, Mak TCW, Williams ID (2001) Inorg Chem Commun 4:467
256. Wu LP (1996) J Coord Chem 37:361
257. Wu LP, Munataka M, Kuroda-Sowa T, Maekawa M, Suenaga Y (1996) Inorg Chim Acta 249:183
258. Pan L, Huang X, Li J, Wu Y, Zheng N (2000) Angew Chem Int Ed 39:527
259. Wu Y, Zheng N, Yang R, Xu H, Ye E (2002) J Mol Struct 610:181
260. Cao R, Sun D, Liang Y, Hong M, Tatsumi K, Shi Q (2002) Inorg Chem 41:2087
261. Pan L, Woodlock EB, Wang X (2000) Inorg Chem 39:4174
262. Long DL, Blake AJ, Champness NR, Wilson C, Schröder M (2001) J Am Chem Soc 123:3401

263. Ma BQ, Zhang DS, Gao S, Jin TZ, Yang CH, Xu GX (2000) Angew Chem Int Ed 39:3644
264. Sun YQ, Zhang J, Chen YM, Yang GY (2005) Angew Chem Int Ed 44:5814
265. De Lill DT, Gunning NS, Cahill CL (2005) Inorg Chem 44:258
266. Serpaggi F, Luxbacher T, Cheetham AK, Férey G (1999) J Solid State Chem 145:580
267. Weissman SI (1942) J Chem Phys 10:214
268. Bunzli JCG, Piguet C (2002) Chem Rev 102:1987
269. de Sa GF, Malta OL, de Mello Donega C, Simas AM, Longo RL, Santa-Cruz PA, da Silva Jr EF (2000) Coord Chem Rev 196:165
270. Imbert D, Comby S, Chauvin A, Bunzli JCG (2005) 44:258
271. Pelé F, Surblé S, Serre C, Millange F, Férey G (2007) J Luminesc 122–123:492
272. Uemura T, Horike S, Kitagawa S (2006) Chem Asian J 1:36

Struct Bond (2009) 132: 135–161
DOI:10.1007/430_2008_9

Published online: 25 February 2009

Supramolecular Chemistry of 4,4′-Bipyridine-N,N'-dioxide in Transition Metal Complexes: A Rich Diversity of Co-ordinate, Hydrogen-Bond and Aromatic Stacking Interactions

Junhua Jia, Peter Hubberstey, Neil R. Champness, and Martin Schröder

Abstract 4,4′-Bipyridine-N,N'-dioxide (L^1) has enormous flexibility as a supramolecular linker since it can be involved not only in co-ordinate and hydrogen-bonds via its N,N'-dioxide oxygen centres, but the pyridine-N-oxide rings can also form aromatic π–π stacking interactions. Thus, L^1 can bridge between, or act as a pendant ligand to metal centres and can support hydrogen-bonds within a lattice in a site remote from the metal centre. Of the structurally characterised transition metal complexes abstracted from the literature for this review, 26 form molecular compounds, 14 form 1D chains, 9 form 2D sheets of either 3^6, 4^4 or 6^3 topology, while 5 form 3D networks with either $4^{12}6^3$ (α-Po type) or 4^86^68 topology. To target multidimensional architectures it has been found to be necessary to avoid aqueous solutions and strongly co-ordinating anions, and consequently the synthesis of multidimensional L^1-bridged transition metal co-ordination polymers has usually involved reaction of L^1 with metal salts of weakly co-ordinating anions in low molecular weight alcohols. Of the 98 distinct molecules of L^1 reported for complexes in the literature, 42 are bridging, 36 pendant and 20 are non-co-ordinated hydrogen-bonded molecules. Approximately 75% of the bridging L^1 molecules adopt an *anti*-conformation, while the remainder adopt a *syn*-conformation. This prevalence of the *anti*-conformation contrasts markedly with the situation observed for lanthanide compounds, for which approximately 75% adopt a *syn*-conformation. A number of trends in the co-ordination behaviour of L^1 with transition metals can be identified. Co-ordination to metal centres is based on sp^2 hybridised oxygen donors, but the π-interaction between the oxygen p_z orbital and the aromatic ring is sufficiently weak that the oxygen lone pairs are normally twisted out of the plane of

J. Jia, P. Hubberstey, N. R. Champness, and M. Schröder (✉)
School of Chemistry, University of Nottingham, University Park, Nottingham, NG7 2RD, UK
e-mail: m.schroder@nottingham.ac.uk

the pyridine-*N*-oxide by a steric clash between the metal centre and the α-hydrogen of the pyridine ring. As a result of this steric hindrance, <M··· O–N angles increase with decreasing perpendicular distance of the metal from the plane of the pyridine-*N*-oxide. Finally, M···M (M = *d*-block metal) separations in complexes containing *anti*- and *syn*-conformation bridging ligands fall in similar ranges. However, those with *syn*-conformation ligands show an increase in M···M separation with increasing <M···O···O···M torsion angle, while those *anti*-conformation ligands show an increase in M···M separation with increasing <M··· O–N angle.

Keywords: 4,4′-Bipyridine-*N*,*N*′-dioxide · Co-ordination polymers · Metal–organic framework · Supramolecular · Transition metals

Contents

Abbreviations

L^1	4,4′-Bipyridine-*N*,*N*′-dioxide
L^2	2,6-Bis[*N*-2-pyridylethyl)formimidoyl]phenolate
H_4bptc	3,3′, 4,4′-Biphenyltetracarboxylic acid
Hfac	Hexafluoroacetylacetonate

1 Introduction

Metal organic co-ordination frameworks have attracted much interest recently [1–5] owing to their potential as materials for solvent-inclusion [6–11] or gas adsorption [12–15] or with electronic [16, 17] or non-linear optical properties [18, 19]. The rational design and targeted synthesis of multidimensional molecular architectures is also of significance in the quest not only to understand how crystalline and ordered materials may be engineered [20–22], but also to elucidate the underlying processes of self-assembly [23–27].

The architectures of metal organic co-ordination frameworks are comprised of metal centres bridged by organic ligands [28,29]. Initially, the majority of the frameworks were produced by linking metal centres with rigid linear N-donor bidentate bridging ligands, such as 4,4′-bipyridine [1–5]. More recently, less sterically demanding and more structurally flexible ligands, including 4,4′-bipyridine-*N*,*N*′-dioxide (L^1), which can bridge metal centres in both *anti*- and *syn*-conformations as well as forming "double-bridges", have been utilised. We reviewed recently the construction of co-ordination frameworks comprising lanthanide metal centres linked by L^1 arguing that they are best considered as design frameworks based on 4^4- and 6^3-subnet tectons [30–35]. In the present review, we consider the literature available on supramolecular frameworks derived from L^1 with *d*-block transition metal ions. In the only previous review of L^1-bridged *d*-block transition metal co-ordination networks, Roesky and Andruh contrasted the role of L^1 as a bridging ligand to that of *N*,*N*′-donor linkers, particularly, 4,4′-bipyridine [36].

As a supramolecular linker, L^1 has enormous potential. Assuming sp^2 hybridisation of the oxygen donor atoms (Scheme 1), it has four lone pairs of electrons, which can be exploited in either direct Lewis base–Lewis acid co-ordination to a metal centre or hydrogen-bond formation with a co-ordinated protic solvent such as water or methanol. Furthermore, the two pyridyl rings provide the opportunity for the formation of aromatic π–π stacking interactions. The outcome of the competition between metal co-ordination and hydrogen-bond formation arising from the dual role of the *N*,*N*′-dioxide oxygen atoms depends on several factors including the strength of the *N*,*N*′-dioxide oxygen to metal, the solvent or anion to metal, and the solvent to *N*,*N*′-dioxide O–H···O hydrogen-bond interactions. Three scenarios can be envisaged with L^1 acting as pendant ligands (Scheme 1a–c), bridges between metal centres (Scheme 1d–f) or sited within the lattice remote from the metal centres (Scheme 1g–i). In all three cases, lone pairs are available to act as hydrogen-bond acceptors to protic solvents (Scheme 1b, c, e, g–i). It thus follows that any rational design of framework materials is not only dependent on the identity of the metal centre and linker but also on the choices of anion and solvent. These need to be taken into account as the more strongly co-ordinating anions and solvent molecules can also occupy metal centre co-ordination sites, thereby cutting the number available for L^1 molecules and reducing both the co-ordinate connectivity of the metal centre and dimensionality of the resultant framework.

2 Structural Chemistry

Structurally characterised complexes containing both a *d*-block transition metal and L^1 are summarised in Table 1, which also includes data pertaining to the co-ordination properties of L^1. Although over 50 such compounds have been reported, few form co-ordinatively bonded framework materials. Of those that have been described, 1D chains are more common than 2D sheets and 3D networks. In this review, the complexes are considered in order of dimensionality based upon

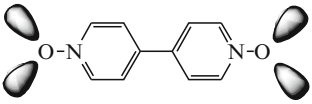

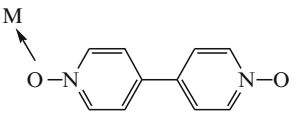

a(18)

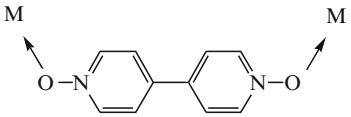

f(9)

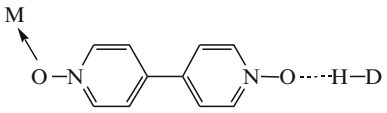

b(12)

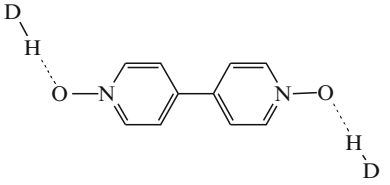

g(9)

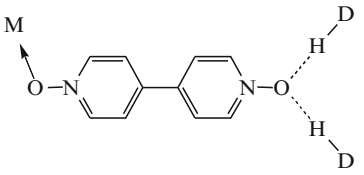

c(6)

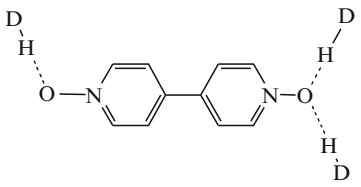

h(3)

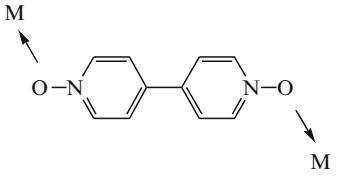

d(27)

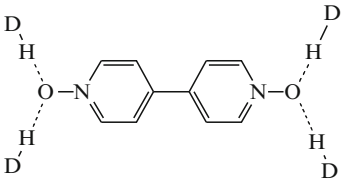

i(8)

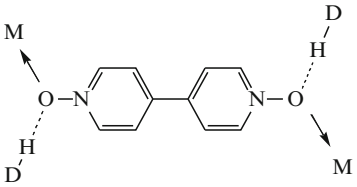

e(6)

Scheme 1 Co-ordinative (**a**–**c** pendant; **d**–**f** bridging) and hydrogen-bonded (**b**, **c**, **e**, **g**–**i**) contacts observed in complexes containing both 4,4′-bipyridine-*N*,*N*′-dioxide and a *d*-block transition metal, M. The number quoted is the frequency of observation in a total of 98 examples. For those systems with a single hydrogen-bonded contact at each end of the 4,4′-bipyridine-*N*,*N*′-dioxide (**g**), the majority (7) lie across an inversion centre giving a pseudo *anti*-conformation arrangement as shown above

Table 1 Structural and conformational data for d-block transition metal complexes of L^1

Compound	Code	Ref.	L^1-type	Symm.	Dihedral angle	M···O–N angle	Distance of M from py plane	M···M distance	M–O···O–M torsion angle
Molecular; mononuclear									
No co-ordinated L^1 molecules									
$[Co(OH_2)_6]\cdot 2Cl\cdot 2(L^1)\cdot 2H_2O$	1	[37]	H-bond type-h	–	2.0				
$[Co(OH_2)_6]\cdot 2Br\cdot 2(L^1)\cdot 2H_2O$	2	[37]	H-bond type-h	–	5.1				
$[Cu(OH_2)_6]\cdot 2Cl\cdot 2(L^1)\cdot 2H_2O$	3	[38]	H-bond type-h	–	2.0				
$[Co(OH_2)_4I_2]\cdot 2(L^1)$	4	[37]	H-bond type-i	C_2	3.8				
$[Co(OH_2)_4(NO_3)_2]\cdot 2(L^1)$	5	[39]	H-bond type-i	–	8.6				
$[Ni(OH_2)_4(NO_3)_2]\cdot 2(L^1)$	6	[39]	H-bond type-i	–	8.4				
One co-ordinated L^1 molecule									
$[Fe(L^1)(OH_2)_5]\cdot SO_4\cdot 4H_2O$	7	[40]	Pendant type-c	–	16.7	133.3	0.268		
$[Co(L^1)(OH_2)_5]\cdot SO_4\cdot 4H_2O$	8	[37]	Pendant type-c	–	2.8	131.2	0.674		
		[41]	Pendant type-c	–	2.1	132.3	0.601		
$[Ni(L^1)(OH_2)_5]\cdot SO_4\cdot 4H_2O$	9	[41]	Pendant type-c	–	2.2	131.4	0.570		
$[Cd(L^1)(OH_2)3I_2]\cdot 0.5(L^1)$	10	[40]	Pendant type-c	–	5.3	127.7	0.737		
			H-bond type-i	i	0				
$[Co(L^1)(OH_2)_3(O_2NO)]\cdot NO_3\cdot (L^1)\cdot H_2O$	11	[37]	Pendant type-c	–	3.1	125.2	0.921		
			H-bond type-g	–	3.7				
Two co-ordinated L^1 molecules									
$[Mn(L^1)_2(OH_2)_2\{N(CN)_2\}_2]$	12	[42]	Pendant type-b	–	No CIF file available				
$[Co(L^1)_2(OH_2)_2\{N(CN)_2\}_2]$	13	[42]	Pendant type-b	–	34.4	119.6	1.753		
$[Cd(L^1)_2(OH_2)_2\{N(CN)_2\}_2]$	14	[43]	Pendant type-b	–	31.8	119.0	1.843		
Four co-ordinated L^1 molecules									
$[Mn(L^1)_4(OH_2)_2]\cdot 2ClO_4\cdot 2H_2O$	15	[44]	Pendant type-b	–	13.1	129.3	0.699		
				–	21.8	131.2	0.744		
$[Co(L^1)_4(OH_2)_2]\cdot 2PF_6\cdot 2H_2O$	16	[44]	Pendant type-b	–	12.0	129.0	0.720		
				–	21.3	130.1	0.813		

(continued)

Table 1 (continued)

Compound	Code	Ref.	L^1-type	Symm.	Dihedral angle	M···O–N angle	Distance of M from py plane	M···M distance	M–O···O–M torsion angle
Six co-ordinated L^1 molecules									
$[Cu(L^1)_6]\cdot 2ClO_4$	17	[38]	Pendant type-a	–	29.3	125.4	1.226		
				–	18.6	125.7	1.534		
				–	14.4	130.0	0.828		
$[Cu(L^1)_6]\cdot 2BF_4$	18	[45]	Pendant type-a	–	27.6	124.4	1.219		
				–	15.3	128.0	0.819		
				–	16.8	124.2	1.559		
$[Zn(L^1)_6]\cdot 2NO_3$	19	[46]	Pendant type-a	–	28.5	124.4	1.267		
				–	12.6	129.2	0.928		
				–	18.3	125.0	1.378		
$[Cd(L^1)_6]\cdot 2NO_3$	20	[45]	Pendant type-a	–	19.4	121.0	1.639		
				–	10.6	128.5	0.967		
				–	29.1	121.1	1.412		
$[Co(L^1)_6]\cdot 2NO_3$	21	[39]	Pendant type-a	–	28.5	125.4	1.250		
				–	12.0	128.7	0.947		
				–	19.4	125.5	1.333		
Molecular; dinuclear									
$\{[Zn_2(\mu\text{-}4,4'\text{-bipy})_2(\mu\text{-}H_2bptc)_2]\cdot(L^1)\}$	22	[47]	H-bond type-g	i	0				
$[\{Cu(OH_2)_2(L^1)\}_2\ (\mu\text{-}L^1)_2]\cdot 2SiF_6\cdot n(solv)$	23	[45]	Bridge type-f	–	10.7	115.6	1.778	11.528	74.0
						124.0	0.866		
			Pendant type-b	–	32.3	137.6	0.236		
$[\{Cu(OH_2)Cl_2(L^1)\}_2(\mu\text{-}L^1)]\cdot 2dmso$	24	[48]	Bridge type-d	i	0	125.3	0.822	12.508	180
			Pendant type-b	–	8.1	125.2	0.834		
Molecular; trinuclear									
$[\{Cu(L^1)_2(OH_2)_2\}\{(\mu\text{-}L^1)(Cu(L^1)_2(OH_2)_2\}_2]\cdot 6ClO_4\cdot 2(L^1)\cdot 6H_2O$	25	[38]	Bridge type-f	–	10.8	135.8	1.050	12.978	61.1
						125.5	0.804		

(continued)

Table 1 (continued)

Compound	Code	Ref.	L^1-type	Symm.	Dihedral angle	M···O–N angle	Distance of M from py plane	M···M distance	M–O···O–M torsion angle
			Bridge type-f	–	21.8	125.6	0.895	12.851	21.4
						135.2	1.086		
			Pendant type-a	–	4.0	127.8	1.279		
			Pendant type-b	–	8.8	127.0	1.177		
			H-bond type-g	–	4.5				
Molecular; tetranuclear									
$[\{Cu_2\{L_2\}(\mu\text{-}OH)\}_2(\mu\text{-}L^1)]\cdot 4ClO_4\cdot 1.33H_2O$	26	[49]	Bridge type-d	i	0	109.8	2.408	12.024	180
1D chains									
$\{[FeCl_3(\mu\text{-}L^1)]\}_\infty$	27	[45]	Bridge type-d	–	38.1	122.8	1.51	12.360	164.3
						122.0	1.72		
$\{[Co(\mu\text{-}L^1)(hfac)_2]\}_\infty$	28	[50]	No CIF file available						
$\{[Cu(\mu\text{-}L^1)(hfac)_2]\}_\infty$	29	[50]	No CIF file available						
$\{[Mn(\mu\text{-}ox)(\mu\text{-}L^1)]\}_\infty$	30	[51]	Bridge type-d	i	0	119.8	1.749	12.537	180
$\{[Co(\mu\text{-}L^1)(H_2O)_4]\cdot 2ClO_4\cdot 2(L^1)\}_\infty$	31	[52]	Bridge type-e	i	0	113.1	2.097	11.831	180
			H-bond type-g	i	0				
			H-bond type-i	i	0				
$\{[Ni\ (\mu\text{-}L^1)(H_2O)_4]\cdot 2ClO_4\cdot 2(L^1)\}_\infty$	32	[52]	Bridge type-e	i	0	112.9	2.049	11.817	180
			H-bond type-g	i	0				
			H-bond type-i	i	0				
$\{[Cu\ (\mu\text{-}L^1)(H_2O)_4]\cdot 2ClO_4\cdot 2(L^1)\}_\infty$	33	[38,52]	Bridge type-e	i	0	107.9	2.42	11.892	180
			H-bond type-g	i	0				
			H-bond type-i	i	0				
$\{[Zn\ (\mu\text{-}L1)(H_2O)_4]\cdot 2ClO_4\cdot 2(L^1)\}_\infty$	34	[52]	Bridge type-e	i	0	113.1	2.122	11.862	180
			H-bond type-g	i	0				
			H-bond type-i	i	0				
$\{[Mn\ (\mu\text{-}L^1)(H_2O)_4]\cdot 2[Cr(bipy)(ox)_2]\cdot 8H_2O\}_\infty$	35	[53]	Bridge type-d	–	12.3	136.3	0.683	13.248	169.2
						137.6	0.151		

(continued)

Table 1 (continued)

Compound	Code	Ref.	L^1-type	Symm.	Dihedral angle	M···O–N angle	Distance of M from py plane	M···M distance	M–O···O–M torsion angle
$\{[Cu\ (\mu\text{-}L^1)(H_2O)\{N(CN)_2\}_2]\}_\infty$	36	[42]	Bridge type-d	–	27.7	116.3	1.765	12.006	163.1
						118.7	1.709		
$\{[Mn\ (\mu\text{-}L^1)(H_2O)_2(C_4H_4O_4)]\}_\infty$	37	[54]	Bridge type-e	i	0	115.1	2.201	12.006	180
$\{[Zn\ (\mu\text{-}L1)(H_2O)_2(C_4H_4O_4)]\}_\infty$	38	[54]	Bridge type-e	i	0	114.3	2.179	11.907	180
$\{[Cu(\mu\text{-}L^1)(\mu\text{-}4,4'\text{-bipy})]$ $\cdot 2ClO_4 \cdot (L^1)\cdot 2H_2O\}_\infty$	39	[38]	Bridge type-d	i	0	129.9	0.988	12.642	180
			H-bond type-g	i	0	–			
$\{[\{Cu(L^1)_2(CH_3OH)_2)(\mu\text{-}L^1)]\cdot 2(PF_6)\}_\infty$	40	[45]	Bridge type-d	i	0	121.0	1.57	12.262	180
			Pendant type-b	–	6.4	122.8	1.54		
2D sheets									
3^6 Topology grids									
$\{[Mn\ (\mu\text{-}L^1)_3]\cdot 2ClO_4\}_\infty$	41	[45]	Bridge type-d	i	0	123.0	1.62	12.403	180
			Bridge type-f	–	24.4	127.9	1.52	12.02	28.9
						129.3	1.24		
$\{[Cu\ (\mu\text{-}L^1)_3]\cdot 2BF_4\}_\infty$	42	[45]	Bridge type-d	i	0	124.4	1.81	12.330	180
			Bridge type-f	–	28.9	125.9	1.22	11.888	33.9
						126.1	1.23		
4^4 Topology grids									
$\{[\{Cd(ONO_2)_2\}(\mu\text{-}L^1)_2]\}_\infty$	43	[45]	Bridge type-f	–	32.0	121.8	1.55	12.254	36.8
						121.6	1.62		
$\{[Cu(H_2O)(\mu\text{-}L^1)_2](S_2O_6)\cdot H_2O)\}_\infty$	44	[41]	Bridge type-d	C_2	22.2	119.0	1.59	11.991	175.4
				i	0	119.7	1.23	11.991	180
$\{[\{Cu(OHMe)_2\}(\mu\text{-}L^1)_2]\cdot 2ZrF_5\}_\infty$	45	[45]	Bridge type-d	i	0	114.7	0.37	11.831	180
				i	0	129.2	1.74	12.62	180
$\{[Et_4N][\{Cu(OHMe)_{0.5}\}(\mu\text{-}L^1)_2$ $(\mu\text{-}FSiF_5)_{0.5}]\cdot 2SbF_6\cdot n(solv)\}_\infty$	46	[45]	Bridge type-d	i	0	118.0	1.63	11.995	180

(continued)

Table 1 (continued)

Compound	Code	Ref.	L^1-type	Symm.	Dihedral angle	M···O–N angle	Distance of M from py plane	M···M distance	M–O···O–M torsion angle
$\{[\{Cu(L^1)_2\}(\mu\text{-}L^1)_2]\cdot 2(PF_6)\}_\infty$	47	[45]	Bridge type-d	i	0	121.0	1.23	12.137	180
				i	0	122.8	1.32	12.343	180
			Pendant type-a	–	16.2	128.7	1.36		
$\{[\{Cu(L^1)_2\}(\mu\text{-}L^1)_2]\cdot 2(SbF_6)\}_\infty$	48	[45]	Bridge type-d	i	0	123.1	1.36	12.185	180
				i	0	121.1	1.33	12.387	180
			Pendant type-a	–	18.0	130.0	1.16		
6^3 Topology grids									
$\{[\{Zn(CH_3OH)_2(L^1)\}(\mu\text{-}L^1)1.5]\cdot 0.5L^1\cdot SiF_6\cdot 3MeOH\}_\infty$	49	[46]	Bridge type-d	i	0	118.0	1.81	12.3	180
			Bridge type-f	–	17.72	125.2	1.63	12.7	56.4
						132.4	0.76		
			Pendant type-b	–	17.9	122.6	1.56		
			H-bond type-g	i	0				
3D networks									
$\{[Sc\ (\mu\text{-}L^1)_3]\cdot 3NO_3\}_\infty$	50	[55]	Bridge type-d	i	0	131.5	0.93	12.8	180
$\{[Sc\ (\mu\text{-}L^1)_3]\cdot 3ClO_4\}_\infty$	51	[55]	Bridge type-d	i	0	134.9	0.72	12.954	180
$\{[Co\ (\mu\text{-}L^1)_3]\cdot S_2O_6\cdot 7C_2H_5OH\}_\infty$	52	[41]	Bridge type-d	i	0	124.5	1.23	12.525	180
			Bridge type-f	–	8.1	119.4	1.78	12.068	44.8
						127.1	0.90		
$\{[Ni\ (\mu\text{-}L^1)_3]\cdot S_2O_6\cdot 7C_2H_5OH\}_\infty$	53	[41]	Bridge type-d	i	0	124.6	1.30	12.410	180
			Bridge type-f	–	10.9	118.7	1.53	12.073	33.3
						123.7	0.95		
$\{[Sc(\mu\text{-}L^1)_3]\cdot 3CF_3SO_3\cdot 2.7CH_3OH\cdot 3H_2O\}_\infty$	54	[55]	Bridge type-f	–	22.6	142.7	0.44	12.250	43.2
						119.1	1.91		
				–	10.6	137.8	0.78	12.173	43.9
						123.8	1.78		
			Bridge type-d	i	0	123.4	1.84	12.416	180
				i	0	129.4	1.15	12.789	180

metal centre to L^1 co-ordinate interactions; thus molecular species are listed first followed by 1D chains, 2D sheets and finally 3D networks.

2.1 Mononuclear Molecular Species

Examples of mononuclear molecular species (Table 1) range from complexes containing no metal co-ordinated molecules of L^1 such as $[M(OH_2)_6] \cdot 2X \cdot 2(L^1) \cdot 2H_2O$ **1**–**3** [37, 38], $[Co(OH_2)_4I_2] \cdot 2(L^1)$ **4** [37] and $[M(OH_2)_4(NO_3)_2] \cdot 2(L^1)$ **5**, **6** [39], through to those containing one, $[M(L^1)(OH_2)_5] \cdot SO_4 \cdot 4H_2O$ (**7** M = Fe; **8** M = Co; **9** M = Ni) [37, 40, 41], $[Cd(L^1)(OH_2)_3I_2] \cdot 0.5(L^1)$ **10** [40] and $[Co(L^1)(OH_2)_3(O_2NO)] \cdot NO_3 \cdot (L^1) \cdot H_2O$ **11** [37], two, $[M(L^1)_2(H_2O)_2\{N(CN)_2\}_2]$ (**12** M = Mn; **13** M = Co; **14** M = Cd) [42, 43], four, $[M(L^1)_4(OH_2)_2] \cdot 2X \cdot 2H_2O$ (**15** M = Mn; **16** M = Co) [44], and six, $\{[M(L^1)_6] \cdot 2X$ (**17** M = Cu; **18** M = Cu; **19** M = Zn; **20** M = Cd; **21** M = Co) [38, 39, 45, 46]. In **1**–**6** the molecules of L^1 are located in the lattice via hydrogen-bonding interactions to co-ordinated water molecules (Scheme 1h, i), while **7**–**21** incorporate L^1 as mono-co-ordinated pendant molecules (Scheme 1a–c). Two examples (**10**, **11**) contain both types of binding interactions, i.e. directly bound to metal cations as well as hydrogen-bonded (Scheme 1i, g, respectively) to co-ordinated water. The extended structures of these species are typified by those of **3** (Fig. 1a) [38], **7** (Fig. 1b) [40], **13** (Fig. 1c) [42], **15** (Fig. 1d) [44] and **17** (Fig. 1e) [38]. Hydrogen-bonding O–H···O between the $[M(OH_2)_6]^{2+}$ cations and un-co-ordinated L^1 in **1** (Fig. 1a; Scheme 1h) results in the construction of a 2D sheet. These sheets are further linked through water ··· water O–H···O and water···anion O–H···Cl hydrogen-bonds to generate a 3D supramolecular structure. Intermolecular water···L^1 O–H·····O hydrogen-bonds between $[M(L^1)(OH_2)_5]^{2+}$ cations in **7** (Fig. 1b; Scheme 1c) together with aromatic π–π stacking interactions afford a 1D ladder motif. These ladders are further linked through water···water and water···anion O–H···O hydrogen-bonds to generate a 3D supramolecular structure. Intermolecular water···L^1 O–H···O and water–$[N(CN)_2]^{2-}$ O–H···N hydrogen-bonds between $[M(L^1)(OH_2)_2[N(CN)_2]$ moieties in **12** (Fig. 1c; Scheme 1b) give a 2D sheet construction. Aromatic stacking interactions between pyridyl moieties lead to super-positioning of the layers and formation of a 3D supramolecular network. Intermolecular water···L^1 O–H···O hydrogen-bonds between the cations $[M(L^1)_4(OH_2)_2]^{2+}$ in **15** (Fig. 1d; Scheme 1b) together with aromatic stacking interactions result in the construction of a 3D diamondoid network. The basic molecular unit of **17** (Fig. 1e; Scheme 1a) is a $[Cu(L^1)_6]^{2+}$ cation in which six pendant molecules of L^1 co-ordinate a Cu(II) centre. Packing of these cations via aromatic π–π stacking interactions gives a 2D sheet structure of bilayer appearance with pseudo-3^6 topology. The sheets align in an eclipsed fashion through aromatic stacking interactions to give an AAA packing motif within which there are triangular channels occupied by counterions.

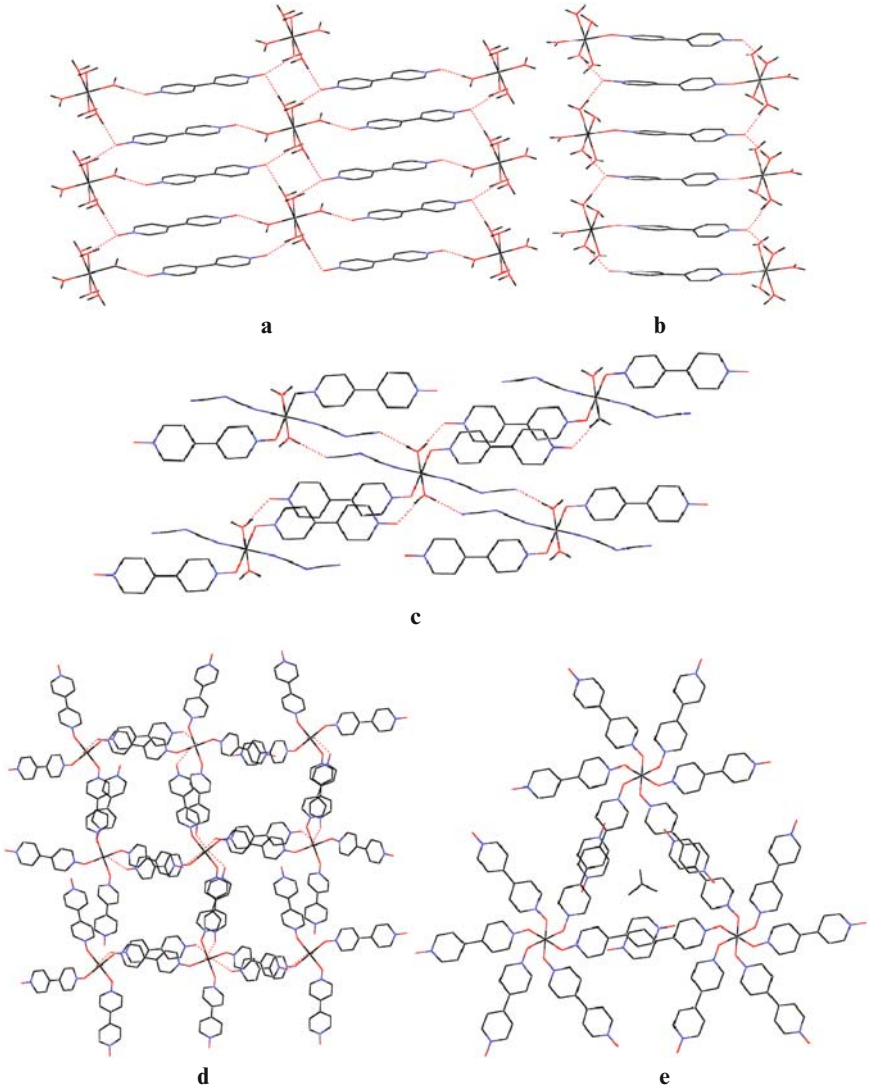

Fig. 1 Views of the supramolecular extended structures of **a** $\{[Cu(OH_2)_6]\cdot 2Cl\cdot 2(L^1)\cdot 2H_2O\}_\infty$ **3** [38], **b** $\{[Fe(L^1)(OH_2)_5]\cdot SO_4\cdot 4H_2O\}_\infty$ **7** [40], **c** $\{[Co(L^1)_2(H_2O)_2\{N(CN)_2\}_2]\}_\infty$ **13** [42], **d** $\{[Mn(L^1)_4(OH_2)_2]\cdot 2ClO_4\cdot 2H_2O\}_\infty$ **15** [44] and **e** $\{[Cu(L^1)_6]\cdot 2ClO_4\}_\infty$ **17** [38]

2.2 Multinuclear Molecular Species

There are 5 examples of multinuclear molecular species (Table 1), 3 of which are binuclear, $\{[Zn_2(\mu\text{-}4,4'\text{-bipy})_2(\mu\text{-}H_2bptc)_2]\cdot(L^1)\}_\infty$ (H_4bptc = 3,3′,4,4′-biphenyltetracarboxylic acid) **22** [47], $[\{Cu(OH_2)_2(L^1)\}_2(\mu\text{-}L^1)_2]\cdot 2SiF_6\cdot n(solv)$

23 [45] and $[\{Cu(OH_2)Cl_2(L^1)\}_2(\mu - L^1)]\cdot$ 2dmso **24** [48]}, one trinuclear, $\{[\{Cu(L^1)_2(OH_2)_2\}\{(\mu\text{-}L^1)(Cu(L^1)_2(OH_2)_2\}_2] \cdot 6ClO_4 \cdot 2(L^1) \cdot 6H_2O$ **25** [38]}, and one tetranuclear $\{[\{Cu_2\{L^2)(\mu\text{-}OH)\}_2(\mu\text{-}L^1)] \cdot 4ClO_4 \cdot 1.33H_2O$ (L^2 = 2,6 − bis[N − 2-pyridylethyl)formimidoyl]phenolate] **26** [49]}. Bridging L^1 ligands only occur in complexes **23**–**26**. In **22** [47], non-co-ordinated guest molecules of L^1 are located by O–H···O hydrogen-bonds (Scheme 1g) in a series of 1D channels within the $\{[Zn_2(\mu\text{-}4,4' - bipy)_2(\mu\text{-}H_2bptc)_2]\}_\infty$ framework. The binuclear species $[\{Cu(OH_2)Cl_2(L^1)\}_2(\mu\text{-}L^1)]$ in **24** [48] is comprised of two crystallographically related $[Cu(OH_2)Cl_2(L^1)]$ moieties linked by a bridging L^1 which adopts an *anti*-conformation (Scheme 1d) and is located across a centre of inversion (Fig. 2a). A similar, but less common arrangement is observed in

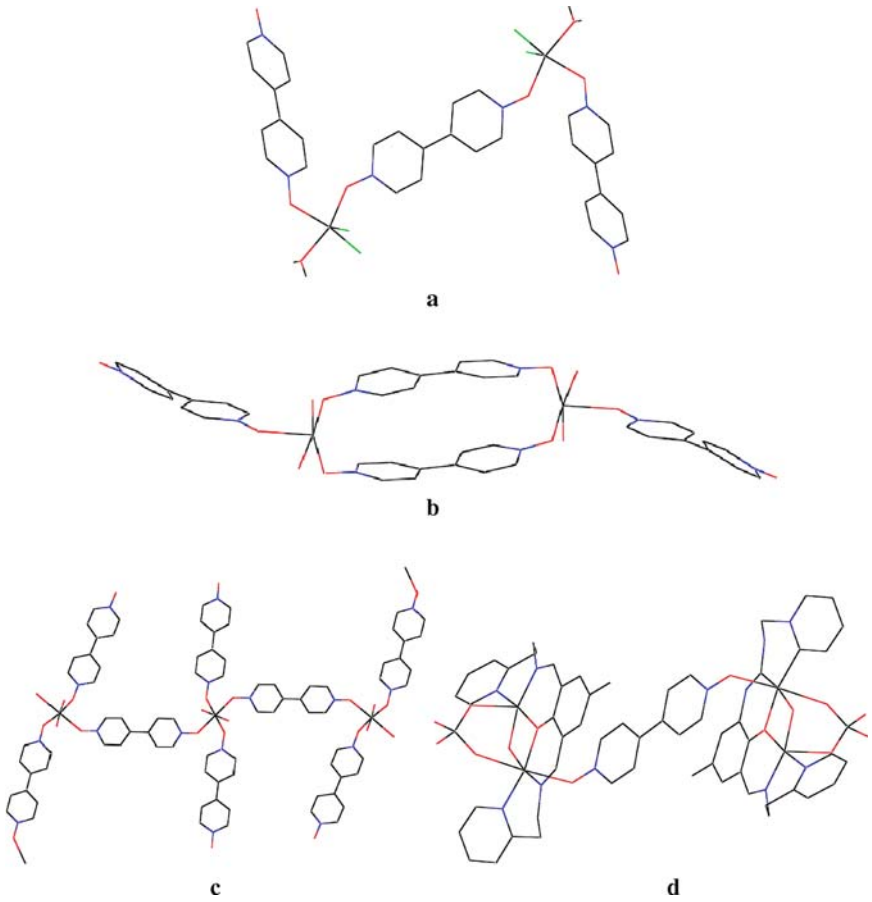

Fig. 2 Views of **a** the binuclear complex $[\{Cu(OH_2)Cl_2(L^1)\}_2(\mu\text{-}L^1)]$ in **24** [48], **b** the binuclear cation$[\{Cu(OH_2)_2(L^1)\}_2(\mu\text{-}L^1)_2]^{2+}$ in **23** [45], **c** the trinuclear cation $[\{Cu(L^1)_2(OH_2)_2\}\{(\mu\text{-}L^1)(Cu(L^1)_2(OH_2)_2\}_2]^{6+}$ in **25** [38] and **d** the tetranuclear cation $[\{Cu_2\{L^2)(\mu\text{-}OH)\}_2(\mu\text{-}L^1)]^{4+}$ in **26** [49]

binuclear $[\{Cu(OH_2)_2(L^1)\}_2(\mu\text{-}L^1)_2]^{2+}$ **23** [45], where two crystallographically related $[Cu(OH_2)_2(L^1)]$ moieties are linked by two molecules of L^1 crystallographically related through an inversion centre (Fig. 2b). This is the only example of a "double-bridge" abstracted for this review, although the double-bridge is a common arrangement in lanthanide co-ordination polymers [30]. In **23** [45], the bridging L^1 molecule adopts a conformation that is almost midway between *anti*- (Scheme 1d) and *syn*- (Scheme 1f) with an $<M\cdots O\cdots O\cdots M$ torsion angle of 74°. This most unusual conformation (a complete list of $<M\cdots O\cdots O\cdots M$ torsion angles is given in Table 1) is probably due to L^1 forming part of the double-bridge. The trinuclear cation $[\{Cu(L^1)_2(OH_2)_2\}\{(\mu\text{-}L^1)(Cu(L^1)_2(OH_2)_2\}_2]^{6+}$ in **25** [38] has a fishbone-like motif; it comprises two crystallographically related $[Cu(OH_2)_2(L^1)_2]$ moieties, each of which is linked by bridging L^1 to a central $[Cu(OH_2)_2(L^1)_2]$ unit that is located across a centre of inversion (Fig. 2c). The bridging molecules of L^1 adopt a *syn*-conformation (Scheme 1f), while the non-co-ordinated lattice L^1 (Scheme 1g) is held in position, parallel to the bridging L^1 molecule, by both water$\cdots L^1O$–$H\cdots O$ hydrogen-bonds and aromatic stacking interactions. Adjacent fishbone units are linked by aromatic π–π stacking interactions to form a 2D sheet of 4^4 topology. The tetranuclear cation $\{[\{Cu_2\{L^2)(\mu\text{-}OH)\}_2(\mu\text{-}L^1)]^{4+}$ in **26** [49] comprises two crystallographically related $[Cu_2\{L^2)(\mu\text{-}OH)]$ complexes linked by a bridging L^1 located across a centre of inversion (Fig. 2d). The bridging L^1 molecule necessarily adopts the *anti*-conformation (Scheme 1d).

2.3 1D 4,4′-Bipyridine–N,N′-Dioxide Bridged Chains

Examples of 1D chain polymer complexes incorporating L^1 (Table 1) are typified by $\{[FeCl_3(\mu\text{-}L^1)]\}_\infty$ **27** [45], $\{[\{M(hfac)_2\}(\mu\text{-}L^1)]\}_\infty$ (hfac = hexafluoroacetylacetonate) (**28** M = Co; **29** M = Cu) [50], $\{[Mn(\mu\text{-}L^1)(\mu\text{-ox})]\}_\infty$ **30** [51], $\{[\{M(H_2O)_4\}(\mu\text{-}L^1)]\cdot 2ClO_4\cdot 2(L^1)\}_\infty$ (**31** M = Co; **32** M = Ni; **33** M = Cu; **34** M = Zn) [38, 52], $\{[\{Mn(H_2O)_4\}(\mu\text{-}L^1)]\cdot 2[Cr(bipy)(ox)_2]\cdot 8H_2O$ **35** [53], $\{[\{Cu(H_2O)\{N(CN)_2\}_2\}(\mu\text{-}L^1)]\}_\infty$ (**36**) [42], $\{[\{M(H_2O)_2\}(\mu\text{-}L^1)(\mu\text{-}C_4H_4O_4)]\}_\infty$ (**37** M = Mn; **38** M = Zn) [54], $\{[Cu(\mu\text{-}L^1)(\mu\text{-}4,4'-\text{bipyridine})]\cdot 2ClO_4\cdot(L^1)\cdot 2H_2O\}_\infty$ **39** [38] and $\{[Cu(L^1)_2(CH_3OH)_2)(\mu\text{-}L^1)]\cdot 2(PF_6)\}_\infty$ **40** [45]. They all comprise alternating metal centres and molecules of L^1 (Fig. 3a). With just two exceptions, L^1 lies across inversion centres giving $<M\cdots O\cdots O\cdots M$ torsion angles of 180°; the exceptions deviate little from the ideal *anti*-conformation with $<M\cdots O\cdots O\cdots M$ torsion angles of 169.2° (**35**) and 163.1°(**36**). The remaining co-ordination sites are occupied either by anions alone (**27**–**30**), solvent molecules alone (**31**–**35**), a mixture of solvent molecules and anions (**36**–**38**) or a mixture of ancillary ligands and anions (**39**). In one case (**40**), pairwise pendant L^1 molecules are attached to each metal centre forming a fishbone-like structure.

Formation of these extended chain structures is highly dependent upon the ancillary ligands. Those containing solely co-ordinated chloride (**27**) or hexafluoroacetylacetonate (**28**, **29**) simply align parallel to one of the crystal axes with minimal

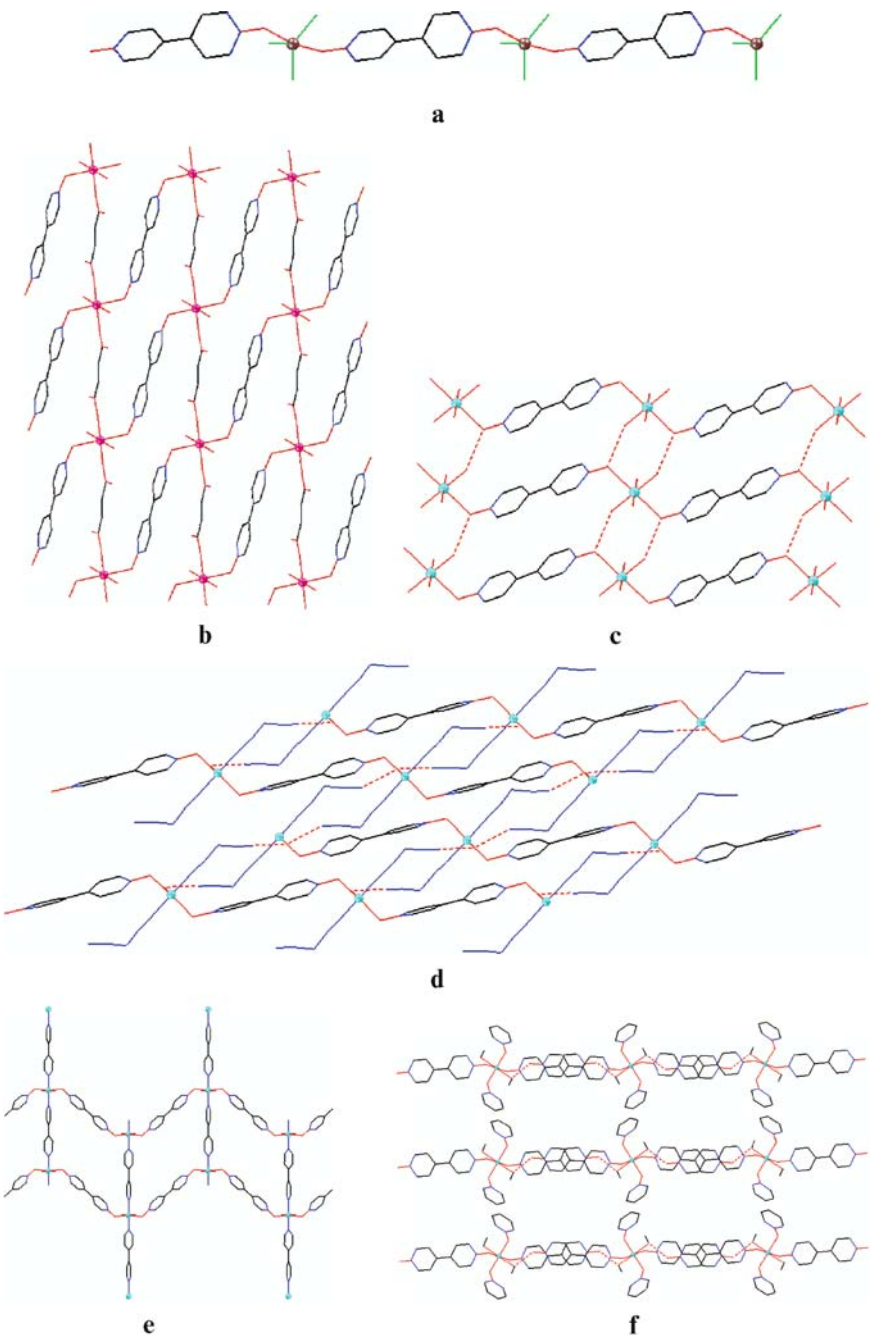

Fig. 3 Views of **a** the 1D chain of alternating metal centres and L^1 bridging ligands in $\{[FeCl_3(\mu\text{-}L^1)]\}_\infty$ **27** [45] and the 2D sheets with pseudo-4^4 topology in **b** $\{[\{Mn(H_2O)_2\}(\mu\text{-}L^1)(\mu\text{-}C_4H_4O_4)]\}_\infty$ **37** [54], **c** $\{[\{Cu(H_2O)_4\}(\mu\text{-}L^1)] \cdot 2ClO_4 \cdot 2(L^1)\}_\infty$ **33** [38], **d** $\{[\{Cu(H_2O)\{N(CN)_2\}_2\}(\mu\text{-}L^1)]\}_\infty$ **36** [42], **e** $\{[Cu\ (\mu\text{-}L^1)(\mu\text{-}4,4'\text{-bipyridine})] \cdot 2ClO_4 \cdot (L^1) \cdot 2H_2O\}_\infty$ **39** [38] and **f** $\{[Cu(L^1)_2(CH_3OH)_2)(\mu\text{-}L^1)] \cdot 2(PF_6)\}_\infty$ **40** [45]

van der Waals interactions. However, for those containing co-ordinated oxalate (**30**) or succinate (**37**, **38**), the anions also act as bridging ligands giving rise to 2D sheets with pseudo-4^4 topology (Fig. 3b). 2D sheets with pseudo-4^4 topology also arise in those materials containing co-ordinated water molecules. Whereas in **31**–**34**, water$\cdots L^1$ O–H$\cdots$O hydrogen-bonds link the chains (Fig. 3c), in **36** the chains are linked by water$\cdots[N(CN)_2]^-$ O–H$\cdots$N hydrogen-bonds (Fig. 3d). A similar pseudo-4^4 grid is also found in the structure of **39**, where the L^1-bridged chains are linked by 4,4′-bipyridine molecules (Fig. 3e). For **40,** in which both co-ordinated methanol and pendant L^1 molecules are present, the chains pack in a parallel fashion such that the non-co-ordinated oxygen atoms of the pendant L^1 molecules from adjacent chains act as hydrogen-bonding acceptors to the OH groups of co-ordinated methanol to form another 2D grid with pseudo-4^4 topology (Fig. 3f); further aromatic interactions between the pendant molecules of L^1 support the formation of this grid.

2.4 2D 4,4′-Bipyridine–N,N'-Dioxide Bridged Sheets

There are a limited number of examples of 2D sheet constructions based on L^1-bridged transition metal centres (Table 1). These generally form grids that are comprised of subnet-tectons [30] of 3^6, 4^4 or 6^3 topologies. 3^6-Grids are found in $\{[M(\mu\text{-}L^1)_3]\cdot 2X\}_\infty$ (**41** M = Mn; **42** M = Cu) [45] with each six-co-ordinate distorted octahedral metal centre linked to six crystallographically related metal centres through bridging molecules of L^1 (Fig. 4) to form layers that are stacked in an eclipsed arrangement through aromatic π–π stacking interactions. Two of the ligands L^1 adopt an *anti*-conformation (Scheme 1d) with the others in a *syn*-conformation (Scheme 1f; Fig. 4). Such grids remain relatively rare with only 7 examples having been described [45, 56–61].

2D grids of 4^4-topology are the principal architectural feature in $\{[\{Cd(ONO_2)_2\}(\mu\text{-}L^1)_2]\}_\infty$ **43** [45], $\{[\{Cu(OH_2)\}(\mu\text{-}L^1)_2]\cdot S_2O_6\cdot H_2O\}_\infty$ **44** [41], $\{[\{Cu(OHMe)_2\}(\mu\text{-}L^1)_2]\cdot 2ZrF_5\}_\infty$ **45** [45], $\{[Et_4N][\{Cu(OHMe)_{0.5}\}(\mu\text{-}L^1)_2(\mu\text{-}FSiF_5)_{0.5}]\cdot 2SbF_6\cdot n(solv)\}_\infty$ **46** [45] and $\{[\{Cu(L^1)_2\}(\mu\text{-}L^1)_2]\cdot 2X\}_\infty$ (**47** X = PF_6^-; **48** X = SbF_6^-) [45]. Typical examples, **43** and **45** [45], are shown in Fig. 5a, b, respectively. The four bridging molecules of L^1, which occupy the equatorial positions of the octahedral (**43**, **45**–**48**), or the basal positions of the square pyramidal (**44**) co-ordination spheres, adopt the *anti*-conformation (Fig. 5b; Scheme 1d), the exception being that in **43**, which adopts a *syn*-conformation (Fig. 5a; Scheme 1f) with a <M$\cdots$O$\cdots$O$\cdots$M torsion angle of 36.8°. The axial co-ordination sites of the distorted octahedral co-ordination spheres are occupied by either NO_3^- anions (**43**), methanol molecules (**45**) or pendant L^1 molecules (**47** and **48**), while those of the Cu(II) centre in **46** are occupied by a SiF_6^{2-} anion and a slightly more remote methanol solvent molecule. The apical co-ordination site of the distorted square pyramidal Cu(II) co-ordination sphere in **44** is occupied by a water molecule. These axial and apical ligands serve to generate extended 3D structures. In **43**, the layers

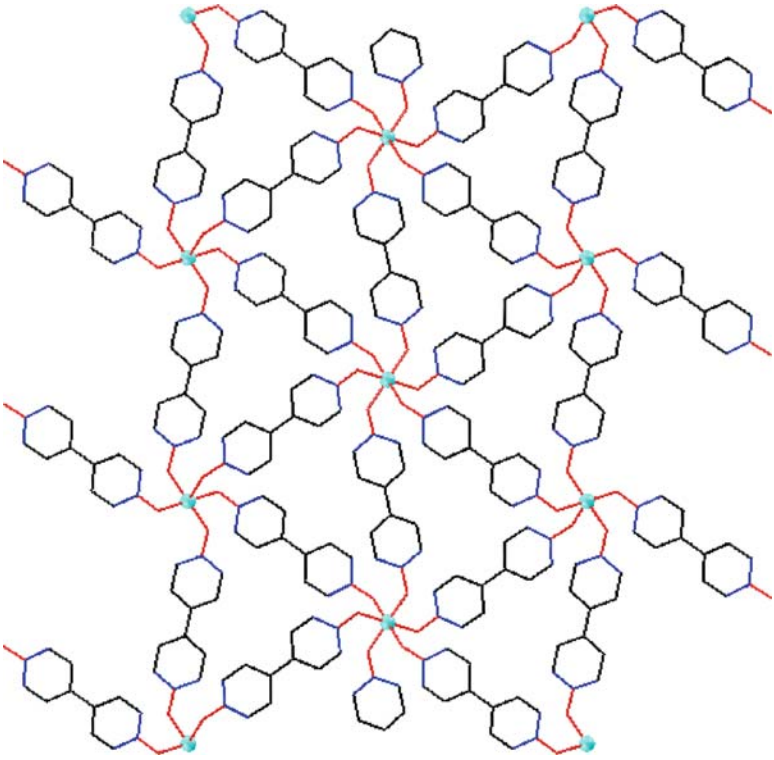

Fig. 4 View of the 2D 3^6 grids in $\{[Cu\ (\mu\text{-}L^1)_3] \cdot 2BF_4\}_\infty$ **42** [45]

align along the *a*-axis in a staggered arrangement through aromatic π–π stacking interactions to give an AB packing mode with the axially located NO_3^- anions interdigitated in the centre of the rectangular cavities of the adjacent sheets. In **44**, the 4^4 sheets are linked via O–H···O hydrogen-bonds between co-ordinated water molecules and dithionate anions. In **45**, the sheets are polycatenated with a dihedral angle of 82.1(1)°. The resultant 3D architecture is further interpenetrated by a 1D $\{[ZrF_5]^-\}_\infty$ chain, which runs through channels in the structure to form a most unusual triply intertwined co-ordination polymer (Fig. 5c) [45, 62–64]. In **47** and **48**, the 2D sheets are aligned parallel such that the pendant ligands L^1 from adjacent sheets form aromatic stacking interactions to give a 3D matrix architecture. In **46** 2D sheets are linked by bridging bidentate $[SiF_6]^{2-}$ anions to give a pillared layer structure stacked along the *c*-axis as shown in Fig. 5d. The 3D extended structure of **46** is based upon a 5-connected metal centre and linear *N*,*N*′-dioxide and $[SiF_6]^{2-}$ linkers to give an overall 4^46^6 topology.

Thus far, only one grid with 6^3 topology, that in $\{[\{Zn(CH_3OH)_2(L^1)\}(\mu\text{-}L^1)_{1.5}] \cdot 0.5L^1 \cdot SiF_6 \cdot 3MeOH\}_\infty$, **49** [46], has been described (Fig. 6) in which octahedral Zn(II) centres are bridged by L^1 to form a 6^3 brickwall net. One of the L^1 bridges lies across an inversion centre and thus necessarily adopts an *anti*-conformation

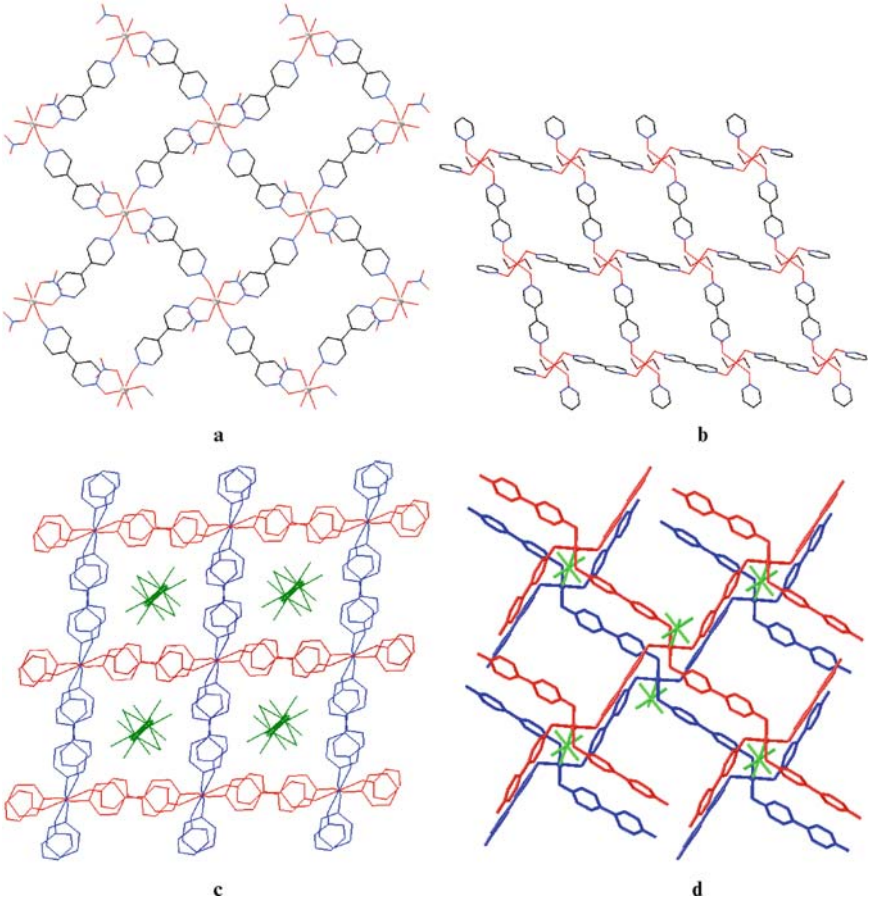

Fig. 5 Views of the 2D 4^4-grids in **a** $\{[\{Cd(ONO_2)_2\}(\mu\text{-}L^1)_2]\}_\infty$ **43** [45] and **b** $\{[\{Cu(OHMe)_2\}(\mu\text{-}L^1)_2] \cdot 2ZrF_5\}_\infty$ **45** [45]. **c** Unusual triply intertwined co-ordination network in $\{[\{Cu(OHMe)_2\}(\mu\text{-}L^1)_2] \cdot 2ZrF_5\}_\infty$ **45** [45]. **d** Linking of the 4^4 sheets in $\{[Et_4N][\{Cu(OHMe)_{0.5}\}(\mu\text{-}L^1)_2(\mu\text{-}FSiF_5)_{0.5}] \cdot 2SbF_6 \cdot n(solv)\}_\infty$ **46** [45] by $[SiF_6]^{2-}$ anions to give a 3D matrix of five-connected 4^46^6 topology

(Fig. 6; Scheme 1d), while the other adopts a *syn*-conformation (Fig. 6; Scheme 1f) with a <M···O···O···M torsion angle of 56.4°. By forming water···L^1 O–H···O hydrogen-bonds with the co-ordinated water molecules, the non-co-ordinated molecules of L^1 (Scheme 1g) modify the 2D framework by connecting the nodes at the centres of the long sides of the brickwall rectangles and convert the 6^3 grid into a pseudo-4^4 grid (Fig. 6). Furthermore, the pendant molecules of L^1 (Scheme 1b) link the sheets through aromatic π–π stacking interactions to construct a 3D open network.

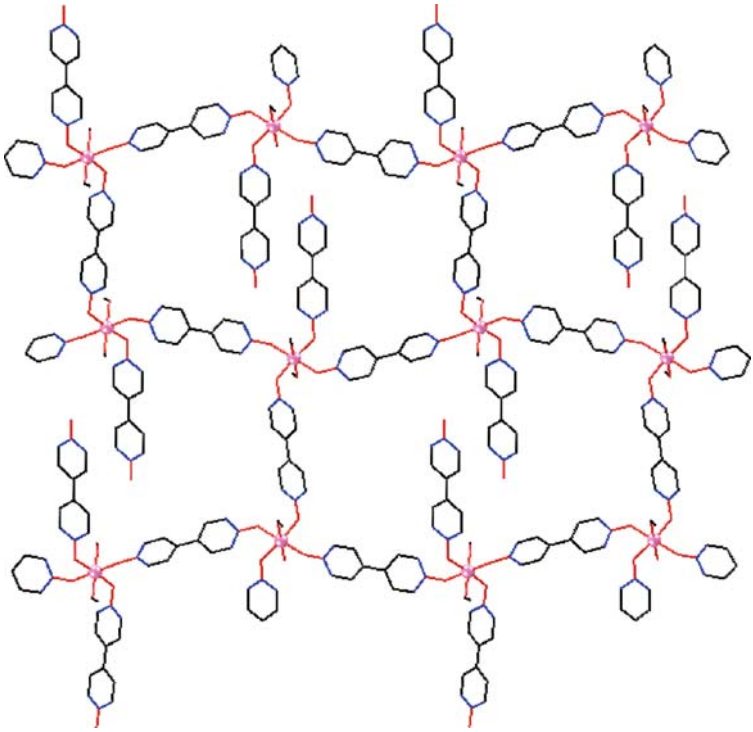

Fig. 6 View of the 2D 6^3 grids in $\{[\{Zn(CH_3OH)_2(L^1)\}(\mu\text{-}L^1)_{1.5}] \cdot 0.5L^1 \cdot SiF_6 \cdot 3MeOH\}_\infty$ **49** [46]

2.5 3D 4,4′-Bipyridine–N,N′-Dioxide Bridged Frameworks

Five examples of this type of 3D co-ordination polymer have been described (Table 1) [41,55]. They fall into two groups, which are topological isomers and, following our earlier analysis [30–35], both structures can be thought of as a series of parallel 4^4 subnet-tectons with each metal centre linked to two other metal centres in both adjacent nets. In $\{[Sc(\mu\text{-}L^1)_3] \cdot 3X\}_\infty$ (**50** $X = NO_3^-$; **51** $X = ClO_4^-$) (Fig. 7a) [55], the molecules of L^1 bridge Sc(III) centres, which are located on crystallographic -3 (S_6) positions, to form a rhombohedral array of $4^{12}6^3$ (α -Po type) topology (Fig. 8a). In $\{[M(\mu\text{-}L^1)_3] \cdot S_2O_6 \cdot 7C_2H_5OH\}_\infty$ (**52** M = Co; **53** M = Ni) [41], and $\{[Sc(\mu\text{-}L^1)_3] \cdot 3CF_3SO_3 \cdot 2.7CH_3OH \cdot 3H_2O\}_\infty$ **54** [55] (Fig. 7b), L^1 bridges Sc(III) centres in a much less symmetrical fashion to give a criss-crossed structure that has displaced linkages between parallel 4^4 subnet-tectons to give a 4^86^68 topology (Fig. 8b). Although the crystallographic symmetry of the structures of **50** and **51** necessitates the adoption of *anti*-conformation for all molecules of L^1, both *anti*- and *syn*-conformation L^1 molecules occur in **52–54** with $<M\cdots O\cdots O\cdots M$ torsion angles of the *syn*-conformation in the L^1 bridges ranging from 33.3 to 44.8° (Table 1).

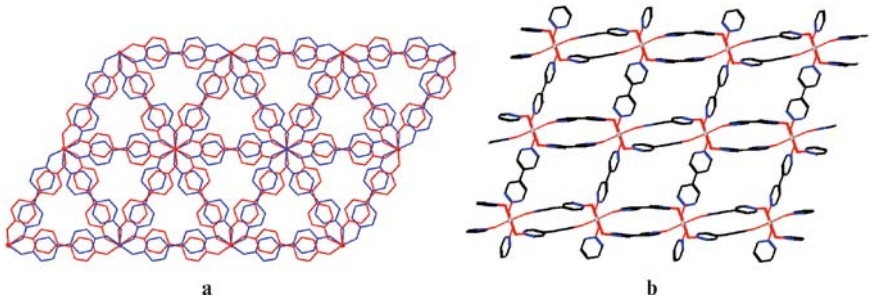

Fig. 7 Views of the 3D structures of **a** $\{[Sc\ (\mu\text{-}L^1)_3]\cdot 3X\}_\infty$ **50** [55] and **b** $\{[Sc\ (\mu\text{-}L^1)_3]\cdot 3CF_3SO_3\cdot 2.7CH_3OH\cdot 3H_2O\}_\infty$ **54** [55] illustrating the channels that accommodate anions and other guest molecules

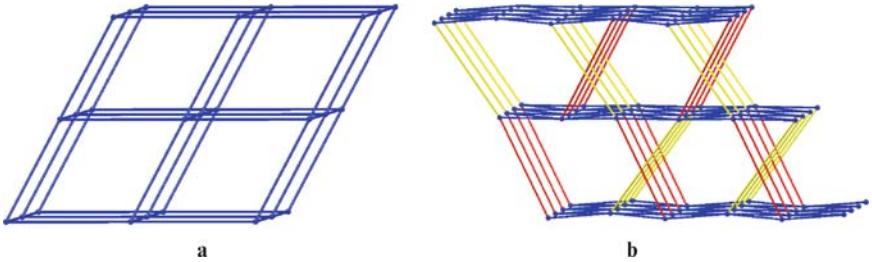

Fig. 8 Schematic representations of the structures of **a** $\{[Sc(\mu\text{-}L^1)_3]\cdot 3X\}_\infty$ **50** [55] and **b** $\{[Sc(\mu\text{-}L^1)_3]\cdot 3CF_3SO_3\cdot 2.7CH_3OH\cdot 3H_2O\}_\infty$ **54** [55] illustrating their $4^{12}6^3$ and 4^86^68 topologies, respectively

3 Synthetic Methodologies

Genuine targeted and designed synthesis of L^1-bridged transition metal co-ordination polymers has yet to be achieved. Nonetheless, considerable progress has been made. It is clear from the structural analyses of isolated materials that it is necessary to avoid aqueous solutions and strongly co-ordinating anions such as halide, nitrate, dicyanamide and hexafluoroacetylacetonate when targeting 1D chains, 2D sheets and 3D networks. Transition metal cationic centres readily bind water and anions to the exclusion of L^1 resulting in molecular rather than polymeric species. The formation of extended framework structures depends upon supramolecular interactions, particularly water$\cdots L^1$ O–H$\cdots$O hydrogen-bonds and aromatic π–π stacking between L^1 pyridyl moieties. Consequently, the synthesis of the multidimensional L^1-bridged transition metal co-ordination polymers considered in this review has involved reaction between L^1 and transition metal tetrafluoroborates, perchlorates, hexafluorophosphates and hexafluoroantimonates in low molecular weight alcohols, typically methanol or ethanol. Reaction stoichiometry does not seem to be as important as anion choice in determining framework formation. For example, in our own experience [45], reaction of L^1 with a series of Cu(II) salts in an equimolar ratio in methanol yields products with diverse L^1: Cu(II) molar ratios ranging from 2:1

in $\{[\{Cu(OH_2)_2(L^1)\}_2(\mu\text{-}L^1)_2] \cdot 2SiF_6 \cdot n(solv)\}_\infty$ **23**, $\{[\{Cu(OHMe)_2\}(\mu\text{-}L^1)_2] \cdot 2ZrF_5\}_\infty$ **45** and $\{[Et_4N][\{Cu(OHMe)_{0.5}\}(\mu\text{-}L^1)_2(\mu\text{-}FSiF_5)_{0.5}] \cdot 2SbF_6 \cdot n(solv)\}_\infty$ **46**, through to 3:1 in $[\{Cu(L^1)_2(CH_3OH)_2)(\mu\text{-}L^1)] \cdot 2(PF_6)\}_\infty$ **40** and $\{[Cu(\mu\text{-}L^1)_3] \cdot 2BF_4\}_\infty$ **42**, 4:1 in $\{[\{Cu(L^1)_2\}(\mu\text{-}L^1)_2] \cdot 2(PF_6)\}_\infty$**47** and $\{[\{Cu(L^1)_2\}(\mu\text{-}L^1)_2] \cdot 2(SbF_6)\}_\infty$ **48**, and to 6:1 in $[Cu(L^1)_6] \cdot 2BF_4$ **18**. In some cases, the crystalline product is only obtained after modification of, or *in situ* production of the anion [45]. Thus, crystallisation of **45** depends upon the conversion of $[ZrF_6]^{2-}$ into $\{[ZrF_5]^-\}_\infty$, while crystallisation of **46** is linked to the formation of $[SiF_6]^{2-}$ by fluoride attack of the pyrex vessel following hydrolysis of $[BF_4]^-$. The choice of metal centre is less important than the choice of anion, as illustrated by the fact that analogous 1D chains $\{[M(\mu\text{-}L^1)(H_2O)_4] \cdot 2ClO_4 \cdot 2(L^1)\}_\infty$ were formed for Co(II) **31**, Ni(II) **32**, Cu(II) **33** and Zn(II) **34** from aqueous solutions containing L^1 and transition metal perchlorate in a 2:1 L^1:M molar ratio [52]. Different products can be obtained by altering either the cation charge and/or reaction media [45, 55]. For example, methanolic solutions containing L^1 and either Mn(II) or Sc(III) perchlorate yield the 2D 3^6 grid $\{[Mn(\mu\text{-}L^1)_3] \cdot 2ClO_4\}_\infty$ **41** or the 3D α-Po framework $\{[Sc(\mu\text{-}L^1)_3] \cdot 3ClO_4\}_\infty$ **51**, respectively.

4 Co-ordination Behaviour of 4,4′-Bipyridine-*N*,*N*′-Dioxide with Transition Metals

As noted earlier, 4,4′ -bipyridine-*N*,*N*′-dioxide fulfils three roles in these polymeric materials. Of the 98 molecules of L^1 in these *d*-block complexes, there are 42 bridging molecules, 36 pendant ligands and 20 non-co-ordinated hydrogen-bonded lattice molecules. These are listed in Table 1 together with their symmetry, if any, with the dihedral angle between pyridine-*N*-oxide rings. For co-ordinated L^1, the <N–O–M angle and the distance of the metal cation from the plane of the co-ordinating pyridine-*N*-oxide are included as are, for the bridging molecules of L^1, the M···M distance and <M···O···O···M torsion angle.

By far the majority of the bridging molecules of L^1 (32) adopt an *anti*-conformation (Fig. 9). Of these, 90% lie across a crystallographic inversion centre giving an <M···O···O···M torsion angle of 180°; for the others the minimum <M···O···O···M torsion angle is 163.1°. The 11 examples that adopt the *syn*-conformation have <M···O···O···M torsion angles that vary from 21.4 to 74.0°. Interestingly, of these 11 examples, 4 occur in multinuclear molecular species and the 74.0° angle is unique owing to the fact that it occurs for the two L^1 molecules that form the double-bridge between Cu(II) centres in the binuclear cation $[\{Cu(OH_2)_2(L^1)\}_2(\mu\text{-}L^1)_2]^{4+}$ in **23** (Table 1; Fig. 2b) [45]. The preponderance of the *anti*-conformation in these compounds contrasts markedly with the situation observed for lanthanide compounds [30–35, 65] for which the number with the *syn*-conformation exceeds that of the *anti*-conformation by a factor close to 3 (Fig. 9). This is probably due to the fact that double-bridges are common in lanthanide

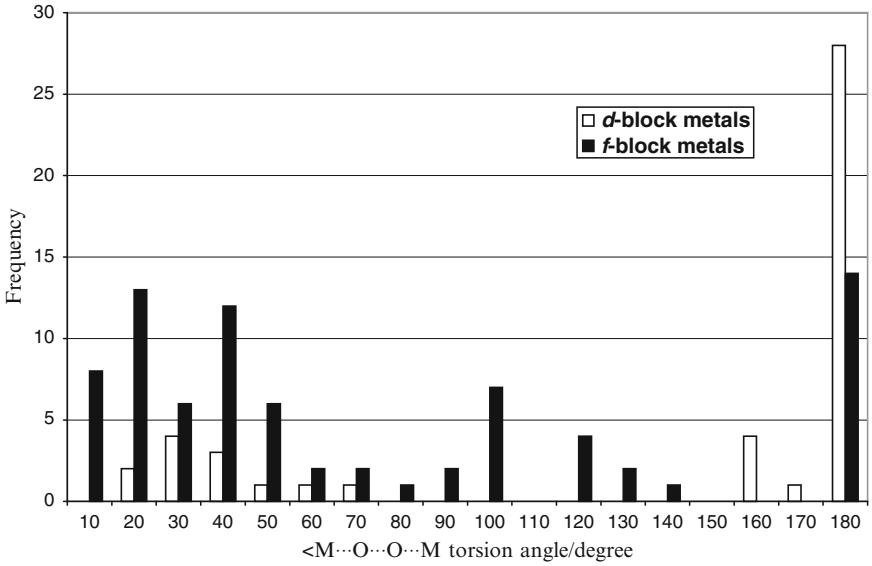

Fig. 9 Frequency of occurrence of L^1 bridged complexes of *d*- and *f*-block metal ions as a function of $<M\cdots O\cdots O\cdots M$ torsion angle

structures [30, 32–35, 65] but extremely rare in *d*-block transition metal chemistry, the only example being that in **23** [45].

Despite the fact that the data quoted in Table 1 for co-ordinated L^1 cover both a wide range of pendant and bridging molecules in both *syn*- and *anti*- bridging conformations with a wide variety of *d*-block transition metal centres, it is possible to identify some trends in the co-ordination behaviour of L^1. The $<M\cdots O$–N angle (θ) ranges from 107.9 to 132.7° with an average of 124.9°, suggesting sp^2 hybridisation of the *N*-oxide oxygen as shown in Scheme 1. However, the metal cation is not co-planar with the pyridine *N*-oxide as would be expected if the oxygen p_z orbital interacts with the π-system of the pyridine ring. In fact, the perpendicular distance of the metal cation from the plane of the pyridine *N*-oxide (*d*) varies from 0.15 to 2.42 Å with an average of 1.28 Å. Consideration of the data (Table 1) shows that a correlation exists between θ and d. As shown in Fig. 10, θ generally decreases as *d* increases. This suggests that the π -interaction between the oxygen p_z orbital and the π -system of the pyridine ring is counterbalanced by steric interactions between the metal centre and the hydrogen on the α-carbon, which forces the metal cation out of the plane of the pyridine *N*-oxide. The calculated $M\cdots H$ distance for a coplanar system (2.64 Å) assuming a typical $M\cdots O$ distance of 2.1 Å corresponds to the minimum van der Waals $M\cdots H$ separation for a *d*-block transition metal–hydrogen contact calculated using Bondi's van der Waals radii ($Zn\cdots H$, 2.59 Å) [66]. Thus, a compromise appears to exist between the π-interaction and this steric clash. The nearer the metal centre is to the plane of the pyridine ring (i.e., as *d* decreases), the

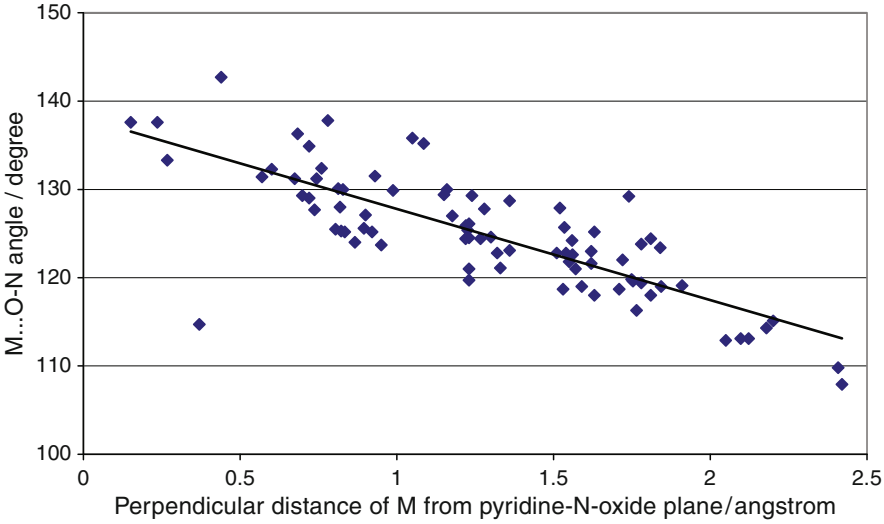

Fig. 10 Variation in the <M···O–N angle (θ) in *d*-block metal complexes as a function of the perpendicular distance of M from the pyridine-*N*-oxide plane for all bridging and pendant molecules of L^1

greater will be the steric interaction, which can only be relieved by an increase in the value for θ.

Interestingly, the distribution of values of θ for lanthanide compounds [65], although similar to that for the *d*-block compounds (Fig. 11), has a higher average value (132.1° *c.f.*, 124.9°). A similar pattern emerges for the distribution of *d* values (Fig. 12; 1.44 Å *c.f.* 1.28 Å). Although the increased average *d* value for the lanthanide compounds can be attributed to the increased size of the metal cation [Ce^{3+}(1.07Å)–Lu^{3+}(0.85 Å); Mn^{2+}(0.91 Å–Ni^{2+}(0.78 Å)] [67], this is not the case for the increase in average θ value, which can be partially attributed to an increased electrostatic contribution to the lanthanide to *N*-oxide interaction.

Assuming comparable M···O distances for the different *d*-block transition metals (ca. 2.1 Å), M···M separations might be expected to decrease with decreasing <M···O···O···M torsion angle giving shorter separations for *syn*-conformation compared to *anti*-conformation L^1 bridges. Considering *syn*-conformation L^1 bridges only (<M···O···O···M torsion angle <75°), the observed M···M separations do indeed decrease with decreasing <M···O···O···M torsion angle (Fig. 13), with the exception of those in **23**, which form the double-bridge in the binuclear cation $[\{Cu(OH_2)_2(L^1)\}_2(\mu\text{-}L^1)_2]^{4+}$, which has an abnormally short M···M separation [45].

Somewhat surprisingly, the M···M separations in complexes containing *syn*-bound L^1 fall in a similar range (∼11.9–12.7 Å) to those for *anti*-conformation L^1 molecules (∼11.8–13.0 Å). For complexes incorporating *anti*-conformation L^1 molecules the variation in M···M separations can be related to the variation in <M···O–N angles. As shown in Fig. 14 for those *anti*-bridging molecules of L^1

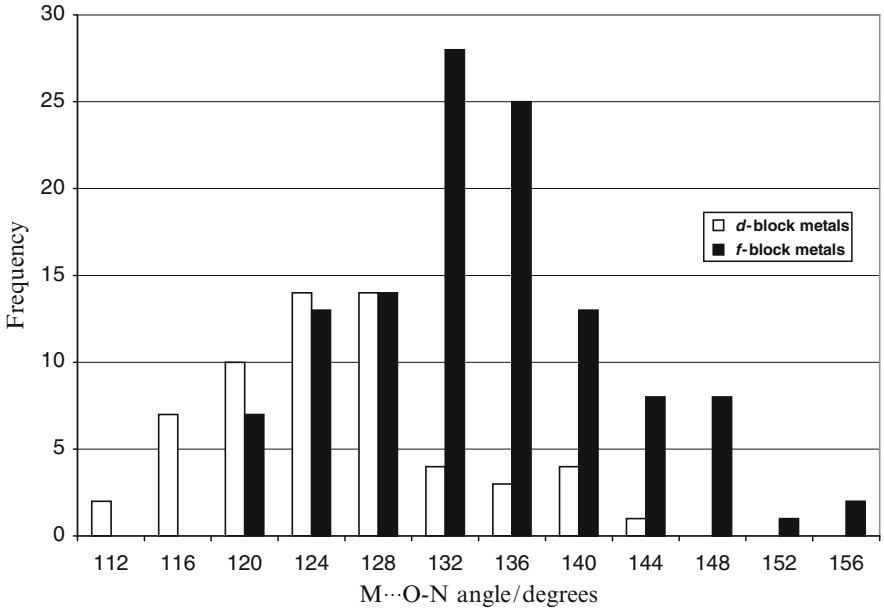

Fig. 11 Frequency of occurrence of <M ··· O-N angles (θ) in bridging and pendant L^1 molecules in *d*- and *f*-block metal complexes

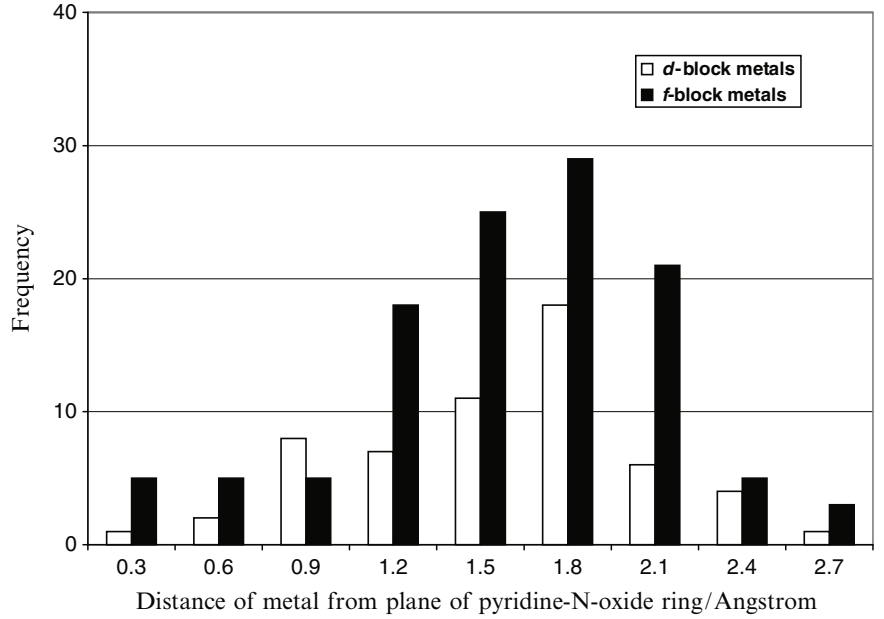

Fig. 12 Frequency of occurrence of the perpendicular distance of the metal cation from the plane of the pyridine *N*-oxide in bridging and pendant molecules of L^1 in *d*- and *f*-block complexes

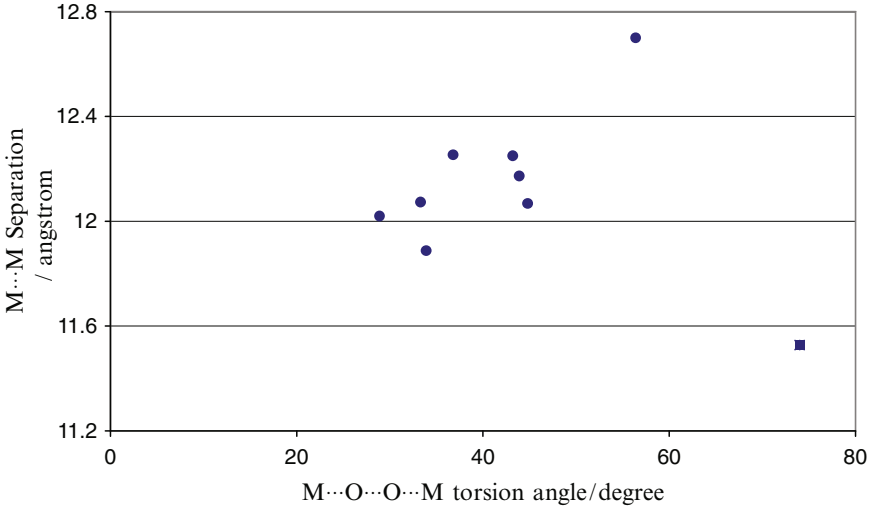

Fig. 13 Variation in M · · · M separation for *d*-block metal complexes as a function of <M · · · O · · · O · · · M torsion angle for molecules of L^1 in a *syn*-conformation. *Square symbol* represents data from compound **23**

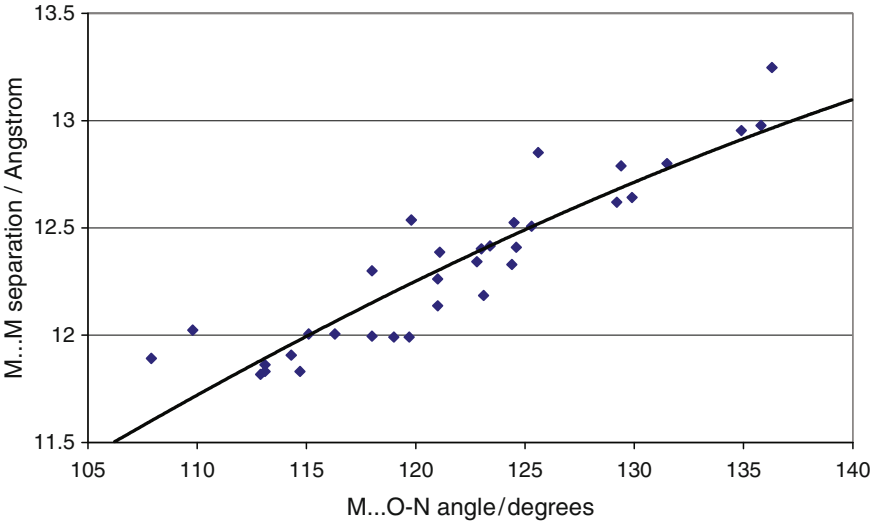

Fig. 14 Variation in M · · · M separation for *d*-block metal complexes as a function of <M · · · O–N angle for molecules of L^1 in an *anti*-conformation and which lie across inversion centres. The *line* represents the data calculated assuming the O · · · O and O · · · M separations to be constant at 9.7 and 2.1 Å, respectively

that lie across inversion centres (i.e., <M···O···O···M torsion angle = 180°), the M···M separation increases with increasing <M···O–N angle, following the line calculated assuming the O···O and O···M separations to be constant at 9.7 and 2.1 Å, respectively.

As noted earlier, many of the *anti*-conformation bridging molecules of L^1 lie across inversion centres. Not only does this result in a <M···O···O···M torsion angle of 180° but also a parallel arrangement of the two pyridine-*N*-oxide rings with a dihedral angle between the corresponding least squares planes of 0°. In contrast, all of the pendant molecules of L^1, all of the *syn*-conformation bridging L^1 molecules and the remainder of the *anti*-conformation bridging L^1 molecules are twisted about the central C–C bond with dihedral angles of up to 34.4° (average 16.5°), 32.0 (average 18.1°), and 38.1° (average 25.1°), respectively. The molecules of L^1 located in the lattice by hydrogen-bonding interactions adopt geometries similar to those of the metal-bridging L^1 molecules in an *anti*-conformation. They exhibit very small dihedral angles (maximum 8.6°; average 1.91°) with a large proportion (60%), particularly type g and type i (Scheme 1), lying across inversion centres.

5 Conclusions

4,4′-Bipyridine -*N*,*N*′-dioxide (L^1) exhibits enormous flexibility as a supramolecular linker and can co-ordinate to metal cations or act as hydrogen-bond acceptors via its O-centres, and/or form aromatic π–π stacking interactions via the pyridine-*N*-oxide rings. To encourage multidimensional architecture construction it is necessary to avoid competing aqueous solutions and strongly co-ordinating anions as transition metal cationic centres readily bind water and anions to the exclusion of L^1, resulting in molecular rather than polymeric species. Thus, the formation of extended frameworks is dependent upon supramolecular interactions, particularly water···L^1 O–H···O hydrogen-bonds and aromatic π–π stacking between L^1 pyridine moieties. Consequently, the synthesis of multidimensional L^1-bridged transition metal co-ordination polymers has generally involved reaction between L^1 and salts of weakly co-ordinating anions in low molecular weight alcohols.

The co-ordinate L^1–transition metal interaction is based on an sp^2 hybridised oxygen but the π -interaction between the oxygen p_z orbital and the aromatic ring is so weak that the oxygen lone pairs can be twisted out of the plane of the pyridine-*N*-oxide by a steric clash between the metal centre and the α -hydrogen of the pyridine ring. As a result, <M···O–N angles increase with decreasing perpendicular distance of the metal from the plane of the pyridine-*N*-oxide.

In contrast to the situation for L^1-bridged lanthanide co-ordination polymers [65], where the bridging L^1 molecules predominantly (ca. 75%) adopt a *syn*-conformation, by far the majority of the bridging L^1 molecules (ca. 75%) in L^1-bridged *d*-block metal co-ordination polymers adopt the *anti*-conformation. This difference is attributed to the fact that "double-bridges" are common in lanthanide structures [30–35, 65] but extremely rare in *d*-block complexes. Although,

contrary to prediction, M···M separations for complexes incorporating *anti*- and *syn*-conformation bridging ligands fall in similar ranges, the M···M separations in complexes incorporating L^1 ligands in an *anti*-conformation are related to the <M···O–N angles, the parameters increasing together as predicted by simple geometrical analysis. For complexes incorporating *syn*-bound ligands of L^1, the M···M separation correlates in part to the <M···O···O···M torsion angle.

Acknowledgments We thank EPSRC for support. M.S. gratefully acknowledges receipt of a Royal Society Wolfson Merit Award and of a Leverhulme Trust Senior Research Fellowship.

References

1. Hoskins BF, Robson R (1990) J Am Chem Soc 112:1546
2. Batten SR, Robson R (1998) Angew Chem Int Ed Engl 37:1460
3. Blake AJ, Champness NR, Hubberstey P, Li WS, Schröder M, Withersby MW (1999) Coord Chem Rev 183:117
4. Moulton B, Zaworotko MJ (2001) Chem Rev 101:1629
5. Khlobystov AN, Blake AJ, Champness NR, Lemenovskii DA, Majouga AG, Zyk NV, Schröder M (2001) Coord Chem Rev 222:155–192
6. Chae HK, Siberio-Pérez DY, Kim J, Go YB, Eddaoudi M, Matzger AJ, O'Keeffe M, Yaghi OM (2004) Nature 427:523
7. Lin X, Blake AJ, Wilson C, Sun XZ, Champness, NR, George MW, Hubberstey P, Mokaya R, Schröder M (2006) J Am Chem Soc 128:10745
8. Kubota Y, Takata M, Matsuda R, Kitaura R, Kitagawa S, Kobayashi TC (2006) Angew Chem Int Ed 45:4932
9. Zeng M-H, Feng X-L, Chen X-M (2004) Dalton Trans, p 2217
10. Wong-Foy AG, Lebel O, Matzger, AJ (2007) J Am Chem Soc 129:15740
11. Ma S, Sun D, Simmons JM, Collier CD, Yuan D, Zhou H-C (2008) J Am Chem Soc 130:1012
12. Lin X, Jia J, Hubberstey P, Schröder M, Champness NR (2007) Cryst Eng Commun 9:438
13. Dincă M, Dailly A, Liu Y, Brown CM, Neumann DA, Long JR (2006) J Am Chem Soc 128:16876
14. Jia J, Lin X, Wilson C, Blake AJ, Champness NR, Hubberstey P, Walker G, Cussen EJ, Schröder M (2007) Chem Commun, p 840
15. Chen B, Liang C, Yang J, Contreras DS, Clancy YL, Lobkovsky EB, Yaghi OM, Dai S (2006) Angew Chem Int Ed 45:1390
16. Ye Q, Song Y-M, Wang G-X, Chen K, Fu D-W, Chan PWH, Zhu J-S, Huang SD, Xiong R-G (2006) J Am Chem Soc 128:6554
17. Bordiga S, Lamberti C, Ricchiardi G, Regli L, Bonino F, Damin A, Lillerud K-P, Bjorgen M, Zecchina A (2004) Chem Commun, p 2300
18. Zhang L-J, Yu J-H, Xu J-Q, Lu J, Bie H-J, Zhang X (2005) Inorg Chem Commun 8:638
19. Khlobystov AN, Brett MT, Blake AJ, Champness NR, Gill PMW, O'Neill DP, Teat SJ, Wilson C, Schröder M (2003) J Am Chem Soc 125:6753
20. Biradha K, Sarkar M, Rajput L (2006) Chem Commun, p 4169
21. Yang W, Lin X, Jia J, Blake AJ, Wilson C, Hubberstey P, Champness NR, Schröder M (2008) Chem Commun, p 359
22. Yang S, Lin X, Blake AJ, Thomas KM, Hubberstey P, Champness NR, Schröder M (2008) Chem Commun, p 6108
23. Swiegers GF, Malefetse TJ (2000) Chem Rev 100:3483
24. Seidel SR, Stang PJ (2002) Acc Chem Res 35:972

25. Blake AJ, Champness NR, Crew M, Hanton LR, Parsons S, Schröder M (1998) J Chem Soc Dalton Trans, p 1533
26. Blake AJ, Brooks NR, Champness NR, Crew M, Hanton LR, Hubberstey P, Parsons S, Schröder M (1999) J Chem Soc Dalton Trans, p 2813
27. Withersby MA, Blake AJ, Champness NR, Cooke PA, Hubberstey P, Realf AL, Schröder M (2000) J Chem Soc Dalton Trans, p 3261
28. Rosi NL, Eddaoudi M, Kim J, O'Keeffe M, Yaghi OM (2002) CrystEngComm 4:401
29. Sui B, Fan J, Okamura T, Sun W-Y, Ueyama N (2005) Solid State Chem 7:969
30. Hill RJ, Long D-L, Champness NR, Hubberstey P, Schröder M (2005) Acc Chem Res 38:337
31. Long D-L, Blake AJ, Champness NR, Wilson C, Schröder M (2001) J Am Chem Soc 123:3401
32. Long D-L, Blake AJ, Champness NR, Wilson C, Schröder M (2001) Angew Chem Int Ed 40:2444
33. Long D-L, Hill RJ, Blake AJ, Champness NR, Hubberstey P, Proserpio DM, Wilson C, Schröder M (2004) Angew Chem Int Ed 43:1851
34. Hill RJ, Long D-L, Turvey MS, Blake AJ, Champness NR, Hubberstey P, Wilson C, Schröder M (2004) Chem Commun, p 1792
35. Long D-L, Blake AJ, Champness NR, Wilson C, Schröder M (2002) Chem Eur J 8:2026
36. Roesky HW, Andruh M (2003) Coord Chem Rev 236:91
37. Bourne SA, Moitsheki LJ (2005) Cryst Eng Commun 7:674
38. Ma B-Q, Sun H-L, Gao S, Xu G-X (2001) Inorg Chem 40:6247
39. Blake AJ, Brett MT, Champness NR, Khlobystov AN, Long D-L, Wilson C, Schröder M (2001) Chem Commun, p 2258
40. Ma B-Q, Gao S, Sun H-L, Xu G-X (2001) Cryst Eng Commun 3:147
41. Mantero DG, Neels A, Stoeckli-Evans H (2006) Inorg Chem 45:3287
42. Nedelcu A, Žak Z, Madalan AM, Pinkas J, Andruh M (2003) Polyhedron 22:789
43. Xu Y, Yuan D, Xu Y, Bi W, Zhou Y, Hong M (2004) Acta Crystallogr Sect E 60:m713
44. Ma B-Q, Sun H-L, Gao S (2005) Inorg Chem 44:837
45. Jia J, Blake AJ, Champness NR, Hubberstey P, Wilson C, Schröder M (2008) Inorg Chem 47:8652
46. Long D-L, Blake AJ, Champness NR Schröder M (2000) Chem Commun, p 2273
47. Wang X-L, Qin C, Wang E-B, Xu L (2005) Eur J Inorg Chem 3418
48. Bourne SA, Moitsheki LJ (2007) J Chem Crystallogr 37:359
49. Visinescu D, Pascu GI, Andruh M, Magull J, Roesky HW (2002) Inorg Chim Acta 340:201
50. Plater MJ, Foreman MRStJ, Slawin AMZ (2000) Inorg Chim Acta 303:132
51. Manna SC, Zangrando E, Drew MGB, Ribas J, Chaudhuri NR (2006) Eur J Inorg Chem 481
52. Ma B-Q, Gao S, Sun H-L, Xu G-X (2001) J Chem Soc Dalton Trans, p 130
53. Bruda S, Andruh M, Roesky HW, Journaux Y, Noltmeyer M, Rivière E (2001) Inorg Chem Commun 4:111
54. Ang SG, Sun BW (2005) Cryst Growth Design 5:383
55. Long D-L, Hill RJ, Blake AJ, Champness NR, Hubberstey P, Wilson C, Schröder M (2005) Chem Eur J 11:1384
56. Williams CA, Blake AJ, Hubberstey P, Schröder M (2005) Chem Commun, p 5435
57. Du M, Jiang X-J, Zhao X-J, (2007) Inorg Chem 46:3984
58. Edgar M, Mitchell R, Slawin AMZ, Lightfoot P, Wright PA (2001) Chem Eur J 5168
59. Burrows AD, Cassar K, Friend RMW, Mahon MF, Rigby SP, Warren JE (2005) Cryst Eng Commun 7:548
60. Hawxwell SM, Adams H, Brammer L (2005) Acta Cryst B62:808
61. Su C-Y, Cai Y-P, Chen C-L, Kang B-S (2001) Inorg Chem 40:2210
62. Biradha K, Fujita M (2002) Chem Commun, p 1866
63. Carlucci L, Ciani G, Proserpio DM (1998) New J Chem 1319
64. Hagrman P, Hagrman D, Zubieta J (1999) Angew Chem Int Ed 38:2638
65. Allen FH, (2002) Acta Crystallogr Sect B 58:380
66. Bondi A (1964) J Phys Chem 68:441
67. Emsley J (1991) The elements, 2nd edn. Clarendon Press, Oxford

Index